Determination of drug absorption parameters in Caco-2 cell monolayers with a mathematical model encompassing passive diffusion, carrier-mediated efflux, non-specific binding and phase II metabolism.

Inauguraldissertation

zur
Erlangung der Würde eines Doktors der Philosophie
vorgelegt der
Philosophisch-Naturwissenschaftlichen Fakultät
der Universität Basel

von

David Werner Blaser
aus Langnau im Emmental (Schweiz)

Basel, 2007

Genehmigt von der von der Philosophisch-Naturwissenschaftlichen Fakultät
auf Antrag von

Herrn Prof. Dr. Hans Leuenberger (Fakultätsverantwortlicher)

Herrn Prof. Dr. Georgios Imanidis (Dissertationsleiter)

Herrn PD Dr. Peter van Hoogevest (Korreferent)

Basel, den 24.4.2007

Prof. Dr. Hans-Peter Hauri
Dekan

meinen Eltern und Johanna

Acknowledgements

Herrn Prof. Dr. Hans Leuenberger danke ich für die Möglichkeit, dass ich meine Dissertation am Institut für Pharmazeutische Technologie der Universität Basel durchführen konnte.

Bei Prof. Dr. Georgios Imanidis möchte ich mich für die wissenschaftliche Betreuung der vorliegenden Arbeit bedanken. Er ließ mir die Freiräume, die Arbeit nach meinen Vorstellungen zu gestalten, war aber auch jederzeit mit interessanten und kritischen Diskussionen eine wertvolle Unterstützung.

Bedanken möchte ich mich bei PD Dr. Peter van Hoogevest für das Interesse an meiner Arbeit und die Übernahme des Korreferates.

Chantal Krömler und Urs Duthaler danke ich recht herzlich für das Engagement und die produktive Zusammenarbeit während Ihrer Diplomarbeiten und das mir entgegengebrachte Vertrauen als Diplomarbeitsbetreuer.

Stefan Winzap danke ich für jegliche technische Unterstützung und für seinen unverzichtbaren Beitrag zum reibungslosen Ablauf des Institutsalltages, Sonja Reutlinger für das Anlernen der Zellkulturtechnik und ihre immer wieder motivierende Art und Frau Christina Erb für ihre Hilfe mit den Textverarbeitungsprogrammen.

Weiterhin möchte ich mich bei meinen Kollegen für die freundliche Atmosphäre und all die Dinge bedanken, die dazu beitrugen, dass mir meine Zeit am Institut in positiver Erinnerung bleiben wird. Besonders bedanke ich mich bei meinen Laborkollegen /-innen Susanne Reitbauer und Marcel Schneider sowie bei Miriam Reiser, Dana Daneshvari und Ervina Brka für die wertvolle Teamarbeit in der Durchführung des Studentenpraktikums in dispersen Arzneiformen.

Ganz besonders aber bedanke ich mich bei Johanna und meiner Familie für die Geduld und die unermessliche Unterstützung auf meinem Weg zur Promotion.

Index

1. ABBREVIATIONS 9

2. SUMMARY 11

3. INTRODUCTION AND OBJECTIVES 14

4. THEORETICAL SECTION 18

4.1. Drug absorption after oral application 18

4.2. The gastro-intestinal tract and the intestinal epithelium 19

4.3. Mechanisms of membrane permeation 20

4.4. Passive transcellular permeation 20

4.5. Paracellular transport 21

4.6. Drug transporters: carrier-mediated influx and efflux. 22

4.7. Pre-systemic Metabolism 23

***4.8. In vitro* assessment of drug permeability: models 23**

***4.9. In vitro* assessment of drug permeability: data analysis 25**

4.10. Non-specific binding / Adsorption 27

4.11. Choice of model compounds 29

5. ANALYSIS OF AMENTOFLAVONE TRANSPORT AND PHASE II METABOLISM IN CACO-2 CELL MONOLAYERS AND ADSORPTION TO THE TRANSWELL SURFACE BY A MATHEMATICAL MODEL FOR DETERMINING DUG ABSORPTION PARAMETERS 31

5.1. Abstract 31

5.2. Introduction 33

5.3. Materials and methods 37

5.3.1. Materials 37

5.3.2. Cell culture 37

5.3.3. MTT-assay 38

5.3.4. Experimental determination of the contact height and mathematical description of the contact area of the transport medium with Transwell surfaces 39

5.3.5. Permeation of Amentoflavone across Transwell polycarbonate membrane without Caco-2 cell monolayers at 4 and 37℃ 40

5.3.6. Extraction of the Transwell plates with methanol 41

5.3.7. TEER 41
5.3.8. Permeation of Amentoflavone across Caco-2 cell monolayers at 4 and 37℃ in presence or absence of inhibitors of active apical efflux 41
5.3.9. Detection of Amentoflavon phase II metabolism in Caco-2 cell monolayers using HPLC-MS 43
5.3.10. Cell lysis 43
5.3.11. HPLC 44
5.3.12. Calculation of normalised fluxes <J> 45

5.4. Theoretical modeling 46
5.4.1. Modelling of adsorption to Transwell surfaces in Transwells without cells 46
5.4.2. Mathematical model for determining drug absorption parameters in Caco-2 cell monolayers 52
5.4.3. Modelling of compound permeation across Caco-2 cell monolayers in Transwells 53
5.4.4. Mathematical model for determining drug absorption parameters in Caco-2 cell monolayers with inclusion of phase II metabolism and adsorption to the Transwell surface 57
5.4.5. Analysis of the permeation data 60
5.4.6. Estimation of adsorption parameters in transwells without cells 61
5.4.7. Analysis of Amentoflavone permeation across Caco-2 cell monolayers 63

5.5. Results and discussion 65
5.5.1. Cell toxicity of the different compounds 65
5.5.2. Determination of the contact height and mathematical description of the contact area of the transport medium with Transwell surfaces (Transwells without cells) 67
5.5.3. Adsorption of Amentoflavone to Transwell surfaces at 4℃ and 37℃ (Transwells without cells,): Estimation of the adsorption parameters and representative fits of the Amentoflavone transport and adsorption in Transwells without cells 68
5.5.4. Comparison of the two different models for adsorption (Transwells without cells, 4℃ and 37℃) 71
5.5.5. Choice of the model for adsorption for analysis of Amentoflavone transport in Transwells with cells 74
5.5.6. Asymmetric transport of Amentoflavone across Caco-2 cell monolayers as measured by the normalised fluxes <J> 75
5.5.7. Cellular accumulation of Amentoflavone / apparent volume of distribution 77
5.5.8. Detection of Amentoflavone phase II metabolism in Caco-2 cell monolayers using HPLC – MS 78
5.5.9. Transport behaviour of the phase II metabolites: formation, efflux and cellular accumulation of Amentoflavone metabolites 81
5.5.10. Analyis of Amentoflavone transport across Caco-2 cell monolayers grown in Transwells based on the transport parameters for passive diffusion and carrier mediated efflux 82
5.5.11. Model derived kinetic parameters for Amentoflavone absorption in Caco-2 cell monolayers 84

5.5.12. Comparison between the measured and calculated amount of Amentoflavone in the cellular compartment 87
5.5.13. Adsorption of Amentoflavone to Transwell surfaces during the transport across Caco-2 cell monolayers 89
5.5.14. Model estimated donor amounts/concentrations for Amentoflavone transport in Transwells with cells 92
5.5.15. Mass balances of Amentoflavone transport in Transwells with cells 93
5.5.16. Conclusion 93

6. INDIVIDUALLY STUDIED ABSORPTION OF DIGOXIN, QUINIDINE, AND VERAPAMIL ACROSS CACO-2 CELLS AND THE INFLUENCE OF BINARY COMBINATIONS ON PASSIVE DIFFUSION AND ACTIVE EFFLUX, AS ANALYSED BY A MATHEMATICAL MODEL FOR DETERMINATION OF DRUG ABSORPTION PARAMETERS. 95

6.1. Abstract 95

6.2. Introduction 97

6.3. Materials and methods 100
6.3.1. Materials 100
6.3.2. Cell culture 100
6.3.3. MTT-assay 100
6.3.4. TEER 102
6.3.5. Individual permeation of Digoxin, Quinidine and Verapamil across Caco-2 cell monolayers at 37℃ 102
6.3.6. Drug permeation of binary combinations of compounds across Caco-2 cell monolayers at 37℃ 103
6.3.7. HPLC 104
6.3.8. Calculation of the apparent permeability coefficient and the efflux ratio 106
6.3.9. Mathematical model for determining drug absorption parameters in Caco-2 cell monolayers 107
6.3.10. Modelling of the reduction of the volume of solution 108
6.3.11. Analysis of compound permeation across Caco-2 cell monolayers 109

6.4. Results and discussion 111
6.4.1. Cell toxicity of the different compounds and combinations 111
6.4.2. Cell permeation of individual drugs 114
6.4.3. Quantification of passive and carrier-mediated transport parameters 119
6.4.4. Transport of binary mixtures of compounds across Caco-2 cell monolayers grown in Transwell plates 131
6.4.5. Conclusion 139

7. APPENDIX 142

7.1. Development of an optimal procedure for TEER-measurements 142

7.2. Detection of Amentoflavon phase II metabolism in Caco-2 cell monolayers using enzymatical cleavage 150

7.3. Amentoflavone **158**

7.4. Digoxin **160**

7.5. Quinidine **167**

7.6. Verapamil **173**

8. REFERENCES **179**

1. Abbreviations

Å	angstrom
a_b	apical to basal transport direction
ABC	ATP-binding cassette
ACE	angiotensin converting enzyme
ADME	absorption, distribution, metabolism, excretion
AF	Amentoflavone
API	active pharmaceutical ingredient
AQ	absorptive quotient
b_a	basal to apical transport direction
BCRP	breast cancer resistance protein
BCS	biopharmaceutical classification system
Caco-2	colon adenocarcinoma cells
C_W	molar number of occupied sites per area
CYP	cytochrome P450 enzymes
D	Digoxin
ER	efflux ratio
Fa	fraction absorbed
FRV	final residual value scaled
HPLC	high performance liquid chromatography
hPepT1	human di/tri-peptide transporter
k_{on}	rate constant for adsorption to the surface
k_{off}	rate constant for desorption of the surface
LC	liquid chromatography
logP	partition coefficient
MS	mass spectrometry
MDCK	Madin-Darby canine kidney
MRP2	multidrug resistance protein 2
MW	molecular weight
OATP	organic anion transporting polypeptide
P	permeability coefficient
P_{app}	apparent permeability coefficient
P-gp	P-glycoprotein
PSA	polar surface area
Q	Quinidine HCl
SHP	succus helix pomatia
SLC	solute carrier family

SQ	secretory quotient
vk	apical efflux rate / pump rate
VP	Verapamil HCL
W	molar number of free sites per area
W_{tot}	total number of binding sites on the surface

2. Summary

Intestinal absorption is required for a sufficiently high bioavailability of drugs administered by the peroral route. Several molecular mechanisms are involved in intestinal absorption and can profoundly influence its magnitude including permeation of the mucosa by passive diffusion, transport across the intestinal wall by carrier mediated processes, chemical and enzymatic alteration of the molecule in the intestinal lumen and/or in the enterocyte, dissolution behaviour of the drug and interaction with food ingredients or co-administered drugs at the dissolution and the transport level. These mechanisms typically act simultaneously and each depends on drug molecule and epithelium related chemical and biological factors whose effect is not definitely established. This makes intestinal absorption a rather complex process, which, despite recent advances, is fundamentally still poorly understood. Therefore, experimental verification of drug absorption remains a must in current industrial drug development practice. Prediction of *in vivo* absorption based on *in vitro* methodology may help reduce the volume of necessary clinical investigations. Cell culture techniques predominantly employing the Caco-2 cell line have been established in the last decade as a screening and study tool of intestinal absorption. This technique, although widely used in industrial and academic settings, still poses a number of challenges. These include artefacts like adsorption to container surfaces and cellular accumulation, which might lead to an erroneous estimation of the permeability, poor recovery, and faulty mass balance. The estimation of independent parameters for parallel processes (e.g. passive permeability and active efflux) is still not the common procedure in the analysis of permeation data and the usually employed apparent permeability coefficient P_{app} and efflux ratio (ER) are afflicted with limitations.

The objective of the present work was to establish a methodology for determining the contribution of passive diffusion, carrier-mediated transport, enzymatic degradation and non-specific binding/adsorption to drug absorption measured in the Caco-2 cell system and investigating drug-drug interactions for absorption in this system. Transport experiments across the cell monolayer were conducted in bi-directional modus using model drug compounds (Amentoflavone, Verapamil, Digoxin and Quinidine) that are known to be subject to more than one of the above molecular mechanisms. In order to delineate the contribution of these mechanisms, a model for analysing the experimental data was introduced. This model encompassed quantitative expressions based on biophysical or physicochemical principles of the effect of all these mechanisms on transport and described the variation of drug concentration in the different compartments of the cell system as a result of the simultaneous action of these mechanisms. The

resulting system of differential equations was fitted to the experimental data using regression analysis following numerical integration and relevant parameters reflecting the quantitative effect of each mechanism involved in absorption were deduced. These parameters were the passive permeability coefficient, first and zero order carrier mediated transport rate, first order metabolic rate constant and binding constant. This was done for the above drugs used individually and for selected binary mixtures.

Amentoflavone exhibited strongly asymmetric transport, which was almost not detectable in the apical to basal direction and pronounced in the basal to apical direction. This suggested that Amentoflavone is subject to apical efflux in the Caco-2 cells. This was partly reversed by GF120918 and Vinblastine which are known inhibitors of P-glycoprotein (P-gp) and P-gp and MRP2, respectively, indicating that Amentoflavone was substrate of at least one of these efflux transporters. The active apical efflux was almost abolished at low temperature. Amentoflavone also underwent phase II metabolism in the Caco-2 cells. At least two glucoronides and one sulfate were detected by HPLC-MS, which were hydrolysable by specific enzymes. These metabolites exhibited also apical efflux. Finally, Amentoflavone was strongly adsorbed to the surface of the Transwell plates used in cell culture and transport studies. The adsorption and desorption rate constant and the total number of surface binding sites was determined in blank experiments using the plates without cells. For this, a model describing the time dependent concentration decrease of the drug due to adsorption was employed. These surface adsorption parameters were subsequently used in the model describing the absorption of Amentoflavone in Caco-2 cells. This procedure allowed the determination of absorption parameters that were not biased by non-specific binding effects. Amentoflavone was found to have a rather low passive cell permeability, which combined with its substantial apical efflux resulted in its marginal absorption in the apical to basal transport direction. The metabolic rate constant was smaller than the efflux rate constant but still sufficiently large to produce relevant amounts of metabolite in the course of the cell absorption experiment.

Verapamil, Digoxin and Quinidine were studied in a wide concentration range individually and in binary mixtures to determine the significance of the interplay of passive diffusion and apical efflux on absorption and how this is affected by concomitant administration of a second drug. Passive permeability coefficients were independent of concentration and varied among the three drugs over at least a ten-fold range. The rate of apical mass efflux varied between the three drugs, increased with concentration and seemed to level off for at least one of the three drugs in the studied concentration range. The dominance of one mechanism over the other depended on concentration in a different pattern for the

three compounds. Thus, the outcome of the combination of passive permeation and apical efflux for apical to basal absorption can only be predicted if the passive permeability coefficient and the concentration dependence of the carrier mediated efflux rate are known. All three drugs were substrates of apical efflux carriers. In binary mixtures, they commonly reduced the efflux rate of the concomitant compound. This reduction was mutual yet its extent varied between the compounds. Hence, these apical efflux carrier substrates may also act as inhibitors and vice versa exhibiting at least a partially overlapping specificity.

In conclusion, the introduced model approach and data analysis provide a quantitative insight into the process of drug absorption which can be used for a better understanding and potentially as a means supporting the prediction of *in vivo* absorption based on cell culture data and the delineated effect of the involved mechanisms.

3. Introduction and Objectives

The oral route is generally accepted to be the most convenient for administration of drugs. One prerequisite for an orally administered drug to have a systemic effect is that there is drug uptake from the gastro-intestinal tract, i.e. the drug has to be absorbed from the gut lumen into the blood stream. The unchanged amount of drug that is absorbed determines its bioavailability and the systemic exposure of the body to the drug. The absorption is an important property in the determinants of the ability of a molecule to act as a drug. Poor absorption properties are often encountered in molecules from contemporary drug development programs. These are either due to poor water solubility or low intestinal wall permeability. The issue of solubility and permeability properties and their influence of the absorption have been addressed by the framework of the biopharmaceutic classification system (BCS) [Amidon, Kasim, Takagi]. Drugs that belong to class III (high solubility and low permeability) and IV (low solubility and low permeability) possess unfavourable permeability properties.

The reasons for poor absorption behaviour of a molecule can be based on different physico-chemical and physiological properties: (1) Molecules may not have the ability to easily cross biological membranes by passive diffusion resulting in low permeability. The main properties of a drug influencing its passive permeation through biological membranes are lipophilicity, hydrogen-bonding capacity, charge and size / molecular weight [Camenisch]. Based on these properties a simple rule of thumb to assess a drug's likeliness to be absorbed was defined [Lipinski]. (2) For an increasing number of molecules active efflux out of the cell, caused by proteins located in the apical cell membrane, is identified to have the potential to limit the overall permeability by pumping the drug molecules in the basal to apical direction. The physiological function of these proteins is to prevent uptake of toxic substrates or to facilitate the excretion of such substrates across the intestinal tract or in the liver. The relevant efflux transporters for drugs in clinical use belong to the ATP-binding cassette (ABC) family (e.g. P-glycoprotein, BCRP, MRP2) [Ambudkar, Borst, Litman 2001, Schinkel]. (3) Chemical instability or metabolism are important factors in limiting the absorption of drugs. A drug molecule must withstand pH values between 1.5 and 7.0 in the gastro-intestinal fluid and high enzymatic activity that can both lead to degradation [Rowland]. Both the liver and the intestinal epithelium constitute metabolic barriers where an absorbed drug molecule may be metabolised. Metabolism is divided into phase I metabolism, that is the modification of the parent drug by oxidation reactions, e.g. by Cytochrome (CYP) P450 enzymes, and phase II metabolism, that is the conjugation of the parent compound or its phase I metabolite with hydrophilic moieties as glucuronic acid, sulfate or glutathione.

The liver may provide the main metabolising organ of the body but also the intestine constitutes an appreciable metabolic barrier where a drug molecule undergoing absorption may be metabolised before reaching the systemic circulation. Of the phase I metabolising enzymes, CYP3A is the dominant subfamily in the small intestine where it constitutes about 70% of the total CYP protein [de Waziers, Kolars, McKinnon]. Several phase II enzymes are expressed in the intestine at levels that are comparable to those in the liver. (4) Further reasons for poor absorption can be drug-drug interactions (e.g. complex forming, chemical reactions, inhibition of or competition for carrier-mediated uptake) or interactions of drugs with food components (e.g. protein binding).

For the assessment and prediction of absorption and permeation properties at the different drug administration sites of the human body and the study of the underlying processes many *in vitro* and *in situ* methods were developed with different levels of complexity and sophistication [Avdeef 2003, Bohets, Deli, Ghibellini, Hidalgo 1989 & 2001, Kansy, Schlatter, Tavelin]. One of most frequently used and best established cell lines for the determination of drug permeability across intestinal membranes is the human colon adenocarcinoma cell line Caco-2, grown on semi-permeable filter supports [Artursson 1991 B, Hidalgo 1989]. Caco-2 cells spontaneously differentiate into enterocyte-like cells and in spite of their colonic origin, a number of active transport mechanisms normally found in the absorptive enterocytes of the small intestine are present in this cell line [Bailey]. The use of the Caco-2 cell model permits the investigation of simultaneous absorption routes at the same time (e.g. passive diffusion, active efflux, metabolism), and much insight into the different steps of absorption has been gained by the use of the Caco-2 cell model [Artursson 1997].

Some of the problems and disadvantages that are affiliated with the use of the Caco-2 cell model are the following: (1) The Caco-2 cell model normally requires, without optimising the culturing conditions, culture on filters for three weeks before it can be used for drug transport experiments. (2) A lab-to-lab and cell batch to cell batch variability is an often-encountered problem with the results of *in vitro* permeability studies. Depending on the exact protocol of the culturing conditions, the results of permeability measurements for selected compounds may differ for different labs, passages, selected clones and culturing conditions [Anderle, Behrens 2003 & 2004, Briske-Anderson, Hosoya, Yu]. (3) Artefacts like non-specific binding to container surfaces and cellular accumulation lead to an erroneous estimation of the permeability of compounds as well as to poor recovery of the compound and faulty mass balance [Balimane 2005, Ingels]. Under *in vitro* conditions the adsorption to solid surfaces and to cells depends on the composition of the experimental buffer or medium, the chemical identity of the compound itself, and the type

of the solid surface [Grohganz, Palmgren]. (4) Up to date the estimation of independent parameters for parallel processes (e.g. passive permeability and active efflux) is not the common procedure in the analysis of permeation data derived from *in vitro* models. The usually employed apparent permeability coefficient P_{app} is afflicted with limitations as this approach uses the initial drug amount in the donor, linear drug transport with time that is applicable to early time points only and furthermore assumes negligible back flux and no mass balance problems [Tran 2004, Youdim]. Additionally, substrates for active apical efflux are identified by calculation of the efflux ratio (ER), and by performing transport experiments with inhibition of the carrier-mediated component. To identify substrates by calculation of the ER the estimated P_{app} values have to be within an optimal range. For substrates that have P_{app} values outside of this range, the identification as a substrate is prone to fail by using this approach [Polli]. These issues and some proposed solutions are addressed in literature [Balimane 2005, Bentz, Ingels, Tran 2004, Troutman 2003 B, Youdim].

Objectives

The purpose of this PhD thesis was to establish a methodology for determining unbiased parameters in *in vitro* cell culture models describing the absorption of some model drug compounds in the Caco-2 cell system. For this a mathematical model had to be developed and evaluated describing the processes involved in this system. The aim was to provide a tool to investigate permeation and metabolism in the Caco-2 cells grown on permeable filter supports in Transwell® plates and to determine the effect of non-specific binding to the surface of Transwell® plates on the permeation. This methodology should result in model-derived parameters that delineate passive and carrier-mediated effects on permeation and allow the study of drug-drug interactions on permeation based on the quantification of the contribution of different concurrent transport mechanism to epithelial permeation. The final benefit is to gain basic understanding of drug absorption and provide the means for prediction.

This model should encompass passive diffusion, carrier-mediated efflux, non-specific binding to the Transwell® surfaces and phase II metabolism and be used for the quantitative analysis of model compound bi-directional transport across Caco-2 cell monolayers. Model drugs (Amentoflavone, Digoxin, Quinidine, Verapamil) should be considered to exhibit efflux, phase II metabolism and non-specific binding. To gain knowledge on the concentration dependent behaviour of the relevant processes and parameters and to study drug-drug interactions on the level of passive diffusion and carrier-mediated transport, experiments are conducted with single compounds and binary combinations of the same compounds. To assess the effect of non-specific binding to the

surface of Transwell® plates, rate constants for adsorption and desorption are determined in experiments without cells and then used in the experiments with cells. Using this model to analyse experimental data should provide estimates of the model parameters of each process, including the passive permeability, the efflux rate, the metabolic rate constant, and the kinetic parameters for non-specific binding to the surface. Finally the model derived kinetic parameters are compared to the conventionally determined apparent permeability coefficient P_{app}.

4. Theoretical section

4.1. Drug absorption after oral application

The oral route is generally accepted to be the most convenient for administration of drugs. Orally administrable drug formulations are preferred to their non-oral alternatives (e.g. intravenous injections, pulmonary and transdermal delivery) for reasons such as better suitability for self-medication, lower production cost, established formulation strategies and better patient compliance.

In order to be efficient, drugs that are orally administered must possess properties that are compatible with oral administration. Several criteria must be met. For instance, the drug molecule must be sufficiently soluble in the gastrointestinal fluids (stomach and/or intestine), withstand pH values between 1.5 and 7.0 [Rowland] and high enzymatic activity (degradation and metabolism) and last but not least permeate to a sufficient degree in the epithelium of the intestinal mucosa.

The introduction of modern drug discovery technologies, such as combinatorial chemistry and high-throughput screening, has resulted in huge numbers of lead compounds being identified. Unfortunately the compounds generated in high-throughput drug discovery programs are generally more lipophilic, less soluble and of higher molecular weight than conventional drugs [Lipinski]. These characteristics often entail unfavourable biopharmaceutical properties, which can lead to termination of the clinical development of new drugs due to the poor bioavailability after oral administration [Kennedy, Venkatesh].

There is a growing research effort aimed at developing experimental and theoretical methods that allow the prediction of biopharmaceutical properties earlier in development, ideally already based on the chemical structure. The solubility and permeability of a drug molecule are considered to be of the most important properties that determine absorption and the influence of these two properties on the extent of absorption has received considerable attention [Amidon]. While appropriate and advanced formulation strategies can modify the solubility of a drug molecule to some extent, the possibilities improve the membrane permeability are limited. It is therefore crucial to assess the solubility and permeability of new potential drug molecules as early as possible during the development process to enable the identification of molecules or lead structures possessing good solubility and membrane permeability properties and to ensure appropriate formulation strategies. In recent years the biopharmaceutic classification system (BCS) has been established and many commercialised drugs have been classified according to this system [Amidon, Kasim, Takagi]. The BCS points to the

solubility and permeability as important factors for the intestinal absorption of orally administered drugs. This classification divides the compounds into four classes: Class I substances defined as having a high permeability and high solubility; Class II ones have a high permeability and low solubility; Class III drugs have a low permeability and a high solubility and class IV is appropriate for drugs with a low permeability and a low solubility. The limit between having a high and low permeability has been set to a fraction absorbed (Fa) of 90%. For classification as a highly soluble compound, the highest dose to be given should be soluble in 250ml of aqueous media in the range from pH 1 to pH 7.5 [Amidon, Lennernäs].

The aqueous solubility of a drug substance is an important physicochemical parameter that has a significant role in various physical and biological processes and serves a wide range of needs throughout the various phases of discovery and development. Solubility is used to characterise compounds belonging to a chemical series and to determine whether these compounds are soluble enough for structure–activity relationship screens. In further stages, solubility data are used to assess absorption, distribution, metabolism and elimination parameters and to develop formulations for safety screens, pre-clinical and early clinical use [Bhattachar]. Reviewing the fundamentals of solubility from the molecular level and the current methods used solubility measurement and prediction, is beyond the scope of this thesis and there is comprehensive literature available on this topic [Avdeef 2001, Bhattachar, Delaney]. Another essential step in modern drug discovery and development is the evaluation and analysis of the ADME properties in general, and in the framework of the BCS system especially the permeability properties.

4.2. The gastro-intestinal tract and the intestinal epithelium

One prerequisite for an orally administered drug to have a systemic effect is that there is drug uptake from the gastro-intestinal tract. However, the intestine may not only be well suited for the absorption of nutrients but also it also protects the organism from potentially harmful microorganisms and xenobiotics (e.g. therapeutically used drugs).

The first hindrance to drug absorption is the acidic environment in the stomach, which can degrade not only bacteria but also some drug substances. In addition the intestinal membrane along the intestine is covered with a tight epithelium, which contains various enzymes that not only degrade nutrients for uptake and can convert xenobiotics into hydrophilic metabolites to assist in their elimination from the body.

Once in solution a drug molecule encounters a system of sequential barriers during its transport from the intestinal lumen into the blood stream. The epithelial surface in contact

with the content of the intestinal lumen is greatly amplified by the macroscopic valve-like folds (circular folds), the tiny finger-like projections called villi, and the microvilli with the associated glycocalyx (brush-border structure) [Daugherty]. The brush-border of the enterocytes presents a considerable catabolic barrier of enzymatic activities. Furthermore the epithelial surface of the gastro-intestinal tract is coated by mucus that is secreted by the goblet cells and contains mucin glycoproteins, enzymes and electrolytes. The functional unit of the intestinal epithelium is the crypt-villus axis. Within the axis the epithelium is spatially separated into proliferating and differentiating cells, with the functional, absorptive cells (enterocytes) situated on the villus tip [Pageot]. The intestinal epithelium contains three different types of cells: endocrine cells secreting digestive hormonal peptides, the exocrine secreting goblet cells (mucus) and the Paneth cells (antimicrobial peptides). The absorptive cells (enterocytes) are the most abundant of the epithelial cells, accounting for 80 – 90% of the total number.

4.3. Mechanisms of membrane permeation

Among the different properties that determine the transfer and distribution of a drug molecule in the human body one property of particular importance is the ability to cross biological membranes. The permeability across the different membranes a drug encounters during its passage through the body shapes its pharmacokinetic profile, affecting its absorption, distribution and elimination. Permeation across the cell membranes takes place by three main mechanisms that are subsequently discussed: transcellular diffusion, paracellular diffusion and active transport (either transport into the cells or efflux out of the cells). The main properties of a drug influencing its permeation through biological membranes are lipophilicity, hydrogen-bonding capacity, charge and size / molecular weight [Camenisch], some of which can be described by partition coefficients (e.g. $\log P_{octanol/water}$) or molecular surface area descriptors such as the polar surface area (PSA) [Goodwin, Stenberg].

4.4. Passive transcellular permeation

The cell membrane of epithelial cell consists in the same manner as all other mammalian cell membranes of a lipid bilayer with embedded proteins (e.g. ion channels, glycoproteins, transporters). The membrane composition (phospholipids, proteins, cholesterol) varies between different cell types and may therefore influence the membrane properties. The presence of different lipids and different embedded proteins provides unique properties to cell membranes throughout the body [Seydel]. The structure of the cell membrane has traditionally been described by the fluid mosaic model [Singer], and more recently been further developed by the lipid raft hypothesis [Simons].

These lipid rafts are membrane microdomains that are enriched in cholesterol and sphingolipids. The dynamic clustering of sphingolipids and cholesterol forms rafts that move within the fluid bilayer and they have been implicated in processes as diverse as signal transduction, endocytosis and cholesterol trafficking. Although a vast number of publications dealing with lipid rafts exist, there is still scepticism about the real nature of their existence and more work is still needed to formally confirm the lipid raft hypothesis [Shaw].

Epithelial cells are polarized, meaning that they possess a distinct apical membrane facing the intestinal lumen and a basolateral membrane facing the sub-epithelial tissues, with different protein and lipid compositions, and thus different permeability properties. The apical membrane contains, for instance, lower levels of glycosphingolipids than the basolateral membrane of epithelial cells [van Meer]. The lipoid nature of the cell membranes restricts the transport of ions and hydrophilic molecules. Passive transcellular transport can be divided into several subsequent steps. The first step is the partitioning of the solute into the apical membrane, which is followed by diffusion through the cytoplasm or if the solute is very lipophilic, the transport across the cell may also involve lateral diffusion in the lipid bilayer of the cell membrane. Finally, the solute exits through the basolateral membrane. The diffusion of small solutes in the cytoplasm is normally a rapid process, and thus the rate of passive transcellular permeability is mainly determined by the rate of transport across the cell membrane.

4.5. Paracellular transport

For lager and more hydrophilic compounds (charged molecules and peptides) transcellular diffusion if often restricted or depending on the pK_a of the molecules absent at physiological pH values and their molecular size. Transport of these compounds across the epithelial cell layer can occur via water-filled pores between the cells, a process known as paracellular transport. The dimensions of the paracellular space itself lies between 10 and 30 – 50Å [Morishita]. The adjacent epithelial cells are connected to each other by the tight junctions, which establish a seal between adjacent cells restricting solute transport by this route of absorption [Salama, Shin]. The calculated human pore sizes (radii) are, jejunum 6–8 Å, ileum 2.9–3.8 Å and colon less than 2.3 Å [Smith]. For Caco-2 cell monolayers grown in the Transwell system the effective pore radius was calculated to be 12.0 +/- 1.9Å [Ho]. Furthermore the surface area presented by the pores constitutes only a small fraction (0.01% - 0.1%) of the total intestinal membrane surface area [Nellans, Pappenheimer]. It is therefore unlikely that this pathway contributes

significantly to the overall transport of most drugs *in vivo*, although small molecules (MW <200 Da) may be exceptions [Avdeef 2001, Karlsson, J.].

4.6. Drug transporters: carrier-mediated influx and efflux.

The transcellular transport in the apical to the basolateral direction is in the simplest case only driven by passive diffusion caused by concentration gradients across the cell (membrane).

For an increasing number of molecules non-diffusion contributions to the permeation are discovered, which are caused by proteins, embedded in the apical or the basal cell membrane. The physiological function of these proteins is to either extract nutrients, vitamins and other compounds essential for the organism from the luminal contents [Lee V.H., Tsuji] or to prevent uptake of toxic substrates or to facilitate the excretion of such substrates across the mucosa of the intestinal tract [Ambudkar], what would explain the broad and sometimes overlapping substrate specificity of the efflux proteins. Carrier-mediated influx mechanisms enhance the transcellular permeability to a limited number of drugs, like the β-lactam antibiotics, ACE inhibitors and phosphate analogs, all of which are structurally similar to the native substrates of transport proteins [Lee, V.H., Tsuji]. The extent of this enhancement depends on the structural similarity between the drug and the natural substrate of the transporter, as well as on drug concentration and physiological factors. Examples for influx transporter, which may play a role in drug absorption and distribution, are the human di/tri-peptide transporter (hPepT1) located in the apical membrane of the enterocytes [Daniel] and Caco-2 cells [Adibi] members of the human organic anion transporting polypeptide (OATP) family (solute carrier family 21A, SLC21A) and the organic cation transporter family (SLC22A) [Sai].

Contrary to the carrier-mediated influx, the efflux proteins located in the apical cell membrane have the potential to limit the overall permeability by pumping the drug molecules in the basal to apical direction. The relevant efflux transporters for drugs in clinical use belong to the ATP-binding cassette (ABC) family. These transporters extrude their substrates in an ATP-dependent manner from the cells in which they are expressed [Borst, Schinkel]. Efflux transporters that are present in the apical membrane of enterocytes include P-glycoprotein (P-gp, ABCB1), the breast cancer resistance protein (BCRP, ABCG2), and the multidrug resistance associated protein 2 (MRP2, ABCC2) [Borst, Chan, L.M.S., Schinkel]. P-gp was one of the first ABC-transporters that were identified to be involved in the efflux of compounds and in multidrug resistance [Juliano]. P-gp has a very broad substrate specificity and transports a vast number of structurally diverse compounds such as anticancer drugs, HIV protease inhibitors and antibiotics

[Hunter, Schinkel]. P-gp is binds its substrates in the cytosolic leaflet of the lipid membrane and flips them to the extracellular leaflet or exports them to the extracellular environment [Loo, Meier]. MPR2 is also located in the apical membrane of enterocytes and transports anionic drugs and endogenous compounds, including their glutathione-, glucuronide- and sulfate conjugates [Suzuki]. As phase II enzymes are present in the human intestine, MRP2 may be responsible for the secretion of the conjugates formed in the intestine.

4.7. Pre-systemic Metabolism

Both the intestine and the liver constitute appreciable metabolic barriers where an absorbed drug molecule may be metabolised before reaching the systemic circulation. Metabolism is divided into phase I metabolism, that is the modification of the parent drug by oxidation reactions, e.g. by Cytochrome (CYP) P450 enzymes, and phase II metabolism, that is the conjugation of the parent compound or its phase I metabolite with hydrophilic moieties as glucuronic acid, sulfate or glutathione.

The liver is the main metabolising organ and enzymes of the CYP1 – 3 families account for about 70% of the total liver CYP content with the CYP3A isoform constituting about 30% of this total [Shimada]. CYP3A is also the dominant subfamily in the small intestine where it constitutes about 70% of the total CYP protein, which represents 50% of the liver content [de Waziers, Kolars, McKinnon]. Several phase II enzymes are expressed in the intestine at levels that are comparable to those in the liver. The conjugates formed through phase II metabolism are often too hydrophilic to diffuse out of the cell and therefore require transporters to assist their exit out of the cell (e.g. MRP2).

Caco-2 cells lack expression of appreciable quantities of CYP3A4 and other enzymes of the cytochrome family, responsible for oxidative metabolism [Crespi, Cummins, Hochman, Schmiedlin-Ren] but differentiated Caco-2 cells express phase II enzymes such as UDP-glucuronosyltransferases, sulfotransferases and glutathione-S-transferases [Galijatovic, Meunier]. Phase II metabolic activity in Caco-2 cells has been demonstrated in general for a diversity of compounds and especially for several different flavonoids [Chen, J., Galijatovic, Hu, Liu].

4.8. *In vitro* assessment of drug permeability: models

In vivo studies of the intestinal membrane permeability of compounds in humans are costly and, if performed with relatively unknown or hazardous compounds, potentially harmful for the volunteers. Therefore, *in vivo* permeability can only be determined for a small number of well-characterised drugs. In the early stages of the drug development

process, many compounds have to be considered and these compounds are poorly characterised. Such studies can be performed in experimental animals instead of humans, but the cost and throughput still severely restrict the capacity of these experiments.

Therefore, for the rapid assessment of the ADME properties of compounds many *in vitro* and *in situ* methods were developed with different levels of complexity and sophistication [Bohets, Hidalgo 2001]. Cell free, lipid based assays like PAMPA [Avdeef 2003, Kansy] allow higher throughput and easier miniaturization compared to cell models that allow mechanistic studies. To study the drug permeability at different sites in the human body, cell models for intestinal permeation (e.g. Caco-2 and 2/4/A1), for the blood – brain barrier (primary cell culture and immortalized cell lines), for hepatic drug metabolism and transport and for the renal drug transport are accessible [Deli, Ghibellini, Hidalgo 1989, Schlatter, Tavelin]. The different models can be wild – type (Caco-2, MDCK), transfected (h-MDR1-MDCKII), or downregulated cell lines [Hilgendorf].

The use of *in vitro* cell permeation experiments across cell monolayers to study the absorption of substances is widely accepted and popular [Artursson 2001, Balimane 2005 & 2006]. Depending on the compounds used and the experimental setting, the purpose of these studies can be the general assessment of the permeability of a compound [Artursson 2001], the development of structure – permeability relationships [Chen, I.J.], the development of *in vitro – in vivo* correlations [Artursson 1991 B, Usansky, Yee], the identification of transporters (influx and efflux) involved in cellular permeation [Maeda], the study of transporter kinetics and development of comprehensive models of transporter function [Tran 2005], the study of the interplay between transporters and metabolism [Benet], the study of drug – drug interactions [Rautio] and the study of formulation effects [Kapitza, LeCluyse].

One of most frequently used cell lines for the determination of drug permeability across membranes is the human colon adenocarcinoma cell line Caco-2, grown on semi-permeable filter supports [Artursson 1991 B, Hidalgo 1989]. Caco-2 cells spontaneously differentiate into enterocyte-like cells with the paracellular permeability comparable to that of human colon. In spite of its colonic origin, a number of active transport mechanisms normally found in the absorptive enterocytes of the small intestine are present in this cell line [Bailey]. Disadvantages of cell culture models is that the cells must be grown on filters for up to several weeks before they can be used for drug transport experiments. Caco-2, for example, normally requires, without optimising the culturing conditions, culture on filters for three weeks before it can be used for drug transport experiments. Furthermore depending on the exact protocol for the culturing

conditions, the results of permeability measurements for selected compounds may differ for different labs, passages, selected clones and culturing conditions [Anderle, Behrens 2003 & 2004, Briske-Anderson, Hosoya, Yu]. An advantage of cell culture models compared to liposomal systems is that they measure the transport of the drug across a cell membrane, rather than an interaction of the drug with the lipid bilayer. Another advantage is that parallel transport routes, both passive and active, can be studied and much insight into the different steps of absorption has been gained by the use of the Caco-2 cell model [Artursson 1997].

4.9. *In vitro* assessment of drug permeability: data analysis

Properties that influence the ease with which a drug can be absorbed (e.g. from an oral dosage form) include dissolution rate and solubility (determining how fast the drug reaches its maximum concentration C_{max} within the solution), and the permeability coefficient P (determining the rate at which the drug will cross the biological barrier). Together, these factors comprise Fick's first law, describing the flux J_{Wall} of a drug across the respective biological barrier:

$$J_{Wall} = P_{Wall} \bullet C_{\max}$$

(Equation 1)

When examining drug permeability across *in vitro* models it is customary to use the shown approximate solution for the permeability coefficient P_{app}:

$$P_{app} = \frac{V_R * dC_R}{dt * A * C_{D0}}$$

(Equation 2)

where P_{app} is the apparent permeability coefficient, V_R the volume of the receiver chamber, A is the area of the permeability barrier, C_{D0} the initial drug concentration in the donor chamber, and dC_R/dt the change in concentration of compound in receiver compartment over time.

This approach is afflicted with limitations: The equation uses the initial drug amount in the donor, linear drug transport with time that is applicable to early time points only and furthermore assumes negligible back flux and no mass balance problems such as due to stability and binding to cells (cellular retention) and / or the apparatus [Tran 2004, Youdim].

Active apical efflux [e.g. P-glycoprotein] substrates are identified by comparison of apical to basal and basal to apical transport namely by calculation of the efflux ratio (ER), and by performing transport experiments with inhibition of the carrier-mediated component. Involvement of a carrier-mediated efflux mechanism is indicated if the ER is > 2.0. For compounds with an ER close to equality, active efflux is unlikely whereas for compounds with ER of 1.5 to 2.0, follow-up experiments with a potent, specific inhibitor of P-gp, e.g. GF120918, are required to demonstrate that the compound undergoes P-gp-mediated efflux.

This approach has several inherent shortcomings and disadvantages: the ER is time dependent, some substrates with high passive permeability (e.g. Verapamil) may not be detected by this approach, no direct quantification of the passive permeability and the apical efflux is possible, and no direct quantification of the influence of inhibitors and/or concurrently applied compounds can be performed. The common practice to calculate passive permeability for the typical P-gp substrates is to simply subtract passive transport curves from the active transport curves. For semiquantitative work this might be adequate but it neglects the reversibility of transport, which is substantial over the longer time courses. For basal to apical transport, at any given timepoint, active transport results in higher concentrations of a drug in the apical compartment than with passive diffusion alone. Thus, the passive backdiffusion of drug from the apical compartment will be greater with active transport than with just passive diffusion alone. In the opposite transport direction, apical to basal, the subtraction is just as inaccurate because the passive backdiffusion is less with active transport than with just passive diffusion alone [Tran 2004]. Although improvements can be made [Youdim], the usage of the approximate equation still requires the establishment of the linear phase of permeability because the equation is just the initial slope of the transport curve. To identify substrates for active efflux transporters like P-glycoprotein by calculation of the ER the estimated P_{app} values have to within an optimal range. For substrates that have P_{app} values outside of this range, the identification as a substrate is prone to fail by using this approach [Polli]. Recently it was shown that the effects of P-glycoprotein mediated efflux on the absorptive and secretory transport may not be symmetrical, per given donor concentration [Troutman 2003 A].

During the past few years the awareness of the necessity of more detailed and precise analysis of data derived from *in vitro* permeation experiments arose. The approaches of different research groups were for instance focused on modelling and determination of (sub-) cellular pharmacokinetics and distribution [Duvvuri, Zhang] or on the consideration of the influence of the aqueous boundary layer on estimated transporter kinetics from

overexpresion systems [Balakrishan]. Other attempts to estimate a more accurate permeability coefficient [Tran 2004] rely on the usage of potent efflux inhibitors like GF120918. Even if the inhibition is almost complete, for compounds with very poor permeability it might be still almost impossible to estimate permeability coefficients. As the P-gp-mediated efflux activity observed during absorptive and secretory transport can be asymmetric for certain substrates, Troutman and Thakker studied the influence of the transport direction on the apical active efflux and introduced two new parameters, absorptive quotient (AQ) and the secretory quotient (SQ), to express the functional activity of P-gp during absorptive and secretory transport, respectively [Troutman 2003 A & B]. The permeability of a P-gp substrate is determined in absorptive and secretory directions in absence and in presence of the potent efflux inhibitor GF120918, and the contribution of P-gp in attenuating the permeability calculated. The relationship between attenuation of absorptive transport and enhancement of secretory transport of compounds by P-gp is asymmetric, and different for different sets of compounds.

An alternative approach to the use of the apparent permeability coefficient and its improvements is the use of biophysical modelling of the transmembrane events involving passive diffusion and efflux mechanisms. The intent of such modelling is to delineate and quantify the mass transfer mechanisms that take place during permeation. This approach may furthermore provide means for the evaluation of the influence of type and concentration of the chosen compound as well as the influence of a second substance or of excipients on the permeation in terms of passive diffusion and active efflux, depending on the exact mode of modelling. These models can provide information about critical parameters and the behaviour of the system if the parameters are changed. In the study of efflux transporters the modelling and the measurement of the kinetic characteristics of transport can be a powerful approach to enhancing the understanding of their function and mechanism or probe different hypothesis about the exact mode of efflux [Litman 2003, Tran 2005]. Other modelling approaches including both, passive diffusion and active efflux focused on the use of these procedures as tools for improving the prediction ability of *in vitro* models [Rodriguez-Ibáñez].

4.10. Non-specific binding / Adsorption

Molecules adsorb on virtually all surfaces, such as packaging materials for pharmaceutical products [Yahya]. The amount they adsorb is roughly proportional to the amount of the surface [Cussler]. The degree of adsorption depends on the chemical nature of the adsorbent (the material that is adsorbing) and the adsorbate (the substance

being adsorbed), the surface area of the adsorbent, the temperature and the concentration of the adsorbate [Martin].

Adsorption to the container surfaces can lead to an erroneous estimation of the permeability of compounds or other *in vitro* parameters [Karlsson, M.] as well as to poor recovery of the compound and a low mass balance [Ingels, Balimane 2005]. Under *in vitro* conditions the adsorption to solid surfaces and to cells depends on the composition of the experimental buffer or medium, the chemical identity of the compound itself, and the type of the solid surface [Grohganz, Palmgren]. Different attempts to minimize the impact of the adsorption in permeability studies in Transwells have been proposed, including pre-treatment of the device with albumin, postexperimental washing with organic solvents, calculation of the permeability from the disappearance from the donor compartment or the addition of serum albumin or different excipients to the receiver compartment [Chan, O.H., Krishna, Lee, Y.-G.]. All of these proposed options have drawbacks like being labour-intensive or tedious, interference with analytical methods, the possibility to affect the membrane fluidity or transporter function or the susceptibility to chemical and / or metabolic degradation and cellular accumulation.

The types of adsorption are generally recognized as physical or van der Waals' adsorption, and chemical adsorption or chemisorption. Physical adsorption, associated with van der Waals' forces, is reversible, the removal of the adsorbate from the adsorbent being known as desorption. Chemisorption, in which the adsorbate is attached to the adsorbent by primary chemical bonds, is irreversible [Martin]. The adsorption of molecules to surfaces is usually described in isotherms, in which the amount adsorbed on a solid is plotted depending on the solution concentration at constant temperature. Three commonly cited isotherms are the linear, Langmuir, and Freundlich types [Cussler]. The simple linear isotherm of the type "concentration in the adsorbent = constant ● concentration in the solution" is frequently assumed even though it rarely occurs. The Freundlich isotherm is given by type "concentration in the adsorbent = constant1 ● (concentration in the solution)$^{\text{constant2}}$" where both constants are empirically determined. This isotherm suggests that a plot of the concentration in the absorbent versus the concentration in solution should be linear on log-log coordinates. The theoretical base for this isotherm is vague. The Langmuir isotherm is more common than the linear isotherm and has a clear theoretical basis. This isotherm assumes that a limited number of sites on the adsorbent are subject to a mass balance and these sites are assumed to be subject to a chemical equilibrium. Langmuir developed an equation based on the theory that the molecules or atoms are adsorbed on active sites of the solid to form a layer one molecule thick (monolayer). The fraction of centers occupied by

molecules at concentration C is represented by θ, and the fraction of sites not occupied is 1 – θ.

4.11. Choice of model compounds

The naturally occurring biflavonoid Amentoflavone (Figure 1) was chosen as model compound as it may be expected to have poor permeability due to its molecular weight of 538.458g/mol and the number of hydrogen bond donors (6) and acceptors (10). It is transported by P-gp [Gutmann 2002] and preliminary studies of the Amentoflavone transport in Caco-2 cell monolayers in our group indicated phase II metabolism of Amentoflavone during the permeation experiments [unpublished]. Phase II metabolic activity in Caco-2 cells has been demonstrated in general as well as for several different flavonoids, including Apigenin, the monomer of Amentoflavone [Chen, J., Galijatovic, Hu, Liu]. The preliminary studies showed poor mass balances for Amentoflavone that could not be fully explained by the phase II metabolism. Based on these findings and the demonstrated property to strongly bind to plasma membranes [Lenne-Gouverneur] and due to sparingly solubility and strong lipophilicity (5.753 +/- 1.0, both calculated using Advanced Chemistry Development (ACD) Software Solaris V4.67) Amentoflavone was assumed to possess a tendency for cellular accumulation and adsorption/non-specific binding to plastic surfaces.

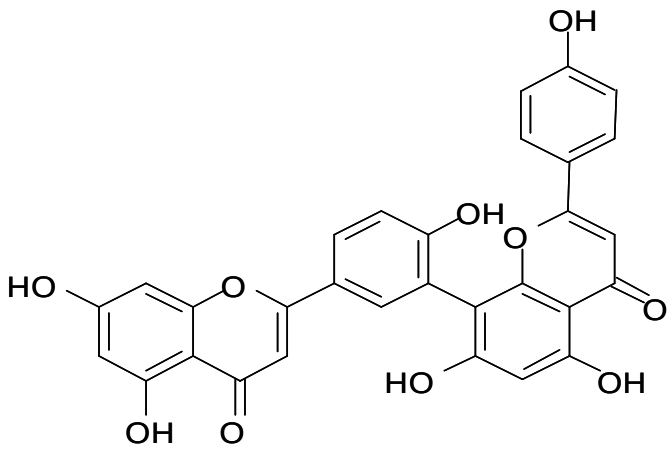

Figure 1: Chemical structure of Amentoflavone ($C_{30}H_{18}O_{10}$).

Verapamil (molecular weight 454.60g/mol, logP 4.7, calculated by PubChem), Quinidine (molecular weight 324.42g/mol, logP 2.6, calculated by PubChem) and Digoxin (molecular weight 780.94g/mol, logP 2.2, calculated by PubChem) are all known to be substrate of P-glycoprotein [Engman, Keogh, Litman 2001, Makhey, Meier, Neuhoff 2003, Troutman 2003 A]. Verapamil and Quinidine are ionisable compounds, with pK_a values of 8.97 +/- 0.50 (ACD Software Solaris V8.14) for Verapamil and 9.28 +/- 0.70 (ACD Software Solaris V8.14) for Quinidine, whereas Digoxin can be considered as

neutral molecule in the relevant pH range for the transport studies. Literature findings indicate high permeability for Verapamil and Quinidine and rather moderate to poor passive permeability for Digoxin [Varma].

5. Analysis of Amentoflavone transport and phase II metabolism in Caco-2 cell monolayers and adsorption to the Transwell surface with a mathematical model for determining dug absorption parameters

5.1. Abstract

Purpose

The present study's aim was the development of a mathematical model for delineating the passive and carrier mediated contributions to the absorption of Amentoflavone in Caco-2 cell monolayers with the integration of phase II metabolism and adsorption to the Transwell surface to the model.

Material and methods

The epithelial membrane transport kinetics and phase II metabolism of Amentoflavone (2 – 10µM) were studied using Caco-2 monolayers cultured in Transwells. Adsorption of Amentoflavone was studied in Transwells without cells. The system of differential equations of the developed mathematical model was fitted to experimental concentration data, and optimal values of the kinetic parameters were deduced using the software EASY-FIT.

Results

Amentoflavone showed polarised transport behaviour, while no concentration-dependent effect was observed. The apical efflux was significantly reduced by the addition of the inhibitors GF120918 and Vinblastine. Along with Amentoflavone sulfate and glucuronide metabolites of Amentoflavone were identified by LC/MS. Apical efflux of the phase II metabolites was significantly favoured compared to basolateral efflux. The addition of Vinblastine resulted in almost complete inhibition of the apical efflux of Amentoflavone and a higher cellular accumulation of Amentoflavone. Furthermore the distribution of the metabolites equalized between the compartments whereas the total amount remained unaffected.

Kinetic parameters of the transport could be calculated with the developed model which included passive and carrier mediated transport, metabolism and non-specific adsorption.Model estimated passive permeability coefficient of Amentoflavone was independent of concentration. Model estimated apical efflux parameters varied for different situations and expressed the mass efflux rate of Amentoflavone elicited by P-glycoprotein in Caco-2 cells. The apical efflux parameter also reflected inhibition of the efflux by Vinblastine. Furthermore an overall phase II metabolic rate constant in the cell

was estimated. By integrating surface adsorption, cellular transport was corrected for this distorting effect.

Conclusions

Transport, phase II metabolism and adsorption of the poorly permeable substance Amentoflavone in Caco-2 cell monolayers could be well described by the proposed model of cellular transport. For each of these processes kinetic parameters could be derived from transport experiments.

5.2. Introduction

In the course of the past 15 years the assessment of permeability across Caco-2 cell monolayers became one of the most popular tools for mechanistic studies of absorption of substances in human small intestine [Ingels, Balimane 2005]. This cell model has been extensively characterised and found to be useful in the field of drug permeability studies [Hidalgo 1989, Artursson 1991A & 2001]. The Caco-2 cells undergo spontaneous enterocytic differentiation in culture and are polarized with well-established tight junctions. Of the most important transport proteins with efflux activity, several (e.g. P-glycoprotein and MRP-2 [Hosoya, Hidaldgo 1996, Hunter, Gutmann 1999, Balimanae 2006]) are functionally expressed in confluent Caco-2 cell monolayers. The cells lack expression of appreciable quantities of CYP3A4 and other enzymes of the cytochrome family, responsible for oxidative metabolism [Crespi, Cummins, Hochman, Schmiedlin-Ren] but differentiated Caco-2 cells express phase II enzymes such as UDP-glucuronosyltransferases, sulfotransferases and glutathione-S-transferases [Meunier, Galijatovic].

The *in vitro* assessment of the permeability of a drug has to take into account different mechanisms influencing the absorption, all of which have to be known and/or controlled in order to estimate quantitative parameters that describe the different contributions to the overall permeation. A compound that permeates across Caco-2 cell monolayers, passively diffuses along a concentration gradient, may be subject to active efflux by different efflux transporters, phase II metabolism and non-specific cellular accumulation. Further confounding or limiting factors may be poor solubility, chemical instability or adsorption to container surfaces. Properties that influence the ease with which a drug can be absorbed (e.g. from an oral dosage form) include dissolution rate and solubility (determining how fast the drug reaches its maximum concentration C_{max} within the solution), and the permeability coefficient P (determining the rate at which the drug will cross the biological barrier). Together, these factors comprise Fick's first law (Equation 3), describing the flux J_{Wall} of a drug across the respective biological barrier:

$$J_{Wall} = P_{Wall} \bullet C_{\max}$$

(Equation 3)

When examining drug permeability across *in vitro* models it is customary to use the shown approximate solution for the permeability coefficient P_{app} (Equation 4):

$$P_{app} = \frac{V_R * dC_R}{dt * A * C_{D0}}$$

(Equation 4)

where P_{app} is the apparent permeability coefficient, V_R the volume of the receiver chamber, A is the area of the permeability barrier, C_{D0} the initial drug concentration in the donor chamber, and dC_R/dt the change in concentration of compound in receiver compartment over time. The equation uses the initial drug amount in the donor, linear drug transport with time that is applicable to early time points only and furthermore assumes negligible back flux and no mass balance problems such as due to stability and binding to cells (cellular retention) and/or the apparatus [Youdim, Tran 2004]. Active apical efflux (e.g. P-glycoprotein) substrates are identified by comparison of apical to basal and basal to apical transport namely by calculation of the efflux ratio (ER), and by performing transport experiments with inhibition of the carrier-mediated component. Involvement of a carrier-mediated efflux mechanism is indicated if the ER is > 2.0. For compounds with an ER close to equality, active efflux is unlikely whereas for compounds with ER of 1.5 to 2.0, follow-up experiments with a potent, specific inhibitor of P-gp, e.g. GF120918, are required to demonstrate that the compound undergoes P-gp-mediated efflux.

This approach has several inherent shortcomings and disadvantages: the ER is time dependent, some substrates with high passive permeability (e.g. Verapamil) may not be detected by this approach, no direct quantification of the passive permeability and the apical efflux is possible, and no direct quantification of the influence of inhibitors and/or concurrently applied compounds can be performed. The common practice to calculate passive permeability for the typical P-gp substrates is to simply subtract passive transport curves from the active transport curves. For semiquantitative work this might be adequate but it neglects the reversibility of transport, which is substantial over the longer time courses. For basal to apical transport, at any given timepoint, active transport results in higher concentrations of a drug in the apical compartment than with passive diffusion alone. Thus, the passive backdiffusion of drug from the apical compartment will be greater with active transport than with just passive diffusion alone. In the opposite transport direction, apical to basal, the subtraction is just as inaccurate because the passive backdiffusion is less with active transport than with just passive diffusion alone [Tran 2004]. Although improvements can be made [Youdim], the usage of the approximate equation still requires the establishment of the linear phase of permeability because the equation is just the initial slope of the transport curve. Other attempts to estimate a more accurate permeability coefficient [Tran 2004] rely on the usage of potent

efflux inhibitors like GF120918. Even if the inhibition is almost complete, for compounds with very poor permeability it might be still almost impossible to estimate permeability coefficients. As the P-gp-mediated efflux activity observed during absorptive and secretory transport can be asymmetric for certain substrates, Troutman and Thakker introduced two new parameters, absorptive quotient (AQ) and the secretory quotient (SQ), to express the functional activity of P-gp during absorptive and secretory transport, respectively [Troutman 2003 A & B]. The permeability of a P-gp substrate is determined in absorptive and secretory directions in absence and in presence of the potent efflux inhibitor GF120918, and the contribution of P-gp in attenuating the permeability calculated. The relationship between attenuation of absorptive transport and enhancement of secretory transport of compounds by P-gp is asymmetric, and different for different sets of compounds.

Molecules adsorb on virtually all surfaces, such as packaging materials for pharmaceutical products [Yahya]. The amount they adsorb is roughly proportional to the amount of the surface [Cussler]. The degree of adsorption depends on the chemical nature of the adsorbent (the material that is adsorbing) and the adsorbate (the substance being adsorbed), the surface area of the adsorbent, the temperature and the concentration of the adsorbate [Martin]. Adsorption to the container surfaces can lead to an erroneous estimation of the permeability of compounds or other *in vitro* parameters [Karlsson, M.] as well as to poor recovery of the compound and a low mass balance [Ingels, Balimane 2005]. Under *in vitro* conditions the adsorption to solid surfaces and to cells depends on the composition of the experimental buffer or medium, the chemical identity of the compound itself, and the type of the solid surface [Grohganz, Palmgren]. Different attempts to minimize the impact of the adsorption in permeability studies in Transwells have been proposed, including pre-treatment of the device with albumin, postexperimental washing with organic solvents, the calculation of the permeability from the disappearance from the donor compartment or the addition of serum albumin or different excipients to the receiver compartment [Chan, O.H., Krishna, Lee, Y.-J.]. All these have drawbacks like being labour-intensive or tedious, interference with analytical methods, the possibility to affect the membrane fluidity or transporter function or the susceptibility to chemical and/or metabolic degradation and cellular accumulation.

By reason of the shortcomings of the traditional way to treat data of transport experiments and to able to directly estimate the transport parameters from concentration-time profiles, we developed a mathematical model to describe the transport of drug between the apical, the basal, and the cellular compartment [Kapitza]. The developed model took into account passive permeation described by the permeability coefficient P

and carrier mediated efflux described by the kinetic parameter vk. In this publication we present extensions to the model with inclusion of phase II metabolism and adsorption to the Transwell surface. A modelling approach helps to identify the system critical parameters and to gain information on the system behaviour when the conditions are modified. To test our model we needed a model compound that is poorly permeable, undergoes active apical efflux and phase II metabolism, is subject to non-specific binding to surfaces (adsorption) and shows to a certain extent cellular accumulation. The naturally occurring biflavonoid Amentoflavone was chosen as model compound as it may be expected to have poor permeability due to its molecular weight of 538.458g/mol and the number of hydrogen bond donors (6) and acceptors (10). It is transported by P-gp [Gutmann 2002] and preliminary studies of the Amentoflavone transport in Caco-2 cell monolayers in our group indicated phase II metabolism of Amentoflavone during the permeation experiments [unpublished]. Phase II metabolic activity in Caco-2 cells has been demonstrated in general as well as for several different flavonoids, including Apigenin, the monomer of Amentoflavone [Chen, J., Galijatovic, Hu, Liu]. The preliminary studies showed poor mass balances for Amentoflavone that could not be fully explained by the phase II metabolism. Based on these findings and the demonstrated property to strongly bind to plasma membranes [Lenne-Gouverneur] and due to sparingly solubility and strong lipophilicity (5.753 +/- 1.0, both calculated using Advanced Chemistry Development (ACD) Software Solaris V4.67) we assumed a tendency for cellular accumulation and adsorption.

5.3. Materials and methods

5.3.1. Materials

The human colon adenocarcinoma cell line Caco-2 was a gift of Prof. H. P. Hauri, Biocenter, University of Basel, and originated from the American Type Culture Collection (ATCC, Rockville, MD, USA). Dulbecco's modified Eagle's medium (DMEM) (with l-glutamine, 4500mg/l D-glucose, without sodium pyruvate), l-glutamine 200mM (100x), MEM non-essential amino acids solution (100x, without l-glutamine), foetal bovine serum FBS, Trypsin-EDTA (10x) liquid, and Dulbecco's Phosphate Buffered Saline (without Ca^{2+} Mg^{2+}) were all purchased from Gibco (Gaithersburg, MD, USA). For cell culture DMEM was supplemented with 10% (v/v) FBS, 2mM l-glutamine, and 1% MEM. Transport media used for the permeation studies and the cytotoxicity experiments were made with Dulbecco's modified Eagle's medium (DMEM) base (without glucose, l-glutamine, phenol red, sodium pyruvate and sodium bicarbonate) (SIGMA-Aldrich, Fluka Chemie GmbH, Buchs, Switzerland). This was dissolved in bi-distilled and autoclaved water and supplemented with glucose (4.5g/l), HEPES (4.76g/l), NaCl (1.987g/l) and l-glutamine (0.876g/l), the pH was adjusted to 7.40 and the final medium was subjected to sterile filtration. Glucose, Hepes, NaCl and l-glutamine were all obtained from SIGMA-Aldrich, (Fluka Chemie GmbH, Buchs, Switzerland). Petri dishes (56.7cm^2), 24-well plates and 96-well plates were from Nunc (Roskilde, Denmark) and the 6-well Transwell plates were from Costar, Corning (NY, USA). Amentoflavone (HPLC grade) was from Extrasynthèse (Genay, France). Vinblastine sulfate and Tween 80 (polyethylensorbitan monooleate) were obtained from SIGMA-Aldrich (Fluka Chemie GmbH, Buchs, Switzerland). GF120918 was obtained from Dr. F. Hyafil, Glaxo Wellcome, (Centre de Recherches France, les Ulis cedex, France). Nile blue A, sodium dodecyl sulfate (SDS) and the thiazolyl blue tetrazolium bromide for the MTT assay were purchased from Fluka (Fluka Chemie GmbH, Buchs, Switzerland). All other reagents were of analytical grade.

5.3.2. Cell culture

Caco-2 cells were grown in petri dishes and maintained at 37°C in an atmosphere of 8% CO_2 and in equilibrium with distilled water using culture medium. They were passaged by treatment with 0.25% trypsin and 2.65mM EDTA with a splitting ratio of 1:12. The medium was changed every alternate day until the petri dishes reached 90% confluence. Cells were used in the 7h experiments at passage number 60 – 65 and in 5h experiments at passage 82 – 92.

5.3.3. MTT-assay

Mitochondrial activity of the cell was evaluated by the 3-(4,5-dimethylthiazol-2-yl)-2,5-diphenyl-2*H*-tetrazolium bromide (MTT) assay. This assay is based on the reduction of MTT by hydrogenase activity in functionally intact mitochondria [Mosmann]. The hydrogenase catalyses the conversion of the yellow MTT reagent to blue formazan crystals. Caco-2 cells were seeded on 6-well Transwell plates at a density of 114,000cells/cm^2 and used for experiments 20 – 24 days post-seeding. Medium was changed every other day. The effect of concentration of Amentoflavone, Vinblastine and GF120918 was investigated using 3 wells per group. The treatment of the cells with respect to the preparation steps before incubation and the incubation time was the same as in the transport experiments with the compound and concentration in question. After removing the culture medium, cells of the 6-well Transwell plates were rinsed on the apical side with 3.5ml and on the basal side with 4ml D-PBS (with Ca^{2+} und Mg^{2+}) and 1600µl of the transport medium was added to the apical compartment and 2800µl to the basal compartment of each well. The plates were then incubated for 60min in the incubator (Sorvall Heraeus, Heracell, Kendro, Switzerland). Then the compounds were added to the transport medium and the cells incubated for either 5h or 7h in the incubator hood (TH 15, Edmund Bühler GmbH, Tübingen & Hechingen, Germany) at 37℃ in a water vapour saturated atmosphere and shaken at 75rpm on a compact shaker (KS 15, Edmund Bühler GmbH, Tübingen & Hechingen, Germany). After removing the incubation solutions, the cells of the 6-well Transwell plates were rinsed on the apical side with 3.5ml and on the basal side with 4ml D-PBS (with Ca^{2+} und Mg^{2+}). The inserts were then transferred to petri dishes and 1500µl culture medium and 150µl MTT solution (5mg/ml in D-PBS (without Ca^{2+}, Mg^{2+})) was added to the apical compartment of each well resulting in a final MTT concentration of 0.45mg/ml. The cells were then incubated for another 4h in the incubator. Subsequently the cells of the 6-well Transwell plates were lysed and developed formazan crystals were dissolved by adding 1500µl lysis buffer containing 10% SDS in 0.01 M HCl [Tada] and incubation for 15 h in the incubator. The amount of formazan was quantified in quadruplicate by transferring 200µl to a 96-well plate and measuring the absorbance at 580nm (reference wavelength 650nm) using an ELISA plate reader (VERSAmax, Molecular Devices, Sunnyvale, CA, USA). 10µl of ethanol absolutum were added to avoid foam. Mitochondrial activity was expressed relative to a control group treated with transport media.

5.3.4. Experimental determination of the contact height and mathematical description of the contact area of the transport medium with Transwell surfaces

A mathematical description of the course of the contact area of the transport medium with the Transwell surface during the transport experiments was determined form experimentally measured contact heights. This description is later on used in the calculations of Amentoflavone adsorption to the surface and the calculations the amount bound to the surface depending on the concentration in the solution.

Firstly the contact height of the donor and acceptor solutions was determined in the Transwell apparatus without cells by colouring the Transwell surface with a solution of Nile Blue A 0.002g/ml (0.2% (m/v)). The Transwell plates were kept for 60min at 37℃ in a water vapour saturated atmosphere in the incubation hood and agitated on an orbital compact shaker at 75min^{-1}. The Volumes used in the apical and basal compartment respectively were corresponding to the volumes after a certain number of sample drawings of 117µl. The volumes for the specified time periods were the following: 0 – 0.5h: apical compartment 1600µl and basal compartment 2800µl; 0.5h – 2.5h: apical compartment 1483µl and basal compartment 2683µl; 2.5 – 5h: apical compartment 1366µl and basal compartment 2566µl; 5 – 7h: apical compartment 1249µl and basal compartment 2449µl. The polycarbonate membrane of the Transwell plates was either free or sealed with adhesive tape on the basal side of the membrane, to mimic the situation with or without cells. The contact height was determined at the following three points in the Transwell system: the inner surface of the insert (apical compartment), the outer surface of the insert (basal compartment) and the surface of the cavity / well (basal compartment).

The experimentally determined contact height was plotted against the apical and basal volumes and a linear relationship was calculated for each compartment by linear regression analysis with Microsoft Excel®. For calculation of the contact areas all contact heights were recalculated for the given volumes and used in the calculations of the contact areas. The contact areas with the solution were calculated as subsequently described. The contact area in the apical compartment is equal to the contact height of the solution with the Transwell insert times the circumference of the polycarbonate filter. The circumference of the filter was calculated from a filter area of 470mm^2 as specified by the Transwell producer. The circumference used in the calculations was 76.852mm. The calculation of the total contact area in the basal compartment was done by addition of the contact area with the basal side of the Transwell insert and the contact area with the rest of the basal compartment. The contact area with the basal side of the insert is

the outer circumference of the insert times the contact height. The outer circumference is calculated from the experimentally measured outer diameter of the insert. The outer circumference used in the calculations was 86.08mm. The contact area with the rest of the basal compartment was calculated from the addition of the basal base area with the contact area from the contact height of solution. The base area was calculated from the experimentally measured area radius of 17.45mm, resulting in a base area of 956.623mm^2 and a base area circumference of 109.642mm that was multiplied with the contact height.

The reduction of the contact area was modelled as a continuous reduction over time and not as it is in reality as a stepwise reduction at discrete times. Timepoints for certain areas were exactly one hour after the nominal time for sample drawing in the „free case" (without adhesive tape), and exactly between the time for two sample drawings for the „sealed case" (with adhesive tape). The first point reflecting the area for the initial volumes was set after 15min. The reduction of the contact area in the apical and the basal compartment due to sampling as a function of time, was accounted for by polynomial relations (Equation 5), the parameters of which were determined empirically using regression analysis with EASY-FIT® using the model type "explicit", the numerical method "DFNLP", a scaling of 1 and an termination tolerance of 0. The point of origin and the endpoint were free.

$$Area(S)_{compartment} = Area(S)_{comaprtment,0} + (a \bullet t) + (b \bullet t^2) + (c \bullet t^3)$$

(Equation 5)

5.3.5. Permeation of Amentoflavone across Transwell polycarbonate membrane without Caco-2 cell monolayers at 4 and 37℃

To study the impact of adsorption on the transport behaviour of Amentoflavone, permeation experiments in Transwell plates without cells were performed both at 37℃ and at 4℃. Before the experiments the Transwell pl ates without cells were incubated for 19 – 22 days with culture medium in the incubator. The medium was not changed. The Transwell plates were washed on the apical side with 3.5ml and on the basal side with 4ml D-PBS (with Ca^{2+} und Mg^{2+}) 37℃ and 1600 µl of the transport medium were added to the apical compartment and 2800µl were added to the basal compartment. The drug was then added in both the apical and the basal compartment. The transport direction was therefore apical and basal (a&b). Different concentrations of Amentoflavone (2, 5, 7.5 & 10µM) were used in these permeation studies. Three wells were used for each concentration. The permeation experiments were performed over 7h and sampling and time points were the same as in experiments with cells. After the permeation experiment

the Transwell plates were once washed on the apical side with 3.5ml and on the basal side with 4ml D-PBS (without Ca^{2+} und Mg^{2+}) 4°C and then subject to methanol extraction.

5.3.6. Extraction of the Transwell plates with methanol

The Transwell plates were extracted with methanol after the transport experiment and the removal of the cell monolayer to estimate the amount of substance bound to the surface and the filter material. In cell free experiments with Amentoflavone in Transwell plates the extraction was also performed. 1600µl Methanol 37°C were added to the apical side and 2800µl to the basal side. The plate was sealed with parafilm to avoid undesired evaporation. The Transwell plates were extracted for 45min at 37°C in a water vapour saturated atmosphere in the incubation hood and agitated on an orbital compact shaker at $75min^{-1}$. Subsequently 500µl were taken per compartment and in each case combined with 500µl water 37°C and mixed in a microtube. 234µl of this water-methanol extract mixture were combined with 26µl of a solution of Tween 80 0.1% (v/v), mixed and then analysed by HPLC.

5.3.7. TEER

The transepithelial electrical resistance (TEER) of cultured cells on Transwell inserts was monitored before and after each permeation experiment with an EVOM epithelial voltohmmeter (World Precision Instruments WPI, Berlin, Germany). Before the experiment, Caco-2 monolayers were washed on the apical side with 3.5ml and on the basal side with 4ml D-PBS (containing Ca^{2+} und Mg^{2+}) and 1600µl of the transport medium were added to the apical compartment and 2800µl to the basal compartment. The 6-well Transwell plates were then incubated for at least 60min in the incubator (Sorvall Heraeus, Heracell, Kendro, Switzerland) before the pre-experiment TEER measurement. Before the post-experiment TEER measurement the withdrawn sampling volume was replaced with transport medium. The TEER measurements were performed at 37°C in the Endohm-24 Chamber (World Precision I nstruments WPI, Berlin, Germany) containing 4.6ml transport medium. Physiologically and morphologically well-developed confluent Caco-2 monolayers (at least 18 days old) with TEER values above $250\Omega cm^2$ were used in the experiments.

5.3.8. Permeation of Amentoflavone across Caco-2 cell monolayers at 4 and 37°C in presence or absence of inhibitors of active apical efflux

Cells were seeded at a density of 114,000 cells/cm^2 onto 6-well Transwell plates with an insert area of $4.7cm^2$ and a pore size of the polycarbonate membrane of 0.4µm. Culture

medium was changed every other day and cell monolayers were used between 18 and 22 days post seeding for the 7h experiments and 20 – 24 days postseeding for the 5h experiments.

The drug was added from a stock solution after the TEER measurement either in the apical or in the basal compartment with respect to the cell monolayer. The transport directions were therefore apical to basal (a_b) and basal to apical (b_a). Bidirectional transport of different concentrations of Amentoflavone alone (37℃: 2 (only b_a), 5, 7.5 & 10µM; 4℃: 5 & 10 µM; with 5µM also an experiment with addition of Amentoflavone in the apical and basal compartment at same time (a&b) was performed) was investigated in these permeation studies. In some experiments, the efflux inhibitor Vinblastine was added at a concentration of 70µM to the solution in both compartments to investigate the effect on the overall transport and metabolism of Amentoflavone in Caco-2 cell monolayers. After a pre-incubation period of 30min at 37℃ and 75rpm with Vinblastine, Amentoflavone was added at a concentration of 5µM to either the apical or basal compartment and the permeation was studied for 7h at 37℃. GF120918 (0.1 and 1 µM) and Vinblastine (3.9, 25 and 70µM) were added in both compartments at the same time as Amentoflavone in the basal compartment to study their impact on the b_a transport of Amentoflavone over 5h. Three wells were used in each group at least (concentration, transport direction, inhibitors and temperature). The receiver compartment contained transport medium with the same ethanol concentration as the drug solution (0.5% (v/v)). Permeation of drug across the cell monolayer was monitored by sampling the solutions in both compartments, at predefined time points for the duration of 7h in the case of all experiments with Amentoflavone alone or in experiments with Vinblastine 70µM and the duration of 5h for Amentoflavone 5µM in basal to apical direction alone or incubated together with either GF120918 0.1 or 1µM or together with Vinblastine 3.9, 25 or 70µM.

Samples were drawn after 30, 150, 300 and 420min during the 7h experiments and after 30, 150 and 300min during the 5h experiments. Sampling volume was 117µl for the 7h experiments and 200µl for the 5h experiments. In the first case 13µl of a solution of Tween 80 0.1% (v/v) were added to the sample. The samples were mixed with a reagent mixer. The withdrawn volume was not replaced. The samples were collected in polypropylene vials (Milian AG, Geneva, Switzerland and Agilent Technologies, USA / Basel, Switzerland) except for the samples of the 5h experiments that where collected in glass vials (Infochroma AG, Zug, Switzerland and Schmidlin Labor & Service AG, Sarbach, Switzerland). The starting volume of the apical solution was 1600µl and the one of the basal solution 2800µl. During the permeation experiment the Transwell plates were

kept at 4 or 37°C in a water vapour saturated atmosphere in the incubation hood and agitated on an orbital compact shaker at 75min^{-1}. After the permeation experiments performed at 37°C the TEER values of the cell monolayers were measured again. No TEER measurement was performed after the transport experiments performed at 4°C. After the 7h experiments the cell monolayers were furthermore subject to cell lysis and the Transwell plates were subject to methanol extraction.

5.3.9. Detection of Amentoflavone phase II metabolism in Caco-2 cell monolayers using HPLC-MS

Caco-2 cells of passage 60 were grown for 19 days on a petri dish. After removing the culture medium, cells were rinsed once with 15ml D-PBS (without Ca^{2+} und Mg^{2+}) and 25ml of the transport medium with 10µM Amentoflavone (containing 1% ethanol (v/v)) were added. The petri dish was kept at 37°C in a water vapour saturated atmosphere in the incubation hood and agitated for 7h on an orbital compact shaker at 50min^{-1}. As a control transport medium 10µM Amentoflavone (containing 1% ethanol (v/v)) was incubated in centrifuge tubes 50ml (Falcon Blue Max, in house) and proceeded the same way. The monolayer was checked with the inverted phase contrast microscope (Labovert 090-122.012, Fa. Ernst Leitz Wetzlar GmbH (Leica Mikroskopie Systeme AG, Glattbrugg, Switzerland)) for morphological alterations. Samples were drawn after 30, 150, 300 and 420min. The sampling volume was 117µl. 13µl of a solution of Tween 80 0.1% (v/v) were added to the sample and mixed with a reagent mixer. The withdrawn volume was not replaced. The samples were collected in polypropylene vials (Milian AG, Geneva, Switzerland and Agilent Technologies, USA / Basel, Switzerland). Concentration of Amentoflavone and the formation of new peaks were analysed by HPLC-MS. The spectral properties of the phase II metabolites were assumed to be the same as the ones of Amentoflavone itself.

5.3.10. Cell lysis

Subsequently to the TEER measurement after the 7h transport experiments the Caco-2 monolayers were washed on the apical side with 3.5ml and on the basal side with 4ml D-PBS (without Ca^{2+} und Mg^{2+}) 4°C. The inserts were transferred to petri dishes and 0.3ml trypsin 37°C were added to each insert. The petri dishes were incubated for 15min in the incubator, 1ml culture medium was added and the cells were scraped of with a cell scraper and collected into centrifuge tubes 15ml (Falcon Blue Max, in house). The suspension was spun 5min at 1000rpm (SIGMA 302-K, SIGMA Laborzentrifugen GmbH, Osterode am Harz, Germany) and the supernatant was discarded. The pellet was resuspended in 750µl water 37°C and transferred to a microtube.

At this stage positive controls of Amentoflavone were added to blank cell pellets to correct the recovery in the samples from transport experiments. The suspension was vortexed and frozen in the refrigerator at -80°C for at least 15min. The samples were thawed in the thermomixer (model 5436, Eppendorf / Dr. Vaudaux AG, Schönenbuch, Switzerland) at 37°C and supplemented with 750 µl MeOH 37°C, vortexed for 10s and put into an ice-water mixture for 20min. The microtubes were shaken in the thermomixer for 10min at 37°C and 1400min $^{-1}$, followed by a centrifugation in the Eppendorf centrifuge (5415C, Eppendorf / Dr. Vaudaux AG, Schönenbuch, Switzerland) at 14000rpm. The water-methanol supernatant was transferred to a microtube and stored in the refrigerator at 4°C. 750 µl Methanol 37°C was added to the pellet. The mixture was subject to 6 pulses with the ultrasonic disintegrator (Branson Sonifier 250, Model 101-063-197, output control: 2 / duty cycle: 30%, SKAN AG, Basel, Switzerland) followed by 5min in the thermomixer at 37°C and 1400min $^{-1}$ and a centrifugation in the Eppendorf centrifuge at 14000rpm. The supernatant was transferred to a microtube and subject to evaporation by nitrogen. The pellet was treated again as described. As the methanol was evaporated the water-methanol extract was added to the residue. The microtubes were shaken for 3min in the thermomixer at 37°C and 1400min $^{-1}$ and centrifuged in the Eppendorf centrifuge at 14000rpm for 25min. 234µl of this water-methanol extract mixture were combined with 26µl of a solution of Tween 80 0.1% (v/v), mixed and then analysed by HPLC-MS.

5.3.11. HPLC

Drug concentration in the samples of the 7h experiments was determined by HPLC-UV-MS (Agilent series 1100, Agilent Technologies, USA) with an isocratic pump G1310A, an autosampler G1313A, a variable wavelength detector G1314A, and a mass spectrometer detector G1946C. The MS detector employed atmospheric pressure electrospray ionisation and was operated in the SIM mode at negative polarity with capillary voltage 4000V, variable fragmentor (m/z 537 120V, m/z 610 100V and m/z 720 100V), drying gas flow 10l/min, drying gas temperature 350°C and nebulizer pressure 20psig. A C-8 reversed phase column (CC 125/2 Nucleosil 100 – 5 C8ec, 5µm, Macherey-Nagel, Oensingen, Switzerland) and the following mobile phase was used: H_2O (bi-distilled and filtered through 0.45µm)/MeOH/THF/acetic acid 96%(v/v) = 51.5/23 /12/13.5. 1.993g/l ammonium acetate was dissolved in the mobile phase. The pH-value at 25°C was 3.0 – 3.3. The flow rate was 0.20ml/min and the injection volume 100µl. Amentoflavone was detected at 341nm in UV and at m/z 537 in MS, Amentoflavone glucuronidate and sulfate were detected at 341nm in UV and at m/z 713 and 617, respectively in MS. All ions correspond to the de-protonated form. Quantification was performed using the AUC

measured in the UV against a set of external standard solutions within the linear response concentration range. MS was only for identification of the peaks.

Drug concentration in the samples of the 5h experiments was determined by HPLC-UV (Agilent series 1050, Agilent Technologies, USA) with an isocratic pump 79852AX, an autosampler 79855A and a variable wavelength detector 79853A. A C-18 reversed phase column (Spherisorb ODS2, 5µm, RP18, 4mm x 250mm, HP) and the following mobile phase was used: H_2O (bi-distilled and filtered through 0.45µm)/MeOH/THF/glacial acetic acid = 38/45 /15/2. The flow rate was 0.8ml/min and the injection volume 50µl. Amentoflavone was detected at 341nm in UV. Quantification was performed against a set of external standard solutions within the linear response concentration range.

5.3.12. Calculation of normalised fluxes <J>

Normalised fluxes <J> into the receiver compartment were calculated for Amentoflavone in the apical to basal as well as in the basal to apical transport direction according to (Equation 6):

$$< J >= \frac{\Delta A}{\Delta t * S * C_{D0}}$$

(Equation 6)

where ΔA is the total amount of Amentoflavone transported [nmol] (in solution and withdrawn) to the receiver compartment after 7h, Δt is the change in time [s], S is the area of the monolayer [cm^2], and C_{D0} is the initial concentration in the donor compartment at time 0. The calculation of the normalised flux <J> was preferred to the calculation of P_{app} as especially in the apical to basal transport direction only very small amounts (close to the limit of detection) permeated and no reliable slope (P_{app}) could be determined.

5.4. Theoretical modelling

5.4.1. Modelling of adsorption to Transwell surfaces in Transwells without cells

The types of adsorption are generally recognized as physical or van der Waals' adsorption, and chemical adsorption or chemisorption. Physical adsorption, associated with van der Waals' forces, is reversible, the removal of the adsorbate from the adsorbent being known as desorption [Martin]. The adsorption of molecules to surfaces is usually described in isotherms, in which the amount adsorbed on a solid is plotted depending on the solution concentration at constant temperature. Three commonly cited isotherms are the linear, Langmuir, and Freundlich types [Cussler]. The Langmuir isotherm assumes that a limited number of sites on the adsorbent are subject to a mass balance and these sites are assumed to be subject to a chemical equilibrium. Langmuir developed an equation based on the theory that the molecules or atoms are adsorbed on active sites of the solid to form a layer one molecule thick (monolayer). To describe the adsorption of Amentoflavone from the transport medium used in transport experiments to the Transwell surface, a model was developed based the assumption of a reversible adsorption and on Langmuir isotherms in an equilibrium situation. Assuming that the substance of interest binds only to the surface (forming a monolayer) and does not penetrate into the solid, the adsorption of a substance to a solid surface can be described the following way

$$[C]+[W]\xrightarrow{k_{on}}[C_W]$$

(Equation 7)

and

$$[C]+[W]\xleftarrow[k_{off}]{}[C_W]$$

(Equation 8)

where C is the molar concentration in the solution [mol/l], W is the molar number of free sites per area [nmol/cm^2], C_W is the molar number of occupied sites per area [nmol/cm^2], k_{on} is the rate constant for the adsorption to the surface and k_{off} is the rate constant for the desorption of the surface. Furthermore the adsorption was modelled assuming a saturable process

$$[W]+[C_W]=W_{tot}$$

(Equation 9)

where W_{tot} is the total number of binding sites on the surface [nmol/cm^2]. It is important to be aware, that k_{on}, k_{on} and W_{tot} are assumed to be concentration-independent. For

modelling purposes the equilibrium of the adsorption was defined in a time dependent manner as described in the following equations (Equation 10) - (Equation 12):

$$\frac{d[C]}{dt} = -k_{on} \bullet [C] \bullet [W]$$

(Equation 10)

$$\frac{d[C_W]}{dt} = -k_{off} \bullet [C_W]$$

(Equation 11)

$$\frac{d[C]}{dt} \bullet V = \frac{d[C_W]}{dt} \bullet S$$

(Equation 12)

where the volume V [ml] and the contact area S [cm^2] are time dependent. In this time dependent definition of the equilibrium, the reverse reaction (k_{off}) was defined by the decrease of C_W and not as usually done in textbooks by the increase of C. The units of the rate constants according to this definition are for k_{on} [cm^2/(nmol•min)] and k_{off} [1/min]. The volume and therefore the contact area with the Transwell surface change over time as a result of the sampling. The reduction of volume and the contact area are modelled as described in chapter 5.4.5.In order to determine the rate constants governing the adsorption to the Transwell surface at 4 and 37℃ t he experiments in Transwell plates without cells were conducted. These transport data were analysed by the subsequently developed system of differential equations. The aim was to describe the change of molar amount depending on the time. All modelling was done under the assumption of mass preservation. The general description of the change of concentration in the apical compartment is

$$\frac{dC_A}{dt} = \frac{dM_A}{dt} \bullet \frac{1}{dV_A}$$

(Equation 13)

and general description for the change of concentration of substance bound to the surface is

$$\frac{dC_{WA}}{dt} = \frac{dM_{WA}}{dt} \bullet \frac{1}{dS_A}$$

(Equation 14)

The change in the molar amount in solution in the apical compartment was modelled as subsequently described. The change of the molar amount in solution in the apical

compartment due to adsorption from the solution to the Transwell surface over time can be defined by

$$-k_{on} \bullet C_A \bullet W_A \bullet V_A = \frac{dM_A}{dt}$$

(Equation 15)

The subscript "A" denotes the apical compartment, V the volume of solution [ml], P the permeability coefficient over the polycarbonate filter [cm/min] and S_M the area of the filter support [cm^2]. The amount desorbing from the Transwell surface into the solution is expressed by

$$k_{off} \bullet C_{WA} \bullet S_A = \frac{dM_A}{dt}$$

(Equation 16)

in terms of the change in the molar amount in solution over time. The molar amount that gets lost from solution due to sampling is expressed by

$$+\frac{dV_A}{dt} \bullet C_A$$

(Equation 17)

the term being with a plus sign as the change in volume itself is negative and will set the whole expression to negative. The change of the molar amount in solution that is caused by diffusion through the Transwell membrane is expressed by

$$+P \bullet (C_A - C_B) \bullet S_M$$

(Equation 18)

and is generally set to plus as it is not known in which compartment the concentration is bigger. The whole term will be positive is there is diffusion from the apical to the basal compartment and negative if there is diffusion from the basal to apical compartment. As a result of the adsorption to the surface there may emerge concentration differences between the two compartments, resulting in diffusion across the Transwell membrane. On the other hand, if the membrane is not sealed, sampling may cause convection, resulting in a substance transport by the fluid flow. As there is no knowledge on the direction of the convection, it is neglected in the modelling. By neglecting the convection the estimated values for the passive permeability coefficient through the Transwell membrane will not reflect the true permeability across the polycarbonate membrane. In any case the fluid flow caused by the convection will be smaller than the volumes of the

sampling. Taken these different simultaneous mechanisms together, the change of the molar amount in solution in the apical compartment, can be described by

$$\frac{dM_A}{dt} = -k_{on} \bullet C_A \bullet W_A \bullet V_A + k_{off} \bullet C_{WA} \bullet S_A + \frac{dV_A}{dt} \bullet C_A + P \bullet (C_A - C_B) \bullet S_M$$

(Equation 19)

The change of the molar amount adsorbed to the surface in the apical compartment, can be described by

$$\frac{dM_{WA}}{dt} = k_{on} \bullet C_A \bullet W_A \bullet V_A - k_{off} \bullet C_{WA} \bullet S_A + \frac{dS_A}{dt} \bullet C_{WA}$$

(Equation 20)

with adsorption to and desorption of the surface and

$$+ \frac{dS_A}{dt} \bullet C_{WA}$$

(Equation 21)

being the molar amount that gets lost from the surface by drying up due to sampling. The term is with a plus sign as the change in contact area itself is negative and will set the whole expression to negative. Equal equations can be defined for the basal compartment and the basal surface. k_{on} and k_{off} for the adsorption in the basal compartment are the same as in the apical compartment. To get an equation that describes the change of the molar concentration of drug in the apical solution, (Equation 13) was differentiated and the chain rule applied

$$\frac{dM_A}{dt} = \frac{dC_A \bullet V_A}{dt} = \frac{dV_A}{dt} \bullet C_A + \frac{dC_A}{dt} \bullet V_A$$

(Equation 22)

The two equations (Equation 22)and (Equation 19) are set equal

$$\frac{dV_A}{dt} \bullet C_A + \frac{dC_A}{dt} \bullet V_A = -k_{on} \bullet C_A \bullet W_A \bullet V_A + k_{off} \bullet C_{WA} \bullet S_A + \frac{dV_A}{dt} \bullet C_A + P \bullet (C_A - C_B) \bullet S_M$$

(Equation 23)

and converted

$$\frac{dC_A}{dt} \bullet V_A = -k_{on} \bullet C_A \bullet W_A \bullet V_A + k_{off} \bullet C_{WA} \bullet S_A + P \bullet (C_A - C_B) \bullet S_M$$

(Equation 24)

$$\frac{dC_A}{dt} = -k_{on} \bullet C_A \bullet W_A + k_{off} \bullet C_{WA} \bullet \frac{S_A}{V_A} + P \bullet (C_A - C_B) \bullet \frac{S_M}{V_A}$$

(Equation 25)

and as

$$W_{tot} = [W_A] + [C_{WA}]$$

(Equation 26)

is inserted, we get

$$\frac{dC_A}{dt} = -k_{on} \bullet C_A \bullet (W_{tot} - C_{WA}) + k_{off} \bullet C_{WA} \bullet \frac{S_A}{V_A} + P \bullet (C_A - C_B) \bullet \frac{S_M}{V_A}$$

(Equation 27)

The equation includes the substance in solution and the substance bound to the surface, resulting in the total amount of substance (mass balance). The number of free binding sites on the surface was eliminated from the equation, as the information we get with this number is not important for the transport characterisation. (Equation 14), describing the change of the molar concentration of drug bound to the apical surface was also differentiated and the chain rule applied

$$\frac{dM_{WA}}{dt} = \frac{dC_{WA} \bullet S_A}{dt} = \frac{dS_A}{dt} \bullet C_{WA} + \frac{dC_{WA}}{dt} \bullet S_A$$

(Equation 28)

The two equations (Equation 28) and (Equation 20) are set equal

$$\frac{dS_A}{dt} \bullet C_{WA} + \frac{dC_{WA}}{dt} \bullet S_A = k_{on} \bullet C_A \bullet W_A \bullet V_A - k_{off} \bullet C_{WA} \bullet S_A + \frac{dS_A}{dt} \bullet C_{WA}$$

(Equation 29)

and converted

$$\frac{dC_{WA}}{dt} \bullet S_A = k_{on} \bullet C_A \bullet W_A \bullet V_A - k_{off} \bullet C_{WA} \bullet S_A$$

(Equation 30)

$$\frac{dC_{WA}}{dt} = k_{on} \bullet C_A \bullet W_A \bullet \frac{V_A}{S_A} - k_{off} \bullet C_{WA}$$

(Equation 31)

and as

$$W_{tot} = [W_A] + [C_{WA}]$$

(Equation 32)

is inserted, we get

$$\frac{dC_{WA}}{dt} = k_{on} \bullet C_A \bullet (W_{tot} - C_{WA}) \bullet \frac{V_A}{S_A} - k_{off} \bullet C_{WA}$$

(Equation 33)

The same modelling with subsequent differentiation and conversion were performed for the equations for concentration in the basal solution depending on time and the concentration of the adsorbed substance to the basal surface depending on time, resulting in the following system of differential equations for the description of the overall transport and adsorption in Transwell plates without cells under the assumption of mass preservation.

Concentration in the solution (Transwell without cells):

$$\frac{dC_A}{dt} = -k_{on} \bullet C_A \bullet (W_{tot} - C_{WA}) + k_{off} \bullet C_{WA} \bullet \frac{S_A}{V_A} + P \bullet (C_A - C_B) \bullet \frac{S_M}{V_A}$$

(Equation 34): apical compartment solution

$$\frac{dC_B}{dt} = -k_{on} \bullet C_B \bullet (W_{tot} - C_{WB}) + k_{off} \bullet C_{WB} \bullet \frac{S_B}{V_B} - P \bullet (C_A - C_B) \bullet \frac{S_m}{V_B}$$

(Equation 35): basal compartment solution

Adsorption to the Transwell surface (Transwell without cells):

$$\frac{dC_{WA}}{dt} = k_{on} \bullet C_A \bullet (W_{tot} - C_{WA}) \bullet \frac{V_A}{S_A} - k_{off} \bullet C_{WA}$$

(Equation 36): apical compartment surface

$$\frac{dC_{WB}}{dt} = k_{on} \bullet C_B \bullet (W_{tot} - C_{WB}) \bullet \frac{V_B}{S_B} - k_{off} \bullet C_{WB}$$

(Equation 37): basal compartment surface

The time dependent variables of this system of differential equations are C_A and C_B that are measured during the experiment and C_{WA} and C_{WB}. The constants in the equations are k_{on}, k_{off}, W_{tot} and P. These equations were used in Easy-Fit® in the fittings of the permeation data of Amentoflavone in Transwell plates without cells. Permeation data were analysed using this theoretical model for transport and adsorption in Transwell plates without cells.

5.4.2. Mathematical model for determining drug absorption parameters in Caco-2 cell monolayers

In an earlier publication our group already presented a mathematical model to describe the transport of drug between the apical, the basal, and the cellular compartment [Kapitza]. This model enables a direct estimation of the relevant transport parameters from concentration-time profiles. The developed model took into account passive permeation described by the permeability coefficient P and carrier mediated efflux described by the kinetic parameters v_{max} and K. The transport processes considered for modelling drug permeation in the Caco-2 cell monolayer and the relevant processes in the basic model are displayed in (Figure 2). Extensions to the model with inclusion of phase II metabolism and adsorption and the detailed derivation of the model equations are treated in this chapter.

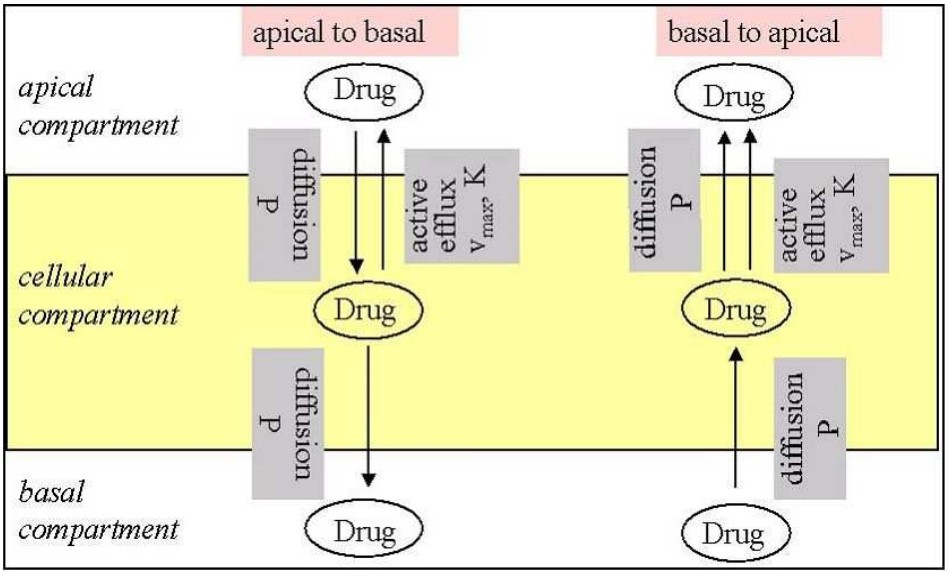

Figure 2: Transport processes considered for modelling drug permeation in the Caco-2 monolayer and relevant processes

This model was based on the following assumptions:

1) Three different compartments are considered in which drug concentration varies with time, the apical, the cellular and the basal compartment.

2) Drug may move between the apical and the cellular and the cellular and the basal compartment in both directions by passive diffusion. Passive diffusion through the apical and the basal cell membrane is symmetrical and is characterized in both cases by the permeability coefficient, P. No effect of electrical membrane potential on the transport is considered.

3) Drug is subject to carrier mediated active efflux from the cellular to the apical compartment. This follows saturable kinetics that may be characterized by two

macroscopic kinetic parameters, v_{max}, the maximum transport rate and K, the mass in the cellular compartment for which one-half of the maximum rate is attained, often referred to as affinity or dissociation constant. One global set of parameters is used to describe carrier-mediated efflux.

4) No two different orientations or conformations of the carrier at the two faces of the membrane are explicitly involved. The drug concentration in the apical compartment does not influence efflux transport and the entire mass of drug present in the cellular compartment is substrate of the transporter.

5) The total mass of drug in the three compartments is preserved.

5.4.3. Modelling of compound permeation across Caco-2 cell monolayers in Transwells

In order to determine the kinetic constants governing the permeation across Caco-2 cell monolayers grown in Transwells the following mathematical model was developed based on the above mentioned assumptions. The equations describing the kinetics of cellular transport were defined as changes of molar amounts over time. The advantage of this procedure is that the different and changing volumes (cellular volume, donor and acceptor volume) of the three compartments don't cause problems, as they are accounted for by separate equations. The situation is different from the treatment of data of enzyme kinetics where e.g. a substrate concentration of 1M results in a product concentration of 1M provided that a 1:1 conversion takes place.

The change of concentration in the apical compartment, can be generally described by

$$\frac{dC_A}{dt} = \frac{dM_A}{dt} \bullet \frac{1}{V_A}$$

(Equation 38)

The change of the molar amount in solution in the apical compartment for the apical to basal transport direction was modelled as subsequently described. The change of the molar amount in solution in the apical compartment caused by concentration gradient driven diffusion across the apical cell membrane into the cellular compartment is defined by

$$J = \frac{dM_{Aab}}{dt \bullet Sm} = -P \bullet \left(C_{Aab} - C_{Cab}\right) \rightarrow \frac{dM_{Aab}}{dt} = -P \bullet \left(C_{Aab} - C_{Cab}\right) \bullet Sm$$

(Equation 39)

The subscript "A" denotes the apical compartment and the subscript "C" the cellular compartment, V the volume of solution [ml], the indices ab (lower case) denote

permeation in the apical to basal direction, P the permeability coefficient across the cell membrane [cm/min] and S_M the area of the cell monolayer [cm^2]. The term is set to minus. If the concentration in the apical compartment is bigger than in the cellular compartment the whole term will be negative reflecting the loss of substance in the apical compartment due to diffusion from the apical to the cellular compartment.

The molar amount that being effluxed from the cellular compartment into the apical compartment by a carrier-mediated mechanism is described by the Michaelis-Menten equation

$$+\frac{v_{\max} \bullet M_{Cab}}{K + M_{Cab}}$$

(Equation 40)

The molar amount that gets lost from solution due to sampling is expressed by

$$+\frac{dV_A}{dt} \bullet C_{Aab}$$

(Equation 41)

the term being with a plus sign as the change in volume itself is negative and will set the whole expression to negative.

Taken these three different mechanisms affecting the amount of substance in the apical compartment together, we get an equation describing the course of the molar amount of substance in the apical compartment over time

$$\frac{dM_{Aab}}{dt} = -P \bullet \left(C_{Aab} - C_{Cab}\right) \bullet Sm + \frac{v_{\max} \bullet M_{Cab}}{K + M_{Cab}} + \frac{dV_A}{dt} \bullet C_{Aab}$$

(Equation 42)

The change of the molar amount in solution in the basal compartment for the apical to basal transport direction can be described a similar manner by

$$\frac{dM_{Bab}}{dt} = P \bullet \left(C_{Cab} - C_{Bab}\right) \bullet Sm + \frac{dV_B}{dt} \bullet C_{Aab}$$

(Equation 43)

For modelling the amount of substance in the basal compartment only the change of the molar amount in solution caused by diffusion across the basal cell membrane and the molar amount that gets lost from solution due to sampling have to be taken into account. The processes causing a change of the molar amount in the cellular compartment for the apical to basal transport direction are diffusion across the apical and the basal cell

membrane and carrier-mediated transport across the apical membrane. The situation in the cellular compartment can therefore be described by

$$\frac{dM_{Cab}}{dt} = P \bullet (C_{Aab} - C_{Cab}) \bullet Sm - \frac{v_{\max} \bullet M_{Cab}}{K + M_{Cab}} - P \bullet (C_{Cab} - C_{Bab}) \bullet Sm$$

(Equation 44)

As the modelling is done under a mass balance approach the overall change for all three equations together is zero. This is true for situations in which only passive diffusion and carrier-mediated transport is integrated to the model. Equal equations can be defined for the basal to apical transport direction. To describe the change in amount in the three different compartments there are for each transport direction three equations with 6 variables (C_A, C_C, C_B, M_A, M_C, M_B). The change of the volume of solution is modelled as described in chapter 5.4.5. To reduce the number of variables, the molar amounts should be expressed in concentration or vice versa.

To get an equation that describes the change of the molar concentration of drug in the apical solution, (Equation 38) was differentiated and the chain rule applied

$$\frac{dM_{Aab}}{dt} = \frac{dC_{Aab} \bullet V_A}{dt} = \frac{dV_A}{dt} \bullet C_{Aab} + \frac{dC_{Aab}}{dt} \bullet V_A$$

(Equation 45)

The two equations (Equation 45) and (Equation 42) are set equal

$$\frac{dV_A}{dt} \bullet C_{Aab} + \frac{dC_{Aab}}{dt} \bullet V_A = -P \bullet (C_{Aab} - C_{Cab}) \bullet Sm + \frac{v_{\max} \bullet M_{Cab}}{K + M_{Cab}} + \frac{dV_A}{dt} \bullet C_{Aab}$$

(Equation 46)

and converted

$$\frac{dC_{Aab}}{dt} \bullet V_A = -P \bullet (C_{Aab} - C_{Cab}) \bullet Sm + \frac{v_{\max} \bullet M_{Cab}}{K + M_{Cab}}$$

(Equation 47)

$$\frac{dC_{Aab}}{dt} = -P \bullet (C_{Aab} - C_{Cab}) \bullet \frac{Sm}{V_A} + \frac{v_{\max} \bullet M_{Cab}}{K + M_{Cab}} \bullet \frac{1}{V_A}$$

(Equation 48)

The Michaelis-Menten term describes the efflux across a membrane (area) and the maximum velocity is in [nmol/(s•cm^2)] and not as in enzyme kinetics where the reaction takes place in solution in [nmol/s]. Therefore the term has to be extended by the area of the monolayer Sm resulting in the following equation

$$\frac{dC_{Aab}}{dt} = -P \bullet \left(C_{Aab} - C_{Cab}\right) \bullet \frac{Sm}{V_A} + \frac{v_{\max} \bullet M_{Cab}}{K + M_{Cab}} \bullet \frac{Sm}{V_A}$$

(Equation 49)

The same approach was applied to the basal compartment to get an equation describing the change of the molar concentration of drug in the basal solution.

The differentiated form of (Equation 38) for the basal compartment was set equal to (Equation 43)

$$\frac{dV_B}{dt} \bullet C_{Bab} + \frac{dC_{Bab}}{dt} \bullet V_B = P \bullet \left(C_{Cab} - C_{Bab}\right) \bullet Sm + \frac{dV_B}{dt} \bullet C_{Bab}$$

(Equation 50)

and converted

$$\frac{dC_{Bab}}{dt} \bullet V_B = P \bullet \left(C_{Cab} - C_{Bab}\right) \bullet Sm$$

(Equation 51)

$$\frac{dC_{Bab}}{dt} = P \bullet \left(C_{Cab} - C_{Bab}\right) \bullet \frac{Sm}{V_B}$$

(Equation 52)

To equation that describes the change of the molar amount of drug in the cellular compartment is the following

$$\frac{dM_{Cab}}{dt} = P \bullet \left(C_{Aab} - C_{Cab}\right) \bullet Sm - \frac{v_{\max} \bullet M_{Cab}}{K + M_{Cab}} - P \bullet \left(C_{Cab} - C_{Bab}\right) \bullet Sm$$

$$with$$

$$M_C = C_C \bullet V_C$$

(Equation 53)

This model results in the following differential equations describing the change of drug concentration or mass as a function of time in the three compartments during permeation in both directions if the relevant processes are passive diffusion and carrier-mediated transport.

transport direction apical to basal:

$$\frac{dC_{Aab}}{dt} = -P \bullet \left(C_{Aab} - C_{Cab}\right) \bullet \frac{Sm}{V_A} + \frac{v_{\max} \bullet M_{Cab}}{K + M_{Cab}} \bullet \frac{Sm}{V_A}$$

(Equation 54): apical compartment

$$\frac{dC_{Bab}}{dt} = P \bullet (C_{Cab} - C_{Bab}) \bullet \frac{Sm}{V_B}$$

(Equation 55): basal compartment

$$\frac{dM_{Cab}}{dt} = P \bullet (C_{Aab} - C_{Cab}) \bullet Sm - \frac{v_{\max} \bullet M_{Cab}}{K + M_{Cab}} \bullet Sm - P \bullet (C_{Cab} - C_{Bab}) \bullet Sm$$

(Equation 56): cellular compartment

transport direction basal to apical:

$$\frac{dC_{Aba}}{dt} = P \bullet (C_{Cba} - C_{Aba}) \bullet \frac{Sm}{V_A} + \frac{v_{\max} \bullet M_{Cba}}{K + M_{Cba}} \bullet \frac{Sm}{V_A}$$

(Equation 57): apical compartment

$$\frac{dC_{Bba}}{dt} = -P \bullet (C_{Bba} - C_{Cba}) \bullet \frac{Sm}{V_B}$$

(Equation 58): basal compartment

$$\frac{dM_{Cba}}{dt} = P \bullet (C_{Bba} - C_{Cba}) \bullet Sm - P \bullet (C_{Cba} - C_{Aba}) \bullet Sm - \frac{v_{\max} \bullet M_{Cba}}{K + M_{Cba}} \bullet Sm$$

(Equation 59): cellular compartment

C is the molar concentration [µM], M is the molar amount of substance [nmol], the indices A, B, and C (upper case) denote the apical, basal and cellular compartment, respectively, the indices ab and ba (lower case) denote permeation in the apical to basal and the basal to apical direction, respectively, Sm is the surface area of the monolayer [cm^2] and V is volume of solution in each compartment [ml].

5.4.4. Mathematical model for determining drug absorption parameters in Caco-2 cell monolayers with inclusion of phase II metabolism and adsorption to the Transwell surface

In a next step adsorption and phase II metabolism were integrated to the model by extension of the system of differential equations described in chapter 5.4.3 to fully describe all the relevant processes taking place during the absorption of Amentoflavone in Caco-2 cell monolayers grown in Transwell plates. Adsorption was modelled as described in chapter 5.4.1 as a saturable process dependent on the concentration of Amentoflavone in solution and the contact area of the solution with the Transwell surface. The parameters describing the adsorption are the following: k_{on} is the rate constant for the adsorption to the surface [cm^2/(mol•min)], k_{off} is the rate constant for desorption of the surface [1/min], and W_{tot} is the total number of binding sites on the surface

[nmol/cm^2]. The values of the parameters k_{on}, k_{off} and W_{tot} of Amentoflavone were first estimated in cell-free experiments in the Transwell apparatus as described in chapter 5.4.6 and later on used in the fits for Amentoflavone with cell monolayers. The phase II metabolism was modelled as a first-order process. The formed amount of metabolites depends on the amount of Amentoflavone in the cellular compartment and the rate constant k_M [1/min]. The transport behaviour of the metabolites itself was neglected for modelling purposes. The combined amount of the detected sulfates and glucuronidates was quantified at each time point and used in the fitting. The cellular compartment was treated as a sink for the metabolites. The transport processes included in the extended version of the transport model are displayed in Figure 3.

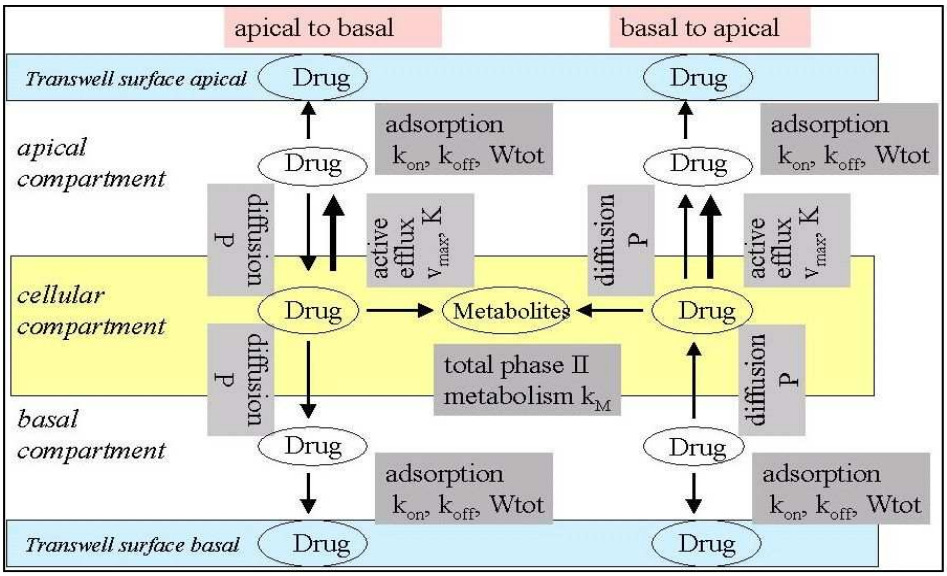

Figure 3: Transport processes considered for modelling drug permeation in the Caco-2 monolayer and relevant processes including phase II metabolism and adsorption.

To consider the adsorption to and the desorption of the surface, the expressions already developed for the transport experiments without cell monolayers ((Equation 34) - (Equation 37)) were integrated to (Equation 54), (Equation 55), (Equation 57) and (Equation 58)) and the system of differential equations describing the change of drug concentration or mass as a function of time in the three compartments during permeation in both directions was extended by the equations for the amounts bound to the surface in the apical and basal compartment. The phase II metabolism was modelled as a first-order process with the formed amount of metabolites depending on the amount of Amentoflavone in the cellular compartment and the rate constant k_M [1/min]. This extension was integrated to the equation for the cellular compartment. An equation for the formed amount of metabolites had to be added for each transport direction. The modelling resulted in the following system of differential equations. The equations are displayed in the full version.

transport direction apical to basal:

$$\frac{dC_{Aab}}{dt} = -P \bullet \left(C_{Aab} - C_{Cab}\right) \bullet \frac{Sm}{V_A} + \frac{v_{\max} \bullet M_{Cab}}{K + M_{Cab}} \bullet \frac{Sm}{V_A} - k_{on} \bullet C_{Aab} \bullet (W_{tot} - C_{WAab}) + k_{off} \bullet C_{WAab} \bullet \frac{S_A}{V_A}$$

(Equation 60): apical compartment solution

$$\frac{dC_{Bab}}{dt} = P \bullet (C_{Cab} - C_{Bab}) \bullet \frac{Sm}{V_B} - k_{on} \bullet C_{Bab} \bullet (W_{tot} - C_{WBab}) + k_{off} \bullet C_{WBab} \bullet \frac{S_B}{V_B}$$

(Equation 61): basal compartment solution

$$\frac{dM_{Cab}}{dt} = P \bullet (C_{Aab} - C_{Cab}) \bullet Sm - \frac{v_{\max} \bullet M_{Cab}}{K + M_{Cab}} \bullet Sm - P \bullet (C_{Cab} - C_{Bab}) \bullet Sm - k_M \bullet M_{Cab}$$

(Equation 62): cellular compartment

$$\frac{dM_{MCab}}{dt} = k_M \bullet M_{Cab}$$

(Equation 63): phase II metabolism

$$\frac{C_{WAab}}{dt} = k_{on} \bullet C_{Aab} \bullet (W_{tot} - C_{WAab}) \bullet \frac{V_A}{S_A} - k_{off} \bullet C_{WAab}$$

(Equation 64): Transwell apical surface

$$\frac{C_{WBab}}{dt} = k_{on} \bullet C_{Bab} \bullet (W_{tot} - C_{WBab}) \bullet \frac{V_B}{S_B} - k_{off} \bullet C_{WBab}$$

(Equation 65): Transwell basal surface

transport direction basal to apical:

$$\frac{dC_{Aba}}{dt} = -P \bullet \left(C_{Aba} - C_{Cba}\right) \bullet \frac{Sm}{V_A} + \frac{v_{\max} \bullet M_{Cba}}{K + M_{Cba}} \bullet \frac{Sm}{V_A} - k_{on} \bullet C_{Aba} \bullet (W_{tot} - C_{WAba}) + k_{off} \bullet C_{WAba} \bullet \frac{S_A}{V_A}$$

(Equation 66): apical compartment solution

$$\frac{dC_{Bba}}{dt} = P \bullet (C_{Cba} - C_{Bba}) \bullet \frac{Sm}{V_B} - k_{on} \bullet C_{Bba} \bullet (W_{tot} - C_{WBba}) + k_{off} \bullet C_{WBba} \bullet \frac{S_B}{V_B}$$

(Equation 67): basal compartment solution

$$\frac{dM_{Cba}}{dt} = P \bullet (C_{Aba} - C_{Cba}) \bullet Sm - \frac{v_{\max} \bullet M_{Cba}}{K + M_{Cba}} \bullet Sm - P \bullet (C_{Cba} - C_{Bba}) \bullet Sm - k_M \bullet M_{Cba}$$

(Equation 68): cellular compartment

$$\frac{dM_{MCba}}{dt} = k_M \bullet M_{Cba}$$

(Equation 69): phase II metabolism

$$\frac{C_{WAba}}{dt} = k_{on} \bullet C_{Aba} \bullet (W_{tot} - C_{WAba}) \bullet \frac{V_A}{S_A} - k_{off} \bullet C_{WAba}$$

(Equation 70): Transwell apical surface

$$\frac{C_{WBba}}{dt} = k_{on} \bullet C_{Bba} \bullet (W_{tot} - C_{WBba}) \bullet \frac{V_B}{S_B} - k_{off} \bullet C_{WBba}$$

(Equation 71): Transwell basal surface

5.4.5. Analysis of the permeation data

Modelling of the reduction of the volume of solution

The reduction of the volume of solution in the apical and the basal compartment due to sampling as a function of time was accounted for by polynomial relations describing this reduction. The reduction was modelled as a continuous reduction over time and not as it is in reality as a stepwise reduction at discrete times. Two cases had to be distinguished for the modelling of the reduction of the volume in Transwells, the first one being Transwells with cells or sealing of the membrane ("sealed case") and the second one with no cell monolayer or any other sealing on the membrane ("free case").

For the modelling of the reduction of the volume in the sealed case, timepoints for certain volumes were exactly between the times for two sample drawings. The first point reflecting the initial volumes was set after 15min. The parameters of the polynomial relations were determined empirically using regression analysis with EASY-FIT® using the model type "explicit", the numerical method "DFNLP", a scaling of 1 and a termination tolerance of 0.00000001. The point of origin and the endpoint were free for the fitting. The values for the different parameters, $V_{apical,0,calculated}$ and $V_{basal,0,calculated}$ were determined for the transport experiments over 7h with sampling volumes of 117µl and sampling after 30, 150, 300 and 420 minutes. The determined relations were later on used in the fittings of the data of transport experiments. For a sampling volume of 117µl regression analysis yielded in the following polynomial relations for the reduction of the volume in the sealed case

$$V_{apical}(t) = 1.630764 - 0.0021457 \bullet t + 0.0000064596 \bullet t^2 - 0.00000000957 \bullet t^3$$

(Equation 72)

$$V_{basal}(t) = 2.83076424 - 0.0021457 \bullet t + 0.0000064597 \bullet t^2 - 0.00000000957 \bullet t^3$$

(Equation 73)

These relations are only valid if there is no fluid flow between the apical and basal compartment. This is the case if there is an intact cell monolayer on the membrane of the Transwell or if the membrane is sealed in any other way. If the membrane is not sealed

sample drawings in the apical and basal compartment without replacement of the withdrawn solution may result in fluid flow, thus possibly equalizing an imbalance in liquid level in the two compartments. For these reasons the reduction in volume for experiments without cells cannot be described with the same relations even if the sample volume is the same. For the calculation of the contact area the contact height of the solution with the Transwell surface was also experimentally measured for the case without any sealing of the membrane (see chapter 5.3.4). The reduction of the contact height of the solution in the apical compartment due to sampling as a function of time was calculated by the following polynomial relations, the parameters of which were determined empirically using regression analysis with EASY-FIT® with the same settings as in the sealed case. Only experiments over 7h and with a sampling volume of 117µl were performed with a free membrane. For these conditions the regression analysis yielded in the following polynomial relations for the height of contact in the apical compartment in the free case.

$$Height_{apical}(t) = 0.56601380 - 0.0005277 \bullet t + 0.0000013207 \bullet t^2 - 0.000000001717 \bullet t^3$$

(Equation 74)

This polynomial relation is applied to describe to the course of the apical volume resulting in the decrease of volume (starting volume 1.6ml). After estimation of the apical volumes for different time points, the basal volume is calculated based on the assumption of conservation of volume in the two compartments. The total initial volume is known (1.6 + 2.8ml) as well as the volume withdrawn as samples (0.117ml) and the calculated apical volumes. With these data the basal volume can be calculated. The reduction of the volume of solution in the free case was accounted for by the same polynomial relations as in the sealed case (see (Equation 72 and (Equation 73). The parameters were determined the same way as described above. The regression analysis yielded in the following polynomial relations for the reduction of the volume in the free case.

$$V_{apical}(t) = 1.64832392 - 0.0033815 \bullet t + 0.000010895 \bullet t^2 - 0.00000001517 \bullet t^3$$

(Equation 75)

$$V_{basal}(t) = 2.81033228 - 0.0006778 \bullet t + 0.0000007337 \bullet t^2 - 0.000000001965 \bullet t^3$$

(Equation 76)

5.4.6. Estimation of adsorption parameters in transwells without cells

The concentration variables defined by the system of differential equations, (Equation 34) to (Equation 37), were fitted to the experimental concentration data. Concentration data

of both compartments obtained from concomitant incubation in the apical and the basal compartment were fitted at the same time. Numerical solution of the equations and least squares fit were performed using the software Easy-Fit® and optimal values of the kinetic parameters k_{on}, k_{off}, W_{tot} and P were deduced.

The regression analysis with EASY-FIT® was performed using the model type "ODE" (ordinary differential equations), the numerical method "DFNLP", a scaling of 0, an initial stepsize of 0.000001 to 0.00000001 and a final accuracy (absolute and relative) of 0.000001 to 0.00000001. Data obtained from transport experiments at 37℃ and at 4℃ were analysed separately. The transport parameters were determined for every single concentration and temperature. The reduction of the volume of solution over time was accounted for by the already mentioned polynomial equations. The reduction of the contact area over time was accounted for by the experimentally determined polynomial relations shown in chapter 5.5.2.

Two attempts were differentiated for the parameter estimation with Easy-Fit®. The first way of fitting the experimental data was to only include the measured concentrations at the defined time points and obtain $C_{Aa\&b}(0)$ and $C_{Ba\&b}(0)$ from the model simulation ("Model without $C_{Donora\&b}(0)$"). Doing so we assumed that already the donor concentration is affected by adsorption (to pipettes and other materials used in the preparation of the donor solutions) and most probably lower than the expected respectively the intended donor concentrations. The second way of fitting the experimental data was to assume that $C_{Aa\&b}(0)$ and $C_{Ba\&b}(0)$ were close to the expected respectively the intended donor concentrations ("Model with $C_{Donora\&b}(0)$"). Doing so, we integrated the not experimentally measured donor concentrations to the fitting along with the measured concentrations at the defined time points. With this attempt we also obtained from the model simulation values for $C_{Aa\&b}(0)$ and $C_{Ba\&b}(0)$ that best fit with the rest of the data. If all parameters to be estimated were free in the fittings, in most instances a strong correlation between k_{on}, k_{off}, W_{tot} and P occurred in the regression analysis, which meant that these parameters could not be deduced individually from each other. Therefore all fittings were performed using step-by-step procedure, beginning with all parameters. After the first fitting the parameters estimated for all concentrations used at the same temperature were compared, and the parameter (k_{on}, k_{off} or W_{tot}) with the most consistent values estimated was set as a constant in the next fitting. Again comparison and selection of the parameters was performed and a second parameter (k_{on}, k_{off} or W_{tot}) was set as a constant in the next fitting. After the third round of fitting the data the last left parameter (k_{on}, k_{off} or W_{tot}) could be determined. The regression analysis resulted in values for k_{on},

k_{off}, W_{tot} and P. Furthermore the course of C_{WA} and C_{WB} dependent on the time was obtained from model simulation.

5.4.7. Analysis of Amentoflavone permeation across Caco-2 cell monolayers

Permeation data were analysed using this theoretical model for the kinetics of cellular transport. The concentration variables defined by the system of differential equations were fitted to the experimental concentration data. Concentration data of both compartments obtained from the apical to basal and the basal to apical direction of permeation were simultaneously fitted. This provided a more stable regression analysis compared to the separate evaluation of each permeation direction. Previous work using the transport model [Kapitza] showed that in most instances a strong correlation between v_{max} and K occurred in the regression analysis, which meant that these parameters could not be deduced individually from each other. Therefore all fittings in the present work were performed using the approximation of first order kinetics for the carrier-mediated efflux (M_C << K) for the estimation of the transport parameters

$$\frac{v_{\max} \bullet M_{Cxy}}{K + M_{Cxy}} = vk \bullet M_{Cxy}$$

(Equation 77)

This approximation yielded in all situations better results as estimated by the final residual values of the fittings than the approximation of zero order kinetics for the carrier-mediated efflux (M_C >> K) that was previously used. The reduction of the volume of solution over time was accounted for by the already mentioned polynomial equations. The reduction of the contact area over time was accounted for by the experimentally determined polynomial relations shown in chapter 5.5.2. The non-specific binding to Transwell surface was calculated by the kinetic parameters estimated in chapter 5.5.3. Numerical solution of the equations and least squares fit were performed using the software Easy-Fit® and optimal values of the kinetic parameters P, vk, and k_M applicable to the different experimental conditions were deduced. The regression analysis with EASY-FIT® was performed using the model type “ODE” (ordinary differential equations), the numerical method “DFNLP”, a scaling of 1, an initial stepsize of 0.00000001 and a final accuracy (absolute and relative) of 0.00000001. The transport data obtained by the methods described in chapter 5.3.8 was used in the fittings. Transport parameters were determined for every single concentration (only data from 7h experiments). A cell monolayer volume of 0.0094ml was used based on a monolayer thickness of 20µm and a monolayer area of 4.70cm^2. The regression analysis resulted in values for the passive

permeability coefficient P, the rate constant vk, which expresses the apical efflux rate in nmol/(cm^2●s) and the rate constant k_M which describes the formation of the metabolites [1/min]. Furthermore the drug concentrations at time zero, $C_{Aab}(0)$ and $C_{Bba}(0)$ and the drug mass in the cellular compartment were obtained from model simulation.

5.5. Results and discussion

5.5.1. Cell toxicity of the different compounds

The possibility of adverse effects elicited by the different compounds and combinations used on cultured Caco-2 cell monolayers was evaluated by determining the mitochondrial dehydrogenase activity of the cells by using the MTT assay. This is an established method addressing one aspect of cell functionality and is widely used as a criterion of cytotoxicity. The MTT assay detects specifically mitochondrial metabolic activity and the ability of the cells for proliferation. The results of the MTT assay are shown in (Figure 4) and (Figure 5). For the 7h incubation with Amentoflavone and Vinblastine and combinations of the two compounds, mitochondrial activity values of the cells were in the range between 89.51% (Amentoflavone 5µM b_a) and 101.59% (Vinblastine 70µM a&b & Amentoflavone 5µM a_b) of the control. None of these values was statistically significant different from the control as determined by the Student's t-test at $p < 0.05$.

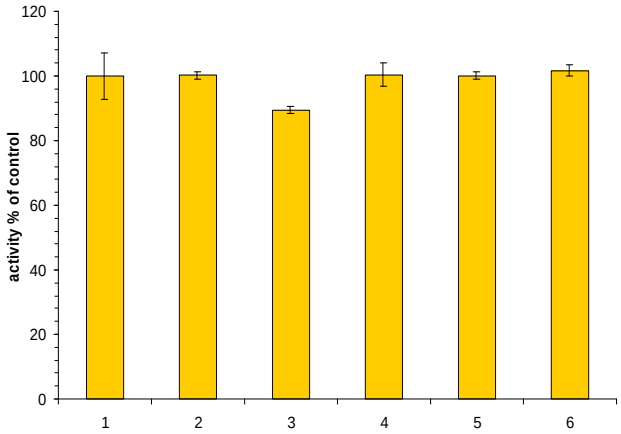

Figure 4: Mitochondrial dehydrogenase activity of the cells determined by the MTT assay following 7h incubation in 6-well Transwell plates. Results are expressed in percent of control obtained with transport medium + 0.5% Ethanol (v/v) and given as mean and standard deviation with n = 4. Column: 1 transport medium + 0.5% EtOH (v/v), 2 Amentoflavone 5µM a_b, 3 Amentoflavone 5µM b_a, 4 Vinblastine 70µM a&b, 5 Vinblastine 70µM a&b & Amentoflavone 5µM a_b, 6 Vinblastine 70µM a&b & Amentoflavone 5µM b_a.

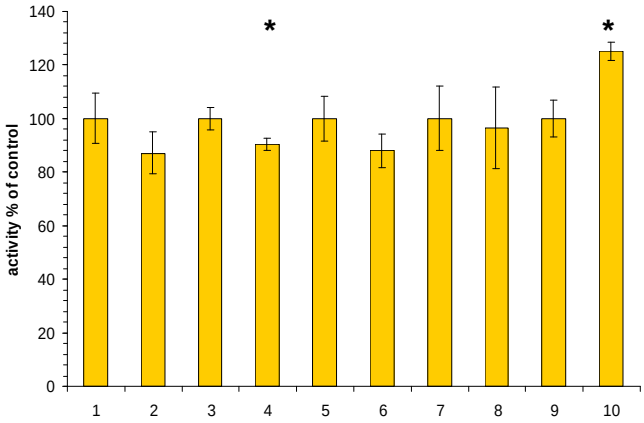

Figure 5: Mitochondrial dehydrogenase activity of the cells determined by the MTT assay following 5h incubation in 6-well Transwell plates (passage 82 - 92, 20 – 24 days post seeding). Results are expressed in percent of control obtained with transport medium + 0.5% Ethanol (v/v) and Amentoflavone 5µM a_b and given as mean and standard deviation with n = 3. Columns: 1, 3, 5, 7 and 9 transport medium + 0.5% EtOH (v/v)) and Amentoflavone 5µM a_b, 2 GF120918 0.1µM a&b and Amentoflavone 5µM a_b, 4 GF120918 1µM a&b and Amentoflavone 5µM a_b, 6 Vinblastine 3.9µM a&b & Amentoflavone 5µM a_b, 8 Vinblastine 25µM a&b & Amentoflavone 5µM a_b, 10 Vinblastine 70µM a&b & Amentoflavone 5µM a_b. * denotes results that are statistically significant from the control at p < 0.05.

For the 5h incubation with Amentoflavone and varying concentrations of Vinblastine and GF120918, mitochondrial activity values of the cells were in the range between 87.15% (GF120918 0.1µM a&b) and 125.17% (Vinblastine 70µM a&b) of the control. The effects of two combinations, the reduction of GF120918 0.1µM a&b and Amentoflavone 5µM a_b to 90.31% and the increase of Vinblastine 70µM a&b & Amentoflavone 5µM a_b to 125.17%, were statistically significant (Student's t-test) at $p < 0.05$. No positive correlation between concentration of GF120918 or Vinblastine and the effect on the mitochondrial activity in the studied concentration range was observed. Taken together the employed compounds and concentrations had overall no significant cytotoxic effect on the cells. The statistically significant effects observed in a two instances in the MTT assay in the 6-well Transwell plates were not consistent between the two incubation times (Vinblastine) or within the series of applied concentrations (both Vinblastine and GF120918. Hence, they do not appear to be systematic. The test in the Transwell plates corresponds exactly to the experimental setup used in the permeation studies except for the fact, that no samples were drawn. A masking of cytotoxicity of the compounds by an interaction of the MTT assay with high concentrations of some P-glycoprotein and MRP substrates leading to false cell viability values during concomitant incubation [Vellonen] cannot be ruled out.

5.5.2. Determination of the contact height and mathematical description of the contact area of the transport medium with Transwell surfaces (Transwells without cells)

The contact height and based on the height the contact area of different volumes of transport medium with the Transwell surface during the transport experiments was determined by colouring the surface with a solution of Nile Blue A. The volumes corresponded to the volumes for certain time points during the transport experiments. The polycarbonate membrane of the Transwell was either free or sealed to mimic the situation with or without cells. The solution in the apical compartment is in contact with the inner surface of the Transwell insert, the solution in the basal compartment is in contact with the outer surface of the Transwell insert and the surface of the Transwell cavity. The experimentally determined height of contact was plotted against the apical and basal volumes and linear relationships were calculated by linear regression in Microsoft Excel®. The relations describing the course of the contact height are displayed in (Table 1). These relations describe the contact height for experiments with donor volumes of 1600µl (apical compartment) and 2800µl (basal compartment), sampling volumes of 117µl and sampling after 30, 150, 300 and 420min.

Table 1: Equations describing the course of the height of contact between the solution and the different parts of the Transwell plates.

	contact height [mm] free membrane	contact height [mm] sealed membrane
apical compartment: inner surface insert	H = 0.0026 • volume [µl] + 1.4239 R^2 = 0.9614	H = 0.0045 • volume [µl] – 1.2153 R^2 = 0.9197
basal compartment: outer surface insert	H = 0.0043 • volume [µl] – 4.7878 R^2 = 0.9486	H = 0.0041 • volume [µl] – 3.4003 R^2 = 0.9926
basal compartment: surface cavity	H = 0.0038 • volume [µl] – 2.3064 R^2 = 0.9868	H = 0.004 • volume [µl] – 1.9699 R^2 = 0.9581

The relations describing the contact height for all the different parts of the Transwell plates show good linear correlation as evaluated by the correlation coefficient. Therefore the assumption that there is a linear connection between the volume and contact height and the resulting contact area, appears to be correct. Based on the contact height the contact area for the different time points was calculated as described in chapter 5.3.4. The reduction of the contact area was then modelled as a continuous reduction described by polynomial relations and the regression analysis performed with Easy-Fit yielded in the following relations for the contact area in the free case (with possible fluid flow between the two compartments)

$$S_{apical}(t) = 4.34994077 - 0.0040556 \bullet t + 0.000010152 \bullet t^2 - 0.0000000132 \bullet t^3$$

(Equation 78)

$$S_{basal}(t) = 25.1737344 - 0.0158919 \bullet t + 0.000039515 \bullet t^2 - 0.00000005121 \bullet t^3$$

(Equation 79)

and in the sealed case

$$S_{apical}(t) = 4.70576080 - 0.0074206 \bullet t + 0.000022341 \bullet t^2 - 0.0000000331 \bullet t^3$$

(Equation 80)

$$S_{basal}(t) = 26.8842921 - 0.0169706 \bullet t + 0.000051570 \bullet t^2 - 0.00000007563 \bullet t^3$$

(Equation 81)

with S being the contact area in [cm^2] and t being the time in [min]. These descriptions of the contact area were used in the fittings of Amentoflavone data of transport experiments with or without cells.

5.5.3. Adsorption of Amentoflavone to Transwell surfaces at 4°C and 37°C (Transwells without cells,): Estimation of the adsorption parameters and representative fits of the Amentoflavone transport and adsorption in Transwells without cells

Transport experiments with Amentoflavone in Transwell plates without cells were performed as described in chapter 5.3.5, at 4°C and at 37°C. The concentration-time profiles of these experiments with concomitant incubation of Amentoflavone in the apical and basal compartment were used to determine the adsorption parameters k_{on}, k_{off}, W_{tot} of Amentoflavone to the Transwell surface and calculate the amount of Amentoflavone adsorbed to the surface, C_{WA} and C_{WB}, at the two different temperatures. The experimental permeation data were analysed using the theoretical model for transport and adsorption in Transwell plates without cells consisting of (Equation 34) to (Equation 37), and the fitting software Easy-Fit®.

Two attempts were differentiated for the parameter estimation with Easy-Fit®. The first attempt was to include only the measured concentrations at the defined time points for the parameter estimation. Values for the donor concentrations $C_{Aa\&b}(0)$ and $C_{Ba\&b}(0)$ were obtained from the model simulation ("Model without $C_{Donora\&b}(0)$"). For the second attempt we assumed that $C_{Aa\&b}(0)$ and $C_{Ba\&b}(0)$ were close to the intended donor concentrations ("Model with $C_{Donora\&b}(0)$"). The values for the intended donor concentrations $C_{Aa\&b}(0)$ and $C_{Ba\&b}(0)$ were included in the fittings for the parameter estimation. Still values for $C_{Aa\&b}(0)$ and $C_{Ba\&b}(0)$ fitting better to the experimentally observed concentration profiles were obtained from the model simulation. As in most instances a strong correlation between k_{on}, k_{off}, W_{tot} and P occurred in the regression analysis and these parameters could not be deduced individually from each other all fittings were performed using step-by-step procedure and one parameter after the other was estimated. This procedure used for the

parameter estimation for the two assumptions and the two temperatures resulted in the values shown in (Table 2).

Table 2: Estimated values for W_{tot}, k_{on} and k_{off} for the two assumptions for calculating the adsorption to Transwell plates without cells.

	model without $C_{Donor\ a\&b}(0)$		model with $C_{Donor\ a\&b}(0)$	
	37℃	4℃	37℃	4℃
W_{tot} [nmol/cm^2]	0.5	1.3	0.65	1.7
k_{on} [cm^2/(nmol • min)]	0.001565	0.000601	0.03	0.0165
k_{off} [1/min]	0.00085	$3.75 \bullet 10^{-35}$	0.0165	0.0195

One has to be aware, that the estimation of the adsorption parameters was performed under the assumption of concentration independency of the k_{on}, k_{off} & W_{tot}, be it for different experiments or during one defined experiment. The non-specific binding can be described by these parameters at each time point during the experiment. The estimated parameters differed for the two temperatures (4℃ and 37℃) as well as for the two models (model with $C_{Donora\&b}(0)$ and model without $C_{Donora\&b}(0)$). W_{tot} was in both models bigger for the lower temperature, indicating a higher binding capacity of the surface at 4℃. If this finding demonstrates a real higher capacity of if the higher number is just artefact of the model and fitting procedure reflecting therefore rather a virtual binding capacity, is uncertain, as at 4℃ the model encounters stronger adsorption. The model with $C_{Donora\&b}(0)$ shows slightly higher values for W_{tot} than the model without $C_{Donora\&b}(0)$. Again this may be due to the fact that there is more Amentoflavone in the system that adsorbs (see chapter 5.5.4) and therefore the higher value results. Further inspection shows that the values for k_{on} and k_{off} are at both temperatures higher for the model with $C_{Donora\&b}(0)$ than for the model without $C_{Donora\&b}(0)$. Surprisingly these values are generally lower at 4℃ than at 37℃, indicating that the values for W_{tot} has a stronger impact on the total amount adsorbed than k_{on} and k_{off}. In one case the value for k_{off} is even higher than the one for k_{on}, further complicating any systematic interpretation of these parameters.

Taken together there is strong evidence that the estimated adsorption parameters are rather descriptive values than reflecting real processes taking place in the Transwell plates. (Figure 6) and (Figure 7) show representative fits for Amentoflavone permeation after simultaneous addition in the apical and basal compartment. The fitting was done with the model with $C_{Donora\&b}(0)$ and with the model without $C_{Donora\&b}(0)$. The experimental data used for the fittings in (Figure 6) and (Figure 7) were the same. (Figure 8) and (Figure 9) show representative calculated courses of C_{WA} and C_{WB} (amounts bound to the surface) depending on time that were obtained from model simulation for the fits of the experimental data used in (Figure 6) and (Figure 7) with the respective models.

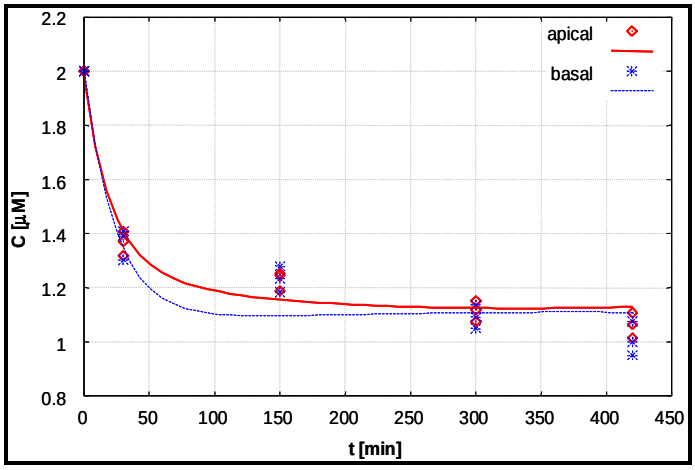

Figure 6: Representative fit of Amentoflavone 2µM apical and basal in Transwell plates without cells at 37°C. The fitting was done with th e model with $C_{Donora\&b}(0)$.

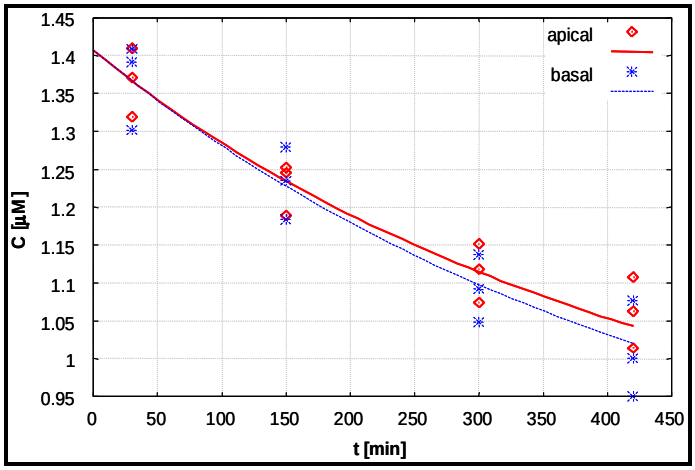

Figure 7: Representative fit of Amentoflavone 2µM apical and basal in Transwell plates without cells at 37°C. The fitting was done with th e model without $C_{Donora\&b}(0)$.

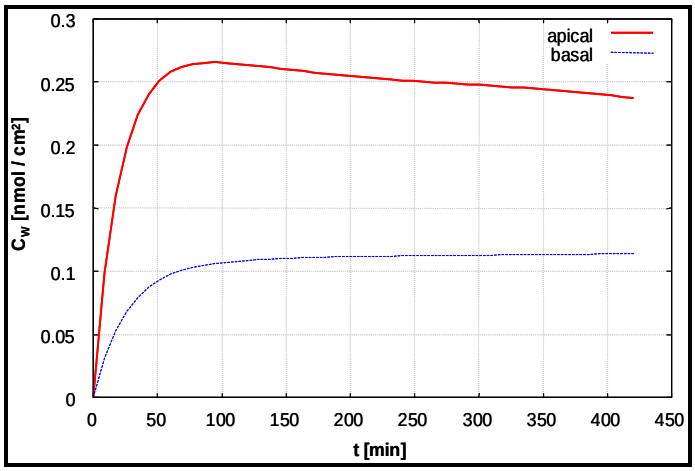

Figure 8: Representative calculated course of the adsorption of Amentoflavone 2µM apical and basal in Transwell plates without cells at 37°C. The fitting was done with the model with $C_{Donora\&b}(0)$.

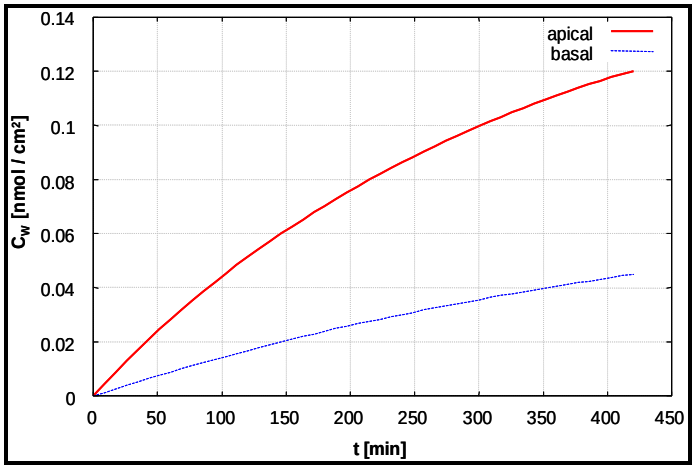

Figure 9: Representative calculated course of the adsorption of Amentoflavone 2µM apical and basal in Transwell plates without cells at 37°C. The fitting was done with the model without $C_{Donora\&b}(0)$.

The model with $C_{Donora\&b}(0)$, taking into account the aspired donor concentration in the fitting, results in concentration-time fits, that do describe all the measured concentrations as well as the fits with the model without $C_{Donora\&b}(0)$. The first model shows strong initial adsorption (during the first 60min) as displayed by the initial drop in concentration (Figure 6) and by the model calculated amounts bound to the surface (Figure 8). After this first phase of adsorption the concentration as well as the amount bound to the surface remains more or less constant. The model without $C_{Donora\&b}(0)$ results in fits that don't show an initial drop in concentration (Figure 7). This model describes the adsorption as a continuous process, taking place over the whole incubation period as displayed by the calculated amounts bound to the surface (Figure 9). The way the adsorption is modelled assumes that over the whole incubation time the driving force for the non-specific binding remains the same and that the adsorption can be described as a whole by the estimated set of adsorption parameters. In case of the likely situation that the adsorption is in reality more complex than our simple model (e.g. binding is a two step process or there is an initial and a steady-state phase with different adsorption parameters), we would fail in a complete description of the adsorption. The main focus of the model with $C_{Donora\&b}(0)$ is the initial decrease in concentration due to non-specific binding whereas the model without $C_{Donora\&b}(0)$ is good in delineating the decrease in concentration in the second part of the concentration-time profile, describing the adsorption as a continuous process taking place over the whole period of the experiment whereas.

5.5.4. Comparison of the two different models for adsorption (Transwells without cells, 4°C and 37°C)

Measured and calculated amount of Amentoflavone adsorbed to the Transwell surface

After each transport experiment the Transwell plates were extracted with methanol to estimate the amount of Amentoflavone bound to the surface during the incubation. (Table 3) shows the experimentally determined amount of Amentoflavone bound to the surface as well as the model-derived total amounts (model without $C_{Donora\&b}(0)$ and model with $C_{Donora\&b}(0)$) adsorbed the surface after incubation in Transwells without cells.

Table 3: Amounts of Amentoflavone (AF) extracted from the Transwell plates without cells after concomitant incubation in the apical and basal compartment for 7h at 4℃ and 37℃ compared to the calculated amounts of Amentoflavone adsorbed to the Transwell surface with the model without $C_{Donora\&b}(0)$ and with the model with $C_{Donora\&b}(0)$. Experimental results are given as mean and standard error of the mean with n = 3. E = experimental values, C = calculated with the model without $C_{Donora\&b}(0)$, C0 = calculated with the model with $C_{Donora\&b}(0)$.

AF conc.	amount extracted 37℃ [nmol]			amount extracted 4℃ [nmol]		
[µM]	E	C	C0	E	C	C0
2	2.473 +/- 0.136	1.526	3.829	3.074 +/- 0.145	1.311	4.386
5	5.587 +/- 0.368	2.356	7.323	9.387 +/- 0.217	3.677	10.159
7.5	6.826 +/- 0.225	2.810	9.432	14.200 +/- 0.762	4.556	14.933
10	11.258 +/- 0.605	6.692	11.187	20.691 +/- 0.898	6.324	22.722

The experimentally determined amounts of Amentoflavone extracted from the surface after concomitant incubation in the apical and basal compartment for 7h at 37℃ were for 2µM 28.1% +/- 1.5, for 5µM 25.4% +/- 1.7, for 7.5µM 20.7% +/- 0.7, and for 10µM 25.6% +/- 1.4 of the initial amount at the start of the experiment. The same experiments performed at 4℃ yielded in the following extraction rates: 2µM 34.9% +/- 1.6, for 5µM 42.7% +/- 1.0, for 7.5µM 43.0% +/- 2.3, and for 10µM 47.0% +/- 2.0 of the initial amount at the start of the experiment. These results are not indicating a saturation effect in the concentration range tested, neither for experiments performed at 4℃ nor for experiments performed at 37℃. Regarding these results the assumption of a linear relationship for the amount adsorbed and the concentration in the solution as used in the theoretical modelling is reasonable. Furthermore a strong dependency of the adsorption on the temperature is demonstrated by the results.

The model with $C_{Donora\&b}(0)$ yields generally in higher amounts bound to the surface compared to the experimentally measured values, whereas the model without $C_{Donora\&b}(0)$ yields in lower amounts compared to the experimentally measured values. For experiments performed at 4℃ the amounts calculated with the model with $C_{Donora\&b}(0)$ were closer to the experimentally measured amounts than ones calculated with the model without $C_{Donora\&b}(0)$, having deviations of +42.7%, +8.2%, +5.2%, and +9.8% compared to deviations of –57.4%, -60.8%, -67.9%, and -69.4%. For experiments performed at 37℃ the amounts calculated with the model with $C_{Donora\&b}(0)$ were with one exception closer to the experimentally measured amounts than ones calculated with the

model without $C_{Donora\&b}(0)$, but the deviations were bigger than the ones for the calculations for experiments at 4°C, having deviati ons of +54.9%, +31.1%, +38.2%, and -0.6% compared to deviations of -38.3%, -57.8%, -58.8%, and -40.6%. By assumption of correctly estimated experimentally values for the amount of Amentoflavone adsorbed to the surface, the model with $C_{Donora\&b}(0)$ is generally better in predicting the adsorption, resulting in most cases in a overestimation of the amount adsorbed to the surface. One other option would be an experimental underestimation of the amount adsorbed to the surface. The possibility of overestimation of the adsorbed amounts by the experiment cannot be ruled out, but would imply a systematic error in the extraction procedure used, as we are not aware of any inconsistencies in the estimated values, neither in the concentration series nor between the two different temperatures.

Model estimated donor amounts

The fittings of the experimental concentration data with either the model with $C_{Donora\&b}(0)$ or model without $C_{Donora\&b}(0)$ yielded in calculated donor concentrations fitting best to the observed concentration profiles, based on which donor amounts were calculated to be compared to the intended donor amounts (Table 4).

Table 4: Estimated donor amounts for transport experiments in Transwell without cells at 4°C and 37°C with model with $C_{Donora\&b}(0)$ and model without $C_{Donora\&b}(0)$.

	model without $C_{Donora\&b}(0)$				model with $C_{Donora\&b}(0)$			
Amentoflavone concentration [µM]	2	5	7.5	10	2	5	7.5	10
donor amount calculated 37°C [nmol]	6.28	16.88	26.06	34.08	8.91	22.35	33.40	44.23
37°C: calc. % of intended	71.32	76.70	78.98	77.46	101.28	101.59	101.21	100.53
donor amount calculated 4°C [nmol]	5.51	14.88	21.93	26.53	8.90	22.30	33.45	44.60
4°C: calc. % of intended	62.61	67.62	66.46	60.30	101.14	101.36	101.35	101.36

The most striking difference between the two models was, that with the model with $C_{Donora\&b}(0)$ the resulting donor amounts were almost identical to the intended ones, with no difference between the two temperatures, whereas for the model without $C_{Donora\&b}(0)$ donor amounts between 60 – 80% of the intended was resulted, with slightly worse results for experiments performed at 4°C. The resul ts of the first model imply that the permeation experiments were performed with concentrations that corresponded to the intention whereas the results of the latter model imply a substantial divergence from the intention. The divergence would be especially problematic for the data treatment of

experiments with cells in which more parallel processes take place than in the simple system of Transwell plates without cells.

Mass balances of Amentoflavone transport in Transwells without

Mass balances were calculated for all permeation experiments without cells by addition of the amount in solution after 7h, the amount withdrawn during the experiment and the amount extracted with methanol from the Transwell surface. The intended donor amount provided the reference for calculation. (Table 5) shows the mass balances for both the experiments at 4℃ and at 37℃.

Table 5: Mass balances of Amentoflavone after concomitant incubation in the apical and basal compartment in Transwell plates without cells for 7h at 4℃ and 37℃.

AF conc.	recovery [%]	
[µM]	37℃	4℃
2 a&b	81.08 +/- 2.42	82.73 +/- 0.32
5 a&b	89.89 +/- 2.13	92.61 +/- 0.71
7.5 a&b	89.99 +/- 2.0	95.07 +/- 1.66
10 a&b	83.69 +/- 4.93	91.59 +/- 3.58

At 37℃ between 81% and 90% of the initial amount were experimentally detected, whereas at 4℃ even higher recoveries resulted (83% – 95%). If the experimentally detected amounts in solution and withdrawn are seen as true values, the only values that may be imprecise and can be better estimated by the model are the amount bound to the surface and the initial donor amounts. If the experimental amounts (including the extracted amounts) are set into relation with the calculated donor amounts for the model with $C_{Donora\&b}(0)$ the recovery is slightly lower, as the calculated donor concentrations are higher for the model than the intended ones. By integration of the calculated amount adsorbed to the surface, the recovery results between 94% and 96.5%. If the experimental amounts (including the extracted amounts) are set into relation with the calculated donor amounts for the model without $C_{Donora\&b}(0)$ the recovery is dramatically higher, as the calculated donor concentrations are lower for the model than the intended ones. At 37℃ the resulting recovery is between 107 % and 117% whereas at 4℃ the recovery is between 132% and 151%. By integration of the calculated amount adsorbed to the surface, the recovery results between 94% and 100%. Again, the comparison between the experimentally determined amounts and mass balances compared to the model derived values are more consistent with the model with $C_{Donora\&b}(0)$.

5.5.5. Choice of the model for adsorption for analysis of Amentoflavone transport in Transwells with cells

The non-specific binding/adsorption taking place in Transwell plates during incubation with Amentoflavone, was found to be temperature- and concentration dependent and not

saturated in the concentration range of the performed experiments. To describe this adsorption a mathematical description of the adsorption was developed.

For the derivation of the kinetic parameters describing the adsorption two different models were compared. For both models the set of kinetic parameters was derived from fittings of experimental data of concomitant incubation of different concentrations of Amentoflavone at two distinct temperatures in Transwell plates without cells. The kinetic parameters describing the adsorption, k_{on}, k_{off} & W_{tot}, were found to be concentration-independent. With these parameters and the relations derived in the theoretical section, the adsorption over the whole incubation time can be described. The fitting of the experimental concentration data for the derivation of the adsorption parameters with the first model was performed taking into account only experimentally measured concentration values ("model without $C_{Donora\&b}(0)$"). For the second model the assumption of a donor concentration close to the expected one was taken and this values were integrated to the fitting ("model with $C_{Donora\&b}(0)$"). The main focus of the model with $C_{Donora\&b}(0)$ is the initial decrease in concentration due to non-specific binding whereas the model without $C_{Donora\&b}(0)$ describes the adsorption as a continuous process taking place over the whole period of the experiment whereas.

The fittings with both models were almost equally well as estimated by the final residual values of the fittings (data not shown). As the model with $C_{Donora\&b}(0)$ generally better predicted the experimentally measured adsorption and the values estimated with this model were found to be more consistent than with the model without $C_{Donora\&b}(0)$, the set of kinetic parameters of the first model was chosen for the fittings of Amentoflavone transport in Transwell plates with cells, modelling the adsorption as almost exclusively initial event and not a continuous process.

5.5.6. Asymmetric transport of Amentoflavone across Caco-2 cell monolayers as measured by the normalised fluxes <J>

For the analysis of the transport data of Amentoflavone no apparent permeability coefficient P_{app} was calculated as in the apical to basal permeation direction Amentoflavone showed only poor permeability. Therefore we used an normalised flux value <J> to compare different concentrations and experimental settings, as this value takes into account the whole permeated substance at the end of the experiment. Amentoflavone showed strong asymmetrical transport behaviour in confluent monolayers of Caco-2 cells (Table 6) indicating the involvement of an active efflux in the apical cell membrane during Amentoflavone transport. No concentration dependency of Amentoflavone transport was detected, neither in the apical to basal nor in the basal to apical direction. No saturation effect of Amentoflavone transport appears to happen in

the analysed concentration range. Low temperature (4℃) reduced the normalised flux <J> in the basal to apical transport direction about 50 fold, most probably by abolishing almost all of the efflux activity. The normalised flux in the apical to basal transport direction was reduced to non-detectable or inaccurate values.

Table 6: The concentration dependent normalised fluxes <J> of the Amentoflavone in the apical to basal (a_b) and basal to apical (b_a) transport direction after 7h incubation at 4 & 37℃ and in presence of Vinblastine 70 µM a&b (Vb). Data are presented as mean and standard error of the mean of 3 – 6 monolayers. NP = not performed.

	a_b			b_a			
	5µM	7.5µM	10µM	2µM	5µM	7.5µM	10µM
<J> 37℃ [cm/s ● 10^6]	0.0080 +/- 0.0025 0.0266 +/- 0.0024 (Vb)	0.0038 +/- 0.0002	0.0043 +/- 0.0002	0.6967 +/- 0.0207	0.5403 +/- 0.0596 0.2140 +/- 0.0051 (Vb)	0.5599 +/- 0.0764	0.5374 +/- 0.0611
<J> 4℃ [cm/s ● 10^6]	not detectable	NP	0.0005 +/- 0.0005	NP	0.0092 +/- 0.0011	NP	0.0091 +/- 0.0005

The addition of inhibitors of apical active efflux, Vinblastine and GF120918, to the apical and basal solution during Amentoflavone transport, resulted in a concentration dependent reduction of the normalised fluxes of Amentoflavone 5µM in the basal to apical direction (Table 7).

Table 7: The concentration dependent normalised fluxes <J> of the Amentoflavone in the basal to apical (b_a) transport direction after 5h incubation at 37℃ and in presence of different concentrations of Vinblastine or GF120918. Data are presented as mean and standard error of the mean of 3 – 15 monolayers. No permeation of Amentoflavone in the apical to basal transport direction was detected in these experiments.

	GF120918 a&b [µM]			Vinblastine a&b [µM]			
	-	0.1µM	1µM	-	3.9µM	25µM	70µM
<J> b_a AF 5µM 37℃ [cm/s ● 10^6]	5.196 +/- 0.209	3.797 +/- 0.132	2.039 +/- 0.102	5.307 +/- 0.410	3.235 +/- 0.072	3.569 +/- 0.344	0.357 +/- 0.023

The addition of GF120918 to the transport medium resulted in a clear concentration-dependent inhibitory effect on the apical efflux, as displayed by the normalised flux <J> of Amentoflavone in the b_a direction, where 1µM resulted in a decrease of the normalised flux <J> to 39.24% compared to the normalised flux <J> without inhibition. For Vinblastine also a concentration-dependent inhibitory effect on the apical efflux was observed. The inhibitory effect of Vinblastine 3.9µM and 25µM was similar, whereas the addition of Vinblastine 70µM resulted in a decrease of the normalised flux <J> in the b_a

direction to 6.73% compared to the normalised flux <J> without inhibition. The effects of GF120918 and Vinblastine on the normalised flux <J> of Amentoflavone are indicative for an involvement of P-glycoprotein in the apical efflux in Caco-2 cell monolayers. This would be in agreement with literature [Gutmann 2002], where Amentoflavone was identified as P-gp substrate. The inhibitory effect of GF120918 1µM is not complete. Concentrations of 1 – 2µM of GF120918 are usually used for complete inhibition in studies on P-gp mediated transport [Troutman 2003 B, Tran 2004]. Vinblastine in a concentration of 70µM resulted in an almost complete inhibition of the efflux activity in Caco-2 cell monolayers of passage 82 – 92 at culture days 20 – 24. If the more complete inhibitory effect of Vinblastine, a known combined inhibitor of P-gp and MRP-2, indicates an involvement of another efflux transporter than P-gp in the basal to apical transport of Amentoflavone is uncertain. The same Vinblastine concentration resulted in a decrease of the normalised flux <J> in the b_a direction to 39.61% compared to the normalised flux <J> without inhibition if Caco-2 cell monolayer of passage 60 – 64 were used at culture days 20 – 22. The Caco-2 cells showed a higher efflux activity at passages 82 – 92 as measured by the normalised flux <J>. The normalised flux in the basal to apical direction was almost 10 fold higher at higher passages.

5.5.7. Cellular accumulation of Amentoflavone / apparent volume of distribution

For the analysis of the cellular accumulation of Amentoflavone, at the end of the transport experiment, the apparent volumes of distribution V_D [ml] (Table 8) were compared. The volume of distribution was calculated by dividing the molar amount found in the cell by the donor concentration.

Table 8: The apparent volume of distribution V_D of Amentoflavone in the cellular compartment after 7h incubation at 4℃ or 37℃ and in presence of Vinblastine 70µM a&b (Vb). Data are presented in % of donor amounts as mean and standard error of the mean of 3 – 6 monolayers. NP = not performed.

	a_b			b_a				a&b
	5µM	7.5µM	10µM	2µM	5µM	7.5µM	10µM	
V_D 37℃ [ml]	0.0152 +/- 0.0007 0.2497 +/- 0.0132 (Vb)	0.0163 +/- 0.0023	0.0153 +/- 0.0006	0.0182 +/- 0.0019	0.0229 +/- 0.0030 0.4708 +/- 0.0194 (Vb)	0.0265 +/- 0.0048	0.0350 +/- 0.0040	NP
V_D 4℃ [ml]	0.0361 +/- 0.0007	NP	0.0218 +/- 0.0016	NP	0.0604 +/- 0.0012	NP	0.0394 +/- 0.0046	0.0878 +/- 0.0096

The apparent volume of distribution V_D of Amentoflavone after 7h transport was depending of the transport direction. For equal concentrations in the basal to apical direction bigger amounts were detected compared to the apical to basal direction. Low temperature (4℃) resulted in a stronger accumulation of Amentoflavone in the cellular compartment compared to 37℃. The effect was more pronounced for donor concentrations of 5µM than for 10µM. Again the accumulation was bigger for the basal to apical transport direction. The use the apical efflux inhibitor Vinblastine 70µM resulted in a 16.4 times higher accumulation in the a_b direction and a 20.6 times higher accumulation in the b_a direction for Amentoflavone 5µM. The tendency for accumulation is lower in the case of 4℃ than for the use of Vinblastine 70µM. Only for the experiments at 37℃ in the basal to apical transport direction a tendency for accumulation could be observed. For 37℃ a_b and 4℃ no evident tendency is observable. Taken together, Amentoflavone accumulates in the Caco-2 cell monolayers during the transport. The accumulation is stronger during inhibition of apical efflux transporters and at 4℃ than for uninhibited experiments at 37℃. For basal to apical transport the accumulation is stronger whereas no clear-cut concentration dependency is observable.

5.5.8. Detection of Amentoflavone phase II metabolism in Caco-2 cell monolayers using HPLC – MS

Caco-2 cell monolayers grown on petri dishes were incubated with Amentoflavone and samples were taken after 30, 150, 300 and 420min and subsequently analysed by HPLC-MS as described. In addition to Amentoflavone with retention of approximately 10min, new peaks were detected in UV at 341nm with retention between 4 – 6min (Figure 10). The peaks were not resolved by the method used and had at least 3 maxima. The AUC of these peaks was increasing with time (not shown). No new peaks were detected in the control samples consisting of Amentoflavone at the same concentration incubated in centrifuge tubes 50ml (chromatogram not shown). Therefore it's not likely that these peaks are degradation products of Amentoflavone.

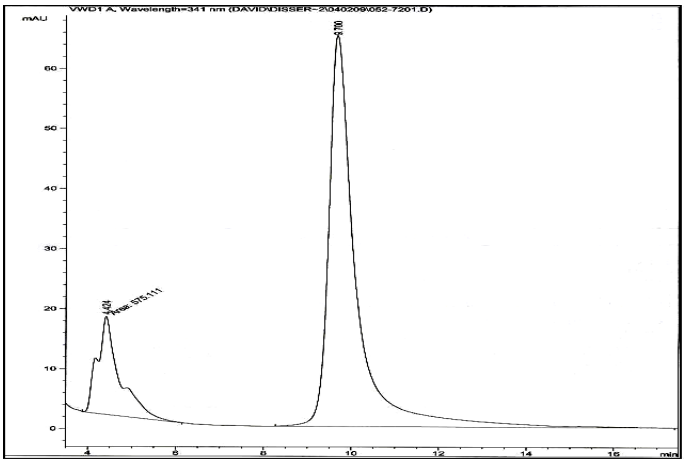

Figure 10: Representative UV chromatogram with the peaks of the Amentoflavone metabolites between 4 and 6min and Amentoflavone with retention of 9.7min.

Using negative ion mass spectra single ion mode (SIM) Amentoflavone (molecular weight 538.46g/mol) could be detected at m/z = 537. In the timeframe of the newly detected UV peaks, using negative ion mass spectra SIM two different new ions, m/z = 617 and m/z = 713 could be detected ((Figure 11) and (Figure 12)). m/z = 617 is indicative for the conjugation of a sulfuric acid moiety (80g/mol) to Amentoflavone whereas m/z = 713 is indicative for the conjugation of a glucuronic acid moiety (176g/mol) to Amentoflavone. Furthermore m/z = 537 was also detected at retention of the newly developed peaks while there was no unchanged Amentoflavone is present in UV. The peak of m/z 537 has more or less the same shape as newly developed peaks in UV (not shown). This may be due to cleavage of the conjugates in the mass detector because of the fragmentor voltage used for ionisation.

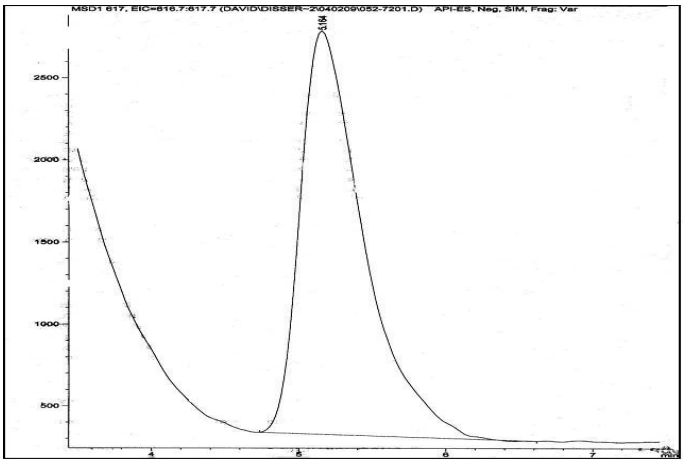

Figure 11: Chromatogram of m/z = 617 corresponding to the sulfate conjugates of Amentoflavone.

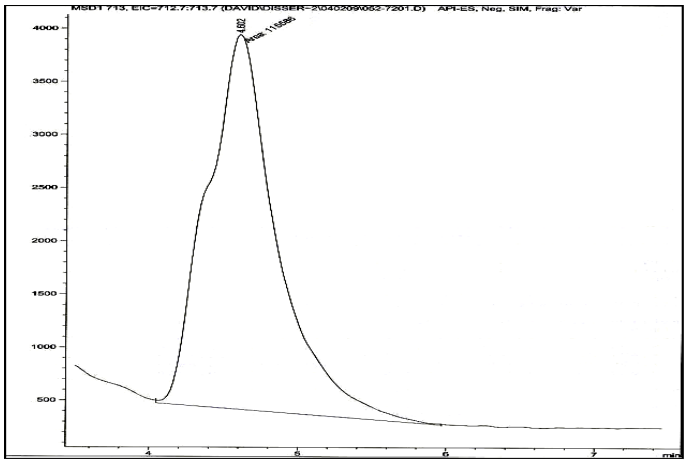

Figure 12: Chromatogram of m/z = 713 corresponding to the glucuronide conjugates of Amentoflavone.

To further concentrate evidences for phase II metabolism of Amentoflavone enzymatical cleavage of the metabolites was performed with succus helix pomatia (SHP, from BioSepra, France, a kind gift of Rodolfo Gasser, Hoffmann-La Roche, Ltd., Basel, Switzerland; data not shown), which contains both, sulfatase and β-glucuronidase. Each step of the cleavage procedure was monitored by HPLC-MS and concentrations and chromatograms of the samples with Amentoflavone and the Amentoflavone conjugates were compared to blank samples with a defined amount of Amentoflavone or just transport medium. Samples were treated either with SHP or water. After the incubation with SHP in samples with Amentoflavone conjugates neither the glucuronide metabolite nor the sulfate metabolite were detectable as monitored with m/z = 617 & m/z = 713 whereas in samples treated with water metabolite peaks were still detectable in MS. The possibility of protein binding masking the metabolites was ruled out by mass balance calculations and comparison to the peaks of samples without metabolites treated with SHP.

The quantification of the metabolites in UV was based on the following assumptions. No differentiation between the two different types of Amentoflavone conjugates was done. They were quantified together as one pool of metabolites as with the methods used the sulfate and glucuronidate conjugates could not be separated from each other. It was assumed that the metabolites had the same molar absorption coefficient as the parent compound. The UV spectral properties of the metabolites were determined with a UV scan during the analysis of samples containing metabolites (not shown). The course of the measured spectrum for the metabolites was the same as for Amentoflavone. The maxima for both curves are at approximately 270nm und 341nm. The quantification of the metabolites was therefore performed against a set of external standard solutions of Amentoflavone within the linear response concentration range. Taken all these results

together it's likely that Amentoflavone undergoes phase II metabolism in Caco-2 cell monolayers resulting in Amentoflavone sulfate and Amentoflavone glucuronide. These metabolites have the same spectral properties in UV as the parent compound and can therefore be quantified by using standard curves of Amentoflavone. With the HPLC methods used the metabolites cannot be separated and are quantified together. At least 3 different maxima of Amentoflavone conjugates could be detected indicating that there is not only one distinct sulfate or glucuronide but also different ways of conjugating the new group to Amentoflavone. Amentoflavone contains several hydroxyl groups to which the conjugation may be performed. This was also described for other substances [Galijatovic]. As the position of the conjugation to Amentoflavone was not the main focus of the present work, no further effort was taken to elucidate the exact number and structure of the different sulfates and glucuronides. The amounts of conjugates quantified together as we were only interested in the total amount of conjugates. Quantification of the conjugates was always performed with the UV chromatograms. The MS chromatograms were only used for assurance of the identity of the UV peaks in different samples.

5.5.9. Transport behaviour of the phase II metabolites: formation, efflux and cellular accumulation of Amentoflavone metabolites

The Amentoflavone metabolites were formed in every transport experiment performed at 37°C, whereas at 4°C no metabolites could be detect ed. The metabolites started to emerge in both compartments after 30min incubation time and the total amounts formed increased in an almost linear manner over time (Figure 16).

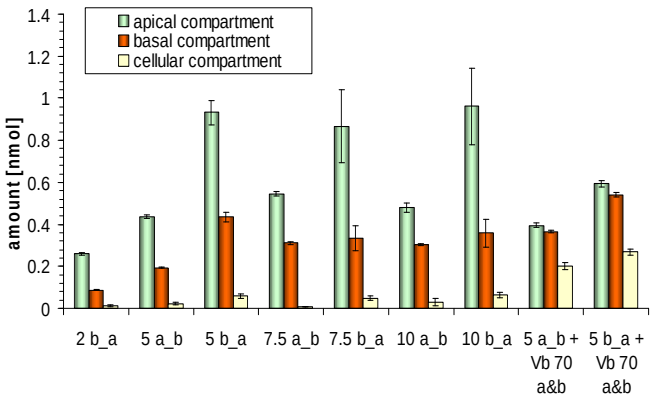

Figure 13: The concentration dependent efflux of the Amentoflavone metabolites into the apical and basolateral compartment and the accumulation of the Amentoflavone metabolites in the cellular compartment after 7h incubation at 37°C. Data are presented as mean and standard error of the mean of 3 – 6 monolayers.

In each experiment the concentrations detected in the apical compartment were higher than in the basal compartment (not shown), indicating polarised transport behaviour of

the metabolites. (Figure 13) displays the inequality in the distribution of the cumulative amounts of Amentoflavone metabolites formed after 7h incubation of Amentoflavone solely at 37°C. The amount found in the apical comp artment was almost twice as much as in the basal compartment, independent of the transport direction and donor concentration. The polarity of the distribution was almost completely abolished by the addition of Vinblastine 70µM in the apical and basal compartment, indicating the involvement of an apical efflux transporter in the transport of the metabolites. The sensitivity to Vinblastine is indicative for MRP-2, as Vinblastine is a known inhibitor of this efflux transporter [Chan, L.M.S.]. It is furthermore generally accepted that phase II metabolites are substrates for MRPs [Jia, Konig, O'Leary, Vaidyanathan]. The inhibition of the active efflux results in an enhanced cellular accumulation of the phase II metabolites compared to the situation without Vinblastine. In the basal to apical transport direction the total amount of the metabolites formed after 7h is higher than in the apical to basal direction for the same donor concentrations of Amentoflavone. No clear-cut concentration dependency on the total amounts of metabolites formed is observable in the concentration range used in the transport studies. The presence of Vinblastine in the incubation medium results in slightly higher total amounts of metabolites in the apical to basal transport direction whereas in the basal to apical transport direction no such tendency was observed.

5.5.10. Analysis of Amentoflavone transport across Caco-2 cell monolayers grown in Transwells based on the transport parameters for passive diffusion and carrier mediated efflux

Permeation data were analysed using the theoretical model for the kinetics of cellular transport presented in chapter 5.4.4. The concentration variables defined by the system of differential (Equation 60) to (Equation 71) were fitted to the experimental concentration data and optimal values of the parameters P, vk and k_M applicable to the different experimental conditions were deduced. Adsorption was integrated to the model equations and described by the set of kinetic parameters derived with the model with $C_{Donora\&b}$ (0). Numerical solution of the equations and least squares fit were performed using the software EASY-FIT (Prof. K. Schittkowski, University of Bayreuth, Germany). Concentration data of both compartments obtained from the apical to basal and the basal to apical direction of permeation were used simultaneously in the fitting. This provided a more stable regression analysis compared to the separate evaluation of each permeation direction. The drawn lines in Figure 14 to Figure 16 represent the representative best fits of Amentoflavone permeation and phase II metabolism. This is considered in all cases to be satisfactory.

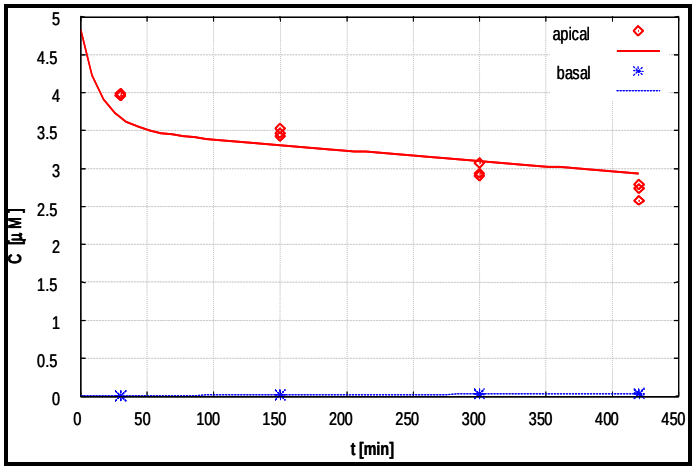

Figure 14: Representative fit of Amentoflavone 5µM apical to basal transport across Caco-2 cell monolayers at 37°C. Experimental points and model-based fitted curves. (◊) Apical concentration. (∗) Basal concentration.

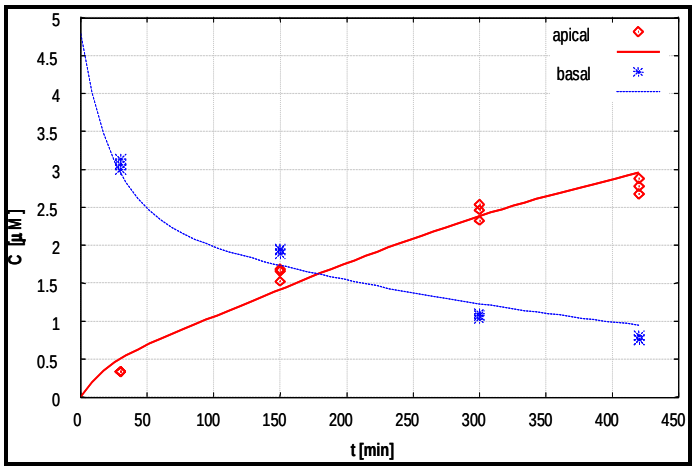

Figure 15: Representative fit of Amentoflavone 5µM basal to apical transport across Caco-2 cell monolayers at 37°C. Experimental points and model-based fitted curves. (◊) Apical concentration. (∗) Basal concentration.

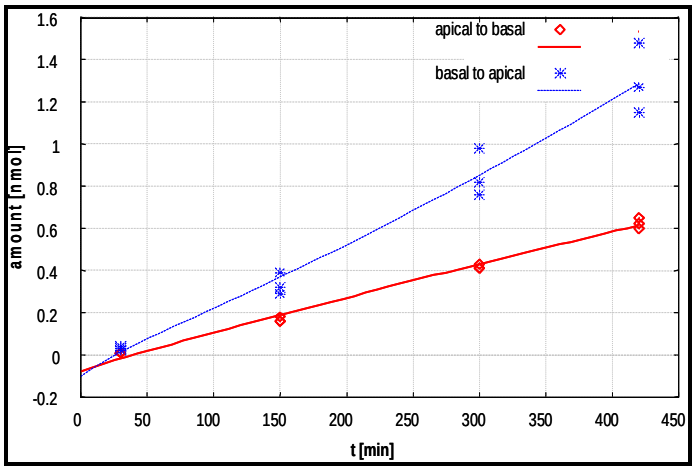

Figure 16: Representative fit of the total amount of Amentoflavone phase II metabolites formed during Amentoflavone 5µM apical to basal and basal to apical transport across Caco-2 cell monolayers at 37°C. Experimental points and model-based fitted curves. (◊) a_b transport. (∗) b_a transport.

For proper fitting of the transport data of experiments performed at 37℃, small adjustments of the model equations had to be done. (Equation 69), describing the formation of the phase II in the basal to apical transport direction, was changed to

$$\frac{dM_{MCba}}{dt} = 2 \bullet k_M \bullet M_{Cba}$$

(Equation 82)

as the experimentally detected formed total amount of metabolites was twice as much as in the apical to basal direction. This adjustment was not done for the fittings of experimental data in presence of Vinblastine or of experiments performed at 4℃ as the formed amounts of metabolites were either equal in both transport directions or no metabolites at all were formed. To simulate a lag time in the formation and excretion of the metabolites in the fitting of data from experiments performed at 37℃ (Amentoflavone alone or in presence of Vinblastine), the values of $M_{MCab}(0)$ and $M_{MCba}(0)$, the total amounts of metabolites formed at the start of the experiment, were integrated to the fitting as parameters to be estimated, resulting in negative values. This is in contradiction to reality with the amounts being zero at the start of the experiment, but is a straightforward way to model the delay in the formation and detection of the metabolites. This provided more stable fits than setting the initial values of $M_{MCab}(0)$ and $M_{MCba}(0)$ to zero or manually to negative values. For the fitting of the data of experiments performed at 4℃, the initial values of $M_{MCab}(0)$ and $M_{MCba}(0)$ were set to zero. We generally assumed, for experiments at 37℃ with Amentoflavone alone or in presence of Vinblastine, the amounts of metabolites in the cellular compartment but not being detected due to concentrations below the limit of detection of the analytical method, to be 6.5% of the total measured amounts of metabolites. This value was also integrated to the fitting (MmCab_fit = 0.935 • MmCab). An estimate of the goodness of the fits is the final residual value (FRV). The FRVs for fits of experimental data performed at 4℃ and 37℃ were all in the same range (37℃: 5 µM 0.0694, 7.5µM1st experiment 0.133, 7.5µM 2nd experiment 0.234, 10µM1st experiment 0.146, 10µM 2nd experiment 0.234 / 4℃: 5 µM 0.0679, 10µM 0.839 / Vb: 5µM 0.15), indicating the estimated values among the different experiments are of equal quality.

5.5.11. Model derived kinetic parameters for Amentoflavone absorption in Caco-2 cell monolayers

The estimated transport parameters for Amentoflavone alone at 37℃ are given in (Table 9). (Table 10) displays the transport parameters for Amentoflavone at 4℃ or at 37℃ in presence of Vinblastine 70µM.

Table 9: Kinetic parameters of Amentoflavone for transport (a_b and b_a) across Caco-2 cell monolayers for 7h at 37°C estimated by regress ion analysis with Easy-Fit. Active efflux was modelled as first order process and adsorption was calculated with the model with $C_{Donora\&b}(0)$.

$C_{Donor(0)}$ [µM]	5	7.5 1st	7.5 2nd	10 1st	10 2nd
C(0) a_b [µM]	4.83	5.55	6.26	6.87	8.02
C(0) b_a [µM]	4.80	5.48	5.77	7.65	7.64
P ● 10^{6} [cm/s]	38.1	29.5	42.0	23.1	33.6
vk [1/(s●cm^2)]	0.218	0.352	0.829	0.197	0.497
k_M [1/s]	0.0558	0.143	0.0842	0.0729	0.0528

Table 10: Kinetic parameters of Amentoflavone for transport (a_b and b_a) across Caco-2 cell monolayers for 7h at 4°C or at 37°C in presenc e of Vinblastine 70µM a&b (Vb) estimated by regression analysis with Easy-Fit. Active efflux was modelled as first order process and adsorption was calculated with the model with $C_{Donora\&b}(0)$.

$C_{Donor(0)}$ [µM]	5 / 4°C	10 / 4°C	5 / Vb
C(0) a_b [µM]	4.71	10.32	3.80
C(0) b_a [µM]	3.46	6.42	4.79
P ● 10^{6} [cm/s]	0.926	0.649	14.056
vk [1/(s●cm^2)]	0.0001	0.0045	0.0151
k_M [1/s]	0	0	0.0293

Consistent values of the passive permeability coefficient were always obtained. For the range tested no concentration dependency of the passive permeability was observed. The passive permeability was slightly lower than the model estimated permeability for Indinavir (53 * 10^{-6} cm/s) and Saquinavir (89 * 10^{-6} cm/s) [Kapitza]. As for Amentoflavone only calculated lipophilicity values (logP) are available no distinct interpretation is possible. The calculated values differ based on the source (5.753 +/- 1.0, for ACD Software Solaris V4.67, 3.102 +/- 0.829, for ACD Software Solaris V8.14 and 2.2, value calculated by PubChem) making it impossible to compare and discuss the findings based on the lipophilicity of Amentoflavone.

The passive permeability coefficient of Amentoflavone did depend on the temperature at which the transport experiments were performed. The estimated values for 4°C were about 40 fold lower than the values for 37°C. This is in agreement with diffusion theory and validates the model. The reason why the permeability coefficient calculated for the presence of Vinblastine in only about half of that without inhibition could not be anticipated on theoretical grounds and, being marginal in magnitude, cannot be further discussed unless rigorously reproduced. One reason might be due to an underestimation of the amount present in the cellular compartment (chapter 5.5.12).

Preliminary studies with Amentoflavone showed a high level correlation (r = 1) between v_{max} and K in the regression analysis (correlation matrices not shown), which meant that these parameters could not be deduced individually from each of these experiments. The

best fit was obtained when (Equation 77) was used to describe carrier-mediated transport i.e., for a transporter mediated efflux rate dependent of drug mass in the cellular compartment. The model estimated values varied for the different concentrations but were all in the same range, not showing a clear concentration effect. Again the effects of temperature and inhibition were well reflected by the model. Low temperature (4℃) lead to an almost complete abolishment of the apical carrier-mediated transport, represented by 100 – 1000 times lower values for vk. The addition of Vinblastine as inhibitor of carrier-mediated transport resulted in a 10-fold reduction of the estimated values for vk compared to no inhibition, demonstrating the ability of the model to display inhibition. As no value of v_{max} was established, no values for K could be deduced for the different experimental settings. The deduced kinetic parameter of apical efflux is global in the sense that it does not differentiate between different transporters that may be involved. This is sufficient for the delineation of the contributions of passive and carrier mediated transport processes, which was one of the objectives of the present work. For Amentoflavone up to now only P-glycoprotein was identified as a transporter involved in its transport across cell monolayers. Therefore the parameters vk can be regarded as an estimate of the mass efflux rate elicited by P-glycoprotein in Caco-2 cells. Distinguishing between parameters for individual transporters in the employed Caco-2 experimental model entails the availability and use of high specificity, high affinity inhibitors for the transporters.

For Amentoflavone transport at a concentration of 5µM, out of the efflux rate (vk = 0.218 $1/(s \bullet cm^2)$) and the average amount in the cellular compartment ($M_C$average = 0.00055nmol) an average mass efflux rate of 0.0001199 $nmol/(s \bullet cm^2)$ corresponding to 0.303 ng/s was calculated. The value is about 100 fold lower than the one calculated for Saquinavir and Indinavir (v_{max} = 0.0175µg/s) [Kapitza].

The model estimated rate constants for total phase II metabolism, k_M, are concentration independent. The effect of low temperature, with no experimental determinable phase II metabolism, is well reflected by rate constants of zero. For the presence of Vinblastine the estimated rate constant is slightly smaller than without inhibition, whereas experimental total amounts remained unaffected. This might be explained by slightly higher calculated amounts of Amentoflavone in the cellular compartment in presence of Vinblastine (chapter 5.5.12), while the total amounts are equal, resulting in a smaller estimated value for k_M, as the metabolism is modelled as first order process.

5.5.12. Comparison between the measured and calculated amount of Amentoflavone in the cellular compartment

A representative fit of the calculated amount of Amentoflavone in the cellular compartment during a_b and b_a transport is shown in (Figure 17).

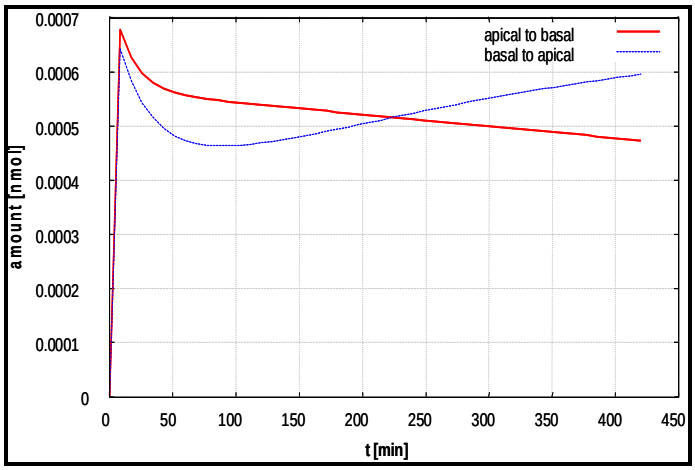

Figure 17: Calculated amounts of Amentoflavone in the cellular compartment during Amentoflavone 5µM apical to basal or basal to apical in Transwell plates with cells at 37°C. The fitting was done with the model with $C_{Donora\&b}(0)$ and the active efflux was modelled as a first order process.

In the simulation, Amentoflavone shows fast distribution into the cellular compartment within the first 10min of transport. After this initial binding the amount in the cellular compartment remains approximately constant. It is noteworthy that for a certain donor concentration both directions of transport result in similar time-profile and the final amounts of substance in the cellular compartment. The drug amounts in the cellular compartment obtained from model simulation and the comparison with the experimentally measured cell associated amounts are shown in (Table 11).

Table 11: The calculated amounts of Amentoflavone accumulated in the cellular compartment after 7h are compared to the experimental amounts. Vb = Vinblastine 70µM in the apical and basal compartment. Active efflux was modelled as first order process and adsorption was calculated with the model with $C_{Donora\&b}(0)$. NP = not performed.

AF conc. [µM]	amount cell 37℃ [nmol]		amount cell 4℃ [nmol]	
	calculated	experimental	calculated	experimental
5 a_b	0.0003	0.0759 +/- 0.0036	0.0076	0.1804 +/- 0.0037
5 a_b & Vb	0.0011	1.2485 +/- 0.0662	NP	
7.5 a_b	0.0002	0.1221 +/- 0.0173	NP	
10 a_b	0.0004	0.1528 +/- 0.0061	0.0010	0.2183 +/- 0.0157
5 b_a	0.0004	0.1145 +/- 0.0150	0.0048	0.3019 +/- 0.0058
5 b_a & Vb	0.0016	2.3539 +/- 0.0972	NP	
7.5 b_a	0.0003	0.1987 +/- 0.0359	NP	
10 b_a	0.0005	0.3504 +/- 0.0396	0.0004	0.3935 +/- 0.0457

The model obtained values didn't show a clear-cut concentration dependency, neither at 4℃ nor at 37℃. For the simulation of the 37℃ the basal to apical direction resulted in slightly higher calculated amounts whereas for 4℃ the opposite is true. The simulations for low temperature resulted in most cases in slightly higher cellular amounts compared to 37℃. The model estimated effect of Vinblastine addition is an enhancement of the cellular accumulation of Amentoflavone. Contradictory to former findings [Kapitza] the calculated values were about two orders of magnitude lower than the experimental values found by extracting the cell monolayer. This may be explained by the fact that in their study also adsorption appeared but was not integrated to the fittings, and as the model is based on mass preservation the loss of drug was accounted to the cell compartment.

The results indicated the necessity to integrate the possibility of the cellular compartment acting as a sink for at least parts of the drug permeating through this compartment in case of experimentally measured cellular accumulation, mimicking thereby binding to cell membranes, accumulation in subcellular compartments or binding to the cytoskeleton. Assuming a total geometrical cellular volume of 0.0094ml (chapter 5.4.7), the estimated volumes of distribution (chapter 5.5.7) of the experimentally measured cellular amounts are in the same range whereas the model-derived volumes of distribution differ by a factor of about 100 from the experimental values. It is a fact, that the model-estimated amounts are lower than the experimental values, the model doesn't need higher amounts of substance in the cellular compartment for good fittings. In the steady-state there is

apical efflux and phase II metabolism that diminish the cell-associated amounts. The cellular compartment is modelled as one homogeneous compartment. The concentration of drug in the compartment C_C is integrated to all the equations describing the processes in the cell (diffusion across the apical and basal membrane, apical efflux, phase II metabolism). The way the modelling is done assumes that all substance present in the cell takes part in these processes, whereas in reality only parts of the substance present in the cell is subject to these processes. The cell is an inhomogeneous compartment and the substance can distribute into a diversity of subcellular compartments or bind to membranes etc. To conclude, for the steady-state situation model estimated cellular amounts are lower than the experimentally determined amounts and lower than the respective donor concentrations.

5.5.13. Adsorption of Amentoflavone to Transwell surfaces during the transport across Caco-2 cell monolayers

After the transport experiments with cells, the Transwell plates were extracted with methanol to estimate the amount of Amentoflavone bound to the surface during the incubation. (Figure 18) shows the experimentally determined amount of Amentoflavone bound to the surface as well as the model derived total amounts (model with $C_{Donora\&b}(0)$) adsorbed the surface after incubation in Transwells without cells.

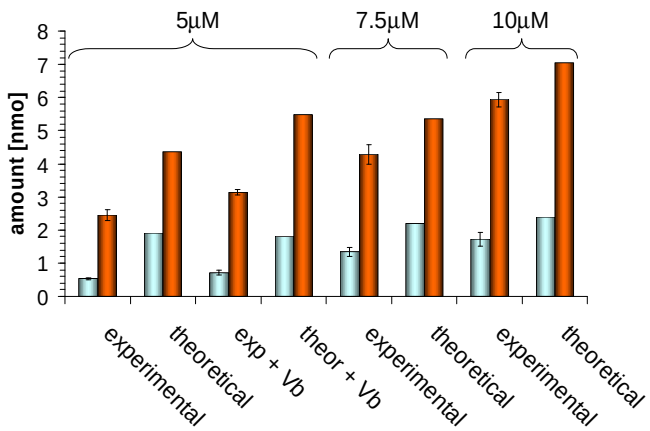

Figure 18: Amounts of Amentoflavone (AF) extracted from the Transwell plates after apical to basal (a_b) and basal to apical (b_a) transport across Caco-2 cell monolayers for 7h at 37°C. The experimental amounts are compared to the calculated amounts of Amentoflavone adsorbed to the Transwell surface. Active efflux was modelled as first order process and adsorption was calculated with the model with $C_{Donora\&b}(0)$. Experimental results are given as mean and standard error of the mean with n = 3 – 6. The light blue column indicates a_b transport and the orange column b_a transport. Vb = addition of Vinblastine 70µM in the apical and basal compartment.

The experimentally determined amounts of Amentoflavone extracted from the surface after apical to basal transport for 7h at 37°C were for 5µM 6.7% +/- 0.4, for 5µM + Vb 9.0% +/- 0.9, for 7.5µM 11.2% +/- 1.1, and for 10µM 10.8% +/- 1.3 of the initial amount at

the start of the experiment. The same experiments performed in the basal to apical transport direction yielded in the following extraction rates: 5µM 17.5% +/- 1.2, for 5µM + Vb 22.4% +/- 0.6, for 7.5µM 20.4% +/- 1.4, and for 10µM 21.2% +/- 0.8 of the initial amount at the start of the experiment. The results are not indicating a saturation effect in the concentration range tested. The basal to apical transport resulted in much higher amounts adsorbed to the Transwell surface, for the absolute amounts as well as the percentage value. This may be explained by the bigger contact area in the basal compartment and the better distribution of Amentoflavone between the two compartments during basal to apical transport, whereas in the apical to basal transport direction almost no Amentoflavone permeates. Representative calculated concentrations of Amentoflavone bound to the surface of the apical and basal compartment during a_b and b_a transport are shown in (Figure 19) and (Figure 20).

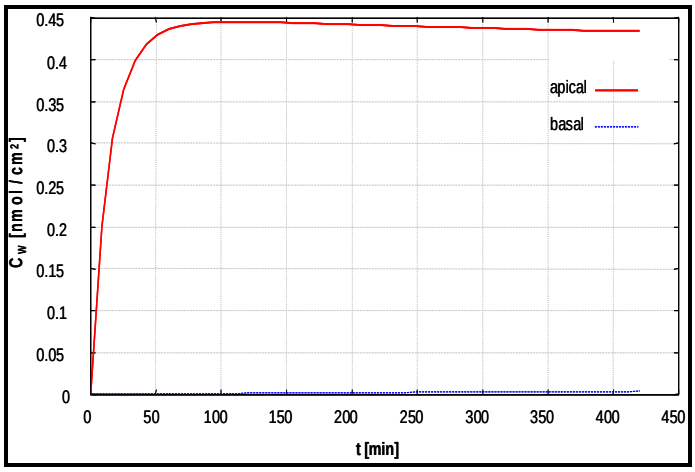

Figure 19: Calculated amounts of Amentoflavone adsorbed to the apical or basal Transwell surface during Amentoflavone 5µM apical to basal in Transwell plates with cells at 37°C. The fitting was done with the model with $C_{Donora\&b}(0)$ and the active efflux was modelled as a first order process.

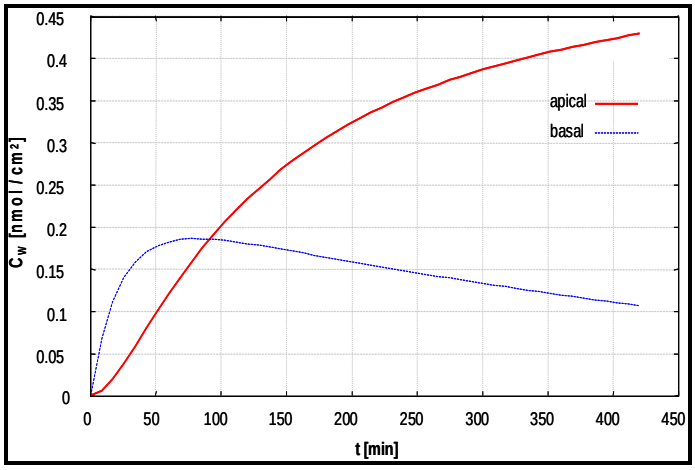

Figure 20: Calculated amounts of Amentoflavone adsorbed to the apical or basal Transwell surface during Amentoflavone 5µM basal to apical in Transwell plates with cells at 37°C.

The fitting was done with the model with $C_{Donora\&b}(0)$ and the active efflux was modelled as a first order process.

For both transport directions, in the donor compartment a fast initial binding of Amentoflavone to the surface with a maximum concentration bound after 60min is observable. In the a_b direction the concentration of substance bound to the surface remains roughly constant, as the decrease in the solution concentration after 60min is small. The strong decrease in the solution concentration (as the determinant factor in adsorption) in the basal compartment during b_a transport results in desorption of substance after the maximum concentration bound to the surface is reached. In the a_b direction only small amounts permeate to the basal compartment, resulting in almost negligible surface concentrations. Contrarily, in the b_a direction there is a constant flux to the apical compartment, resulting in an adsorption profile comparable to the solution concentration profile.

The adsorbed amounts calculated by the model are generally higher compared to the experimentally measured values, with the deviations in the basal to apical direction being smaller than in the apical to basal direction. Likewise the deviations were smaller for higher donor concentrations. For basal to apical transport direction the amounts calculated with the model with deviated from the experimentally measured by +78.6%, +75.5%, +25.4%, and +18.5% compared to apical to basal transport direction with deviations of +259.0%, +151.1%, +63.9%, and +39.2%. The reason for the better consistence of the calculated values for the basal to apical transport with the experimental values than for the apical to basal transport is ambiguous.

One reason for the high values of the calculated amounts bound to the surface may be the fact that the model estimated amounts for Amentoflavone associated with the cellular compartment are too low (chapter 5.5.12). The model equations may attribute some of the Amentoflavone present in the system to the surface rather than to the cellular compartment. But this may only explain part of the difference between the experimental and the calculated amounts. Another option would be an experimental underestimation of the amount adsorbed to the surface as discussed for the situation without cells (chapter 5.5.4). The effect of the addition of Vinblastine on the adsorption of Amentoflavone is unclear, as we only used one concentration combination of the two compounds. The experimentally determined amounts bound to the surface are higher after the addition of Vinblastine, whereas the calculated amounts are in the same range for both experimental settings. Further exploration of different concentration combinations would be needed to gain more insight into the effect of Vinblastine on Amentoflavone adsorption in Transwells.

The experimental amounts extracted for experiments performed at 4°C exhibited a contradictorily behaviour. For the apical to basal transport smaller amounts were extracted than for the experiments performed at 37°C (for 5µM 0.4862nmol +/- 0.0425 vs. 0.5328nmol +/- 0.0317 and for 10µM 1.2022nmol +/- 0.0609 vs. 1.7199nmol +/- 0.2126) whereas in the basal to apical direction the expected higher amounts bound to the surface were found for the lower temperature (for 5µM 5.6654nmol +/- 0.1452 vs. 2.4488nmol +/- 0.1618 and for 10µM 11.4381nmol +/- 1.0478 vs. 5.9362nmol +/- 0.2149). These experimentally determined amounts reflected in the apical to basal transport direction for 5µM 6.1% +/- 0.5 and for 10µM 15.0% +/- 0.8 and in the basal to apical transport direction for 5µM 27.0% +/- 0.7 and for 10µM 40.9% +/- 3.7of the initial amount at the start of the experiment. The deviations of the calculated amounts from the experimentally determined ones were extreme for the apical to basal direction (for 5µM +607.6% and for 10µM +343.1%) whereas the basal to apical direction was well described by the model (for 5µM -6.2% and for 10µM -17.8%). Taken together these values indicated, the model cannot precisely describe in all cases the adsorption in the situation with cell monolayers present in the Transwell. For the basal to apical transport direction the model yields nevertheless in quite reasonable estimates of the adsorption. For a more accurate description of the adsorption during apical to basal transport further exploration of the adsorption behaviour would be necessary. As the model for adsorption only included the plastic surface of the surface and the polycarbonate membrane of the Transwell was neglected, the possible influence of the filter support on the adsorption should be evaluated.

5.5.14. Model estimated donor amounts/concentrations for Amentoflavone transport in Transwells with cells

The drug concentrations at time zero, $C_A(0)$ and $C_B(0)$, obtained from the best fit were smaller than the theoretical concentrations of the prepared aqueous solutions despite the integration of the adsorption to the model equations. The donor concentrations obtained for the apical to basal transport at 4°C were in better agreement with the intended ones (88 – 103%) than for the basal to apical transport (64 – 78%), again indicating the vital role of the basal compartment with its larger surface in the adsorption and that the model is an approximation of the reality with the adsorption parameters being descriptive for both compartments together and not for one compartment alone. The donor concentrations obtained for transport at 37°C yielded in better concordance for the apical to basal and the basal to apical transport direction, with no tendency for one direction resulting generally in higher donor concentrations. The estimated donor concentrations were in the range of 68.7 – 96.6% of the intended donor concentrations with the majority

of the values in the range of 75 – 85%. The lower calculated donor concentrations is to be attributed to some loss of drug during preparation as the time from the preparation of the solutions until the addition to cells was longer than during the experiments without cells. A second possible reason could be an initial binding of the drug to the cells resulting in lower solution concentrations than in Transwells without cells but with the same donor amounts, and therefore leading to lower calculated donor concentrations.

5.5.15. Mass balances of Amentoflavone transport in Transwells with cells

Mass balances were calculated for the permeation experiments by addition of the amount in solution after 7h, the amount withdrawn during the experiment, the amount metabolised and the amount extracted with methanol from the Transwell surface. The intended donor amount provided the reference for calculation. The mass balances for experiments performed at 37℃ yielded in the apical to basal direction recovery rates of 55.6 – 74.6% and in the basal to apical direction 61.4 – 77.7% if only experimental values were regarded. If the measured amounts were set into relation with the model derived donor concentrations recovery rates were in the a_b direction between 71.5 and 96.4% and in the b_a direction between 75.2 and 99.9%. By replacing the experimentally measured amounts adsorbed by the model derived values recovery rates in the a_b direction were mainly between 85.4 and 95% with two outliners of 77.1 and 113.9%. In the b_a direction recovery rates with the calculated amounts adsorbed were all between 88.3 and 103.4%. The mass balances for experiments performed at 4℃ yielded in the apical to basal direction recovery rates of 57.3 and 75.4% and in the basal to apical direction 65.7 and 66.9% if only experimental values were regarded. If the measured amounts were set into relation with the model derived donor concentrations recovery rates were in the a_b direction 59.7 and 75.6% and in the b_a direction between 95.5 and 101.2%. By replacing the experimentally measured amounts adsorbed by the model derived values recovery rates in the a_b direction were 98.1 and 96.1% and in the b_a direction 92.0 and 90.0%.

5.5.16. Conclusion

In the present study the transport of Amentoflavone in the Caco-2 model was studied. Amentoflavone showed polarised transport behaviour elicited by P-glycoprotein, was subject to glucuronidation and sulfatation by the cells and strongly adsorbed to the Transwell apparatus. We employed mathematical modelling encompassing passive diffusion, carrier-mediated transport, carrier inhibition, phase II metabolism and non-specific binding in order to describe the processes taking place in the transport and to estimate unbiased transport parameters that are characteristic for the drug and the cell

culture system in use. The quantitative assessment of kinetic phenomena taking place in the cell culture system used in the drug absorption studies could be well described by the proposed model of cellular transport. The model-based evaluation of the experimental results of this study shows that the developed model for describing the kinetics of permeation in the Caco-2 cell monolayer makes it possible to distinguish in a quantitative fashion between the contribution of passive permeation and carrier-mediated efflux to drug transport in this system. Reasonable values for the passive permeability coefficient and for the carrier-mediated transport, were obtained by the model. The influence of temperature and inhibition was well reflected by the two parameters. The estimated kinetic constants for metabolism and adsorption are not a complete description of the processes taking place in reality but are useful tools to describe the transport. The inclusion of adsorption and phase II metabolism to the model allowed us in the first place to analyse Amentoflavone transport, as the cellular transport could be corrected for this distorting effects. This analysis is proposed as a tool for independently determining the contribution of the individual transport processes to the overall cellular permeation.

6. Individually studied absorption of Digoxin, Quinidine, and Verapamil across Caco-2 cells and the influence of binary combinations on passive diffusion and active efflux, analysed with a mathematical model for determination of drug absorption parameters.

6.1. Abstract

Purpose

The present study's aim was the further evaluation of a mathematical model for delineating the passive and carrier mediated contributions to the absorption of some apical efflux substrates in Caco-2 cell monolayers. Special respect was given to the effect of concentration and binary combinations of substances, on permeation in terms of these two contributing factors, passive diffusion and active apical efflux and the comparison with the conventional approach to analyse data from transport experiments, the calculation of the apparent permeability P_{app}.

Material and methods

The epithelial membrane transport kinetics of the P-glycoprotein substrates Digoxin (0.5 – 100µM), Quinidine (1 – 200µM) and Verapamil (5 – 1000µM) alone and during concomitant incubation of different combinations were studied using Caco-2 monolayers cultured in the Transwell system. The system of differential equations of the developed mathematical model was fitted to experimental concentration data, and optimal values of the kinetic parameters were deduced using the software EASY-FIT. Kinetic analysis of the carrier-mediated transport and the passive permeability was performed with respect to concentrations-dependency of these and parameters and the influence of concomitant transport.

Results

All compounds used showed asymmetrical transport across Caco-2 cell monolayers, the extent of which depended on the compound and the concentration used. The P_{app} values for all three compounds were compared to previously reported ones and found to be comparable. Consistent values for the model estimated passive permeability coefficients were obtained with Verapamil possessing the highest and Digoxin the lowest passive permeability. No concentration dependency of the passive permeability was observed in the range tested. The parameter for the carrier-mediated efflux rate, vk, was different for each compound and concentration, reflecting the different propensity of the drugs to be apically effluxed and allowing quantitative assessment of the efflux. Only for Quinidine saturation of the apical efflux was observed. Comparison of the P_{app} with the model

estimated kinetic parameters demonstrated the sensibility of its values to small deviations in the mode of calculation and the necessity of sink-conditions for the calculation of accurate values of P_{app}. The contributions and the interplay of passive diffusion and active efflux to the net mass flux across the Caco-2 cells were different for all three compounds and changed in a concentrations-dependent manner. The model-derived parameters from transport experiments with concomitant incubation of two compounds, demonstrated different levels and potencies of interactions between the compounds. Depending on the combination and the concentrations used, both reduction and enhancement of the apical efflux rate and the passive permeability were observed.

Conclusions

The present study demonstrates the utility of the proposed mathematical model for kinetic analysis of transport phenomena in confluent monolayers of Caco-2 cells cultured in the Transwell system. The model-derived parameters are less susceptible to distorting effects like non-sink conditions and allow their determination by simple fitting of concentration-time profiles. It was demonstrated, that consistent values for passive permeability and efflux rates are calculable by the model and that interactions between compounds are well reflected by the kinetic parameters.

6.2. Introduction

One essential step in modern drug discovery and development is the evaluation and analysis of the ADME properties of a new active pharmaceutical ingredient (API). For the rapid assessment of these properties many *in vitro* and *in situ* methods were developed with different levels of complexity and sophistication [Bohets, Hidalgo 2001]. Cell free, lipid based assays like PAMPA [Avdeef 2003, Kansy] allow higher throughput and easier miniaturization compared to cell models that allow mechanistic studies. In order to probe the mechanistic aspects of solute transport, simplified models of the respective cellular barrier have been developed in recent years. In many cases, the cells that comprise these barriers, or cells that serve to mimic the barrier of interest, can be maintained in culture [Ho]. To study the drug permeability at different sites in the human body cell models for intestinal permeation (e.g. Caco-2 and 2/4/A1), for the blood – brain barrier (primary cell culture and immortalized cell lines), for hepatic drug metabolism and transport and for the renal drug transport are accessible [Deli, Ghibellini, Hidalgo 1989, Schlatter, Tavelin]. The different models can be wild – type (Caco-2, MDCK), transfected (h-MDR1-MDCKII), or downregulated [Hilgendorf] cell lines.

The use of *in vitro* cell permeation experiments across cell monolayers to study the absorption of substances is widely accepted and popular [Artursson 2001, Balimane 2005]. Depending on the compounds used and the experimental setting, the purpose of these studies can be the general assessment of the permeability of a compound [Artursson 2001], the development of structure – permeability relationships [Chen 2006], the development of *in vitro* – *in vivo* correlations [Artursson 1991 B, Usansky, Yee], to identify transporters (influx and efflux) involved in cellular permeation [Maeda], the study of transporter kinetics and development of comprehensive models of transporter function [Tran 2005], the study of the interplay between transporters and metabolism [Benet], the study of drug – drug interactions [Rautio] and the study of formulation effects [Kapitza, LeCluyse].

In the recent past years the awareness of the necessity of detailed and precise analysis of data derived from *in vitro* permeation experiments arose. The approaches of different research groups can be focused on modelling and experimental determination of (sub-) cellular pharmacokinetics and distribution [Duvvuri, Zhang], more exact estimations of the passive permeability coefficient [Tran 2004], the influence of the transport direction on the apical active efflux [Troutman 2003 A], consideration of the influence of the aqueous boundary layer on estimated transporter kinetics from overexpresion systems [Balakrishnan].

When examining drug permeability and the influence of carrier-mediated transport *in vitro* models it is customary to use an approximate solution for the permeability coefficient P_{app} and based on that the calculation of the efflux ratio under sink conditions. This approach is afflicted with limitations [Youdim, Tran 2004]. To identify substrates for active efflux transporters like P-glycoprotein by calculation of the ER the estimated P_{app} values have to within an optimal range. For substrates that have P_{app} values outside of this range, the identification as a substrate is prone to fail by using this approach [Polli]. Recently it was shown that the effects of P-glycoprotein mediated efflux on the absorptive and secretory transport may not be symmetrical, per given donor concentration [Troutman 2003 A].

An alternative approach to the use of the apparent permeability coefficient and its improvements is the use of biophysical modelling of the transmembrane events involving passive diffusion and efflux mechanisms. The intent of such modelling is to delineate and quantify the mass transfer mechanisms that take place during permeation. This approach may furthermore provide means for the evaluation of the influence of type and concentration of the chosen compound as well as the influence of a second substance or of excipients on the permeation in terms of passive diffusion and active efflux, depending on the exact mode of modelling. These models can provide information about critical parameters and the behaviour of the system if the parameters are changed. In the study of efflux transporters the modelling and the measurement of the kinetic characteristics of transport can be a powerful approach to enhancing the understanding of their function and mechanism or probe different hypothesis about the exact mode of efflux [Litman 2003, Tran 2005]. Other modelling approaches including both, passive diffusion and active efflux focus on the use of these procedures as tools for improving the prediction ability of *in vitro* models [Rodriguez-Ibáñez].

Our group recently published a mathematical model to describe the transport of drug between the apical, the basal, and the cellular compartment [Kapitza], which enables the direct estimation of the transport parameters from concentration-time profiles of permeation experiments. The developed model took into account passive permeation described by the permeability coefficient P and carrier mediated efflux described by the kinetic parameter vk. In another publication [Blaser] we presented extensions to the model with inclusion of phase II metabolism and adsorption to the Transwell surface. In the present publication with used the mathematical model for delineation of cell permeation kinetics of Digoxin, Quinidine, and Verapamil. All three compounds are well known to be P-glycoprotein substrates and inhibitors. The focus was the concentration-dependent assessment of the contributions of passive diffusion and carrier-mediated transport to the overall permeation characteristics. The model derived kinetic parameters

were then compared to the conventional P_{app} values. A second part of the publication deals with the effect of concomitant incubation of two different compounds on the passive permeability and the efflux rate of the two compounds.

6.3. Materials and methods

6.3.1. Materials

The human colon adenocarcinoma cell line Caco-2 was a gift of Prof. H. P. Hauri, Biocenter, University of Basel, and originated from the American Type Culture Collection (ATCC, Rockville, MD, USA). Dulbecco's modified Eagle's medium (DMEM) (with l-glutamine, 4500mg/l D-glucose, without sodium pyruvate), l-glutamine 200mM (100x), MEM non-essential amino acids solution (100x, without l-glutamine), foetal bovine serum FBS, Trypsin-EDTA (10x) liquid, and Dulbecco's Phosphate Buffered Saline (without Ca^{2+} Mg^{2+}) were all purchased from Gibco (Gaithersburg, MD, USA). For cell culture DMEM was supplemented with 10% (v/v) FBS, 2mM l-glutamine, and 1% MEM. Transport media used for the permeation studies and the cytotoxicity experiments were made with Dulbecco's modified Eagle's medium (DMEM) base (without glucose, l-glutamine, phenol red, sodium pyruvate and sodium bicarbonate) (SIGMA-Aldrich, Fluka Chemie GmbH, Buchs, Switzerland). This was dissolved in bi-distilled and autoclaved water and supplemented with glucose (4.5g/l), HEPES (4.76g/l), NaCl (1.987g/l) and l-glutamine (0.876g/l), the pH was adjusted to 7.40 and the final medium was subjected to sterile filtration. Glucose, Hepes, NaCl and l-glutamine were all obtained from SIGMA-Aldrich, (Fluka Chemie GmbH, Buchs, Switzerland). Petri dishes (56.7cm^2), 24-well plates and 96-well plates were from Nunc (Roskilde, Denmark) and the 6-well Transwell plates were from Costar, Corning (NY, USA). Quinidine Hydrochloride Monohydrate (Dihydroquinidine content 11%) and ($^+$/-)-Verapamil Hydrochlorid (minimum 99.0% titration) were obtained from SIGMA-Aldrich (Fluka Chemie GmbH, Buchs, Switzerland). Digoxin (purum; >95.0% (HPLC)), dimethylsulfoxid (DMSO), sodium dodecyl sulfate (SDS) and the thiazolyl blue tetrazolium bromide for the MTT assay were purchased from Fluka (Fluka Chemie GmbH, Buchs, Switzerland). All other reagents were of analytical grade.

6.3.2. Cell culture

Caco-2 cells were grown in petri dishes and maintained at 37°C in an atmosphere of 8% CO_2 and in equilibrium with distilled water using culture medium. They were passaged by treatment with 0.25% trypsin and 2.65mM EDTA with a splitting ratio of 1:12. The medium was changed every alternate day until the petri dishes reached 90% confluence. Cells were used at passage number 60 – 65.

6.3.3. MTT-assay

Mitochondrial activity of the cell was evaluated by the 3-(4,5-dimethylthiazol-2-yl)-2,5-diphenyl-2*H*-tetrazolium bromide (MTT) assay. This assay is based on the reduction of

MTT by hydrogenase activity in functionally intact mitochondria [Mosmann]. The hydrogenase catalyses the conversion of the yellow MTT reagent to blue formazan crystals. Caco-2 cells were seeded on 24-well plates or 6-well Transwell plates at a density of 114,000cells/cm^2 and used for experiments 9 days postseeding (24-well plates) or 22 days post-seeding (6-well Transwell). Medium was changed every other day. The effect of concentration of Digoxin, Quinidine and Verapamil and combinations of these compounds was investigated using 3 wells per group. The treatment of the cells with respect to the preparation steps before incubation and the incubation time was the same as in the transport experiments with the compound and concentration in question. After removing the culture medium, cells of the 24-well plates were rinsed once with 1.5ml D-PBS (with Ca^{2+} und Mg^{2+}) and 1000µl of the transport medium were added to each well. The cells of the 6-well Transwell plates were rinsed on the apical side with 3.5ml and on the basal side with 4ml D-PBS (with Ca^{2+} und Mg^{2+}) and 1600µl of the transport medium was added to the apical compartment and 2800µl of the transport medium was added to the basal compartment of each well. The plates were then incubated for 60min in the incubator (Sorvall Heraeus, Heracell, Kendro, Switzerland). Then the compounds were added to the transport medium and the cells incubated for 3h in the incubator hood (TH 15, Edmund Bühler GmbH, Tübingen & Hechingen, Germany) at 37℃ in a water vapour saturated atmosphere and shaken at 75rpm on a compact shaker (KS 15, Edmund Bühler GmbH, Tübingen & Hechingen, Germany). After removing the incubation solutions, the cells of the 24-well plates were rinsed with 1ml D-PBS (with Ca^{2+} und Mg^{2+}) and 800µl culture medium and 80µl MTT solution (5mg/ml in D-PBS (without Ca^{2+}, Mg^{2+})) was added to each well resulting in a final MTT concentration of 0.45mg/ml. The cells were then incubated for another 4h in the incubator. The cells of the 6-well Transwell plates were rinsed on the apical side with 3.5ml and on the basal side with 4ml D-PBS (with Ca^{2+} und Mg^{2+}). The inserts were then transferred to petri dishes and 1500µl culture medium and 150µl MTT solution (5mg/ml in D-PBS (without Ca^{2+}, Mg^{2+})) was added to the apical compartment of each well resulting in a final MTT concentration of 0.45mg/ml. The cells were then incubated for another 4h in the incubator. Subsequently the cells of the 24-well plates were lysed and developed formazan crystals were dissolved by adding 800µl lysis buffer containing 10% SDS in 0.01 M HCl [Tada] and incubation for 15 h in the incubator. In the case of the 6-well Transwell plates 1500µl lysis buffer were added. The amount of formazan was quantified in quadruplicate by transferring 200µl to a 96-well plate and measuring the absorbance at 580nm (reference wavelength 650nm) using an ELISA plate reader (VERSAmax, Molecular Devices, Sunnyvale, CA, USA). 10µl of ethanol absolutum were added to

avoid foam. Mitochondrial activity was expressed relative to a control group treated with transport media.

6.3.4. TEER

The transepithelial electrical resistance (TEER) of cultured cells on Transwell inserts was monitored before and after each permeation experiment with an EVOM epithelial voltohmmeter (World Precision Instruments WPI, Berlin, Germany). Before the experiment, Caco-2 monolayers were washed on the apical side with 3.5ml and on the basal side with 4ml D-PBS (containing Ca^{2+} und Mg^{2+}) and 1600µl of the transport medium were added to the apical compartment and 2800µl to the basal compartment. The 6-well Transwell plates were then incubated for at least 60min in the incubator before the pre-experiment TEER measurement. Before the post-experiment TEER measurement the withdrawn sampling volume was replaced with transport medium. The TEER measurements were performed at 37°C in the End ohm-24 Chamber (World Precision Instruments WPI, Berlin, Germany) containing 4.6ml transport medium. Physiologically and morphologically well-developed confluent Caco-2 monolayers (at least 18 days old) with TEER values above 250Ωcm^2 were used in the experiments.

6.3.5. Individual permeation of Digoxin, Quinidine and Verapamil across Caco-2 cell monolayers at 37°C

Cells were seeded at a density of 114,000 cells/cm^2 onto 6-well Transwell plates with an insert area of 4.7cm^2 and a pore size of the polycarbonate membrane of 0.4µm. Culture medium was changed every other day and cell monolayers were used between 18 and 22 days post seeding. The drug was added from a stock solution after the TEER measurement either in the apical or in the basal compartment with respect to the cell monolayer. The transport directions were therefore apical to basal (a_b) and basal to apical (b_a). Bidirectional transport of different concentrations of Digoxin (0.5, 1, 2.5, 5, 10, 20, 35, 50, 65, 80 & 100µM), Quinidine HCl (1, 2.5, 5, 7.5, 10, 20, 30, 40, 50, 65, 80, 100, 150 & 200µM), Verapamil HCl (5, 7.5, 12.5, 25, 50, 75, 100, 150, 200, 250, 500, 750 & 1000µM) alone was investigated in these permeation studies. Three wells were used in each group (concentration and transport direction). Permeation of drug across the cell monolayer was monitored by sampling the solutions in both compartments, at predefined time points for the duration of 3h. Samples of 54µl were drawn after 15, 30, 45, 60, 90, 120 and 180min. 6µl of a solution of Tween 80 0.1% (v/v) were added to the sample. The samples were mixed with a reagent mixer. The withdrawn volume was not replaced. The samples were collected in glass vials (Infochroma AG, Zug, Switzerland and Schmidlin Labor & Service AG, Sarbach, Switzerland) except for all experiments including Digoxin in which polypropylene vials (Milian AG, Geneva, Switzerland and Agilent Technologies,

USA / Basel, Switzerland) were used. The starting volume of the apical solution was 1600µl and the one of the basal solution 2800µl. During the permeation experiment the Transwell plates were kept at 37°C in a water vapour saturated atmosphere in the incubation hood and agitated on an orbital compact shaker at 75min^{-1}. After the permeation experiment the TEER values of the cell monolayers were measured again. Only data derived from experiments with final TEER values exceeding 80% of the initial values was used.

6.3.6. Drug permeation of binary combinations of compounds across Caco-2 cell monolayers at 37°C

Caco-2 cells were grown on 6-well Transwell plates as previously described. The drugs were added together after the TEER measurement either in the apical or in the basal compartment with respect to the cell monolayer. Bidirectional transport of different combinations of compounds and concentrations were studied in these permeation studies (Table 12 to Table 14). Three wells were used in each group (compound combination, concentration and transport direction). Permeation of drugs across the cell monolayer was monitored as described before. After the permeation experiment the TEER values of the cell monolayers were measured again. Only data derived from experiments with final TEER values exceeding 80% of the initial values was used.

Table 12: Combinations of Digoxin and Quinidine used to study concomitant transport in Caco-2 cell monolayers.

combination number	Digoxin [µM]	Quinidine [µM]
1	1	250
2	1	250
3	10	250
4	10	250
5	50	5
6	50	50
7	50	250
8	100	1
9	100	10
10	100	50
11	100	100
12	100	250

Table 13: Combinations of Quinidine and Verapamil used to study concomitant transport in Caco-2 cell monolayers.

combination number	Quinidine [µM]	Verapamil [µM]
1	1	500
2	10	25
3	10	100
4	10	250
5	10	500
6	20	250
7	20	500
8	50	50
9	100	25
10	100	50
11	100	100
12	250	5
13	250	25

Table 14: Combinations of Digoxin and Verapamil used to study concomitant transport in Caco-2 cell monolayers.

combination number	Digoxin [µM]	Verapamil [µM]
1	100	5
2	100	25

6.3.7. HPLC

Drug concentration in the samples of the Digoxin experiments was determined by capillary HPLC (Agilent series 1100, Agilent Technologies, USA) with a capillary pump G1376A, an autosampler G1377A µWPS and a variable wavelength detector G1314A. A C-8 reversed phase column (MB 125/1 Nucleosil 100-5 C8ec, Macherey-Nagel, Oensingen, Switzerland) and the following mobile phase was used: H_2O (bi-distilled and filtered through 0.45µm)/MeOH/THF/acetic acid 96% (v/v) = 52/38/9/1. 5g/l ammonium acetate was dissolved in the mobile phase. pH-value at 25°C was 4.92. An isocratic method was used for quantification. The flow rate was 50µl/min, the injection volume 40µl and the runtime 8min. Digoxin was detected at 220nm in UV. Using this method the retention of Digoxin was approximately 4.5min. Quantification was performed against a set of external standard solutions within the linear response concentration range.

Drug concentration in the samples of the Quinidine experiments was determined by capillary HPLC with the same column, mobile phase and injection volume as Digoxin. An isocratic method was used for quantification. The flow rate was 50µl/min, the injection volume 40µl and the runtime 6min. Quinidine was detected at 250nm in UV. Using this method the retention of Quinidine was approximately 3min. Quantification was performed

against a set of external standard solutions within the linear response concentration range.

Drug concentration in the samples of the Verapamil experiments was determined by capillary HPLC with the same column, mobile phase and injection volume as Digoxin. An isocratic method was used for quantification. The flow rate was 50µl/min, the injection volume 40µl and the runtime 6min. Verapamil was detected at 280nm in UV. Using this method the retention of Verapamil was approximately 3.5min. Quantification was performed against a set of external standard solutions within the linear response concentration range. Alternatively, drug concentration in the samples of the Verapamil experiments was determined by capillary HPLC with the same column as Digoxin but a gradient method and the following mobile phases. Mobile phase A: H_2O (bi-distilled and filtered through 0.45µm)/MeOH/THF/acetic acid 96% (v/v) = 59/19/11/11. 1.994g/l ammonium acetate was dissolved in the mobile phase. Mobile phase B: H_2O (bi-distilled and filtered through 0.45µm)/MeOH/THF/acetic acid 96% (v/v) = 10/65/12/13. 1.994g/l ammonium acetate was dissolved in the mobile phase. The flow rate was 50µl/min, the injection volume 40µl and the runtime 15min. The gradient method started with 100% of A. From 0 to 9min the composition of the mobile phase was changed to 100% of B and then until the 10.min back to 100% of A. Verapamil was detected at 280nm in UV. Using this method the retention of Verapamil was approximately 4min. Quantification was performed against a set of external standard solutions within the linear response concentration range.

Drug concentration in the samples of experiments of Digoxin in combination with Quinidine was determined by capillary HPLC with the same column and mobile phase as Digoxin alone. An isocratic method was used for quantification. The flow rate was 50µl/min, the injection volume 40, 20 or 10µl, depending on the concentrations used and the runtime was 8 or 11min. Digoxin was detected at 220 or 240nm in UV and Quinidine at 250nm in UV. Using this method the retention of Quinidine was approximately 3min and the retention of Digoxin was approximately 4.5min. The method could be used within a concentration range of 1µM-100µM for Digoxin and 1µM-250µM for Quinidine. Quantification was performed against a set of external standard solutions within the linear response concentration range.

Drug concentration in the samples of experiments of Digoxin in combination with Verapamil was determined by capillary HPLC with the same column as Digoxin alone and the following mobile phase was used: H_2O (bi-distilled and filtered through 0.45µm)/MeOH/THF/acetic acid 96% (v/v) = 62.4/28/9/0.6. 5g/l ammonium acetate was

dissolved in the mobile phase. pH-value at 25°C was 4.93. An isocratic method was used for quantification. The flow rate was 50µl/min, the injection volume 40µl and the runtime 15min. Digoxin was detected at 240nm in UV and Verapamil at 280nm in UV. Using this method the retention of Verapamil was approximately 6min and the retention of Digoxin was approximately 12min. Quantification was performed against a set of external standard solutions within the linear response concentration range.

Drug concentration in the samples of experiments of Quinidine in combination with Verapamil was determined by capillary HPLC with the same method as Digoxin in combination with Verapamil. An isocratic method was used for quantification. The flow rate was 50µl/min, the injection volume 20µl and the runtime 10min. Quinidine was detected at 250nm in UV and Verapamil at 280nm in UV. Using this method the retention of Quinidine was approximately 4min and the retention of Verapamil was approximately 6min. Quantification was performed against a set of external standard solutions within the linear response concentration range. The method could be used up to a concentration 500µM for Quinidine and 500µM Verapamil at the same time.

6.3.8. Calculation of the apparent permeability coefficient and the efflux ratio

For all compounds used, the apparent permeability coefficient (P_{app}) in the apical to basal as well as in the basal to apical transport direction and the efflux ratio (ER) were calculated after 15min. The P_{app} was calculated using the following relation:

$$P_{app} = \frac{V_R * \Delta C_R}{\Delta t * S * C_{D0}} = \frac{dA}{dt * S} * \frac{1}{C_{D0}}$$

(Equation 83)

where V_R is the volume of the receiver compartment [ml], ΔC_R is the change in concentration in the receiver compartment [µM], Δt is the change in time [s], S is the area of the monolayer [cm^2], A is the amount of drug transported [nmol], and C_{D0} is the initial concentration in the donor compartment. The efflux ratio (ER) was calculated using the following relation. The apparent permeability coefficient in the basal to apical transport direction is divided by the apparent permeability coefficient in the apical to basal transport direction:

$$EfluxRatio = \frac{P_{app\ :\ basal_to_apical}}{P_{app\ :\ apical_to_basal}}$$

(Equation 84)

The apparent permeability coefficients as well as the efflux ratio are displayed depending on the initial concentration used in the donor compartment.

6.3.9. Mathematical model for determining drug absorption parameters in Caco-2 cell monolayers

In an earlier publication our group presented a mathematical model to describe the transport of drug between the apical, the basal, and the cellular compartment [Kapitza]. This model enables a direct estimation of the relevant transport parameters from concentration-time profiles. The developed model took into account passive permeation and carrier mediated efflux. The transport processes considered for modelling drug permeation in the Caco-2 cell monolayer and the relevant processes in the basic model are passive diffusion and carrier-mediated efflux at the apical membrane. For the detailed derivation of the model equations and extensions to the model with inclusion of phase II metabolism and adsorption the reader is referenced to [Blaser]. The present publication only uses the basic model with passive permeation and carrier-mediated efflux, as in preliminary experiments with all three compounds used in this study neither adsorption nor phase II metabolism was detected. Briefly, this model was based on the following assumptions:

1) Three different compartments are considered in which drug concentration varies with time, the apical, the cellular and the basal compartment.

2) Drug may move between the apical and the cellular and the cellular and the basal compartment in both directions by passive diffusion. Passive diffusion through the apical and the basal cell membrane is symmetrical and is characterized in both cases by the permeability coefficient, P. No effect of electrical membrane potential on the transport is considered.

3) Drug is subject to carrier mediated active efflux from the cellular to the apical compartment that is described by the parameter vk, the apical efflux rate.

4) No two different orientations or conformations of the carrier at the two faces of the membrane are explicitly involved. The drug concentration in the apical compartment does not influence efflux transport and the entire mass of drug present in the cellular compartment is substrate of the transporter.

5) The total mass of drug in the three compartments is preserved.

The differential equations describing the change of drug concentration or mass as a function of time in the three compartments during permeation in both directions if the relevant processes are passive diffusion and carrier-mediated transport are the following:

transport direction apical to basal:

$$\frac{dC_{Aab}}{dt} = -P \bullet \left(C_{Aab} - C_{Cab}\right) \bullet \frac{Sm}{V_A} + vk \bullet \frac{Sm}{V_A}$$

(Equation 85): apical compartment

$$\frac{dC_{Bab}}{dt} = P \bullet (C_{Cab} - C_{Bab}) \bullet \frac{Sm}{V_B}$$

(Equation 86): basal compartment

$$\frac{dM_{Cab}}{dt} = P \bullet (C_{Aab} - C_{Cab}) \bullet Sm - vk \bullet Sm - P \bullet (C_{Cab} - C_{Bab}) \bullet Sm$$

$$with$$

$$M_C = C_C \bullet V_C$$

(Equation 87): cellular compartment

transport direction basal to apical:

$$\frac{dC_{Aba}}{dt} = P \bullet (C_{Cba} - C_{Aba}) \bullet \frac{Sm}{V_A} + vk \bullet \frac{Sm}{V_A}$$

(Equation 88): apical compartment

$$\frac{dC_{Bba}}{dt} = -P \bullet (C_{Bba} - C_{Cba}) \bullet \frac{Sm}{V_B}$$

(Equation 89): basal compartment

$$\frac{dM_{Cba}}{dt} = P \bullet (C_{Bba} - C_{Cba}) \bullet Sm - P \bullet (C_{Cba} - C_{Aba}) \bullet Sm - vk \bullet Sm$$

$$with$$

$$M_C = C_C \bullet V_C$$

(Equation 90): cellular compartment

C is the molar concentration [µM], M is the molar amount of substance [nmol], P the permeability coefficient [cm/s], vk the apical efflux rate [nmol/(cm^2•s)], the indices A, B, and C (upper case) denote the apical, basal and cellular compartment, respectively, the indices ab and ba (lower case) denote permeation in the apical to basal and the basal to apical direction, respectively, Sm is the surface area of the monolayer [cm^2] and V is volume of solution in each compartment [ml].

6.3.10. Modelling of the reduction of the volume of solution

The reduction of the volume of solution in the apical and the basal compartment due to sampling as a function of time was accounted for by polynomial relations describing this reduction. The reduction was modelled as a continuous reduction over time and not as it

is in reality as a stepwise reduction at discrete times. For the modelling of the reduction of the volume, timepoints for certain volumes were exactly between the times for two sample drawings. The first point reflecting the initial volumes was set after 15min. The parameters of the polynomial relations were determined empirically using regression analysis with EASY-FIT® using the model type “explicit”, the numerical method “DFNLP”, a scaling of 1 and a termination tolerance of 0.00000001. The point of origin and the endpoint were free for the fitting. The values for the different parameters, $V_{apical,0,calculated}$ and $V_{basal,0,calculated}$ were determined for the transport experiments over 3h with sampling volumes of 54µl and sampling after 15, 30, 45, 60, 90, 120 and 180 minutes. The determined relations were later on used in the fittings of the data of transport experiments. For a sampling volume of 54µl regression analysis yielded in the following polynomial relations for the reduction of the volume.

$$V_{apical}(t) = 1.63560489 - 0.0045391 \bullet t + 0.000017685 \bullet t^2 - 0.00000002258 \bullet t^3$$

(Equation 91)

$$V_{basal}(t) = 2.83560998 - 0.0045382 \bullet t + 0.000017673 \bullet t^2 - 0.00000002253 \bullet t^3$$

(Equation 92)

6.3.11. Analysis of compound permeation across Caco-2 cell monolayers

Permeation data were analysed using this theoretical model for the kinetics of cellular transport. The concentration variables defined by the system of differential equations were fitted to the experimental concentration data. Concentration data of both compartments obtained from the apical to basal and the basal to apical direction of permeation were simultaneously fitted. This provided a more stable regression analysis compared to the separate evaluation of each permeation direction. In previous work the carrier-mediated transport was modelled by Michaelis-Menten kinetics [Kapitza], but in most instances a strong correlation between v_{max} and K occurred in the regression analysis, which meant that these parameters could not be deduced individually from each other. Therefore all fittings in the present work were performed describing the carrier-mediated efflux by the global efflux rate vk, which describes the amount of substance pumped out of the cell per time and area. The reduction of the volume of solution over time was accounted for by the already mentioned polynomial equations. Numerical solution of the equations and least squares fit were performed using the software Easy-Fit® and optimal values of the kinetic parameters P and vk applicable to the different experimental conditions were deduced. The regression analysis with EASY-FIT® was performed using the model type “ODE” (ordinary differential equations), the

numerical method “DFNLP”, a scaling of 1, an initial stepsize of 0.00000001 and a final accuracy (absolute and relative) of 0.00000001. The transport data obtained by the methods described in chapter 6.3.5 and 6.3.6 was used in the fittings. Transport parameters were determined for every single compounds and every combination experiment. A cell monolayer volume of 0.0094ml was used based on a monolayer thickness of 20µm and a monolayer area of 4.70cm^2. The regression analysis resulted in values for the passive permeability coefficient P in cm/s and the rate constant vk, which expresses the apical mass efflux rate of the drugs elicited by P-glycoprotein in Caco-2 cells in nmol/(cm^2●s). Furthermore the drug concentrations at time zero, $C_{Aab}(0)$ and $C_{Bba}(0)$ and the drug mass in the cellular compartment were obtained from model simulation.

6.4. Results and discussion

6.4.1. Cell toxicity of the different compounds and combinations

The possibility of adverse effects elicited by the different compounds and combinations used on cultured Caco-2 cell monolayers was evaluated by determining the mitochondrial dehydrogenase activity of the cells by using the MTT assay. This is an established method addressing one aspect of cell functionality and is widely used as a criterion of cytotoxicity. The MTT assay detects specifically mitochondrial metabolic activity and the ability of the cells for proliferation.

After 3h incubation with Quinidine alone, the mitochondiral activities as reported by the MTT assay, were for 5µM 104.23% +/- 5.38, for 50µM 107.32% +/- 3.54, for 100µM 98.84% +/- 3.58 and for 250µM 94.05% +/- 3.01 of the control. Only the value for 50µM was statistically significant higher from the control as determined by the Student's t-test at $p < 0.05$. After 3h incubation with Digoxin alone, the mitochondiral activities were for 1µM 94.94% +/- 3.56, for 5µM 95.01% +/- 3.14, for 50µM 91.85% +/- 2.78 and for 100µM 86.60% +/- 2.76 of the control. The values for 50µM and 100µM were statistically significant lower from the control as determined by the Student's t-test at $p < 0.05$. After 3h incubation with Verapamil alone, the mitochondiral activities were for 5µM 98.57% +/- 2.19, for 50µM 95.37% +/- 2.02, for 100µM 98.02% +/- 3.83, for 250µM 100.28% +/- 4.65 and for 1000µM 115.50% +/- 4.85 of the control. Only the value for 1000µM was statistically significant higher from the control as determined by the Student's t-test at $p < 0.05$.

Taken together the employed concentrations of Quinidine and Verapamil alone didn't show a concentration – activity trend and had overall no significant cytotoxic effect on the cells. The statistically significant effects observed in each case were not consistent within the series of applied concentrations (both Quinidine and Verapamil). Hence, they do not appear to be systematic and there are not harmful effects of Quinidine and Verapamil alone in the concentration range and incubation time used. For Digoxin we observed a concentration dependent decrease in the mitochondrial activity with the activities for the highest Digoxin concentration used being statistically significant lower compared to the control. Therefore we have to take care, if there are no confounding effects caused by this slightly cytotoxic effect, on the permeation in terms of the passive permeability and the carrier-mediated transport. The results of the MTT assay for combinations of the different compounds are shown in (Figure 21) to (Figure 23).

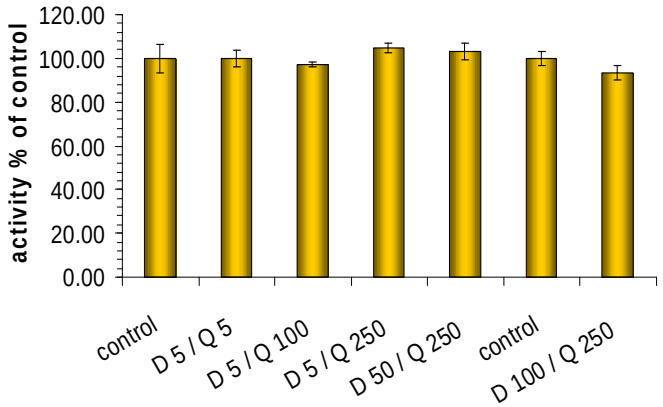

Figure 21: Mitochondrial dehydrogenase activity of the cells determined by the MTT assay following 3h incubation in 24 well plates. Results are expressed in percent of control obtained with transport medium and given as mean and standard deviation with n = 3. D = Digoxin, Q = Quinidine, concentrations are given in µM.

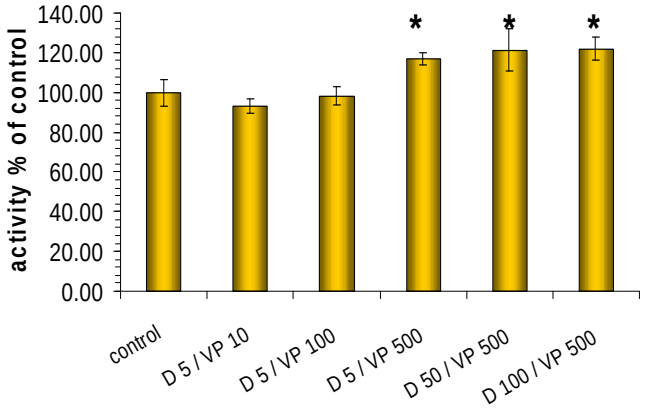

Figure 22: Mitochondrial dehydrogenase activity of the cells determined by the MTT assay following 3h incubation in 24 well plates. Results are expressed in percent of control obtained with transport medium and given as mean and standard deviation with n = 3. D = Digoxin, VP = Verapamil, concentrations are given in µM. * denotes results that are statistically significant from the control at p < 0.05.

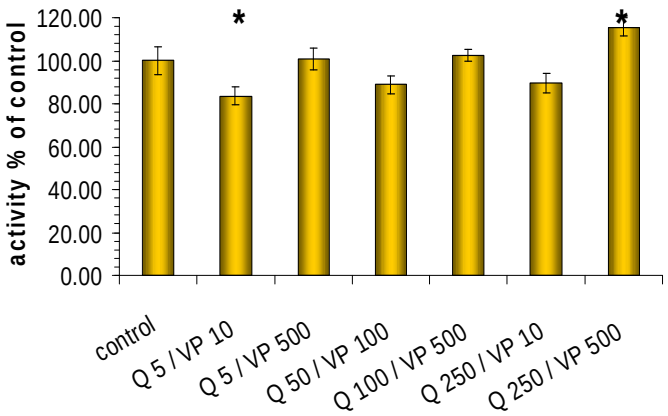

Figure 23: Mitochondrial dehydrogenase activity of the cells determined by the MTT ay following 3h incubation in 24 well plates. Results are expressed in percent of control obtained with transport medium and given as mean and standard deviation with n = 3. Q =

Quinidine, VP = Verapamil, concentrations are given in µM. * denotes results that are statistically significant from the control at p < 0.05.

For the 3h incubation with combinations of Digoxin and Quinidine, mitochondrial activity values of the cells were in the range between 93.44% +/- 3.13 (Digoxin 100µM & Quinidine 250µM) and 104.64% +/- 2.25 (Digoxin 5µM & Quinidine 250µM) of the control. None of these values was statistically significant different from the control as determined by the Student's t-test at $p < 0.05$.

For the 3h incubation with combinations of Digoxin and Verapamil, mitochondrial activity values of the cells for the low Verapamil concentrations (10µM & 100µM) were 93.32% +/- 3.58 and 98.23% +/- 4.67. These values was statistically significant different from the control as determined by the Student's t-test at $p < 0.05$. On the other hand, mitochondrial activity values of the cells for the high Verapamil concentrations were in the range between 117.08% +/- 3.06 (Digoxin 5µM & Verapamil 500µM) and 121.90% +/- 5.88 (Digoxin 100µM & Verapamil 500µM) of the control and all statistically significant different from the control as determined by the Student's t-test at $p < 0.05$.

For the 3h incubation with combinations of Quinidine and Verapamil, mitochondrial activity values were always higher for those combinations with a set Quinidine concentration in which the higher Verapamil concentration was used. No other trends could be observed. Overall the activity values of the cells were in the range between 83.60% +/- 4.08 (Quinidine 5µM & Verapamil 10µM) and 115.73% +/- 4.17 (Quinidine 250µM & Verapamil 500µM) of the control. These two outer extremes were the only values that were statistically significant different from the control as determined by the Student's t-test at $p < 0.05$.

Taken together the employed combinations and concentrations had overall no significant cytotoxic effect on the cells. While in single substance experiments statistically significant reductions of the activity caused by Digoxin were measured, this toxicity not only disappeared if Digoxin was used in combinations, but for the highest concentration combinations with Verapamil even statistically significant higher activities were measured. Aside from the finding of higher mitochondrial activities for higher concentrations during concomitant incubations, no other systematically effects were observed, especially no toxic effects. The observed increase might be possibly explained by the reported masking of cytotoxicity of compounds by an interaction of the MTT assay with high concentrations of some P-glycoprotein and MRP substrates leading to false cell viability values during concomitant incubation [Vellonen]. Therefore care has to be taken

in interpretation of the estimated passive permeability coefficients and the parameters of the carrier-mediated transport for combinations with high concentrations used.

6.4.2. Cell permeation of individual drugs

Measurement of drug permeation in the Caco-2 model was possible for Verapamil at all the employed drug concentrations (5 – 1000µM) in both transport directions. In the apical to basal direction substantial amounts of Verapamil permeated and the concentrations in the two compartments aligned with time, but with none of the concentrations used, an equilibration between the two compartments was reached. Typically after 60 – 90min the concentration difference remained constant (Figure 31). Generally, for all concentrations used, in the basal to apical direction the apical concentration exceeded the basal concentration after approximately 40 – 80min, with the higher concentrations resulting in later points in time. The apical concentrations further increased and after approximately 90min the concentration difference remained constant (Figure 32).

Quinidine was generally well permeable in the basal to apical transport direction. No permeation was measured in the apical to basal direction at 1 and 2.5µM, whereas all other concentrations (5 – 200µM) resulted in measurable permeation in both directions. In the apical to basal the permeation behaviour was typically bi-phasic, after an initial decrease in the donor concentrations up to approximately 90min and the appearance of Quinidine in the acceptor compartment, the concentration difference between the two compartments remained constant (Figure 29). With lower concentrations the initial decrease was rather abrupt and fast and for higher concentrations more gradual. Generally for all concentrations used, in the basal to apical direction the apical concentration exceeded the basal concentration after approximately 30 – 60min, with the higher concentrations resulting in later points in time. The apical concentrations further increased and for lower concentrations only few amounts of Quinidine remained in the donor concentrations (for 1µM after 3h Quinidine is not anymore detectable in the basal compartment, for 5µM the remaining concentration was about 15% and for 10µM about 30% of the initial concentration). For higher donor concentrations (> 20µM) the remaining percentages in the basal compartment were bigger and anyway after approximately 120min the concentration difference remained constant (Figure 30).

Digoxin was the least permeable compound of the selected series. For Digoxin only the higher concentrations (20 – 100µM) resulted in a detectable, permeation in both transport directions. For lower concentrations (0.5 – 10µM) no transport in the apical to basal direction was detectable and transport in the basal to apical direction was rather limited. Generally for all concentrations the apical to basal transport direction resulted in only

small amounts of Digoxin appearing the receiver compartment. The concentrations in the apical donor compartment were fluctuating around the donor concentration by approximately +/-10%. In the basal to apical direction the apical concentration exceeded the basal concentration not until approximately 150 – 180min, independent of the donor concentration ((Figure 27) and (Figure 28)).

In our experiments, to a certain degree all of three chosen substances showed asymmetric transport across the Caco-2 cells indicating that the drugs are subject to active apical efflux by at least P-gp, what is present in these cells [Gutmann 1999, Hidalgo 1996]. Especially Quinidine and Digoxin showed a profound asymmetry in the transport. From literature all three substances are known to be substrate of P-glycoprotein [Engman, Keogh, Litman, Makhey, Meier, Neuhoff 2003, Troutman 2003 A].

For Quinidine transport strong concentration dependent effects on the permeation behaviour through Caco-2 monolayers were observed. The efflux ratio for all concentrations lower than 50µM, was bigger than 2, with a steep increase to higher ER for concentrations below 20µM. The highest ER was calculated for 5µM (~26), but as for lower donor concentrations in the apical to basal direction no transport could be detected, the ER for these concentrations might have even been bigger. As the ER for donor concentrations above 50µM is for all experiments with some variation around 1.5, there is most probably a saturation effect of the efflux transporter affecting the overall permeation of Quinidine. For concentrations above 50µM the P_{app} in the basal to apical direction was in the range of 90 ● 10^{-6} cm/s, with a trend for the values getting gradually higher for lower concentrations, reaching maximum values of approximately 130 ● 10^{-6} cm/s (Figure 24). The P_{app} values for the apical to basal direction were very small for the lowest donor concentrations and gradually increased up to concentrations of about 70 – 80µM and the remained more or less constant around 60 ● 10^{-6} cm/s.

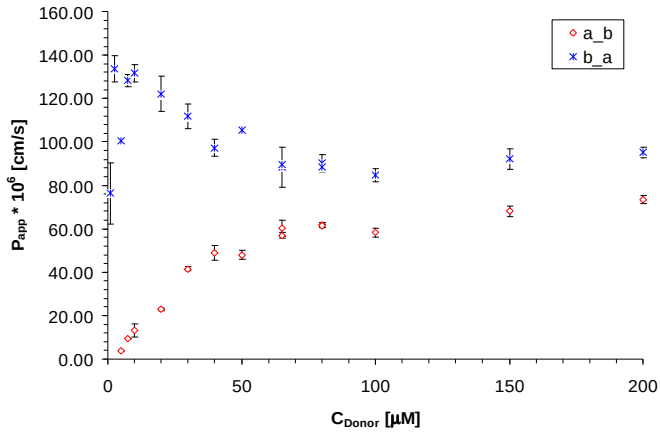

Figure 24: The concentration dependency of the apparent permeability coefficient P_{app} of Quinidine. Results are given as mean of 3 wells with the standard deviation. (◊) Apical to basal permeation. (∗) Basal to apical permeation.

Neuhoff et al. reported for transport of Quinidine at a concentration of 50µM under similar conditions (pH apical and basolateral 7.4) an ER of 4.0 with an P_{app} of 30.4 +/- 1.6 ● 10^{-6} cm/s in the apical to basal direction and 122.3 +/- 8.7 ● 10^{-6} cm/s in the basal to apical direction [Neuhoff 2003] and Troutman et al. reported for transport of Quinidine 1µM an ER of 5.2 with an P_{app} of 20.8 +/- 0.32 ● 10^{-6} cm/s in the apical to basal direction and 109 +/- 2.7 ● 10^{-6} cm/s in the basal to apical direction [Troutman 2003 B]. Korjamo et al. reported in their study for WT-Caco-2 cells P_{app} of ~18 ● 10^{-6} cm/s (apical to basal) and P_{app} of ~90 ● 10^{-6} cm/s (basal to apical) for Quinidine 1µM [Korjamo]. Our values for Quinidine 50µM were comparable to the reported ones with an ER of 2.20 and with an P_{app} of 47.9 +/- 2.2 ● 10^{-6} cm/s in the apical to basal direction and 105.3 +/- 1.6 ● 10^{-6} cm/s in the basal to apical direction. For Quinidine 1µM we couldn't detect any permeation in the apical to basal direction and in the basal to apical direction our estimated P_{app} was 76.3 +/- 14.2 ● 10^{-6} cm/s.

For Verapamil no concentration dependent effect on the permeation behaviour was observed. The efflux ratio was over the whole concentration range tested (5 – 1000µM) around 1.3 – 1.4. The P_{app} for Verapamil in the basal to apical direction was in the range of 110 ● 10^{-6} cm/s for the apical to basal direction approximately 80 ● 10^{-6} cm/s (Figure 25). The findings are consistent with the fact, that P-gp has only little effect on the overall permeation for high permeability compounds [Eytan 1996, 1999 and 2005].

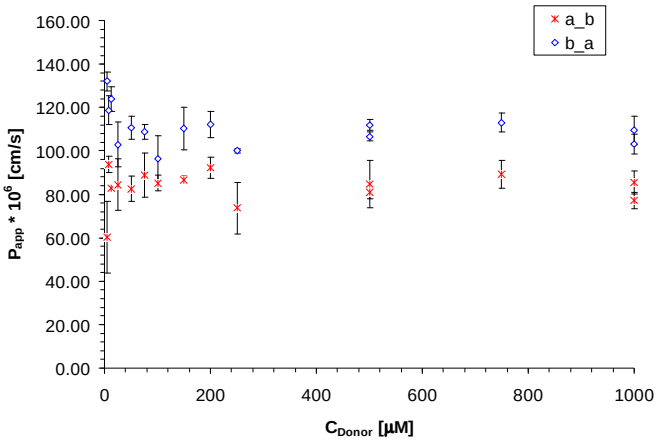

Figure 25: The concentration dependency of the apparent permeability coefficient P_{app} of Verapamil. Results are given as mean of 3 wells with the standard deviation. (◊) Apical to basal permeation. (∗) Basal to apical permeation.

Verapamil is usually used as an inhibitor of P-glycoprotein in transport studies performed with Caco-2 cell monolayers. The transport of Verapamil itself and the contributions of passive diffusion and active, carrier-mediated efflux are less frequently the objective of studies. Some publications report active efflux of Verapamil in Caco-2 cells [Engman, Makhey] and other groups [Pauli-Magnus] didn't measure P-glycoprotein-dependent transport. The measured efflux ratios for Verapamil are in the range of 1 – 2.5 [Engman, Shirasaka, Troutman 2003 B]. The mean value of P_{app} for Verapamil 5 – 1000µM measured with our cells was 83.2 +/- 8.2 ● 10^{-6} cm/s in the apical to basal direction and 110.7 +/- 9.1 ● 10^{-6} cm/s in the basal to apical direction, resulting in a mean ER of 1.33. These values are comparable to the ones reported by Troutman et al., with P_{app} values of 44.5 +/- 3.5 ● 10^{-6} cm/s (apical to basal, 0.1µM) and 117 +/- 1.2 ● 10^{-6} cm/s (basal to apical, 0.1µM) and the enantioselective analysis of Engman et al. yielded in the apical to basal direction P_{app} of 69 – 157 ● 10^{-6} cm/s (R-Verapamil, 2.5 – 80µM) and 85 – 143 ● 10^{-6} cm/s (S-Verapamil, 2.5 – 80µM) with efflux ratios of around 2.0 for 8µM and 1.0 for 80µM. On the other hand the values for the P_{app} of Pauli-Magnus et al. were 12.9 +/- 6.4 ● 10^{-6} cm/s (apical to basal, 5µM) and 11.9 +/- 1.3 ● 10^{-6} cm/s (basal to apical, 5µM) and Shirasaka et al. reported similar values, 12.9 +/- 1.10 ● 10^{-6} cm/s (apical to basal, 0.1µM) and 14.9 +/- 0.54 ● 10^{-6} cm/s (basal to apical, 0.1µM). The lower P_{app} values might be explained by the shorter culturing time before the transport experiments, Pauli-Magnus et al. performed experiments on day 7 after plating and Shirasaka et al. used the cells after 5 days in culture.

Digoxin showed the lowest permeability of all three compounds, not only in the apical to basal direction, with the P_{app} values being generally below 0.3 ● 10^{-6} cm/s or not showing any permeation at all, but also in the basal to apical direction. In this direction the P_{app}

was slightly below 30 ● 10^{-6} cm/s for concentrations above 20µM, and smaller but with more variation for lower concentrations (Figure 26). Neither the P_{app} values nor the ER (between 85 and 285, where calculable) indicated any concentration effects on the permeation of Digoxin, as for example saturation of the transporter.

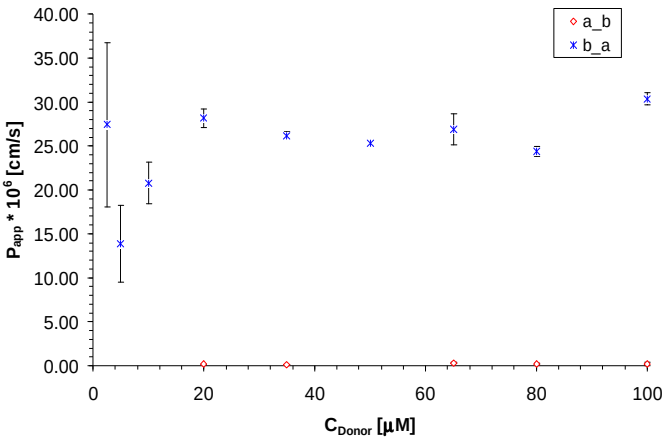

Figure 26: The concentration dependency of the apparent permeability coefficient P_{app} of Digoxin. Results are given as mean of 3 wells with the standard deviation. (◊) Apical to basal permeation. (∗) Basal to apical permeation.

Neuhoff et al. measured P_{app} values for Digoxin around 3.0 ● 10^{-6} cm/s in the apical to basal direction, independent of the concentration used (59nM and 625µM) and P_{app} in the basal to apical direction around 26 ● 10^{-6} cm/s for the lower and around 3 ● 10^{-6} cm/s for the higher concentration [Neuhoff 2006]. Troutman et al. reported similar P_{app} values for Quinidine 10µM with 2.18 +/- 0.10 ● 10^{-6} cm/s in the apical to basal direction and 44.1 +/- 0.85 ● 10^{-6} cm/s in the basal to apical direction [Troutman 2003 B]. P_{app} b_a decreased as the concentration was increased above 50µM and the P_{app} a_b was concentration independent up to concentrations of 200µM. They measured efflux ratios ranging from 11 to 7 in the concentration range tested [Troutman 2003 A]. The mean value of P_{app} for Digoxin measured with our cells was 0.19 +/- 0.08 ● 10^{-6} cm/s in the apical to basal direction (20 – 100µM) and 24.8 +/- 4.9 ● 10^{-6} cm/s in the basal to apical direction (2.5 – 100µM), demonstrating similar permeation characteristics in the basal to apical direction, whereas the permeability in the apical to basal direction in our cells is significantly lower for Digoxin.

For every transport experiment performed, mass balances were calculated by addition of the amount in solution after 3h and the amount withdrawn during the experiment. The intended donor amount provided the reference for calculation. One has to be aware that the intended donor concentration might have different from the effective used donor concentration. As we did not measure the initial concentration, we can just compare the intended concentrations with the calculated ones. The mass balances for experiments

performed with Verapamil yielded in the apical to basal direction recovery rates of 75 – 104% with two thirds of the values between 90 and 100%, and in the basal to apical direction 77 – 103% again with two thirds of the values between 90 and 100%. The mean in the a_b direction was 91.79% +/- 9.34 and in the b_a direction 91.98% +/- 8.63 for a total of 15 different experiments with 3 wells each. For some of the experiments methanol extraction of the Transwell was performed after experiments (data not shown), but no substantial amounts of Verapamil were found to be adsorbed to the surface. Furthermore for the experiments with worse mass balances no trend could be observed, they were spread all over the tested concentration range. The mass balances for experiments performed with Quinidine yielded in the apical to basal direction recovery rates of 78 – 100% with most of the values between 95 and 100% and in the basal to apical direction 81 – 103% again with most of the values between 95 and 103%. The mean in the a_b direction was 94.88% +/- 5.19 and in the b_a direction 97.09% +/- 5.42 for a total of 16 different experiments with 3 wells each. Generally there were in each transport direction only 2 experiments with recovery below 90%. The mass balances for experiments performed with Digoxin yielded in the apical to basal direction recovery rates of 80 – 116% with almost all of the values between 95 and 116% and in the basal to apical direction 75 – 110% with almost all of the values between 94 and 110%. The mean in the a_b direction was 101.76% +/- 12.17 and in the b_a direction 99.01% +/- 12.74 for a total of 11 different experiments with 3 wells each. The lowest recovery was observed with the 2 smallest donor concentrations whereas for the values exceeding 100% the most, no trend was observed.

Taken together the best recovery in terms of consistency and variation was found for Quinidine followed by the Verapamil experiments and the worst results were found for Digoxin experiments with some variation and values exceeding 100% recovery. For the three chosen compounds there are no hints for adsorption to the surface of the Transwell plates, nor metabolism or substantial cellular accumulation in the concentration range tested.

6.4.3. Quantification of passive and carrier-mediated transport parameters

Permeation data were analysed using the theoretical model for the kinetics of cellular transport presented in chapter 6.3.9. As the experimental data didn't indicate adsorption or metabolism, we could use this basic model and not the elsewhere described extended version [Blaser]. The concentration variables defined by the system of differential (Equation 85) to (Equation 90) were fitted to the experimental concentration data and optimal values of the parameters P and vk applicable to the different experimental

conditions were deduced. Numerical solution of the equations and least squares fit were performed using the software EASY-FIT (Prof. K. Schittkowski, University of Bayreuth, Germany). Concentration data of both compartments obtained from the apical-to-basal and the basal-to-apical direction of permeation were used simultaneously in the fitting. This provided a more stable regression analysis compared to the separate evaluation of each permeation direction. The drawn lines in (Figure 27) to (Figure 32) represent the representative best fits of Digoxin, Quinidine and Verapamil permeation. This is considered in all cases to be satisfactory.

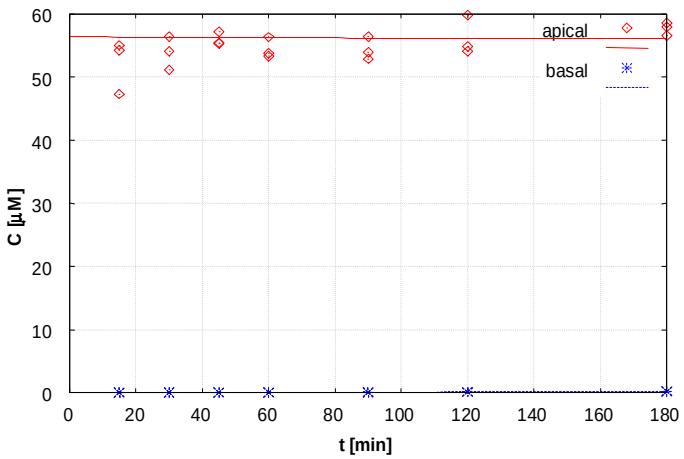

Figure 27: Representative fit of Digoxin 50µM apical to basal transport across Caco-2 cell monolayers at 37℃ (calculated with the model using zero order efflux kinetics). Experimental points and model-based fitted curves. (◊) Apical concentration. (∗) Basal concentration.

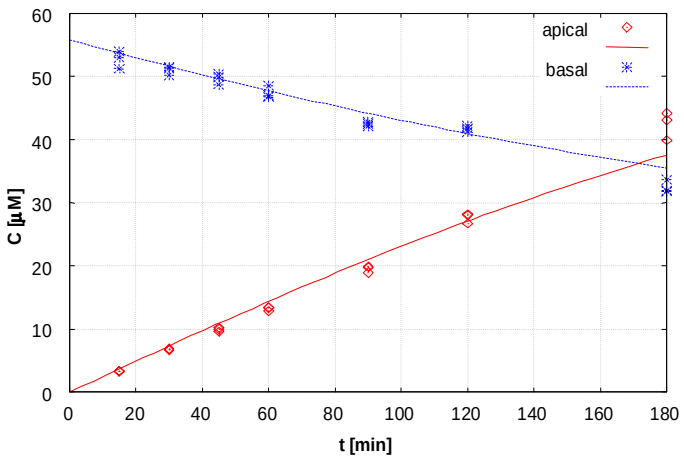

Figure 28: Representative fit of Digoxin 50µM basal to apical transport across Caco-2 cell monolayers at 37℃ (calculated with the model using zero order efflux kinetics). Experimental points and model-based fitted curves. (◊) Apical concentration. (∗) Basal concentration.

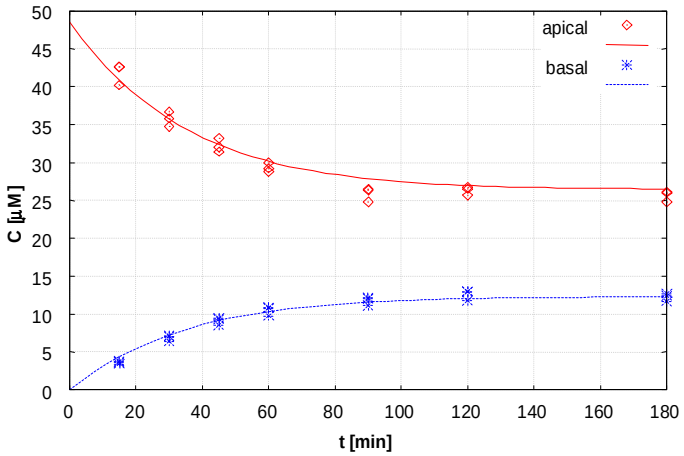

Figure 29: Representative fit of Quinidine 50µM apical to basal transport across Caco-2 cell monolayers at 37℃ (calculated with the model using zero order efflux kinetics). Experimental points and model-based fitted curves. (◊) Apical concentration. (∗) Basal concentration.

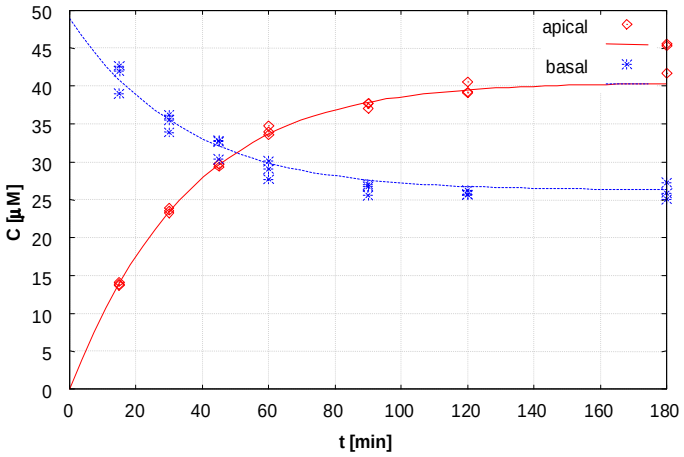

Figure 30: Representative fit of Quinidine 50µM basal to apical transport across Caco-2 cell monolayers at 37℃ (calculated with the model using zero order efflux kinetics). Experimental points and model-based fitted curves. (◊) Apical concentration. (∗) Basal concentration.

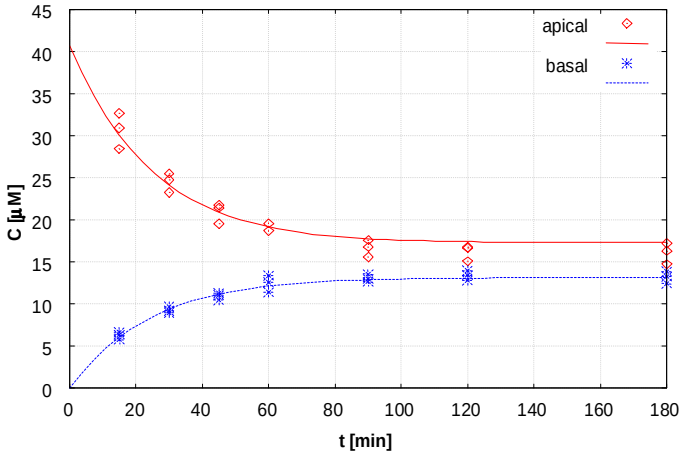

Figure 31: Representative fit of Verapamil 50µM apical to basal transport across Caco-2 cell monolayers at 37℃ (calculated with the model using zero order efflux kinetics). Experimental points and model-based fitted curves. (◊) Apical concentration. (∗) Basal concentration.

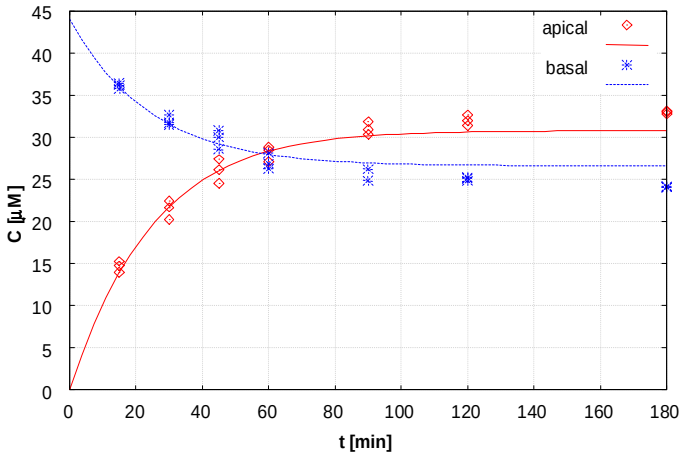

Figure 32: Representative fit of Verapamil 50µM basal to apical transport across Caco-2 cell monolayers at 37°C (calculated with the model using zero order efflux kinetics). Experimental points and model-based fitted curves. (◊) Apical concentration. (∗) Basal concentration.

An estimate of the goodness of the fits is the final residual value (FRV). The Easy-Fit settings were equal for the three compounds. Therefore the estimated FRVs are comparable for the different concentrations of a substance as well as between the substances. The smaller the number of the FRV, the better is the fit. For Verapamil and Quinidine there was a trend for better fits for the higher concentrations, for Digoxin the fits were equally well among the whole concentration range tested. Generally the best fits were obtained for Verapamil data, with FRV values between 0.00182 (500µM) and 0.0516 (7.5µM). Quinidine FRVs were basically in the same range and resulted between 0.00287 (200µM) and 0.0592 (2.5µM) with two outliners of 0.218 (1µM) and 0.159 (5µM). The fits for Digoxin data were about one order of magnitude worse than the ones for the other two compounds. The values were in the range between 0.0145 (5µM) and 0.394 (20µM). The experimental data for which fits were not as good as for the rest (some Quinidine concentrations and Digoxin in general) were generally those with poor apical to basal permeation, demonstrating that the chosen procedure with concomitant fittings of the apical to basal and basal to apical data was the right decision to obtain reasonable and consistent values for the kinetic parameters.

The drug concentrations at time zero, $C_A(0)$ and $C_B(0)$, obtained from the best fit were in the case of Verapamil for most experiments smaller than the theoretical concentrations of the prepared solutions. In the b_a direction the model derived donor concentrations were usually 1 – 2% higher compared to the a_b concentration. For higher donor concentrations the consistency between the intended and the model derived donor concentrations was better than for the lower donor concentrations, with 95.92 – 103.38% for the concentration range between 150 – 1000µM and 81.43 – 93.72 % between 5 –

100µM. For the experiments with Quinidine, the drug concentrations at time zero, C_A (0) and C_B (0), obtained from the best fit were in most instances in quite good concordance with the theoretical concentrations of the prepared solutions. No trend for differences for the model-derived donor concentrations were for the two transport directions was observed. The estimated donor concentrations were in the range of 95.48 – 103.76% of the intended ones, with most values between 95 – 100%. Only the experiment with the worst fit (FRV) was an exception to this with the estimated donor amounts being 82.0, 77.6, 99.82 and 90.3% of the intended ones. Again as with the recovery rates, Digoxin data showed the biggest variation among the set of compound chosen for this study. The drug concentrations at time zero, C_A (0) and C_B (0), obtained from the best fit were for the lower concentrations (0.5 – 5µM) between 83.20 – 100.62% and for the higher concentrations (10 – 100µM) between 98.17 – 112.68%, with most values between 105 – 110%.

The course of the drug mass in the cellular compartment yielded by the model based simulation was similar for Verapamil and for Quinidine ((Figure 33) and (Figure 34)), with an fast initial loading of the cells within the first few minutes, independent of the transport direction. For the apical to basal direction a small decrease of the mass in the cellular compartment follows within the next 60min after which the mass remains about constant. In the basal to apical direction the mass in the cellular compartment further rises to a small amount within the same time and remains then the same for the rest of the experiment. For Digoxin experiments the model simulation yielded in the apical to basal direction in a small initial binding to the cells with no change afterwards, whereas in the basal to apical direction the mass in the cellular compartment continuously increased over time (Figure 35). The medial drug mass over time, averaged for the a_b and b_a transport direction, in the cellular compartment yielded by the model-based simulation was 0.017 – 4.2nmol for Verapamil (5 – 1000µM), 0.0005 – 0.953nmol for Quinidine (1 – 250µM) and 0.0002 – 0.047nmol for Digoxin (0.5 – 100µM).

For all three compounds the resulting model derived mass of drug in the cellular compartment was directly proportional to the donor concentration over the whole range of tested concentrations with correlation coefficients of 0.99 and better. For a selected donor concentration of 100µM the model derived mass in the cell compartment was for Verapamil 0.37nmol, for Quinidine 0.38nmol and for Digoxin 0.047nmol. Generally for equal donor concentrations of Verapamil and Quinidine about the same drug in the cellular compartment resulted, whereas Digoxin mass was always about one order of magnitude lower. The similar cellular accumulation of Quinidine compared to Verapamil is, while having lower passive permeability in line with the stronger apical efflux of the

former compound ((Figure 36) and (Figure 37)). Hence, the different propensity of the two drugs to be apically effluxed can be quantitatively assessed with the present analysis. Digoxin masses in the cellular compartment were also coherent with the estimated kinetic parameters. Demonstrating only slightly higher passive than carrier-mediated fluxes across Caco-2 cell monolayers it is not likely that in the apical to basal direction substantial amounts of Digoxin can accumulate whereas in the basal to apical direction more substance permeates across the cells resulting in higher cellular accumulation.

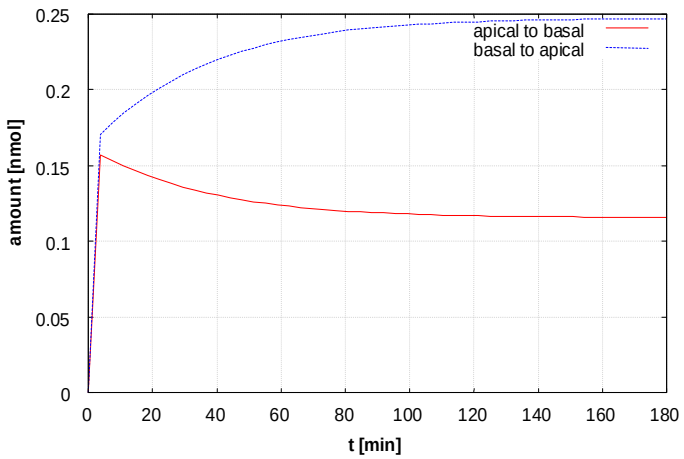

Figure 33: Calculated amounts of Quinidine in the cellular compartment during Quinidine 50µM apical to basal and basal to apical transport at 37°C (calculated with the model using zero order efflux kinetics).

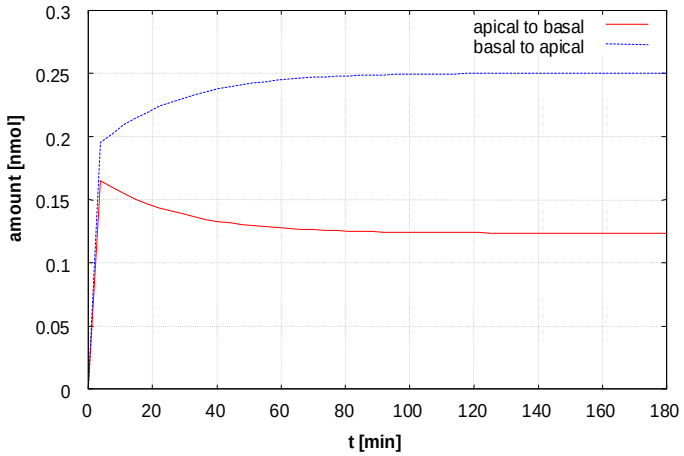

Figure 34: Calculated amounts of Verapamil in the cellular compartment during Verapamil 50µM to basal and basal to apical transport at 37°C (c alculated with the model using zero order efflux kinetics).

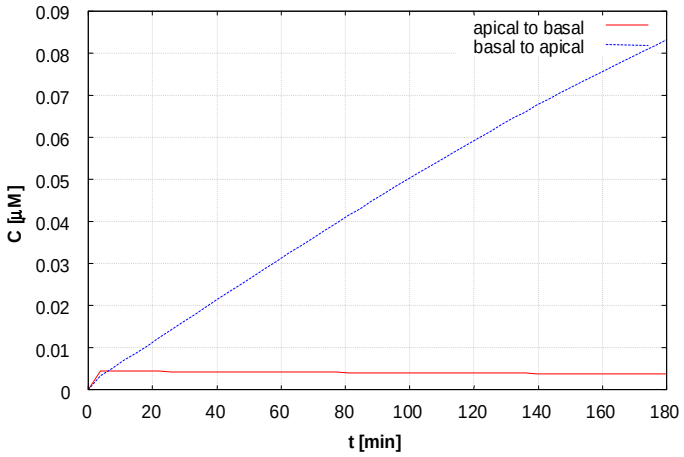

Figure 35: Calculated amounts of Digoxin in the cellular compartment during Digoxin 50µM to basal and basal to apical transport at 37°C (cal culated with the model using zero order efflux kinetics).

The fitting yielded in consistent values of the passive permeability coefficients for all three compounds used. The model derived permeability coefficients of Verapamil, Quinidine and Digoxin for the different donor concentrations used are displayed in (Figure 36). The passive permeability coefficient as modelled is independent of the transport direction and equal for the apical and the basal cell membrane.

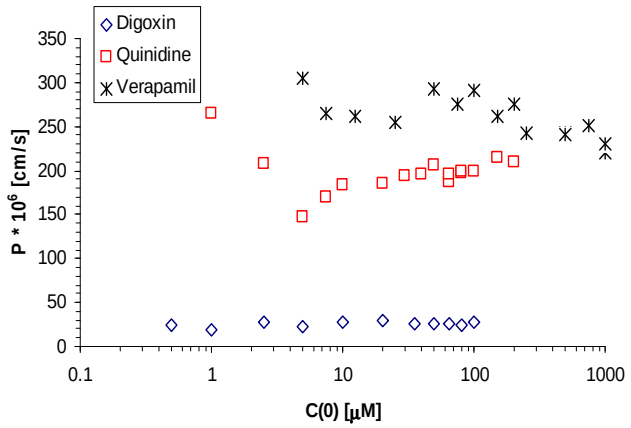

Figure 36: Model derived permeability coefficient of Digoxin 0.5 – 100µM (◊), Quinidine 1 – 200µM (□) and Verapamil 5 – 1000µM (∗) calculated with the model using zero order efflux kinetics.

For the range tested no concentration dependency of the passive permeability was observed. This observation is valid for all three compounds used in the study. The two values for Quinidine, which are obviously different from the rest, are the ones for the concentrations whose fits were not as good as the rest (1& 5µM) as a result of poor permeation with acceptor concentrations around the limit of detection for the analytical method used. Nevertheless for Verapamil there appeared to be a trend for slightly lower permeability coefficients at higher donor concentrations compared to the lower donor concentrations. If this trend is systematic or just a side effect of the tighter fitting of the

experimental data of higher concentrations is unclear. According to diffusion theory there should not be a concentration dependency of the passive permeability coefficient. As there was no clear-cut concentration dependency of the permeability coefficient further discussion of the results will be based upon the mean of the values. The model derived medial passive permeability coefficients for the three drugs in Caco-2 cells at 37°C are given in (Table 15).

Table 15: Model derived passive permeability coefficient of the compounds (calculated with the model using zero order efflux kinetics). Results are given as mean of n different concentrations and standard error of the mean.

concentration range [µM]	Digoxin (n=11)	Quinidine (n=16)	Verapamil (n=15)
	0.5 – 100	1 – 200	5 – 1000
$P \bullet 10^6$ [cm/s]	25.532 +/- 0.827	197.436 +/- 6.161	260.736 +/- 6.201

The rank order of passive permeability across Caco-2 cells was the following: Verapamil showed the highest permeability, followed by the slightly less permeable Quinidine and with one order of magnitude lower permeability Digoxin. For discussion of this rank order one has to keep in mind that both, Verapamil (molecular weight 454.60g/mol, logP 4.7, calculated by PubChem) and Quinidine (molecular weight 324.42g/mol, logP 2.6, calculated by PubChem) are ionisable compounds, with pK_a values of 8.97 +/- 0.50 (ACD Software Solaris V8.14) for Verapamil and 9.28 +/- 0.70 (ACD Software Solaris V8.14) for Quinidine, whereas Digoxin (molecular weight 780.94g/mol, logP 2.2, calculated by PubChem) can be considered as neutral molecule in the relevant pH range for the transport studies. Verapamil can be expected to possess a higher permeability than Quinidine and Digoxin as its lipophilicity, expressed by the (calculated) logP is two orders of magnitude higher. Furthermore at pH 7.4 neither the degree of ionisation with the two pK_a values being close to each other nor the molecular weight will be the crucial criterion for permeability differences between Verapamil and Quinidine. Digoxin with its high molecular weight is prone to have low permeability. This rank order is in agreement with the literature findings for Verapamil and Quinidine having high permeability and for Digoxin rather moderate to poor passive permeability [Varma]. The passive permeability coefficients for Verapamil and Quinidine were higher than the previously model estimated permeability for Indinavir (53 $\bullet$ 10^{-6} cm/s), Saquinavir (89 $\bullet$ 10^{-6} cm/s) and Amentoflavone (33.3 +/- 7.4 $\bullet$ 10^{-6} cm/s) [Blaser, Kapitza] whereas Digoxin has the poorest permeability among these different compounds.

Taken together the model estimated passive permeability coefficients were not concentration dependent and reflected the lipophilicity and molecular weight of the

different compounds. A reasonable rank order for the passive permeability of the Verapamil, Quinidine and Digoxin was obtained that was consistent with literature findings.

Preliminary studies using the mathematical model with Michaelis-Menten kinetics for the apical efflux directly integrated to the equations used for fitting showed a high level correlation between v_{max} and K in the regression analysis, which meant that these parameters could not be deduced individually from each of these experiments [Kapitza]. Therefore all fittings in the present work were performed describing the carrier-mediated efflux by the global efflux / pump rate vk, which describes the amount of substance pumped out of the cell monolayer per time and area. The dependency of the apical pump rate vk, of Quinidine, Digoxin and Verapamil on the model-derived concentrations are displayed in (Figure 37).

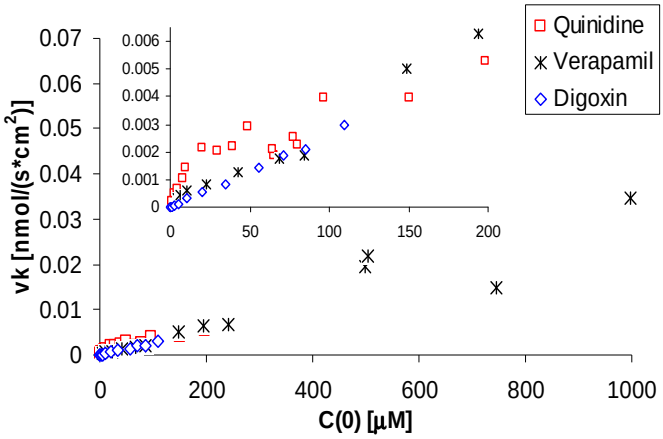

Figure 37: Model derived efflux rate vk of Digoxin (0.5 – 100µM) (◊), Quinidine (1 – 200µM) (□) and Verapamil (5 – 1000µM) (∗) in Caco-2 cell monolayers depending on the estimated donor concentrations for nominal concentrations in the brackets (calculated with the model using zero order efflux kinetics).

All three compounds used in the study are well known P-glycoprotein substrates, therefore the parameters vk can be regarded as an estimate of the mass efflux rate elicited by P-glycoprotein in Caco-2 cells. The model estimated values for the pump rate vk varied for the different compounds and concentrations, demonstrating clear concentration dependency of the efflux for all compounds. This concentration dependency that is the course of the plot was different for the three compounds.

For Quinidine data biphasic behaviour was observed, with the first part showing a linear relationship for the increase of the apical efflux with concentration up to donor concentrations of about 20µM and at higher concentrations a flattening connected to each other with a curvature part, i.e. having the appearance of a hyperbola. This

behaviour of the efflux rate for Quinidine was interpreted as a saturation of the carrier-mediated transport.

The pump rate of Digoxin showed almost perfect linear relationship for the dependency on the estimated donor concentration. As already indicated by the calculated P_{app} and efflux ratios for Digoxin (see chapter 6.4.2) it is most likely that the used concentrations are outside of the saturation range for Digoxin transport by P-glycoprotein.

The behaviour of Verapamil efflux was the most ambiguous of the three P-glycoprotein substrates used. The plot of the pump rate depending on the estimated donor concentrations (Figure 37) might be regarded to have a sigmoidal or linear shape. But most probably also the used Verapamil concentrations are still not in the saturation range for its P-gp mediated efflux.

The comparison of the estimated transport parameters with published results of other groups and the overall permeability P_{app} is not always conclusive. Troutman et al. determined for Verapamil, Quinidine and Digoxin the apparent permeability because of passive diffusion (P_{PD}) across Caco-2 cell monolayers by measuring the transport in the presence of 1µM GW918 [Troutman 2003 A and B]. They stated, that the values in absorptive (a_b) and secretory (b_a) directions were not significantly different, supporting our assumption. For Verapamil (0.1µM) they determined a P_{PD} of 86.3 +/- 3.47 ● 10^{-6} cm/s, for Quinidine (1µM) a P_{PD} of 55.9 +/- 0.99 ● 10^{-6} cm/s and for Digoxin (10µM) a P_{PD} of 14.9 +/- 1.84 ● 10^{-6} cm/s. For both, Verapamil and Quinidine our model estimated passive permeability was more than three times higher than the values obtained by Troutman et al. after inhibition of P-glycoprotein with GW918. For Digoxin the difference is not as big but still our estimated passive permeability is about twice as theirs. This finding is somewhat puzzling, as the apparent permeability coefficient P_{app} obtained for the three compounds with our cells does not differ to the same degree from the P_{app} obtained by Troutman et al. (see chapter 6.4.2) as the passive permeability coefficient. It is generally valid for all three compounds that the P_{app} in the basal to apical direction was almost equal to the values calculated by Troutman et al. (see chapter 6.4.2). In the apical to basal direction the P_{app} obtained for Verapamil and Quinidine with our cells were about twice as big as their values. On the other hand, for Digoxin we measured in the apical to basal direction about tenfold lower P_{app} values than Troutman et al. For Verapamil and Quinidine the data indicate that both must have higher passive permeability in our cells compared to Troutman et al. and that otherwise the efflux activity in our cells must be lower for these two compounds. The higher passive permeability enables the better flux in the a_b direction and compensates in the b_a direction for the diminished carrier-

mediated flux to result in an overall permeability that is comparable to Troutman et al. Contradictory to these interpretation are the findings for Digoxin, for what we found a slightly higher passive permeability. As Digoxin has about the same P_{app} in the basal to apical direction but a ten times lower P_{app} in the apical to basal direction, we would expect a higher efflux activity of our Caco-2 cells compared to Troutman et al. There are no obvious reasons for this behaviour. It is possible that the P_{app} in the apical to basal direction was underestimated as the permeated amounts were always close to the limit of detection of the analytical method used.

These reflections indicate that the exact way of data analysis is crucial for the outcome of the kinetic analysis. By simple observation of the concentration-time profiles of the three compounds ((Figure 27) to (Figure 32)), it is neither possible to derive the quantitative contributions of the passive diffusion and the active efflux to the resulting permeation profile nor to elucidate their interplay. (Table 16) lists, among other data, the P_{app} values and the model-estimated values of passive permeability P of Digoxin, Quinidine and Verapamil, all estimated at a nominal donor concentration of 100µM.

Table 16: The apparent permeability coefficients P_{app}, the model estimated passive permeability coefficients P_{model}, passive and active fluxes of 100µM Digoxin, Quinidine, and Verapamil across Caco-2 cell monolayers. $J_{passive,\ model}$ was calculated by $P_{model} \bullet C(0)_{model}$. ΔC(15min) values denote the concentration differences between the apical and basal compartment 15min after the start of the experiment. P_{app}* are apparent permeability coefficients with the reference concentration ΔC(15min). All calculated values derived from the model using zero order efflux kinetics.

C(0) [µM] nominal / model estimated	Digoxin	Quinidine	Verapamil
	100 / 109.31	100 / 96.64	100 / 84.53
$P_{app} \bullet 10^6$ [cm/s] a_b	0.17 +/- 0.16	58.17 +/- 1.90	85.21 +/- 3.60
$P_{app} \bullet 10^6$ [cm/s] b_a	30.35 +/- 0.71	84.65 +/- 2.98	96.29 +/- 10.59
$P_{model} \bullet 10^6$ [cm/s]	27.61	199.77	291.33
ΔC(15min) [µM] a_b	105.99	73.64	49.60
ΔC(15min) [µM] b_a	88.12	61.81	44.54
$P_{app}^* \bullet 10^6$ [cm/s] a_b	0.16 +/- 0.15	78.99 +/- 2.58	171.79 +/- 7.25
$P_{app}^* \bullet 10^6$ [cm/s] b_a	34.45 +/- 0.81	136.95 +/- 4.82	216.19 +/- 23.78

One should expect the values of the (model estimated) passive permeability to be in between the P_{app} in the apical to basal and basal to apical direction, as in the apical to basal direction the overall flux is reduced by the active efflux at the apical cell membrane, whereas in the basal to apical direction higher fluxes and therefore permeability coefficients should result because of this efflux. Only for Digoxin transport this hypothesis is true, for Quinidine and Verapamil the model estimated passive permeability coefficient is significantly higher than the values for P_{app} in the basal to apical direction. What is the reason for these discrepancies?

If we calculate the model estimated passive flux caused by concentration dependent diffusion across the cell monolayer, $J_{passive,\ model} = P_{model} \bullet C(0)_{model}$, and compare these values to the model estimated active, carrier-mediated flux, $J_{active,\ model}$, which is equal to our pump rate vk, we find for both, Quinidine and Verapamil the passive flux to be greater than the carrier-mediated efflux. For Quinidine 100µM the passive flux $J_{passive,\ model}$ is 19.3058 and the active flux $J_{active,\ model}$ 3.9794pmol/(cm^2•s), for Verapamil 100µM we get for $J_{passive,\ model}$ 24.6261 and for $J_{active,\ model}$ 1.8816pmol/(cm^2•s) and for Digoxin 100µM the $J_{passive,\ model}$ is 3.0180 and the $J_{passive,\ model}$ 2.9864pmol/(cm^2•s). The values for the passive fluxes of Quinidine and Verapamil are about 10 times higher than their corresponding pump rates, meaning that for the overall permeation profile at the chosen donor concentration the passive diffusion is determinant. Contrarily, for Digoxin the passive flux is only slightly higher than the carrier-mediated component, explaining the poor permeability in the apical to basal direction. With one random exception for Digoxin and no exception for Verapamil, the calculated passive fluxes were always bigger than the active flux caused by carrier-mediated efflux. For Digoxin almost no net flux resulted explaining the poor permeability whereas for Verapamil always increasing net fluxes were calculated (Figure 38). For the two lowest concentrations of Quinidine the active part was bigger than passive one followed by an increasing importance of the passive flux. This behaviour resulted in biphasic net flux profile for Quinidine, with only low net flux for the lowest concentrations and for concentrations higher than the threshold of about 10µM an almost linear increase of the net flux with concentration (Figure 38).

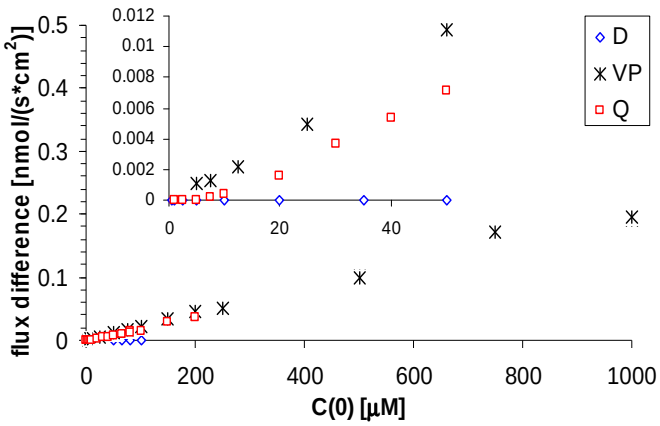

Figure 38: The model derived concentration-dependent net fluxes of Digoxin (◊), Verapamil (∗) and Quinidine (□). The net flux is the flux difference of the $J_{passive,\ model}$ (= P_{model} • $C(0)_{model}$) and the $J_{active,\ model}$ (= efflux / pump rate vk) (calculated values derived form the model using zero order efflux kinetics).

To come back to the discrepancy between the model-estimated passive permeability and the P_{app} values, we have to keep in mind the mode by which the P_{app} value is calculated, namely the division by the donor concentration. From ((Figure 27) to (Figure 32)) it is known that in the case of Digoxin only poor permeation results in the first 15 minutes of the transport experiments, whereas for Quinidine and especially for Verapamil already substantial permeation has taken place (a_b and b_a direction). The results are the following, for Digoxin the sink conditions are most probably maintained, whereas for Quinidine and Verapamil strong deviations from the nominal donor concentration are observable with no maintenance of the sink conditions. These deviations were taken into account for a recalculation of the apparent permeability coefficients, yielding P_{app}*, by using the difference between the actual apical and basal concentration after 15min (ΔC(15min)) as the reference (Table 16). Using this procedure, the underestimation of the permeability of Quinidine and Verapamil was partially corrected, resulting in higher values for P_{app}* than for P_{app} and an alignment yet not equalisation to our values for the passive permeability coefficient. For Digoxin the differences between the apparent permeability coefficients a_b and b_a and our model estimated passive permeability coefficient slightly increased. The P_{app} of Digoxin cannot become much greater, as the active flux generated by P-glycoprotein can only pump out of the cells what is delivered by passive influx. These observations demonstrate the importance of the knowledge of the passive permeability behaviour, the carrier-mediated efflux kinetics and their interplay, for the estimation of the overall permeation of a compound. For example, the concentration-time profiles of Quinidine and Verapamil may look similar ((Figure 29) to (Figure 32)) but the underlying contributions of passive diffusion and active efflux are different (Table 16) and may be, as in the case of the active efflux, concentration-dependent.

6.4.4. Transport of binary mixtures of compounds across Caco-2 cell monolayers grown in Transwell plates

The model was evaluated with respect to the ability to detect and quantify reductions of active efflux rate as estimated by the value of the pump rate vk. Further aspects were the influence of a concomitantly incubated substance on the passive permeability coefficient and the calculated amount of substance in the cellular compartment. The model derived kinetic parameters should allow a direct estimation of the effect of the co-incubated substance on the passive permeability and the active efflux whereas the use of the P_{app} and Efflux ratio does neither directly reveal which of these two fundamental properties was influenced nor to what extent. The same three compounds as used solitary, that is Digoxin, Quinidine, and Verapamil, were used in the same concentration range in

different combinations and concentrations to evaluate the permeation during concomitant incubation. To do so, a pair of compounds was added at the same time to the donor compartment and permeation was followed in both transport directions (apical to basal and basal to apical) for 3 hours. The resulting passive permeability coefficients P and the active efflux rates vk after concomitant incubation of Quinidine with Verapamil are displayed in (Figure 39) to (Figure 42).

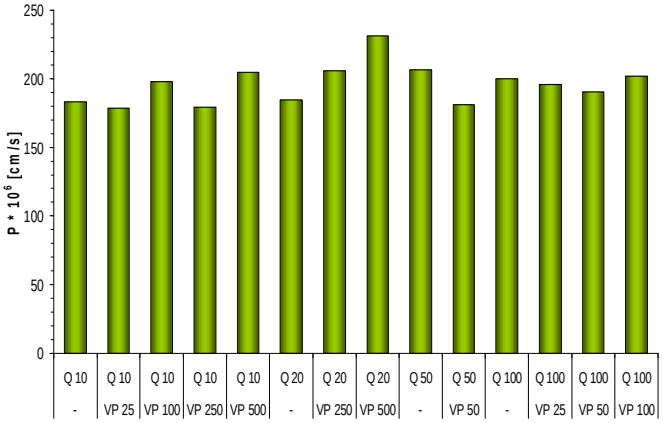

Figure 39: Model estimated passive permeability coefficient P of Quinidine (Q) for transport experiments with concomitant incubation with Verapamil (VP). Numbers on the x-axis display nominal donor concentrations in [µM] (values derived form the model using zero order efflux kinetics).

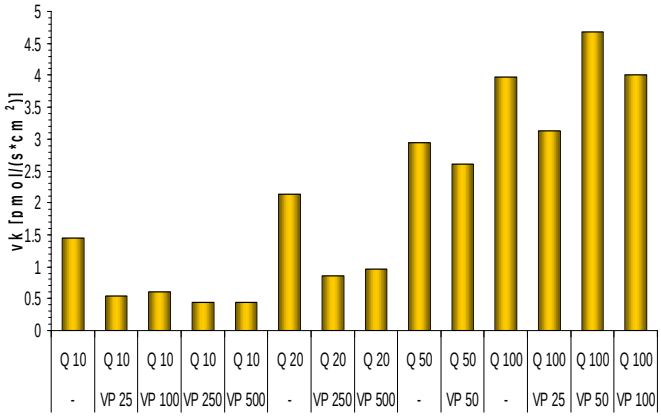

Figure 40: Model estimated efflux rate vk of Quinidine (Q) for transport experiments with concomitant incubation with Verapamil (VP). Numbers on the x-axis display nominal donor concentrations in [µM] (values derived form the model using zero order efflux kinetics).

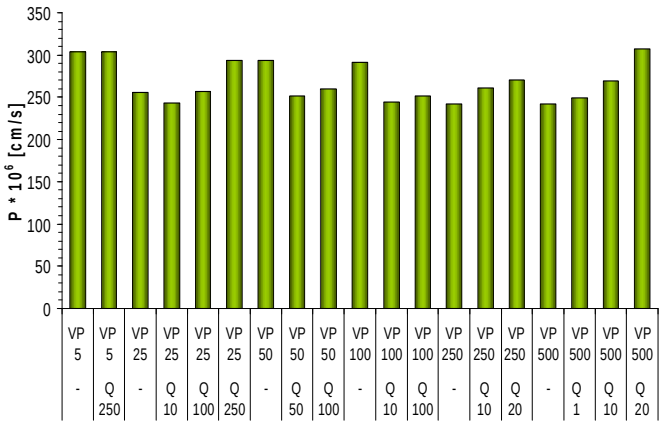

Figure 41: Model estimated passive permeability coefficient P of Verapamil (VP) for transport experiments with concomitant incubation with Quinidine (Q). Numbers on the x-axis display nominal donor concentrations in [µM] (values derived form the model using zero order efflux kinetics).

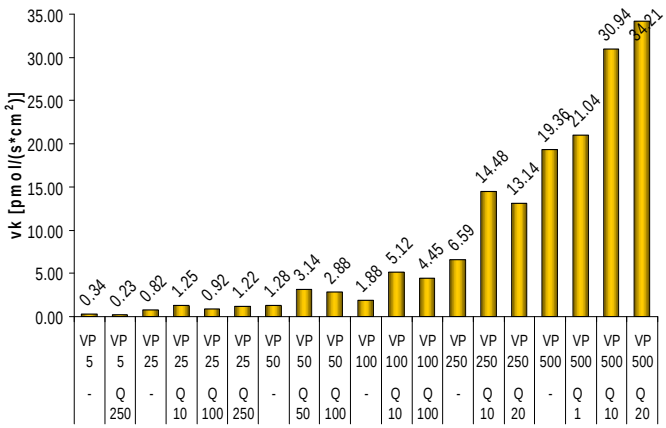

Figure 42: Model estimated efflux rate vk of Verapamil (VP) for transport experiments with concomitant incubation with Quinidine (Q). Numbers on the x-axis display nominal donor concentrations in [µM] (values derived form the model using zero order efflux kinetics).

The model estimated passive permeability coefficients of Quinidine are not strongly affected by the addition of Verapamil to the donor solution. All permeability coefficients were in the same range as the estimated values for Quinidine alone 1 – 200µM. The variations of the values didn't show a clear Verapamil concentration dependency. Some of these values were higher other lower than the control. The other way round, the passive permeability of Verapamil was also not systematically affected by the addition of Quinidine and all calculated values were in the range of the permeability values derived form experiments with Verapamil alone.

The apical efflux rate of Quinidine was influenced by the presence of Verapamil in terms of a reduction of the efflux rate. Verapamil reduced Quinidine efflux rate significantly, and the pump rate vk was greatest affected at the lower donor concentrations of Quinidine

i.e. 10, 20 and 50µM whereas at the higher Quinidine donor concentrations the effect was less pronounced. For the highest concentrations of Quinidine used in these experiments with concomitant incubation, i.e. 100µM, the effect of the second compound on the active efflux was barely detectable. The estimated values for the pump rate were fluctuating between 80 and 120% of the control with no clear-cut concentration dependency. It is more probable that these changes in the values of vk reflect differences in the intrinsic activity of P-glycoprotein for the different cells used in the experiments than effects of the co-incubated compound on the active efflux. Another reason for the reduced potency of Verapamil to diminish the efflux rate of higher Quinidine concentrations might also be, that at lower concentrations of Quinidine higher concentrations of Verapamil were used in each case whereas at higher Quinidine concentrations the respective Verapamil concentrations were smaller or equal to Quinidine concentrations. It is noteworthy that at the lower concentrations of Quinidine the addition of higher concentrations of Verapamil didn't result in a steadily more pronounced reduction of the parameter vk. The pump rate of Quinidine was not further reduced and the effect level was the same, independent of the Verapamil concentration. This can be interpreted as an incomplete influence of Verapamil on Quinidine efflux, due to the fact that there might be a component in the efflux of Quinidine that cannot be influenced by Verapamil (e.g. due to different or not completely overlapping binding sites or other reasons).

The effect of Quinidine on Verapamil efflux is more ambiguous. In the presence of Quinidine no reduction of the efflux rate of Verapamil was measured. At Verapamil concentrations of 5 and 25µM the variations of the pump rate are rather random than caused by Quinidine presence in the transport medium whereas for Verapamil concentrations bigger than 50µM efflux of Verapamil appears to be stimulated or activated by the presence of Quinidine as the efflux rate are enhanced compared to the control values. This phenomenon is observable at concentrations of Quinidine that are smaller or equal to the concentrations of Verapamil. As no higher concentrations were tested, we could only speculate about a possible reduction of Verapamil efflux in such experiments. Another interesting point is that Verapamil cannot reduce the efflux rate of Quinidine to more than a certain degree, even in increasing concentrations, whereas Verapamil itself demonstrates continuously increasing efflux rate in these experiments, again indicating that there is only a partial overlap in the binding sites of Verapamil and Quinidine. Finally, one has to be aware for the interpretation of Verapamil efflux, that already the values for the pump rate derived from single substance experiments with Verapamil didn't show a clear concentration-dependent behaviour and there was obvious

saturation of Verapamil efflux in the range tested. The model-calculated amounts of substance in the cellular compartment of Quinidine for experiments in presence of Verapamil, demonstrate that in those experiments with a clear and sharp reduction of the efflux rate, Quinidine 10 & 20µM, the amount of substance in the cell is enhanced (Figure 43). For the experiments with no or only a small reduction of the efflux rate, Quinidine 50 & 100µM, the amount in the cellular compartment remains mainly unchanged compared to the control values. The amount of Verapamil in the cellular compartment remains mostly unaffected by the presence of Quinidine (Figure 44).

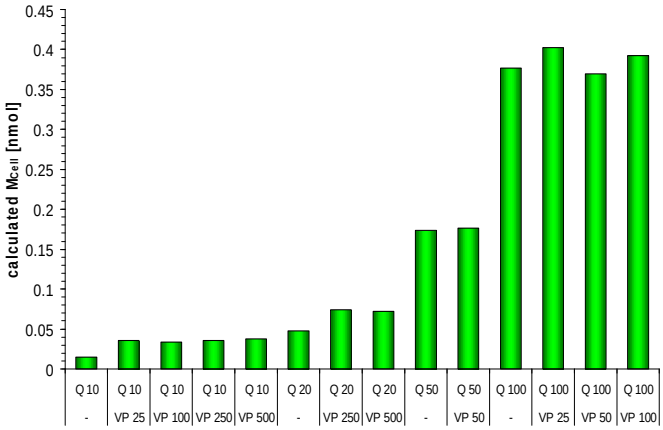

Figure 43: Model estimated amount in the cellular compartment (M_{Cell}) of Quinidine (Q) for transport experiments with concomitant incubation with Verapamil (VP). Numbers display nominal donor concentrations in [µM] (values derived form the model using zero order efflux kinetics).

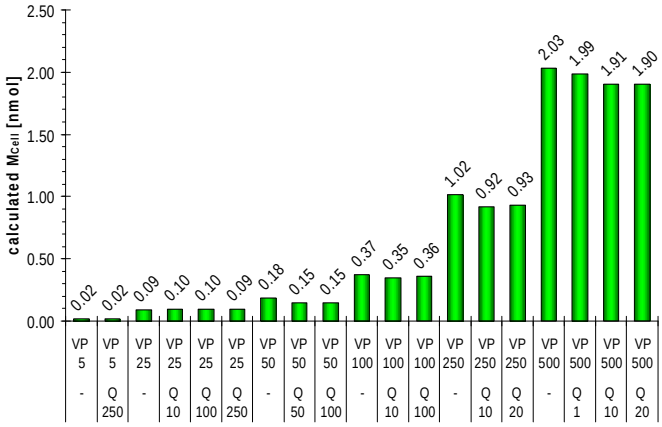

Figure 44: Model estimated amount in the cellular compartment (M_{Cell}) of Verapamil (VP) for transport experiments with concomitant incubation with Quinidine (Q). Numbers display nominal donor concentrations in [µM] (values derived form the model using zero order efflux kinetics).

The resulting passive permeability coefficients P and the active efflux rates vk after concomitant incubation of Quinidine with Digoxin are displayed in (Figure 45) to (Figure 48).

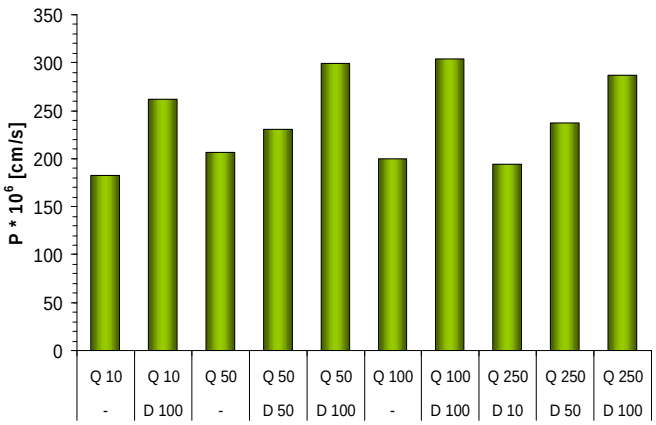

Figure 45: Model estimated passive permeability coefficient P of Quinidine (Q) for transport experiments with concomitant incubation with Digoxin (D). Numbers on the x-axis display nominal donor concentrations in [µM] (values derived form the model using zero order efflux kinetics).

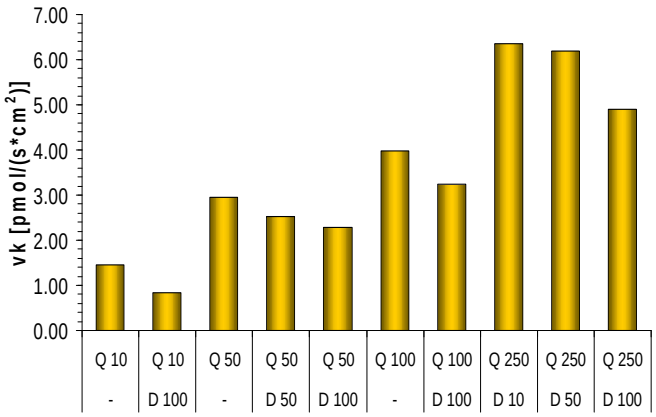

Figure 46: Model estimated efflux rate vk of Quinidine (Q) for transport experiments with concomitant incubation with Digoxin (D). Numbers on the x-axis display nominal donor concentrations in [µM] (values derived form the model using zero order efflux kinetics).

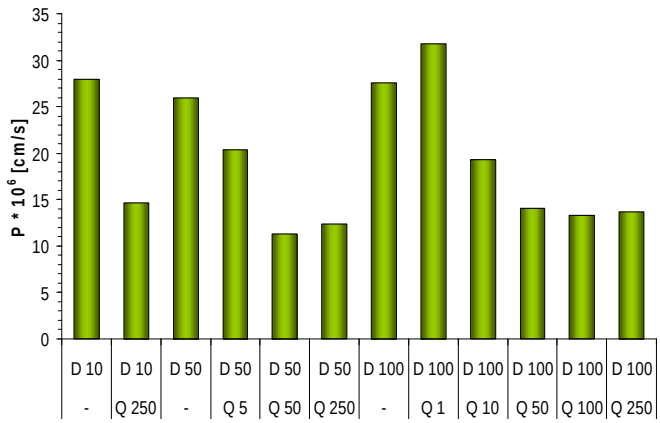

Figure 47: Model estimated passive permeability coefficient P of Digoxin (D) for transport experiments with concomitant incubation with Quinidine (Q). Numbers on the x-axis display nominal donor concentrations in [µM] (values derived form the model using zero order efflux kinetics).

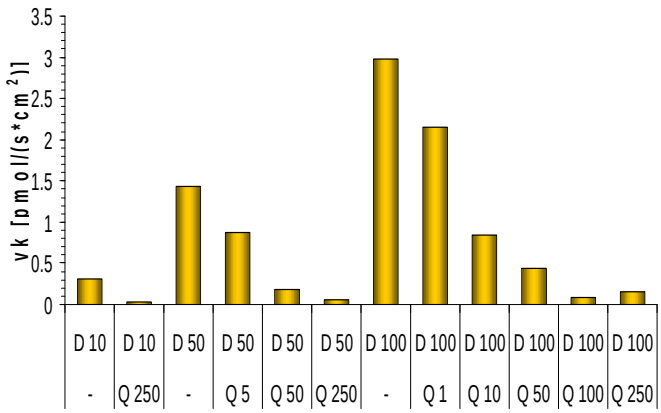

Figure 48: Model estimated efflux rate vk of Digoxin (D) for transport experiments with concomitant incubation with Quinidine (Q). Numbers on the x-axis display nominal donor concentrations in [µM] (values derived form the model using zero order efflux kinetics).

The model estimated passive permeability coefficients of Quinidine are affected by the addition of Digoxin to the donor solution. The concomitant incubation of Quinidine with Digoxin results in a systematic and concentration-dependent enhancement of the permeability coefficient of Quinidine whereas the same concentration of Digoxin, result in similar enhancement of Quinidine permeability, independent of the concentration of Quinidine. On the other hand the passive permeability of Digoxin is also affected by the addition of Quinidine, but the result is a reduction of the value of the permeability coefficient. This reduction is also dependent on the concentration of Quinidine, but after a certain level of reduction is obtained, higher concentrations do not further boost the reduction. There is an interaction between Quinidine and Digoxin on the level of the passive permeability, but the reasons for this interaction are not known. It is not likely that

this effect is an artefact of the parameter estimation procedure as not correlation between P and vk was observed in the fittings. We did not further investigate this finding.

The model estimated apical efflux rate of Digoxin was strongly reduced by the presence of Quinidine. The reduction of Digoxin efflux was observed at all concentrations. Already a small concentration of Quinidine reduced Digoxin efflux, and a further increase in Quinidine concentration demonstrated a clear concentration-dependency of this effect, resulting in some cases in a reduction to less than 10% of the efflux activity of the control. The effect of Digoxin on the efflux rate of Quinidine was less pronounced, but measurable by the model parameter. The reduction of Quinidine efflux by Digoxin also appeared to be concentration-dependent. If comparable concentrations are considered (e.g. 50µM) the higher potency of Quinidine to reduce the efflux of Digoxin compared to the effect of Digoxin on Quinidine efflux is obvious. The model estimated amount of substance in the cellular compartment are in line with these findings ((Figure 49) and (Figure 50)). The amounts of Quinidine in the cellular compartment are only slightly higher in the presence of Digoxin compared to the control, whereas the calculated amounts for Digoxin were several-fold higher in presence of Quinidine, with higher concentrations of Quinidine resulting in higher amounts in the cell.

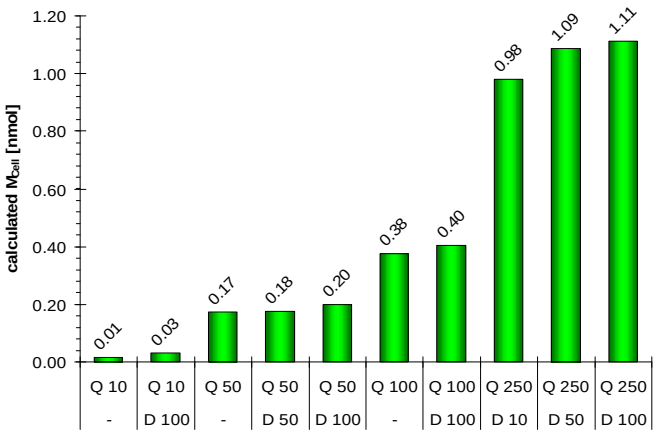

Figure 49: Model estimated amount in the cellular compartment (M_{Cell}) of Quinidine (Q) for transport experiments with concomitant incubation with Digoxin (D). Numbers display nominal donor concentrations in [µM] (values derived form the model using zero order efflux kinetics).

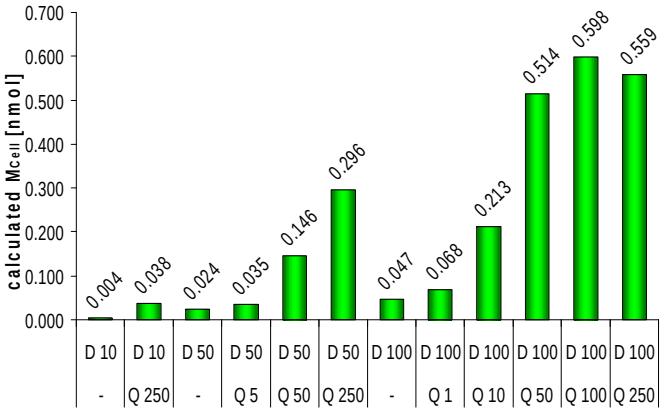

Figure 50: Model estimated amount in the cellular compartment (M_{Cell}) of Digoxin (D) for transport experiments with concomitant incubation with Quinidine (Q). Numbers display nominal donor concentrations in [µM] (values derived form the model using zero order efflux kinetics).

The interaction of Verapamil transport with Digoxin transport was studied for two combinations and only data for Verapamil is available. Verapamil transport was studied at 5 and 25µM, both in combinations with 100µM of Digoxin. Digoxin didn't influence Verapamil transport in a systematic manner. For Verapamil 5µM the resulting passive permeability coefficients P were 304.4 • 10^6cm/s (alone) and 315.8 • 10^6cm/s (in combination with Digoxin 100µM), the active efflux rates 0.34pmol/(s • cm^2) (alone) and 0.26pmol/(s • cm^2) (in combination with Digoxin 100µM) and the calculated amount in the cellular compartment 17.1pmol (alone) and 17.5pmol (in combination with Digoxin 100µM). For Verapamil 25µM the resulting passive permeability coefficients P were 255.2 • 10^6cm/s (alone) and 304.2 • 10^6cm/s (in combination with Digoxin 100µM), the active efflux rates 0.82pmol/(s • cm^2) (alone) and 0.98pmol/(s • cm^2) (in combination with Digoxin 100µM) and the calculated amount in the cellular compartment 92.5pmol (alone) and 102.1 (in combination with Digoxin 100µM). The variations of these results are rather random than an effect of Digoxin on Verapamil transport. Further experiments would be necessary to fully explore the interaction of these two compounds.

6.4.5. Conclusion

Taken together the results from single compound experiments, all compounds used showed asymmetrical transport across Caco-2 cell monolayers, the extent of which depended on the compound and the concentration used. The P_{app} values for all three compounds were comparable to previously reported ones.

The model-estimated passive permeability coefficients were not concentration dependent and reflected among other possible reasons the lipophilicity and molecular weight of the different compounds. A reasonable rank order for the passive permeability of the

Verapamil, Quinidine and Digoxin was obtained that was consistent with literature findings. The model-derived permeability was severalfold higher for Verapamil and Quinidine than previously reported values for passive permeability across Caco-2 cells, whereas Digoxin passive permeability was in the same range as estimated by inhibition with GW918. Reasons for that discrepancy might be either differences in the experimental set-up, the kinetic analysis of the obtained transport data or even be based on differences in the properties of the cell membrane in presence of the P-gp inhibitor compared to the uninhibited situation, the mechanism of which could only be speculated about. It could be furthermore demonstrated that the calculation of the apparent permeability coefficient P_{app} is prone to result in erroneous estimates of the permeability if sink conditions are not strictly maintained. Our model estimated passive permeability coefficients were less susceptible to concentration-dependency and unaffected by the course of the concentration-time profiles with no necessity to maintain sink conditions.

The estimated efflux rates reflected the different propensity of the compounds to efflux by P-glycoprotein. Different patterns of concentration-dependency of the net flux of compound across Caco-2 cell monolayers as estimated by our mathematical model were detected: Verapamil net flux was dominated by the passive flux over the whole concentration range tested and increased with rising concentrations. Digoxin net flux remained always low with no concentration dependent changes as the passive flux and the active flux were about in the same range. The behaviour of Quinidine net flux was biphasic, at low concentrations only small values for the net flux were calculated and after a certain concentration threshold was exceeded the net constantly became bigger. These findings demonstrate the importance of the knowledge of the exact quantitative contributions of simultaneous processes (e.g. passive diffusion and active efflux) to gain understanding of the overall permeation behaviour. For further studies the significance of the model could even be enhanced if the model-derived masses in the cellular compartment are verified by experimental results and the if model derived efflux rate could analysed in detail to derive information about the affinity and capacity of the transporter for different compounds and situations. The effects of binary combinations of compounds on the passive permeability and the active efflux were well reflected by the model-derived respective kinetic parameters and enable to study drug-drug interactions.

Concluding, the present study demonstrates the utility of the proposed mathematical model for kinetic analysis of transport phenomena in confluent monolayers of Caco-2 cells cultured in the Transwell system as the model-derived parameters are less susceptible to distorting effects than the conventional approach for data analysis. The

model provides a tool for the simple determination of the transport parameters by fitting of concentration-time profiles.

7. Appendix

7.1. Development of an optimal procedure for TEER-measurements

The measurement of the transepithelial electrical resistance (TEER) of cultured cells on Transwell inserts was used as an instrument to determine the integrity and viability of the cell monolayer before and after transport experiments. To assure that the chosen measurement procedure was reliable and robust several preliminary tests were performed. STX-2 chopstick electrodes were compared to the Endohm chamber, the influence of the temperature and the influence of the washing step (D-PBS (without Ca^{2+} und Mg^{2+}) vs. D-PBS (with Ca^{2+} und Mg^{2+}) and the number of washing steps) of the cells on the course of the TEER values over time and the absolute values were studied. Furthermore the influence of shaking vs. non-shaking and the presence/absence of carbon dioxide were checked for.

To do so, Caco-2 cells were grown on 6-well Transwell plates as described in the publication part and washed on the apical side with 3.5ml and on the basal side with 4ml D-PBS. 1600µl transport medium were added to the apical compartment and 2800µl transport medium were added to the basal compartment. One set of 6-well Transwell plates was then directly subject to a first TEER measurement and subsequently incubated (incubator or the incubator hood). TEER values were monitored for 7h. A second set of Transwell plates was first incubated for at least 60min in the incubator before the initial TEER measurement and then incubated (incubator or the incubator hood). TEER values were monitored for 7h. TEER values are displayed either as absolute values or relative to the initial value. To assure that the chosen procedure for the measurement of the TEER values was reliable and robust several preliminary tests were performed.

The comparison of the STX-2 chopstick electrodes with the Endohm chamber showed, that the measurement with the Endohm chamber is much more reliable in terms of the values measured and results in stable and reproducible values for the TEER. A representative measurement of TEER values is shown in (Table 17). Values measured with the STX-2 electrode show a bigger variation in comparison to the values measured with the Endohm chamber. The values measured with the STX-2 chopstick electrode are more dependent on the handling of the electrode during the measurement, as there is no defined geometry as in the case of the Endohm chamber. The depth of the insertion into the solution, the angle in which the electrode is hold for measurement and the exact place of the monolayer to which the electrode is placed are only some of the reasons for higher variation of the measurements with the STX-2 electrode. The TEER

measurements are less time consuming with the Endohm chamber as it is only necessary to measure each well one time to get a reliable value. With the STX-2 electrode at least 3 measurements in each of the 3 holes of the insert are necessary. With the STX-2 electrode only the resistance in close proximity to the electrode are measured, therefore not ruling out the possibility that small holes in the monolayer may be overlooked, especially in the centre of the monolayer. As the Endohm chamber measures the resistance of the whole monolayer, the possibility of detecting small changes in the monolayer is bigger.

Table 17: Comparison of the measured TEER values of Caco-2 cell monolayers either measured with STX-2 electrodes (each well n = 9) or the Endohm chamber (each well n = 3). TEER values are displayed after subtraction of the TEER value of the blank polycarbonate membrane (457.64Ω*cm^2 for STX-2 electrodes and 7Ω*cm^2 for the Endohm chamber). The cell monolayers were in both experiments of passage 62 and 18 days post seeding.

STX-2 chopstick electrodes	TEER [Ω*cm^2]	standard deviation [[Ω*cm^2]	standard deviation [%]
well 1	455.20	26.77	5.88
well 2	481.32	16.91	3.51
well 3	454.16	44.96	9.90
well 4	481.32	34.68	7.21
well 5	447.89	55.81	12.46
well 6	467.22	31.60	6.76
Endohm chamber	**TEER [Ω*cm^2]**	**standard deviation [[Ω*cm^2]**	**standard deviation [%]**
well 1	491.20	0.00	0.00
well 2	477.10	0.00	0.00
well 3	425.40	0.00	0.00
well 4	-	-	-
well 5	463.00	0.00	0.00
well 6	438.72	1.36	0.31

The influence of the temperature during and the time needed for the measurements of the TEER values are two critical parameters that can strongly influence the values measured. Time is a critical parameter for all the single procedures during the TEER measurement, be it the removal of the culture medium, the washing of the cell monolayer or the addition of the transport medium. All these steps influence the exposure of the cell monolayer to the air and therefore, as described later, the TEER values. Furthermore the time needed for the measurement itself is also very important as during the measurement step the temperature may decrease. If there is no device or other way of keeping the Transwell plate and the transport medium during the measurement at 37℃, it is critical to perform this step as fast and standardised as possible, but still with all the cautiousness needed. (Figure 51) displays the course of the TEER of a Transwell plate with Caco-2 cell monolayers standing in the laminar flow bench at ambient temperature. The initial measurement (time = 0) was performed after equilibrating the Transwell plate

at 37°C for 60min. A reference sample of transport medium (approximately 30ml) in a bottle showed a decrease to 29.4°C after 15min at the same place as the Transwell plate.

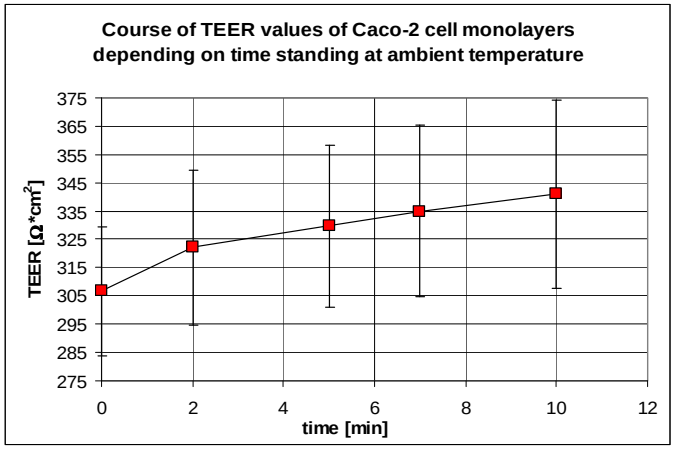

Figure 51: The course of TEER values with time of Caco-2 cell monolayers in Transwell standing in the laminar flow bench at ambient temperature. The cells were 15 days post seeding and the medium for measurement was transport medium including 0.5% ethanol (v/v). The measurement was performed with the STX-2 electrode.

It is obvious from (Figure 51) that already small changes in the temperature of the transport medium may lead to an increase in the measured TEER values. A general tendency is that the TEER values become smaller at higher temperatures.

All TEER measurements were performed in transport medium after the removal of the culture medium from the Transwell plates and a washing step with D-PBS. To investigate the influence of the washing step (D-PBS (without Ca^{2+} and Mg^{2+}) vs. D-PBS (with Ca^{2+} and Mg^{2+}) and the number of washing steps) of the cells on the TEER values and their course, several experiments were performed. In order to compare the effect of the type of D-PBS used, the cell monolayers were washed 1 or 3 times with each type of D-PBS after the removal of the culture medium and TEER values were immediately measured at 37°C in the Endohm chamber. (Figure 52) shows that after washing the cells 3 times the TEER values were approximately 150Ω*cm^2 lower if D-PBS (without Ca^{2+}/Mg^{2+}) was used instead of D-PBS (with Ca^{2+}/Mg^{2+}). With proceeding time of incubation the values rose again after usage of D-PBS (without Ca^{2+}/Mg^{2+}) and after approximately one hour the values were close to the ones after usage of D-PBS (with Ca^{2+}/Mg^{2+}). The TEER values after usage of D-PBS (with Ca^{2+}/Mg^{2+}) drop immediately after the initial measurement, rise again and stay with some variation constant after 60min (Figure 52).

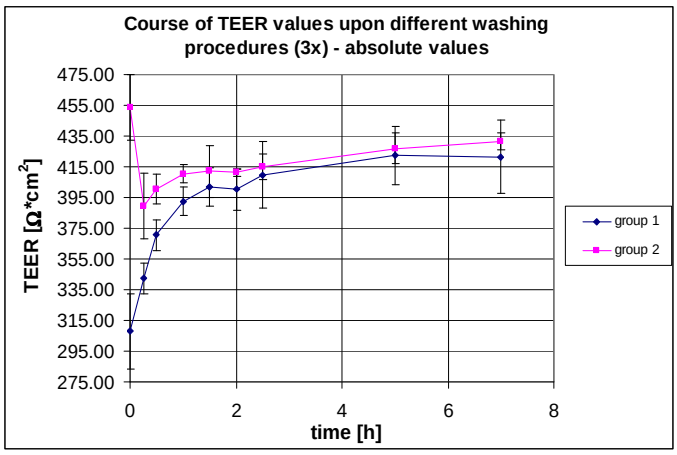

Figure 52: Course of the absolute TEER values over 7h in the incubator hood at 37℃ without shaking. The cells were washed 3 times with D-PBS. Group 1 was washed with D-PBS (without Ca^{2+}/Mg^{2+}) and group 2 was washed with D-PBS (with Ca^{2+}/Mg^{2+}). Each group consisted of 3 wells. Transwell transport medium (including 0.5% Ethanol (v/v) was at 37℃ and the reference solution in the Endohm chamber was at ambient temperature (25 – 30℃). The cell monolayers were of passage 65 and 20 days post seeding.

If the Transwell plates were only washed once with D-PBS (without Ca^{2+}/Mg^{2+}) there were no differences to the values measured after one washing step D-PBS (with Ca^{2+}/Mg^{2+}) (Figure 53). Even the course of the TEER over 7h of incubation was the same in the 2 groups. In both groups there was an initial drop of the values just to rise again during the second half of the incubation time. Although there were no differences between the two groups if the cells were only washed once, D-PBS (with Ca^{2+}/Mg^{2+}) is recommended for the washing step, to rule out the possibility of affecting the TEER values by washing them with a calcium-free buffer after the removal of the culture medium.

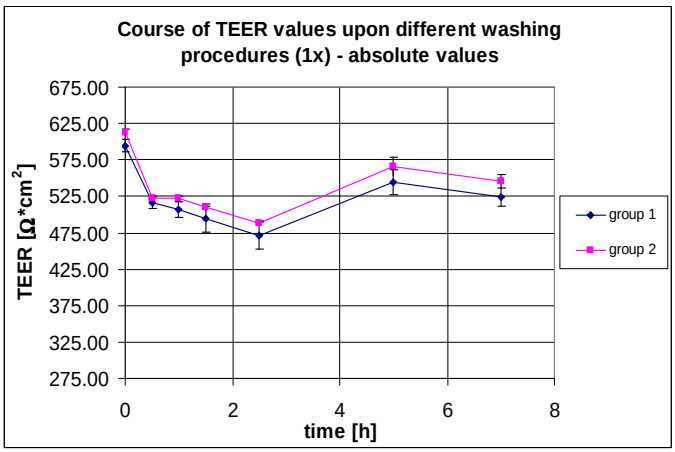

Figure 53: Course of the absolute TEER values over 7h in the incubator hood at 37℃ without shaking. The cells were washed 1 time with D-PBS. Group 1 was washed with D-PBS (without Ca^{2+}/Mg^{2+}) and group 2 was washed with D-PBS (with Ca^{2+}/Mg^{2+}). Each group consisted of 3 wells. Transwell transport medium (including 0.5% Ethanol (v/v) was at 37℃ and the reference solution in the Endohm chamber was at ambient temperature (25 – 30℃). The cell monolayers were of passage 65 and 21 days post seeding.

(Figure 53) shows an initial decrease in the measured TEER values with a subsequent recovery over the next hours (but not up to 100%). This decrease may be due to the exposition of the cell monolayer to the air during the removal of the culture medium and during the washing step. The same applies also if there would be a replacement of the solution in the apical and basal compartment after the initial TEER measurement.

To further investigate the effect of the exposition of the cell monolayer to the air on the course of the TEER values a pre-incubation period before the initial measurement was introduced. After the removal of the culture medium and one washing step with D-PBS (with Ca^{2+}/Mg^{2+}), the transport medium was added to the apical and basal compartment. The cells were then incubated for at least 60min in the incubator at 37°C in an atmosphere of 8% CO_2 and in equilibrium with distilled and autoclaved water. After this period the initial TEER measurement was performed. One Transwell plate was then subject to incubation in the incubator hood at 37°C and 75rpm without a total replacement of the transport medium (500µl were withdrawn in each compartment and replaced), whereas on the second Transwell plate the transport medium was first totally exchanged again before the incubation in the incubator hood at 37°C and 75rpm. The course of the TEER values for the two groups is displayed in (Figure 54).

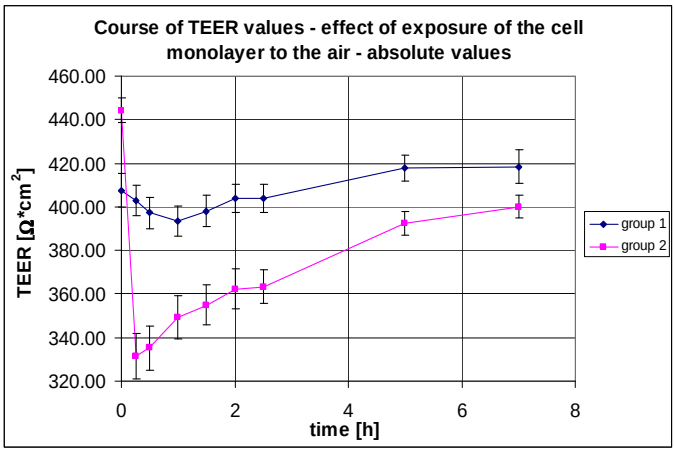

Figure 54: Course of the absolute TEER values over 7h in the incubator hood at 37°C and 75rpm. Group 1 was directly subject to incubation after the initial TEER measurement whereas in group 2 the transport medium was replaced again completely after the initial TEER measurement. Each group consisted of 5 wells. The transport medium in the Transwells and the Endohm chamber was at 37°C for the measurements. The cell monolayers of group 1 were of passage 60 and 21 days post seeding and the cell monolayers of group 2 were of passage 60 and 20 days post seeding.

The TEER values of the cell monolayers in the Transwell plate with replacement of the transport medium after the initial TEER measurement showed an initial decrease down to 80% of the initial values, followed by a continuous recovery back to 95% after 7h of incubation. By contrast the TEER values of the Transwell without replacement of the transport medium after the initial TEER measurement fluctuated between 97.5 and

102.5% of the initial TEER values. These results strongly indicate that the exposure of the cell monolayer to air is a stress factor to the cells and the tight junctions resulting in a loss of TEER. These results are in concordance with literature [Li].

The small initial decrease of the TEER value even without replacement of the transport medium may still be due to the stress cause by the removal of the culture medium and the following washing step. The time for pre-incubation may have not been long enough for a total recovery of the TEER values. But the standard error for the mean TEER values in this case is about the same range as the decrease itself. Therefore 60min pre-incubation are regarded to be long enough to allow afterwards the detection of any changes in the TEER values caused by the medium or transported substances. The transport medium itself or the incubation in the incubator at 37°C and shaking at 75rpm don't seem to affect the TEER for the incubation time of 7h. As in the experiments with Amentoflavone always 0.5% (v/v) Ethanol were included in the transport medium, it is necessary to know the effect of Ethanol on the TEER. It is known from literature [Ma], that Ethanol is able to modulate the tight junctions and therefore the TEER. Therefore the effect of the presence of 0.5% (v/v) in the transport medium was investigated. Ethanol (0.5% (v/v) was added to the transport medium after the initial TEER measurement (without exchange of the whole transport medium) and the TEER was followed for 5h (Figure 55).

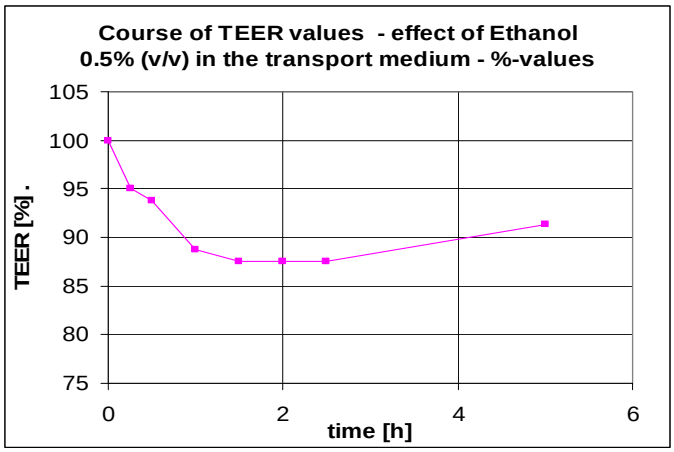

Figure 55: Course of the %-TEER values over 5h in the incubator hood at 37°C and 75rpm in the presence of 0.5% (v/v) Ethanol in the transport medium. The Transwell was directly subject to incubation after the initial TEER measurement and addition of the Ethanol. Only 1 well was measured. The transport medium in the Transwells and the Endohm chamber was at 37°C for the measurements. The cell monolaye rs were of passage 60 and 22 days post seeding.

Within 1.5h after the addition of Ethanol the TEER decreases down to 87.5% of the initial value. Until the end of the incubation of 5h the value shows a recovery up to over 90%. Compared to the incubation without Ethanol the decrease appears to be more

pronounced and the recovery with time smaller. But two control experiments on the course of TEER performed with transport medium without Ethanol according to the "standard measurement procedure" described later revealed that an initial decrease of the TEER values of about 10% is normal (Figure 56). Therefore no effects were detected that could be attributed to the presence of Ethanol (0.5% (v/v) in the transport medium.

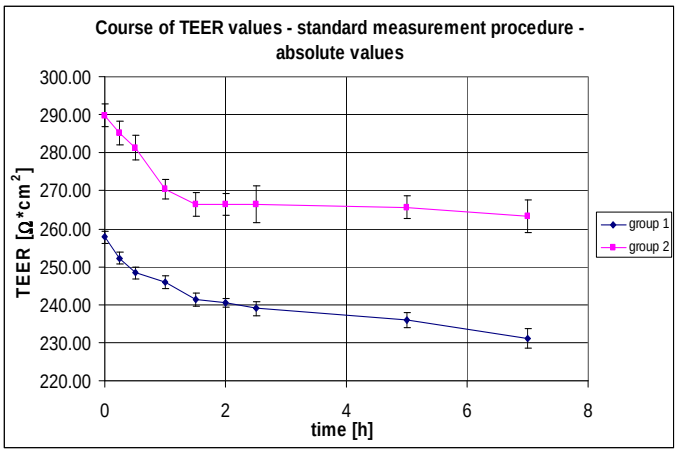

Figure 56: Course of the absolute TEER values over 7h in the incubator hood at 37°C and 75rpm. Measurement in both groups was performed according the standard procedure. Each group consisted of 6 wells. The transport medium in the Transwells and the Endohm chamber was at 37°C for the measurements. The cell monolayers of group 1 were of passage 65 and 18 days post seeding and the cell monolayers of group 2 were of passage 61 and 19 days post seeding.

Further points that may affect the measured TEER values are the density of plating the cells. This influences the homogeneity of the values and the absolute values itself, because the TEER is depending on the time of confluence of the cells on the polycarbonate membrane and the confluence itself is depending on the density of plating. Therefore it is recommended to seed only 2 – 3 wells at a time followed by a rehomogenisation of the cell suspension. Taken all this together the factors affecting the most the measurement and the measured values are the type of the electrode use (Endohm chamber or STX-2-electrode), the temperature at which the measurement is performed, the way of washing the cells (D-PBS (with or without Ca^{2+}/Mg^{2+})) and the exposition of the monolayer to air.

The following protocol ("standard measurement procedure") is recommended to allow a reproducible and meaningful TEER measurement. The Endohm chamber is preferentially used for the TEER measurements, whereas the geometry of the chamber should always be the same. The distance between the lower side of the electrode and the upper part of the case used for the present word was approximately 1.75cm. For resistance measurement, the Endohm chamber can be used directly without preincubation of the electrode. The chamber is filled with Ethanol 70% (v/v) and incubated for 15min for

sterilisation. After the removal of the Ethanol the chamber is washed several times with transport medium. At 37°C the resistance of a blank Transwell plate with transport medium was 7Ω*cm^2. For the measurements the Endohm chamber was filled with 4.6ml and the apical compartment of the Transwell with 1.6ml transport medium 37°C. It is necessary to strictly control the plating density of the cells used for transport experiments and to use always the same plating density. For the measurement itself the culture medium is withdrawn and the Transwell plate should be carefully washed 1 time with D-PBS (with Mg^{2+}/Ca^{2+}) 37°C (apical compartment 3.5ml, basal compartment 4.0ml). After the D-PBS is withdrawn, the transport medium 37°C is added (apical compartment 1600µl and basal compartment 2800µl). The Transwell plate in incubated for 60min in the incubator 37°C in an atmosphere of 8% CO_2 and in equilibrium with distilled and autoclaved water. 4.6ml transport medium 37°C is added to the Endohm chamber. The Transwell plate is taken out of the incubator and the TEER measurements are performed as fast and carefully as possible (1 measurement per well, the well is transferred to the chamber with tweezers). The volume necessary for the addition of the stock solution of the compound for the transport experiments is withdrawn. The cell monolayer should always be covered with transport medium. After the transport experiment the volume withdrawn for sampling is replaced in the apical compartment and the TEER measured again. One limitation of the TEER measurement procedure is, that the lowest TEER value for usage of the cell monolayers for transport studies was never checked for the permeability of a model compound to assess the paracellular permeability e.g. Mannitol.

7.2. Detection of Amentoflavone phase II metabolism in Caco-2 cell monolayers using enzymatical cleavage

To further assure the formation of the Amentoflavone conjugates, a global enzymatical cleavage of the glucuronides and sulfates was performed with Succus helix pomatia (SHP). Caco-2 cells of passage 60 were grown for 19 days on a petri dish as described in the publication part ("Amentoflavone transport"). After removing the culture medium, cells were rinsed once with 15ml D-PBS (without Ca^{2+} und Mg^{2+}) and 25ml of the transport medium with 10µM Amentoflavone (containing 1% ethanol (v/v)) were added. The petri dish was kept at 37°C in the incubation h ood and agitated for 7h on an orbital compact shaker at $50min^{-1}$. As a blank, transport medium with 1% ethanol (v/v) was incubated and treated the same way. At the end of the incubation 117µl of the respective samples were taken and combined with 13µl of a solution of Tween 80 0.1% (v/v), mixed and then analysed by HPLC-MS. The monolayer was checked with the inverted phase contrast microscope for morphological alterations. After the incubation the transport medium with Amentoflavone and the corresponding conjugates as well as the blank samples were centrifuged for 10min at 2000rpm. 117µl of the respective supernatant were taken and combined with 13µl of a solution of Tween 80 0.1% (v/v), mixed and then analysed by HPLC-MS. The supernatant was adjusted to pH 4.80 with acetic acid 50%. The blank was divided into two parts. One part was also adjusted to pH 4.80. The other half (7.00ml) was added with 175µl Amentoflavone solution 250µM and also adjusted to pH 4.80 (final Amentoflavone concentration approximately 6µM). Again 117µl of the respective solutions were taken and combined with 13µl of a solution of Tween 80 0.1% (v/v), mixed and then analysed by HPLC-MS. 2ml of the solutions of each subgroup adjusted to pH 4.80 were transferred to centrifuge tubes 15ml and added with either 300µl SHP (at ambient temperature) or 300µl double distilled water (at ambient temperature). The tubes were incubated in the water bath for 60min at 55°C. After the addition of 2.3ml Methanol (at ambient temperature) the samples were vortexed for 10s and put for 20min in an ice-water-mixture. The samples were centrifuged for 10min at 4500rpm, corresponding 3370g. 117µl of the respective supernatant were taken and combined with 13µl of a solution of Tween 80 0.1% (v/v), mixed and then analysed by HPLC-MS. During each step the molar concentration of Amentoflavone and the Amentoflavone conjugates was measured. During the enzymatical cleavage of the glucuronides and sulfates that was performed with Succus helix pomatia (SHP), the amount of Amentoflavone and the Amentoflavone conjugates was measured in each step (Table 18).

Table 18: Concentration of Amentoflavone (AF) during the treatment with SHP and water.

sample	concentration AF [µM]	concentration AF conjugates [µM]
samples after 7h incubation (n=3)	7.42 +/- 0.36	0.53 +/- 0.08
samples after centrifugation (n=5)	6.24 +/- 0.31	0.51 +/- 0.08
samples after adjustment to pH 4.8 (n=5)	4.16 +/- 0.19	0.39 +/- 0.08
blank after addition of AF and adjustment to pH 4.8 (n=5)	4.18 +/- 0.25	0
samples with AF and AF conjugates after treatment with SHP (n=5)	0.86 +/- 0.15	0
samples with AF and AF conjugates after treatment with H_2O (n=5)	1.84 +/- 0.10	0.20 +/- 0.08
blank with AF after treatment with SHP (n=5)	0.70 +/- 0.14	0
blank with AF after treatment with H_2O (n=5)	1.80 +/- 0.12	0

It is noteworthy that the concentrations of Amentoflavone in the samples incubated with SHP are less than half the ones compared with the samples incubated only with water. That may be explained by a possible binding to the proteins present in SHP. The concentrations of Amentoflavone in the samples that contained conjugates are higher than the one in the blank added with Amentoflavone. This is true for both the samples treated with SHP and the samples treated with water. But the samples had already before the incubation slightly higher concentrations of Amentoflavone than the blanks. The difference in Amentoflavone concentration between the samples and the blanks added with Amentoflavone is bigger for the samples that were treated with SHP than the ones treated with water, even though those show lower concentrations. The less pronounced decrease in Amentoflavone concentration after incubation with SHP in the samples that contained Amentoflavone conjugates in comparison with the blanks, could be explained by a liberation of previously conjugated Amentoflavone. The molar amount of Amentoflavone present in the final solutions after treatment with water in relation with the 2ml volume prior to the treatment result for the samples with Amentoflavone and Amentoflavone-conjugates in slightly higher concentrations than initially measured whereas the calculated concentrations of the blanks with Amentoflavone are slightly lower than initially measured. A possible explanation to these findings would be a cleavage of the conjugates because of the acidic milieu and the increased temperature. As there was no decrease in the concentration of the Amentoflavone conjugates during the treatment with water (see later) this explanation is not likely. A further explanation

would be an evaporation of the Methanol used or impreciseness during pipetting. It is furthermore remarkable that there is a decrease of about 2µM in the Amentoflavone concentrations after adjusting the pH to 4.80, compared to the concentrations after the centrifugation. This decrease cannot be explained as a dilution effect, as only about 2 – 3 drops of acetic acid and sodium hydroxide were used. The decrease is most probably attributed to adsorption to the surface of the centrifugation tubes used. The samples were subject to several decanting steps until measured after the adjustment to pH 4.80 whereas the measurement after the centrifugation was directly performed with samples from the centrifugation tubes used for centrifugation. After the incubation with SHP in samples with Amentoflavone conjugates neither the glucuronide nor the sulfate were detectable as monitored with UV or m/z 617 & m/z 713 ((Figure 58), (Figure 60) and (Figure 62)). In the UV chromatogram of the samples that contained Amentoflavone conjugates, new peaks appeared with slightly later retention than the metabolites ((Figure 62) and (Figure 68)) (metabolites approximately 4.5, 4.8 & 5.6min; new peaks ca. 5.4 & 6.5min). These peaks were also detectable in the blank samples with added Amentoflavone and in the blank samples that consisted only of transport medium that were treated with SHP. As the AUC of these new peaks (Table 19) is in the same range for all subgroups treated with SHP, they were attributed to the presence of SHP. It has to be noted that the AUC of the new peaks is about 5 times bigger than the one in samples with Amentoflavone and Amentoflavone conjugates after treatment with H_2O (AUC 109.90 +/- 5.22 [mAU*s]). The chromatograms of the samples treated with H_2O are shown in ((Figure 57), (Figure 59) and (Figure 61)) and the chromatograms of transport medium, treated with either H_2O or SHP are shown in ((Figure 63) to (Figure 68)).

Table 19: AUC of the newly detected peaks after treatment with SHP.

sample	total AUC [mAU*s]
samples with AF and AF conjugates after treatment with SHP (n=5)	626.38 +/- 17.01
blank with AF after treatment with SHP (n=5)	625.92 +/- 5.37
blank (without AF) after treatment with SHP (n=3)	578.55 +/- 0.64

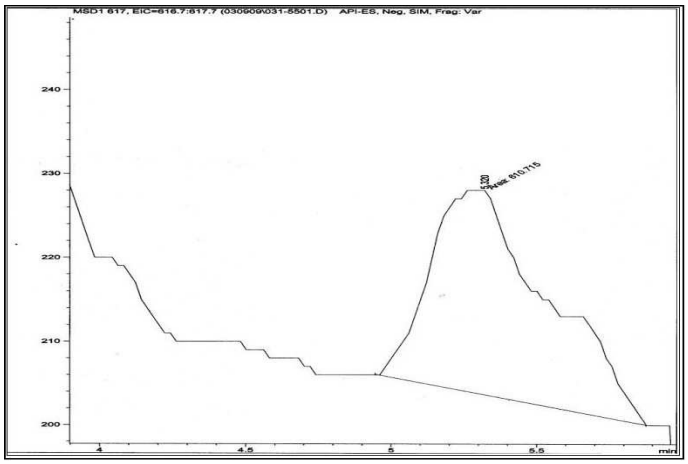

Figure 57: m/z 617 corresponding to the sulfate conjugates in samples containing Amentoflavone and the Amentoflavone conjugates treated with H_2O.

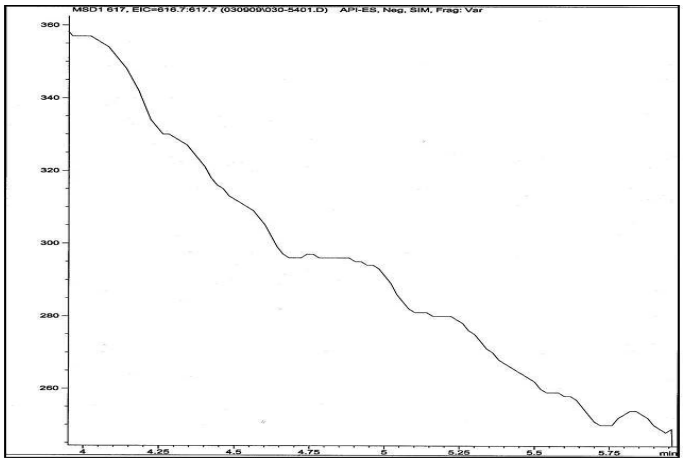

Figure 58: m/z 617 corresponding to the sulfate conjugates in samples containing Amentoflavone and the Amentoflavone conjugates treated with SHP.

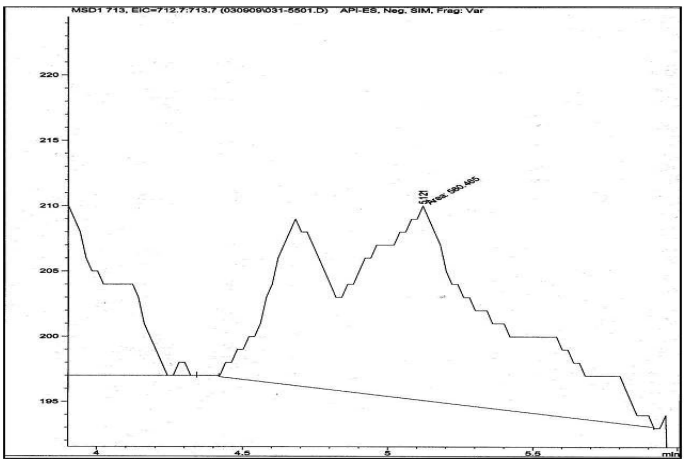

Figure 59: m/z 713 corresponding to the glucuronide conjugates in samples containing Amentoflavone and the Amentoflavone conjugates treated with H_2O.

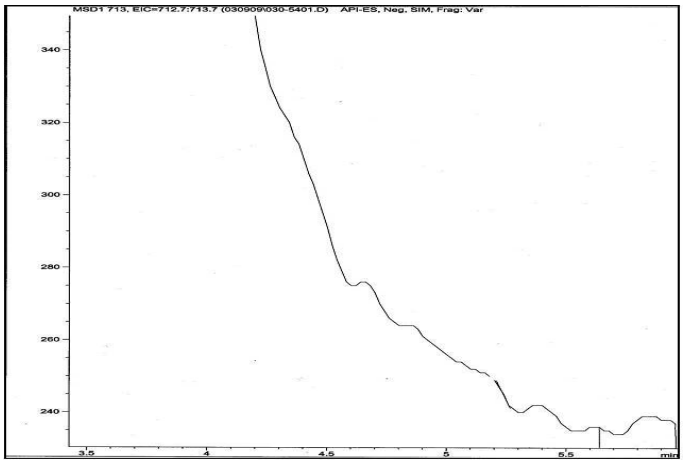

Figure 60: m/z 713 corresponding to the glucuronide conjugates in samples containing Amentoflavone and the Amentoflavone conjugates treated with SHP.

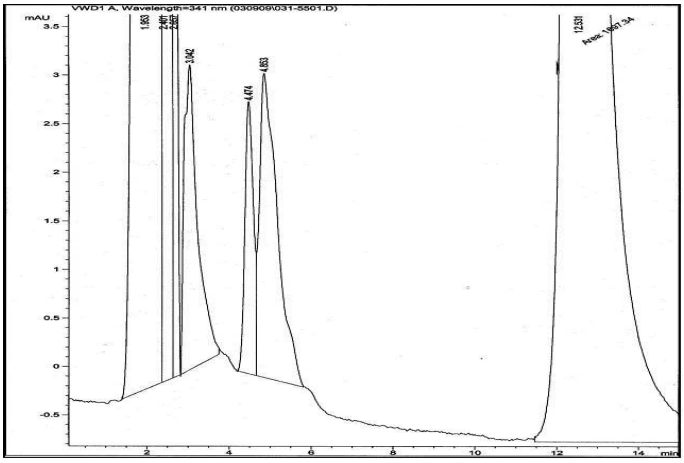

Figure 61: UV chromatogram with the peaks for the sulfate and glucuronide conjugates (retention 4.474 & 4.853min) and the Amentoflavone (retention 12.531min) in samples containing Amentoflavone and the Amentoflavone conjugates treated with H_2O.

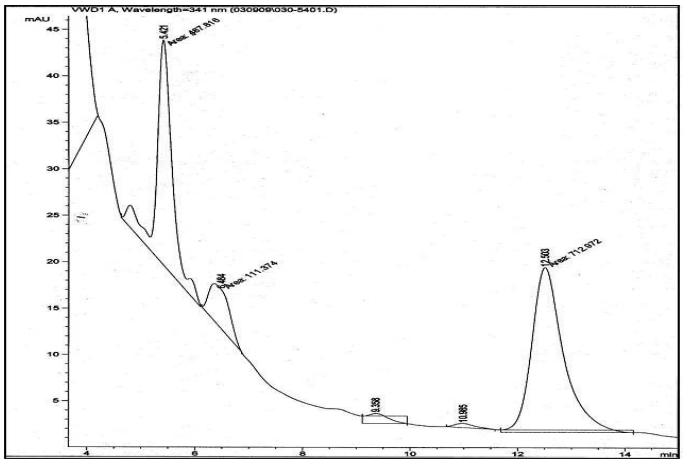

Figure 62: UV chromatogram with the newly developed peaks (retention 5.4 & 6.5min) and the Amentoflavone (retention 12.503min) in samples containing Amentoflavone and the Amentoflavone conjugates treated with SHP.

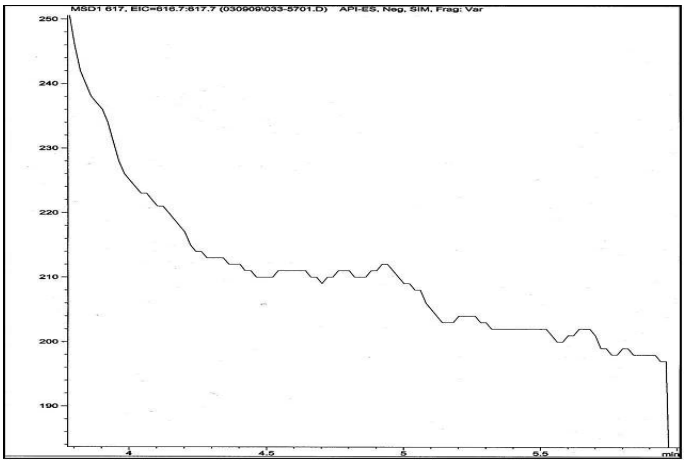

Figure 63: m/z 617 corresponding to the sulfate conjugates in samples of pure transport medium treated with H_2O.

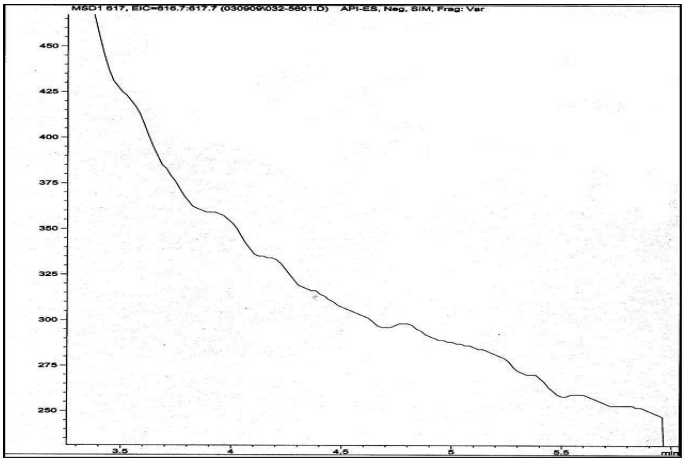

Figure 64: m/z 617 corresponding to the sulfate conjugates in samples of pure transport medium treated with SHP.

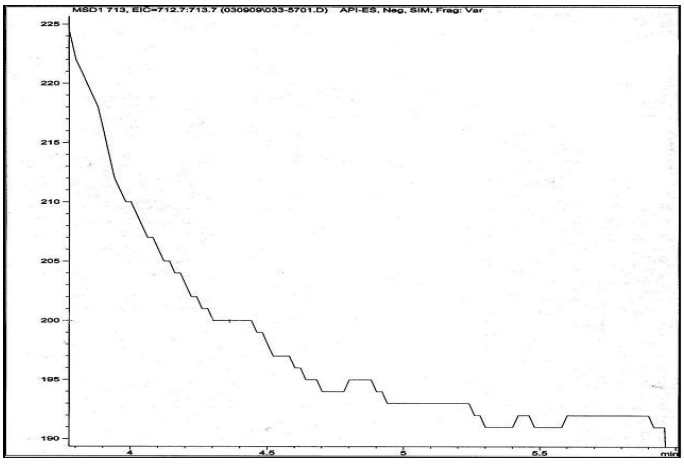

Figure 65: m/z 713 corresponding to the glucuronide conjugates in samples of pure transport medium treated with H_2O.

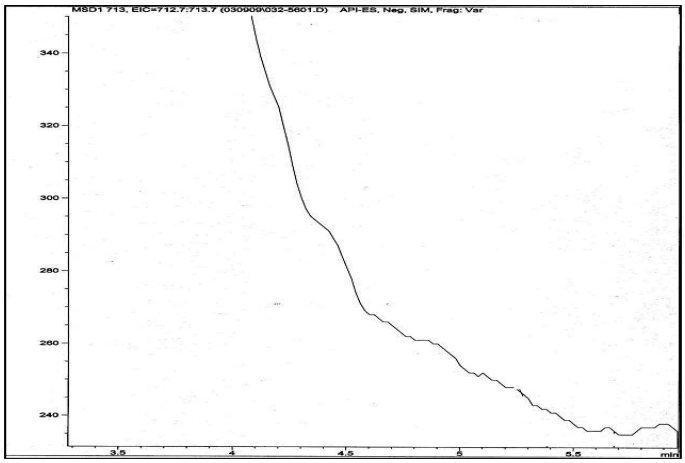

Figure 66: m/z 713 corresponding to the glucuronide conjugates in samples of pure transport medium treated with SHP.

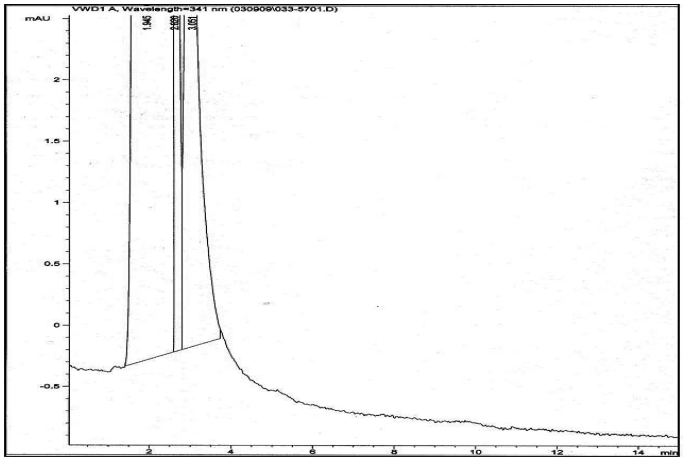

Figure 67: UV chromatogram of samples of pure transport medium treated with H_2O.

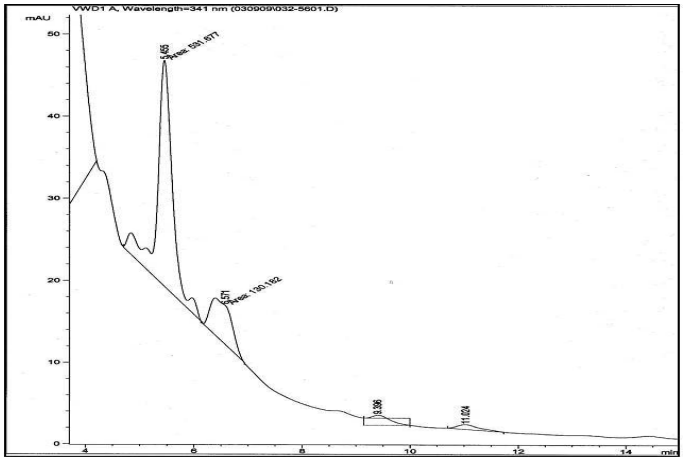

Figure 68: UV chromatogram with the newly developed peaks (retention 5.4 & 6.5min) in samples of pure transport medium treated with SHP.

It cannot be ruled out that the conjugates are subject to protein binding as Amentoflavone itself is. A binding to the proteins present in SHP could also lead to a disappearance of the conjugates even though they were not cleaved. After the adjustment of the pH to 4.80 the concentration and therefore the amount of

Amentoflavone in the samples with Amentoflavone and Amentoflavone conjugates and the blanks with Amentoflavone was approximately the same (Table 18). On condition that the addition of SHP leads to a total cleavage of the Amentoflavone conjugates, the amount of Amentoflavone in the samples that contained the conjugates should be higher to the same amount in comparison to the blanks only containing Amentoflavone. The difference in the amount of Amentoflavone after SHP incubation is 0.736nmole. This is almost the same amount as the there were conjugates before the incubation (0.78nmole, Table 20). The conjugates were therefore no longer detectable because enzymatical cleavage rather than protein binding.

Table 20: Concentration and amount of Amentoflavone and Amentoflavone conjugates during the processing with SHP or water.

	AF in samples	AF conjugates in samples	AF in blank
concentration after adjustment to pH 4.80 [µM]	4.16 +/- 0.19	0.39 +/- 0.08	4.18 +/- 0.25
amount in 2ml after adjustment to pH 4.80 [nmol]	8.32 +/- 0.38	0.78 +/- 0.16	8.36 +/- 0.5
concentration after incubation with H_2O [µM]	1.84 +/- 0.10	0.20 +/- 0.08	1.80 +/- 0.12
amount in 4.6ml after incubation with H_2O [nmol]	8.464 +/- 0.46	0.92 +/- 0.368	8.28 +/- 0.552
concentration after incubation with SHP [µM]	0.86 +/- 0.15	0	0.70 +/- 0.14
amount in 4.6ml after incubation with SHP [nmol]	3.956 +/- 0.69	0	3.22 +/- 0.644

7.3. Amentoflavone

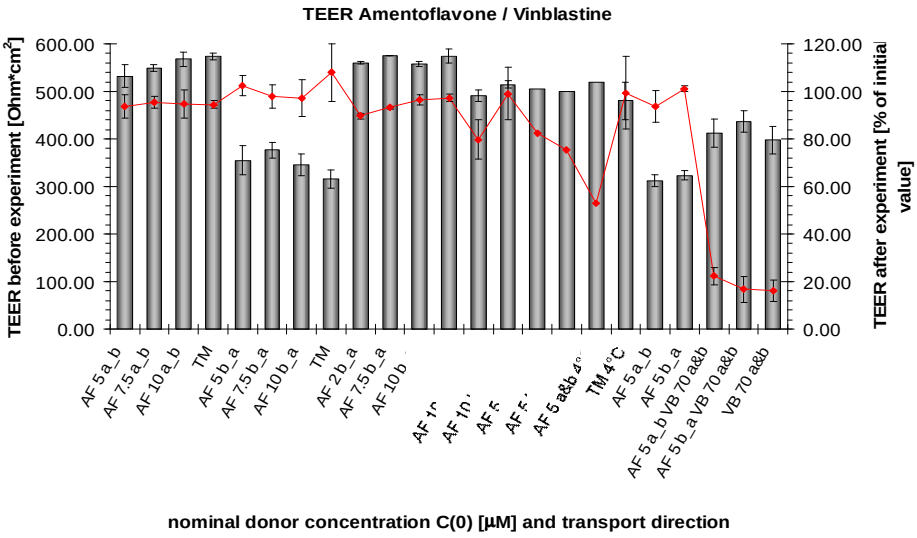

Figure 69: TEER values of Caco-2 cell monolayer used in the experiments with Amentoflavone and Vinblastine (individual or in combination). The grey columns display the absolute values before the experiments and the points connected with a line the TEER values after the experiment in % of the initial values. At least 3 wells were used per group. Numbers display concentrations in [µM]. TM = transport medium.

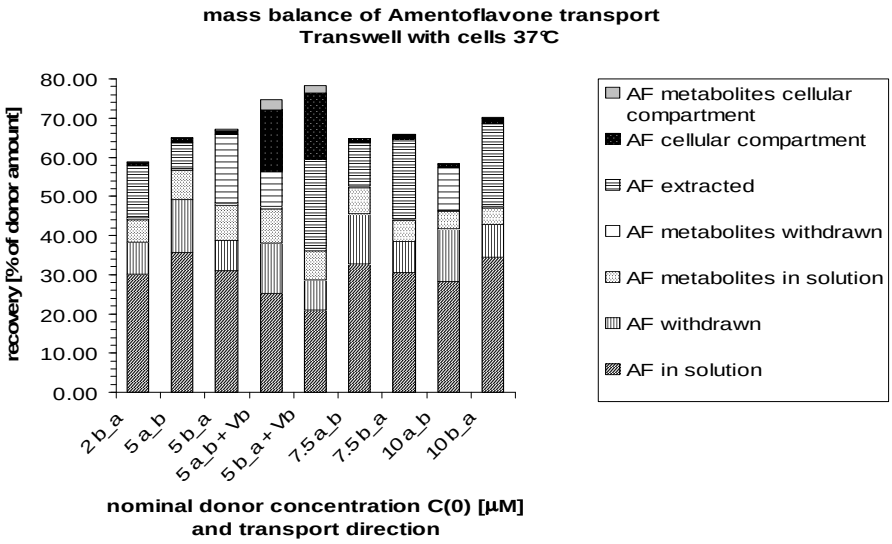

Figure 70: Mass balance of Amentoflavone transport at 37°C in Caco-2 cells grown in Transwell plates (individual transport and combination with Vinblastine). At least 3 wells were used per group. Numbers display concentrations in [µM].

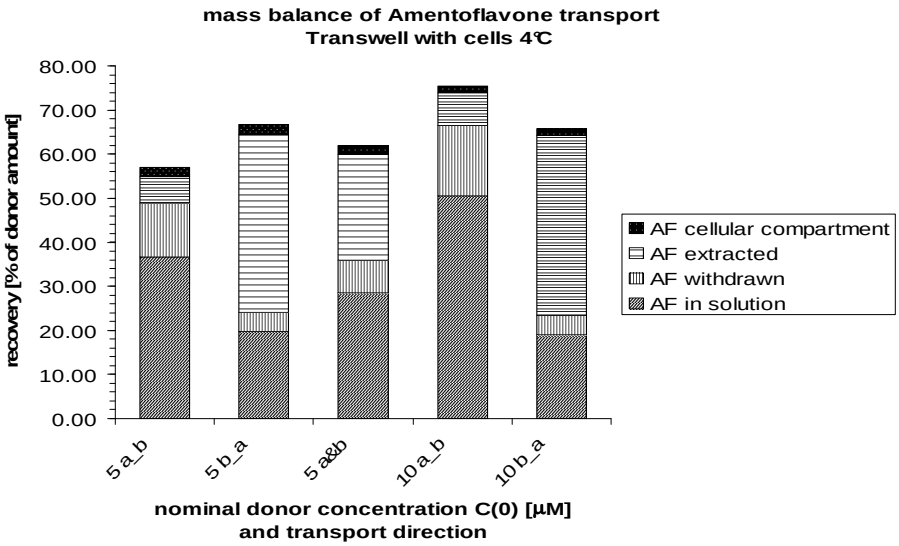

Figure 71: Mass balance of Amentoflavone transport at 4°C in Caco-2 cells grown in Transwell plates (individual transport). At least 3 wells were used per group. Numbers display concentrations in [µM].

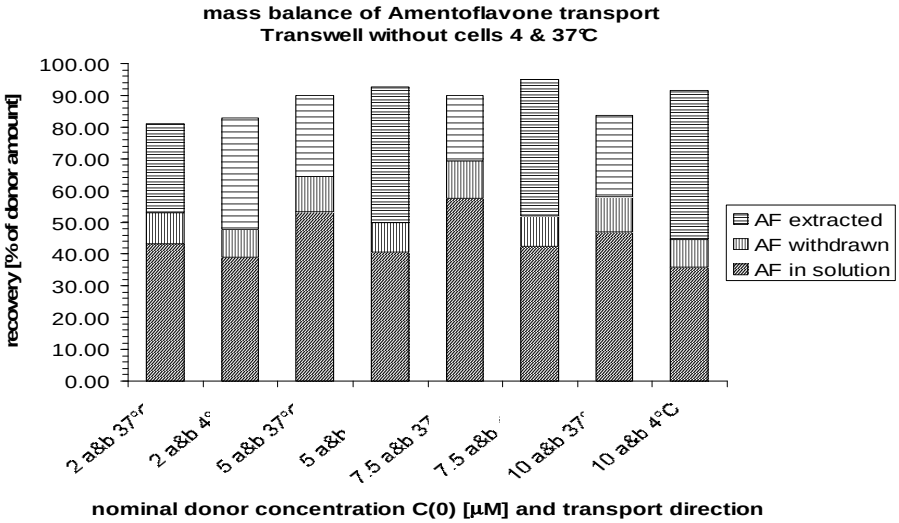

Figure 72: Mass balance of Amentoflavone transport at 4 & 37°C in Transwell plates without cells (individual transport). At least 3 wells were used per group. Numbers display concentrations in [µM].

7.4. Digoxin

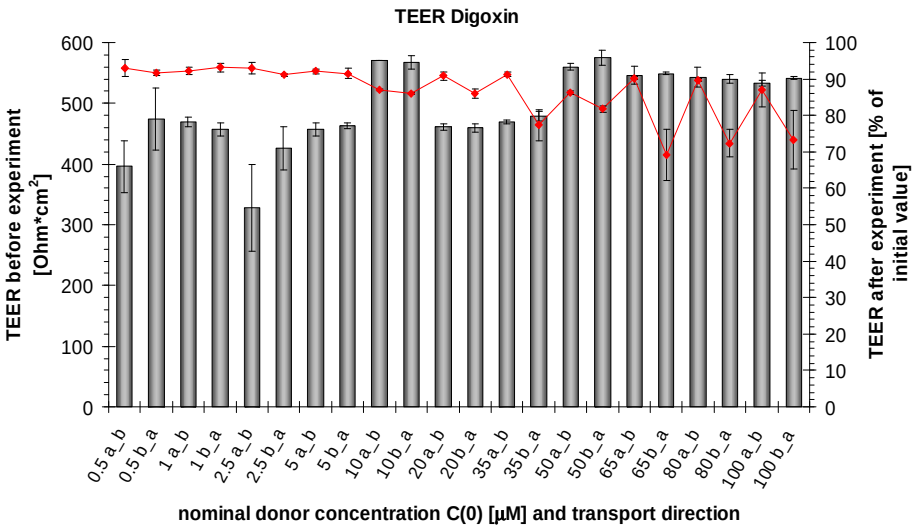

Figure 73: TEER values of Caco-2 cell monolayer used in the experiments with Digoxin (individual transport). The grey columns display the absolute values before the experiments and the points connected with a line the TEER values after the experiment in % of the initial values. At least 3 wells were used per group. Numbers display concentrations in [µM].

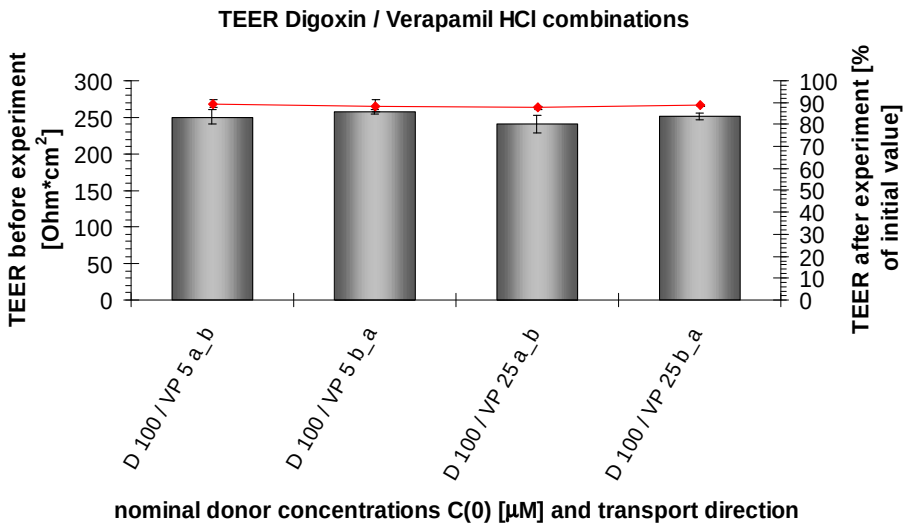

Figure 74: TEER values of Caco-2 cell monolayer used in the experiments with combinations of Digoxin with Verapamil. The grey columns display the absolute values before the experiments and the points connected with a line the TEER values after the experiment in % of the initial values. At least 3 wells were used per group. Numbers display concentrations in [µM].

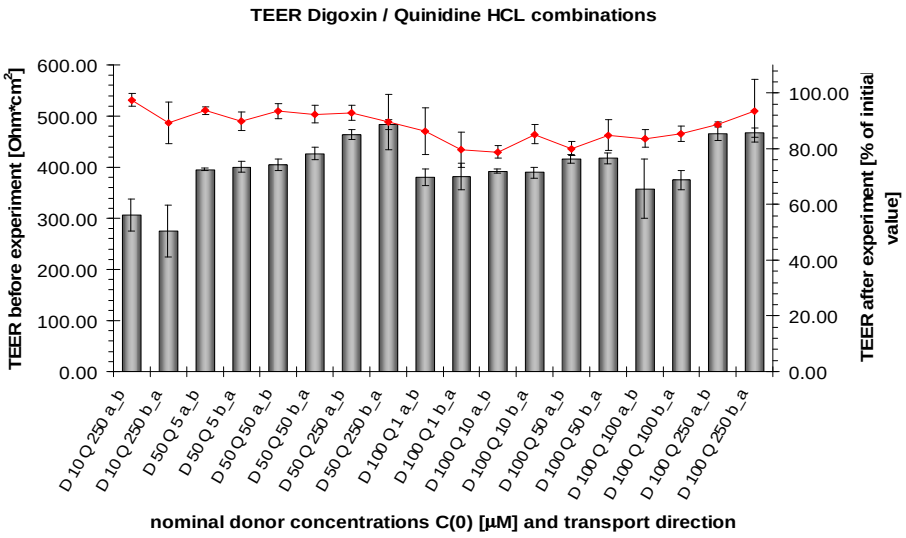

Figure 75: TEER values of Caco-2 cell monolayer used in the experiments with combinations of Digoxin with Quinidine. The grey columns display the absolute values before the experiments and the points connected with a line the TEER values after the experiment in % of the initial values. At least 3 wells were used per group. Numbers display concentrations in [µM].

Table 21: Model estimated kinetic parameters of Digoxin permeation across Caco-2 cell monolayers.

nominal donor concentration [µM]	0.5	1	2.5	5	10	20	35	50	65	80	100
model derived C(0) a_b	0.437	0.887	2.433	5.031	10.855	19.888	34.36	56.339	71.159	85.154	110.971
model derived C(0) b_a	0.416	0.859	2.377	4.986	10.801	20.243	34.388	55.771	70.73	85.794	107.639
average model derived C(0)	0.427	0.873	2.405	5.009	10.828	20.066	34.374	56.055	70.945	85.474	109.305
P ● 10^6 [cm/s]	24.373	18.867	27.215	23.33	27.92	28.658	25.306	25.969	26.694	24.916	27.609
efflux rate vk [nmol/(s●cm^2)]	0.000010179	0.000016258	0.000064992	0.00011678	0.00030307	0.00054787	0.00085304	0.00143825	0.00186169	0.00207638	0.00298635
J_{active} = vk [pmol/(s●cm^2)]	0.010179	0.016258	0.064992	0.11678	0.30307	0.54787	0.85304	1.43825	1.86169	2.07638	2.98635
$J_{passive}$ = P ● C(0) [pmol/(s●cm^2)]	0.010395085	0.016470891	0.065452075	0.116848305	0.30231776	0.575037099	0.869868444	1.455692295	1.893792483	2.129670184	3.017801745
$J_{passive}$ - J_{active} [pmol/(s●cm^2)]	0.000216084	0.000212891	0.000460075	6.8305E-05	-0.00075224	0.027167099	0.016828444	0.017442295	0.032102483	0.053290184	0.031451745
lowest M_{Cell} a_b [nmol]	0.000076	0.000103	0.000175	0.0001	2.7E-09	0.003	0.0026	0.0038	0.0057	0.0072	0.0112
highest M_{Cell} a_b [nmol]	0.00009	0.00016	0.00021	0.000115	3.20E-09	0.0036	0.00305	0.00445	0.0066	0.0085	0.0132
average M_{Cell} a_b [nmol]	0.000083	0.0001315	0.0001925	0.0001075	2.95E-09	0.0033	0.002825	0.004125	0.00615	0.00785	0.0122
lowest M_{Cell} b_a [nmol]	0	0	0	0	0	0.006	0.004	0.003	0.008	0.015	0
highest M_{Cell} b_a [nmol]	0.00058	0.00098	0.00335	0.0067	0.0164	0.036	0.06	0.083	0.11	0.13	0.162
average M_{Cell} b_a [nmol]	0.00029	0.00049	0.001675	0.00335	0.0082	0.021	0.032	0.043	0.059	0.0725	0.081
average M_{Cell} a_b/b_a [nmol]	0.0001865	0.00031075	0.00093375	0.00172875	0.004100001	0.01215	0.0174125	0.0235625	0.032575	0.040175	0.0466
FRV scaled	0.0596	0.0787	0.0195	0.0145	0.0185	0.394	0.0472	0.151	0.0448	0.0517	0.165

Table 22: Model estimated kinetic parameters of Digoxin permeation across Caco-2 cell monolayers in experiments with concomitant incubation with a second compound (Q = Quinidine).

nominal donor concentration [µM]	10 Q 250	50 Q 5	50 Q 50	50 Q 250	100 Q 1	100 Q 10	100 Q 50	100 Q 100	100 Q 250
model derived C(0) a_b	10.765	48.707	48.02	68.34	71.195	91.104	139.853	134.636	132.278
model derived C(0) b_a	8.734	45.929	44.767	65.831	80.633	81.889	136.787	131.707	126.515
average model derived C(0)	9.750	47.318	46.394	67.086	75.914	86.497	138.320	133.172	129.397
$P \bullet 10^6$ [cm/s]	14.63	20.37	11.331	12.4018	31.777	19.327	14.113	13.359	13.723
efflux rate vk [nmol/(s●cm^2)]	0.000025384	0.00086676	0.00018218	5.02209E-05	0.00215568	0.00084461	0.00043663	0.000082509	0.00015304
J_{active} = vk [pmol/(s●cm^2)]	0.0254	0.8668	0.1822	0.0502	2.1557	0.8446	0.4366	0.0825	0.1530
$J_{passive} = P \bullet C(0)$ [pmol/(s●cm^2)]	0.1426	0.9639	0.5257	0.8320	2.4123	1.6717	1.9521	1.7790	1.7757
$J_{passive} - J_{active}$ [pmol/(s●cm^2)]	0.1173	0.0971	0.3435	0.7818	0.2566	0.8271	1.5155	1.6965	1.6227
average M_{Cell} a_b [nmol]	0.04025	0.0265	0.1445	0.2875	0.0143	0.2075	0.49	0.575	0.545
average M_{Cell} b_a [nmol]	0.03575	0.04375	0.1465	0.305	0.1225	0.2175	0.5375	0.62	0.5725
average M_{Cell} a_b/b_a [nmol]	0.038	0.035125	0.1455	0.29625	0.0684	0.2125	0.51375	0.5975	0.55875
FRV scaled	0.0709	0.0766	0.0455	0.0471	0.026	0.0126	0.0169	0.0578	0.0116

Table 23: Apparent permeability coefficient P_{app} of Digoxin permeation in Caco-2 cell monolayers. Values were calculated from the permeated amount of substance after 15min. Values are displayed as mean of 3 measurements with the standard deviation (SD).

Digoxin: nominal donor concentration [µM]	P_{app} a_b • 10^6 [cm/s]	SD	P_{app} b_a • 10^6 [cm/s]	SD	Efflux Ratio
0.5	ND		ND		-
1	ND		ND		-
2.5	ND		27.41	9.35	-
5	ND		13.88	4.36	-
10	ND		20.78	2.38	-
20	0.17	0.05	28.14	1.03	166.39
35	0.09	0.01	26.15	0.42	284.13
50	ND		25.27	0.05	-
65	0.31	0.02	26.87	1.74	85.33
80	0.23	0.07	24.35	0.58	108.17
100	0.17	0.16	30.35	0.71	177.47

Table 24: Apparent permeability coefficient P_{app} of Digoxin permeation in Caco-2 cell monolayers in experiments with concomitant incubation with a second substance (Q = Quinidine). Values were calculated from the permeated amount of substance after 15min. Values are displayed as mean of 3 measurements with the standard deviation.

Digoxin: nominal donor concentration [µM]		P_{app} a_b • 10^6 [cm/s]	SD	P_{app} b_a • 10^6 [cm/s]	SD	Efflux Ratio
10	Q 250	4.74	1.04	7.39	0.12	1.56
50	Q 5	2.27	0.21	19.03	1.21	8.39
50	Q 50	2.52	0.42	7.51	0.36	2.99
50	Q 250	4.10	0.38	5.34	0.63	1.30
100	Q 1	0.95	0.13	20.92	1.24	21.91
100	Q 10	5.53	0.28	16.90	1.14	3.06
100	Q 50	4.86	0.24	7.68	0.31	1.58
100	Q 100	6.62	0.56	8.53	0.08	1.29
100	Q 250	5.87	0.05	9.12	3.93	1.56

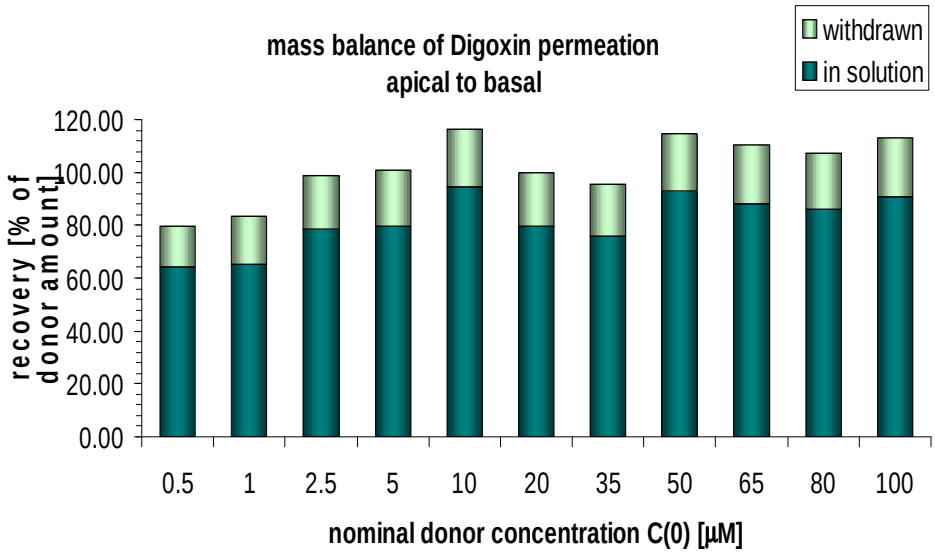

Figure 76: Mass balance of Digoxin transport apical to basal at 37°C in Caco-2 cells grown in Transwell plates (individual transport). At least 3 wells were used per group. Numbers display concentrations in [µM].

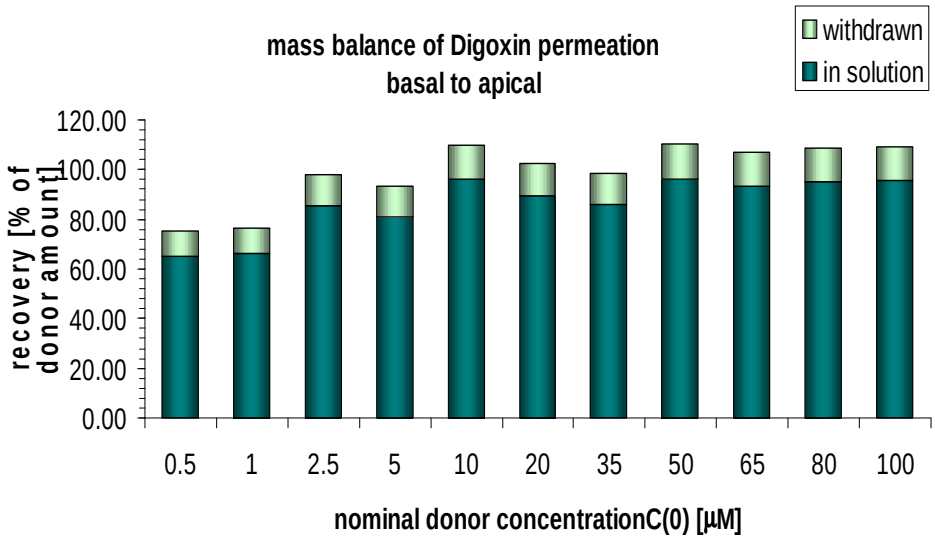

Figure 77: Mass balance of Digoxin transport basal to apical at 37°C in Caco-2 cells grown in Transwell plates (individual transport). At least 3 wells were used per group. Numbers display concentrations in [µM].

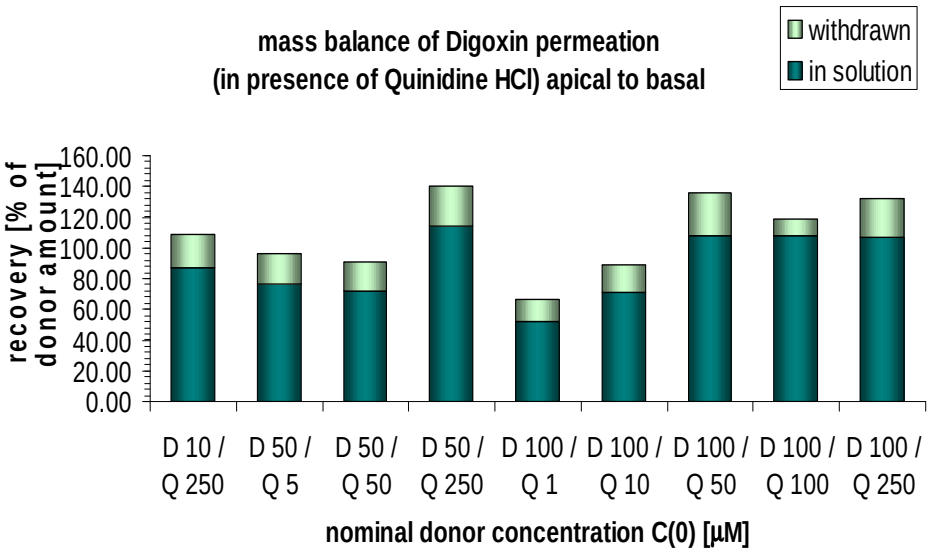

Figure 78: Mass balance of Digoxin transport apical to basal at 37°C in Caco-2 cells grown in Transwell plates (in presence of Quinidine). At least 3 wells were used per group. Numbers display concentrations in [µM].

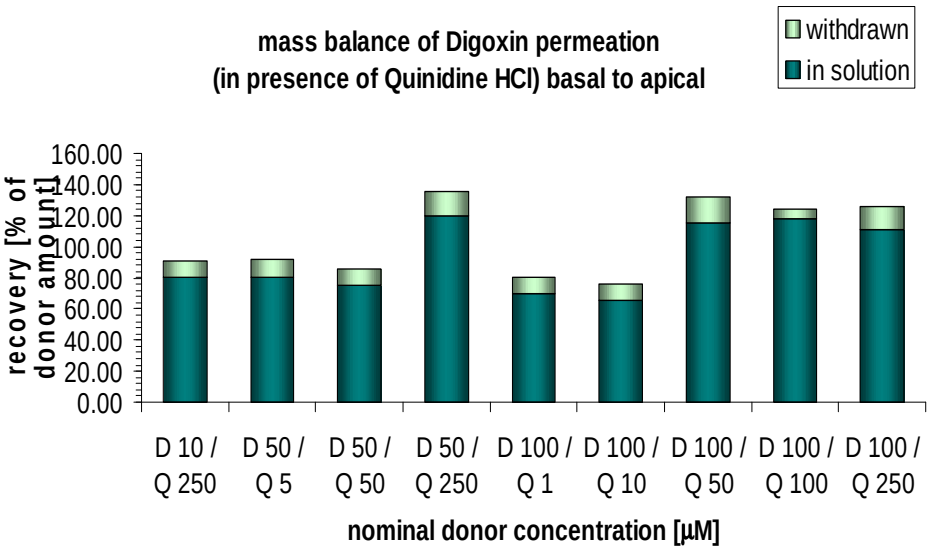

Figure 79: Mass balance of Digoxin transport basal to apical at 37°C in Caco-2 cells grown in Transwell plates (in presence of Quinidine). At least 3 wells were used per group. Numbers display concentrations in [µM].

7.5. Quinidine

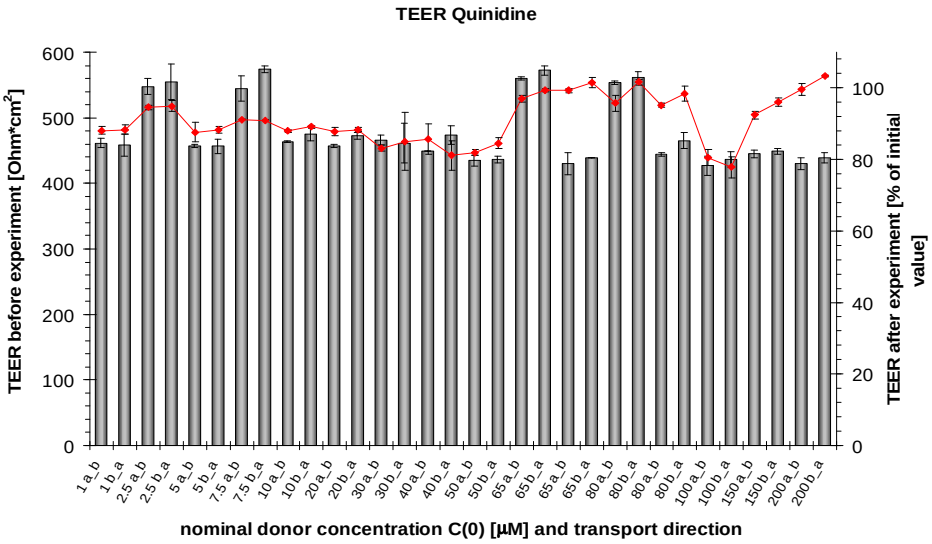

Figure 80: TEER values of Caco-2 cell monolayer used in the experiments with Quinidine (individual transport). The grey columns display the absolute values before the experiments and the points connected with a line the TEER values after the experiment in % of the initial values. At least 3 wells were used per group. Numbers display concentrations in [µM].

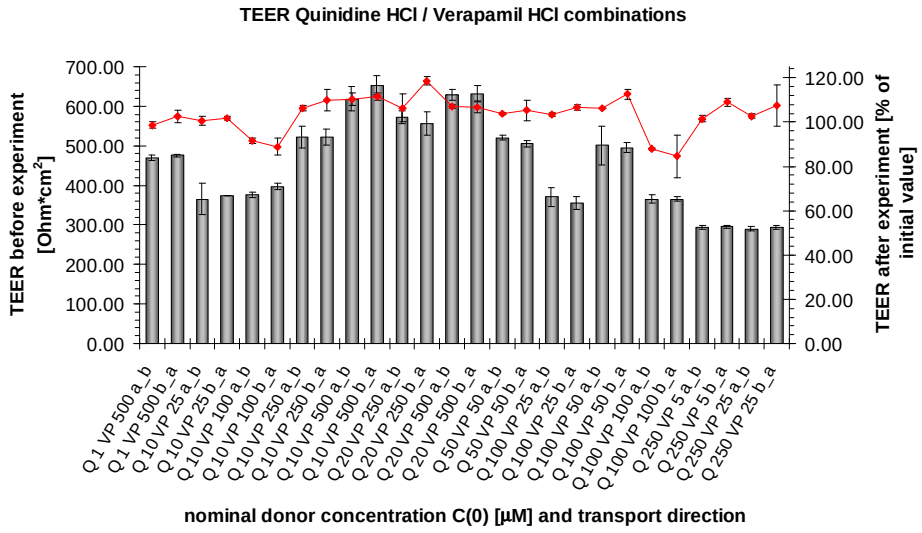

Figure 81: TEER values of Caco-2 cell monolayer used in the experiments with combinations of Quinidine with Verapamil. The grey columns display the absolute values before the experiments and the points connected with a line the TEER values after the experiment in % of the initial values. At least 3 wells were used per group. Numbers display concentrations in [µM].

Table 25: Model estimated kinetic parameters of Quinidine permeation across Caco-2 cell monolayers.

nominal donor concentration [µM]	1	2.5	5	7.5	10	20	30	40	50	65	65	80	80	100	150	200
model derived C(0) a_b	0.82	2.492	4.991	7.69	10.08	19.889	29.156	38.789	48.581	63.608	64.037	78.764	77.555	96.166	145.789	194.402
model derived C(0) b_a	0.776	2.387	4.515	7.345	9.79	19.989	29.784	38.835	48.919	66.159	64.802	80.684	77.009	97.115	154.458	201.366
average model derived C(0)	0.80	2.44	4.75	7.52	9.94	19.94	29.47	38.81	48.75	64.88	64.42	79.72	77.28	96.64	150.12	197.88
$P \bullet 10^6$ [cm/s]	265.57	208.78	147.668	169.15	182.91	184.65	194.14	195.17	206.74	187.49	195.73	197.2	198.67	199.77	215.259	210.075
efflux rate vk [nmol/(s•cm^2)]	0.0002	0.0005	0.0007	0.0011	0.0015	0.0021	0.0021	0.0022	0.0029	0.0019	0.0021	0.0023	0.0025	0.0040	0.0040	0.0053
J_{active} = vk [pmol/(s•cm^2)]	0.2177	0.5202	0.6874	1.0580	1.4546	2.1360	2.0607	2.2153	2.941	1.8779	2.0883	2.2516	2.5278	3.9794	3.978177	5.2997
$J_{passive}$ = P • C(0) [pmol/(s•cm^2)]	0.2119	0.5093	0.7019	1.2716	1.8172	3.6817	5.7213	7.5749	10.0786	12.1650	12.6088	15.7216	15.3536	19.3059	32.3154	41.5705
$J_{passive}$ - J_{active} [pmol/(s•cm^2)]	-0.0058	-0.0109	0.01452	0.2136	0.3626	1.5457	3.6606	5.3597	7.1376	10.2871	10.5205	13.4699	12.8258	15.3265	28.3373	36.2707
lowest M_{Cell} a_b [nmol]	2.05E-10	2.60E-09	0.00113	0.0048	0.0072	0.028	0.062	0.092	0.116	0.18	0.17	0.225	0.22	0.26	0.58	0.76
highest M_{Cell} a_b [nmol]	2.70E-10	3.30E-09	0.00155	0.0065	0.0096	0.038	0.085	0.125	0.158	0.245	0.245	0.31	0.295	0.35	0.425	0.575
average M_{Cell} a_b [nmol]	2.375E-10	2.95E-09	0.00134	0.00565	0.0084	0.033	0.0735	0.1085	0.137	0.2125	0.2075	0.2675	0.2575	0.305	0.5025	0.6675
lowest M_{Cell} b_a [nmol]	0	0	0	0.0063	0.0105	0.043	0.095	0.135	0.175	0.275	0.27	0.34	0.32	0.375	0.67	0.86
highest M_{Cell} b_a [nmol]	0.0019	0.006	0.0115	0.023	0.0325	0.0815	0.144	0.195	0.245	0.365	0.3505	0.45	0.4225	0.52	0.86	1.13
average M_{Cell} b_a [nmol]	0.00095	0.003	0.00575	0.01465	0.0215	0.06225	0.1195	0.165	0.21	0.32	0.31025	0.395	0.37125	0.4475	0.765	0.995
average M_{Cell} a_b/b_a [nmol]	0.000475	0.0015	0.003545	0.01015	0.01495	0.047625	0.0965	0.13675	0.1735	0.26625	0.25888	0.33125	0.31438	0.37625	0.63375	0.83125
FRV scaled	0.218	0.0592	0.159	0.0521	0.0303	0.00959	0.00436	0.00759	0.00877	0.0053	0.00463	0.00457	0.00365	0.00851	0.00503	0.00287

Table 26: Model estimated kinetic parameters of Quinidine permeation across Caco-2 cell monolayers in experiments with concomitant incubation with a second compound (D = Digoxin / VP = Verapamil).

nominal donor concentration [µM]	10 VP 25	10 VP 100	10 VP 250	10 VP 500	10 D 100	20 VP 250	20 VP 500	50 VP 50	50 D 50	50 D 100	100 VP 25	100 VP 50	100 VP 100	100 D 100
model derived C(0) a_b	10.375	9.673	9.423	9.778	9.061	19.046	18.894	49.923	46.251	48.715	100.529	98.214	101.544	96.024
model derived C(0) b_a	10.058	9.749	9.68	9.692	9.149	19.377	18.892	49.6	47.859	48.28	99.613	98.362	99.588	95.482
average model derived C(0)	10.217	9.711	9.552	9.735	9.105	19.212	18.893	49.762	47.055	48.498	100.071	98.288	100.566	95.753
$P \bullet 10^6$ [cm/s]	178.45	197.75	179.28	204.65	262.33	205.57	231.03	180.87	230.05	299.03	196	190.67	201.59	304.13
efflux rate vk [nmol/(s●cm^2)]	0.0005	0.0006	0.0004	0.0004	0.0008	0.0009	0.0009	0.0026	0.0025	0.0022	0.0031	0.0047	0.0040	0.0032
J_{active} = vk [pmol/(s●cm^2)]	0.5354	0.6060	0.4311	0.4430	0.8247	0.8592	0.9625	2.6101	2.5277	2.2929	3.1395	4.6732	4.0136	3.2376
$J_{passive}$ = P ● C(0) [pmol/(s●cm^2)]	1.8231	1.9204	1.7124	1.9923	2.3885	3.9493	4.3648	9.0004	10.8250	14.5022	19.6139	18.7406	20.2731	29.1214
$J_{passive}$ - J_{active} [pmol/(s●cm^2)]	1.2878	1.3144	1.2813	1.5493	1.5638	3.0901	3.4023	6.3903	8.2973	12.2093	16.4744	14.0673	16.2595	25.8837
average M_{Cell} a_b [nmol]	0.0295	0.02625	0.0278	0.0305	0.0235	0.059	0.0588	0.141	0.1395	0.162	0.33	0.295	0.3225	0.33
average M_{Cell} b_a [nmol]	0.04275	0.04075	0.043	0.0445	0.037	0.089	0.0865	0.2125	0.2135	0.235	0.475	0.445	0.4625	0.4775
average M_{Cell} a_b/b_a [nmol]	0.03613	0.0335	0.0354	0.0375	0.03025	0.074	0.0726	0.1768	0.1765	0.1985	0.4025	0.37	0.3925	0.4038
FRV scaled	0.0218	0.0117	0.0258	0.0176	0.0461	0.017	0.0244	0.0165	0.0145	0.0457	0.0128	0.0131	0.0085	0.0319

Table 27: Apparent permeability coefficient P_{app} of Quinidine permeation in Caco-2 cell monolayers. Values were calculated from the permeated amount of substance after 15min. Values are displayed as mean of 3 measurements with the standard deviation (SD). ND = no permeation detected. * values calculated by drawing a straight line from zero to the concentration after 30min.

Quinidine: nominal donor concentration [µM]	P_{app} a_b • 10^6 [cm/s]	SD	P_{app} b_a • 10^6 [cm/s]	SD	Efflux Ratio
1	ND		76.27	14.18	-
2.5	ND		133.65	5.86	-
5	3.92*		100.68	1.25	25.69
7.5	9.45*		128.21	2.84	13.57
10	13.25	3.10	131.74	3.94	9.94
20	22.84	0.60	122.15	8.20	5.35
30	41.59	0.77	111.72	5.73	2.69
40	48.80	3.39	97.28	3.98	1.99
50	47.93	2.17	105.29	1.58	2.20
65	56.96	1.28	88.33	9.28	1.55
65	60.27	3.79	89.79	0.41	1.49
80	61.73	0.99	90.18	4.04	1.46
80	61.39	0.77	88.60	1.98	1.44
100	58.17	1.90	84.65	2.98	1.46
150	68.02	2.49	92.10	4.84	1.35
200	73.49	1.97	95.13	2.41	1.29

Table 28: Apparent permeability coefficient of Quinidine permeation in Caco-2 cell monolayers in experiments with concomitant incubation with a second substance (D = Digoxin / VP = Verapamil). Values were calculated from the permeated amount of substance after 15min. Values are displayed as mean of 3 measurements with the standard deviation.

Quinidine: nominal donor concentration [µM]		P_{app} a_b • 10^6 [cm/s]	SD	P_{app} b_a • 10^6 [cm/s]	SD	Efflux Ratio
10	VP 25	47.98	5.39	83.65	6.89	1.74
10	VP 100	42.56	2.21	103.57	3.28	2.43
10	VP 250	36.39	2.29	59.64	4.90	1.64
10	VP 500	65.42	3.68	77.14	0.51	1.18
10	D 100	77.61	4.84	102.12	9.16	1.32
20	VP 250	51.29	1.97	85.77	5.18	1.67
20	VP 500	68.08	5.80	86.32	3.00	1.27
50	VP 50	44.41	2.58	73.84	3.13	1.66
50	D 50	55.75	3.72	99.45	9.56	1.78
50	D 100	86.66	1.60	126.16	13.38	1.46
100	VP 25	62.05	4.61	96.63	12.88	1.56
100	VP 50	52.43	1.90	81.79	1.36	1.56
100	VP 100	63.79	2.68	88.56	1.15	1.39
100	D 100	92.24	4.30	113.59	6.43	1.23

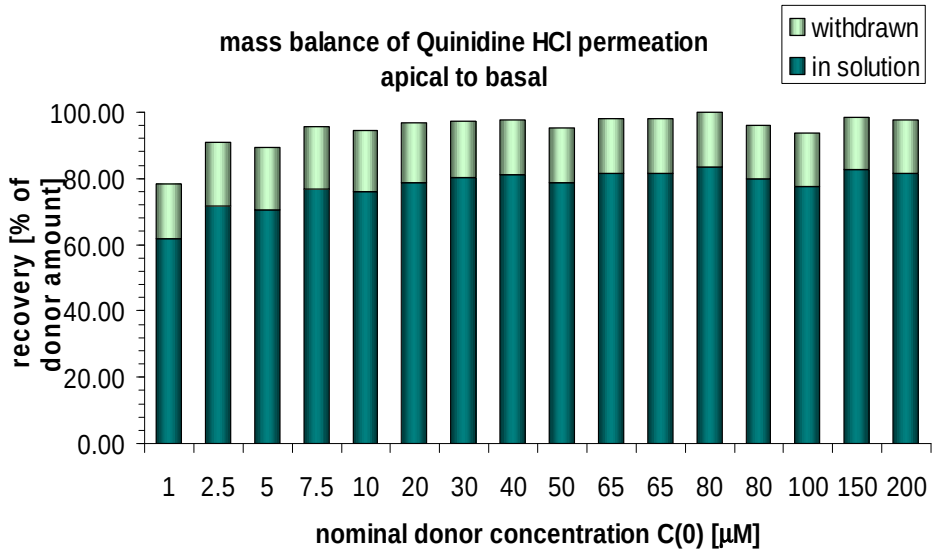

Figure 82: Mass balance of Quinidine transport apical to basal at 37°C in Caco-2 cells grown in Transwell plates (individual transport). At least 3 wells were used per group. Numbers display concentrations in [µM].

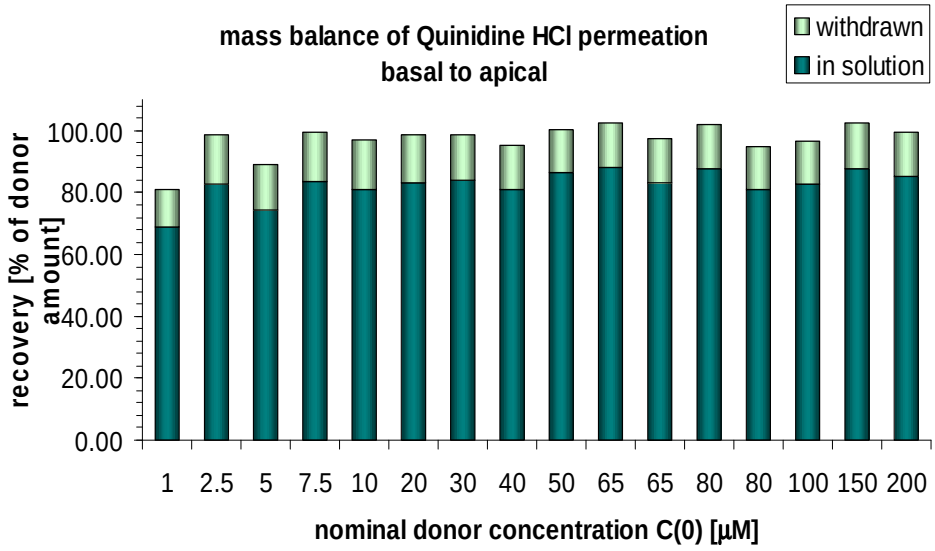

Figure 83: Mass balance of Quinidine transport basal to apical at 37°C in Caco-2 cells grown in Transwell plates (individual transport). At least 3 wells were used per group. Numbers display concentrations in [µM].

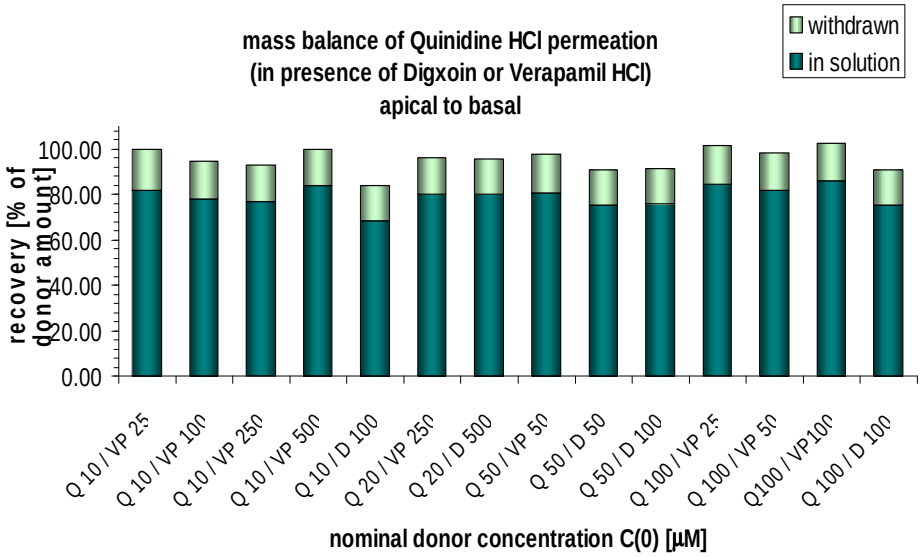

Figure 84: Mass balance of Quinidine transport apical to basal at 37°C in Caco-2 cells grown in Transwell plates (in presence of Digoxin or Verapamil). At least 3 wells were used per group. Numbers display concentrations in [µM].

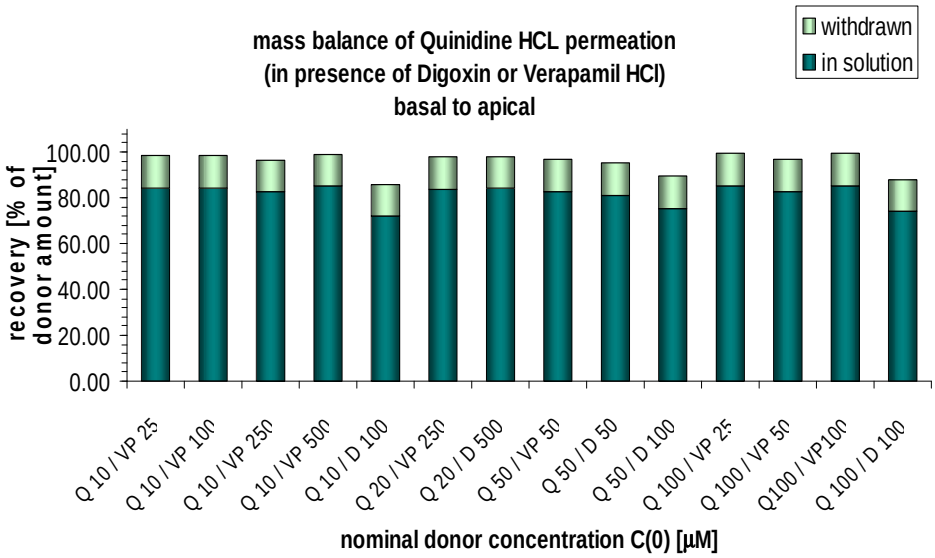

Figure 85: Mass balance of Quinidine transport basal to apical at 37°C in Caco-2 cells grown in Transwell plates (in presence of Digoxin or Verapamil). At least 3 wells were used per group. Numbers display concentrations in [µM].

7.6. Verapamil

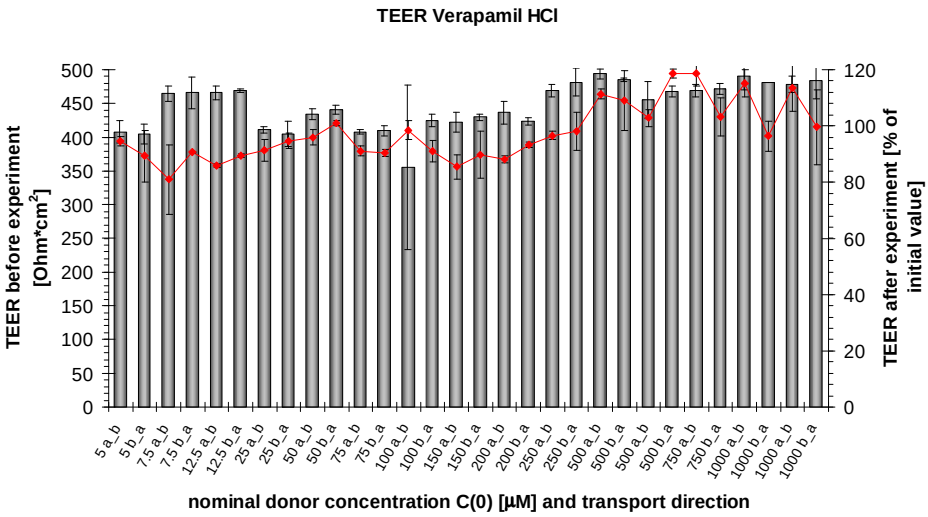

Figure 86: TEER values of Caco-2 cell monolayer used in the experiments with Verapamil (individual transport). The grey columns display the absolute values before the experiments and the points connected with a line the TEER values after the experiment in % of the initial values. At least 3 wells were used per group. Numbers display concentrations in [µM].

Table 29: Model estimated kinetic parameters of Verapamil permeation across Caco-2 cell monolayers.

nominal donor concentration [µM]	5	7.5	12.5	25	50	75	100	150	200	250	500	500	750	1000	1000
model derived C(0) a_b	4.455	6.494	10.346	22.417	40.717	67.787	85.517	150.206	191.834	240.571	513.388	502.722	739.104	972.106656	1004.6382
model derived C(0) b_a	4.686	6.481	11.09	22.571	44.025	68.998	83.539	147.834	196.51	241.695	485.841	505.258	749.668	1033.77653	990.15366
average model derived C(0)	4.57	6.49	10.72	22.49	42.37	68.39	84.53	149.02	194.17	241.13	499.61	503.99	744.39	1002.94	997.40
P ● 10^6 [cm/s]	304.36	265.51	261.2	255.24	293.29	275.47	291.33	262.19	274.93	242.54	242.35	240.42	251.11	220.46	230.64
efflux rate vk [nmol/(s●cm^2)]	0.0003	0.0004	0.0006	0.0008	0.0013	0.0018	0.0019	0.0050	0.0063	0.0066	0.0194	0.02204	0.0149	0.0305	0.0347
J_{active} = vk [pmol/(s●cm^2)]	0.3398	0.4366	0.5815	0.8220	1.2812	1.7873	1.8816	5.0343	6.2889	6.5946	19.3616	22.0412	14.8549	30.4763	34.6934
$J_{passive}$ = P ● C(0) [pmol/(s●cm^2)]	1.3911	1.7225	2.7995	5.7414	12.4270	18.8401	24.6255	39.0716	53.3837	58.4844	121.0815	121.1692	186.9228	221.1085	230.0394
$J_{passive}$ - J_{active} [pmol/(s●cm^2)]	1.0513	1.2859	2.2180	4.9194	11.1458	17.0528	22.7440	34.0373	47.0948	51.8898	101.720	99.1281	172.0678	190.6322	195.3460
lowest M_{Cell} a_b [nmol]	0.0112	0.0163	0.0275	0.065	0.123	0.21	0.27	0.445	0.575	0.72	1.45	1.375	2.3	2.8	2.85
highest M_{Cell} a_b [nmol]	0.015	0.022	0.037	0.087	0.165	0.275	0.355	0.595	0.77	0.95	1.975	1.875	3.1	3.8	3.85
average M_{Cell} a_b [nmol]	0.0131	0.0192	0.0323	0.076	0.144	0.2425	0.3125	0.52	0.6725	0.835	1.7125	1.625	2.7	3.3	3.35
lowest M_{Cell} b_a [nmol]	0.0175	0.024	0.0435	0.093	0.2	0.305	0.375	0.635	0.85	1.05	2	2	3.4	4.4	4.1
highest M_{Cell} b_a [nmol]	0.0245	0.0335	0.0595	0.125	0.25	0.39	0.48	0.82	1.1	1.35	2.7	2.75	4.3	5.8	5.5
average M_{Cell} b_a [nmol]	0.021	0.0288	0.0515	0.109	0.225	0.3475	0.4275	0.7275	0.975	1.2	2.35	2.375	3.85	5.1	4.8
average M_{Cell} a_b/b_a [nmol]	0.0171	0.0240	0.0419	0.0925	0.1845	0.295	0.37	0.6238	0.8238	1.0175	2.03125	2	3.275	4.2	4.075
FRV scaled	0.0275	0.0516	0.031	0.0187	0.0108	0.00659	0.00822	0.00493	0.00327	0.00941	0.0054	0.00182	0.00399	0.00376	0.00372

Table 30: Model estimated kinetic parameters of Verapamil permeation across Caco-2 cell monolayers in experiments with concomitant incubation with a second compound (D = Digoxin / Q = Quinidine).

nominal donor concentration [µM]	5 Q 250	5 D 100	25 Q 10	25 Q 100	25 Q 250	25 D 100	50 Q 50	50 Q 100	100 Q 10	100 Q 100	250 Q 10	250 Q 20	500 Q 1	500 Q 10	500 Q 20
model derived C(0) a_b	4.0769	4.235	25.025	27.77	23.19	23.514	44.886	43.524	89.795	90.352	239.714	234.459	489.216	496.188	491.491
model derived C(0) b_a	4.239	4.56	25.004	24.459	23.464	25.131	45.702	44.289	91.666	91.782	242.34	244.248	488.637	499.504	499.155
average model derived C(0)	4.158	4.398	25.015	26.115	23.327	24.323	45.294	43.907	90.731	91.067	241.027	239.354	488.927	497.846	495.323
$P \bullet 10^6$ [cm/s]	303.46	315.75	242.87	256.94	293.69	304.15	251.71	259.4	244.04	251.39	260.69	270.47	249.34	268.84	306.8
efflux rate vk [nmol/(s●cm^2)]	0.0002	0.0003	0.0013	0.0009	0.0012	0.0010	0.0031	0.0029	0.0051	0.0044	0.0145	0.0131	0.0210	0.0309	0.0342
J_{active} = vk [pmol/(s●cm^2)]	0.2312	0.2567	1.2543	0.9204	1.2185	0.9836	3.1433	2.8812	5.1196	4.4458	14.4820	13.1392	21.0418	30.9411	34.2095
$J_{passive}$ = P ● C(0) [pmol/(s●cm^2)]	1.2618	1.3885	6.0753	6.7099	6.8509	7.3977	11.4010	11.3893	22.1419	22.8933	62.8333	64.7379	121.9089	133.8409	151.9651
$J_{passive}$ - J_{active} [pmol/(s●cm^2)]	1.0306	1.1319	4.8210	5.7894	5.6324	6.4141	8.2576	8.5081	17.0223	18.4476	48.3514	51.5988	100.8671	102.8999	117.7556
average M_{Cell} a_b [nmol]	0.0131	0.0135	0.0788	0.08	0.0758	0.0803	0.1335	0.129	0.275	0.2875	0.73	0.7325	1.625	1.51	1.5
average M_{Cell} b_a [nmol]	0.0203	0.0215	0.1135	0.119	0.1118	0.124	0.168	0.1658	0.415	0.43	1.1025	1.135	2.35	2.3	2.3
average M_{Cell} a_b/b_a [nmol]	0.0167	0.0175	0.0961	0.0995	0.0938	0.1021	0.1508	0.1474	0.345	0.3588	0.9163	0.9338	1.9875	1.905	1.9
FRV scaled	0.0226	0.024	0.0324	0.02	0.017	0.0115	0.0253	0.0233	0.0152	0.0142	0.0171	0.0138	0.00657	0.0158	0.0234

Table 31: Apparent permeability coefficient P_{app} of Verapamil permeation in Caco-2 cell monolayers. Values were calculated from the permeated amount of substance after 15min. Values are displayed as mean of 3 measurements with the standard deviation (SD).

Verapamil: nominal donor concentration [µM]	P_{app} a_b • 10^6 [cm/s]	SD	P_{app} b_a • 10^6 [cm/s]	SD	Efflux Ratio
5	60.34	16.63	132.02	4.40	2.19
7.5	93.67	3.83	118.75	6.44	1.27
12.5	82.73	1.68	123.81	5.68	1.50
25	84.44	11.80	102.96	10.24	1.22
50	82.63	5.84	110.75	5.16	1.34
75	88.84	10.04	108.85	3.26	1.23
100	85.21	3.60	96.29	10.59	1.13
150	86.54	1.82	110.42	9.83	1.28
200	92.31	4.79	112.26	5.99	1.22
250	73.65	11.94	99.96	0.77	1.36
500	84.69	10.87	106.67	2.11	1.26
500	81.10	2.99	111.93	2.38	1.38
750	89.29	6.39	113.09	4.29	1.27
1000	77.13	3.91	103.23	4.56	1.34
1000	85.40	5.27	109.39	6.56	1.28

Table 32: Apparent permeability coefficient P_{app} of Verapamil permeation in Caco-2 cell monolayers in experiments with concomitant incubation with a second substance (D = Digoxin / Q = Quinidine). Values were calculated from the permeated amount of substance after 15min. Values are displayed as mean of 3 measurements with the standard deviation.

Verapamil: nominal donor concentration [µM]		P_{app} a_b • 10^6 [cm/s]	SD	P_{app} b_a • 10^6 [cm/s]	SD	Efflux Ratio
5	Q 250	70.51	5.84	99.96	6.08	1.42
5	D 100	93.77	10.50	94.27	13.68	1.01
25	Q 10	70.96	8.55	98.37	7.33	1.39
25	Q 100	79.16	8.35	103.57	5.44	1.31
25	Q 250	83.44	5.28	107.76	4.18	1.29
25	D 100	84.64	10.14	121.81	7.28	1.44
50	Q 50	60.55	2.70	93.21	3.36	1.54
50	Q 100	62.61	0.22	99.75	3.88	1.59
100	Q 10	66.71	1.90	90.09	2.21	1.35
100	Q 100	70.18	3.95	93.25	1.96	1.33
250	Q 10	74.75	5.09	103.37	7.37	1.38
250	Q 20	75.60	2.91	104.52	5.95	1.38
500	Q 1	80.42	4.70	100.52	3.90	1.25
500	Q 10	79.95	5.52	105.43	1.35	1.32
500	Q 20	90.07	5.31	118.40	5.18	1.31

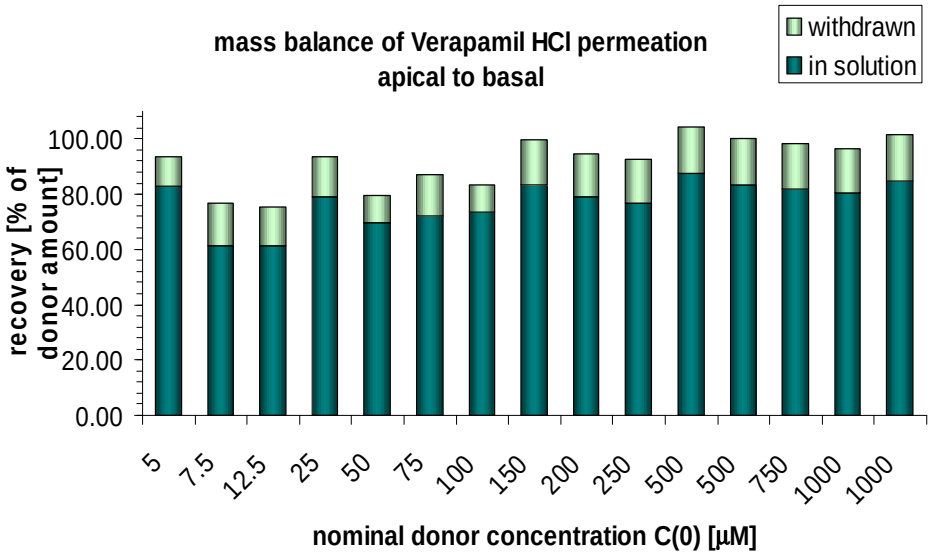

Figure 87: Mass balance of Verapamil transport apical to basal at 37°C in Caco-2 cells grown in Transwell plates (individual transport). At least 3 wells were used per group. Numbers display concentrations in [µM].

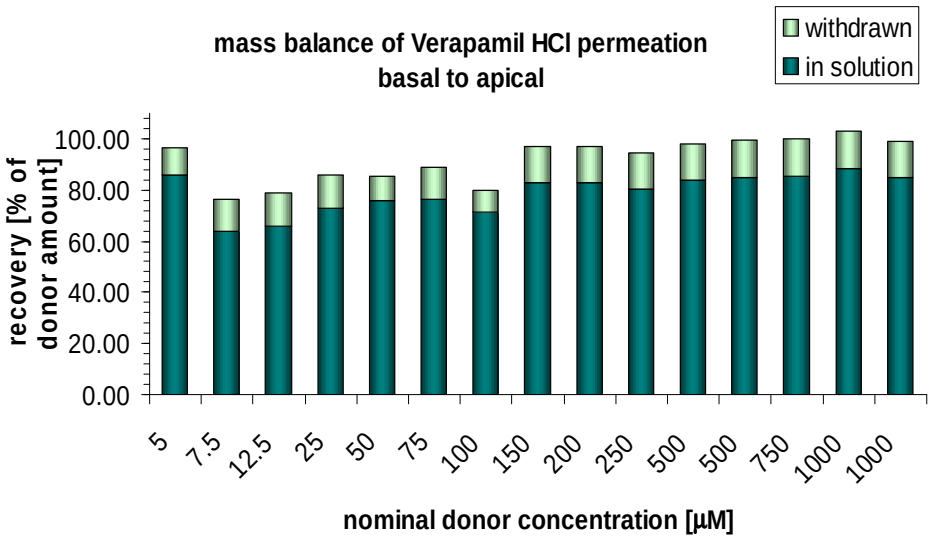

Figure 88: Mass balance of Verapamil transport basal to apical at 37°C in Caco-2 cells grown in Transwell plates (individual transport). At least 3 wells were used per group. Numbers display concentrations in [µM].

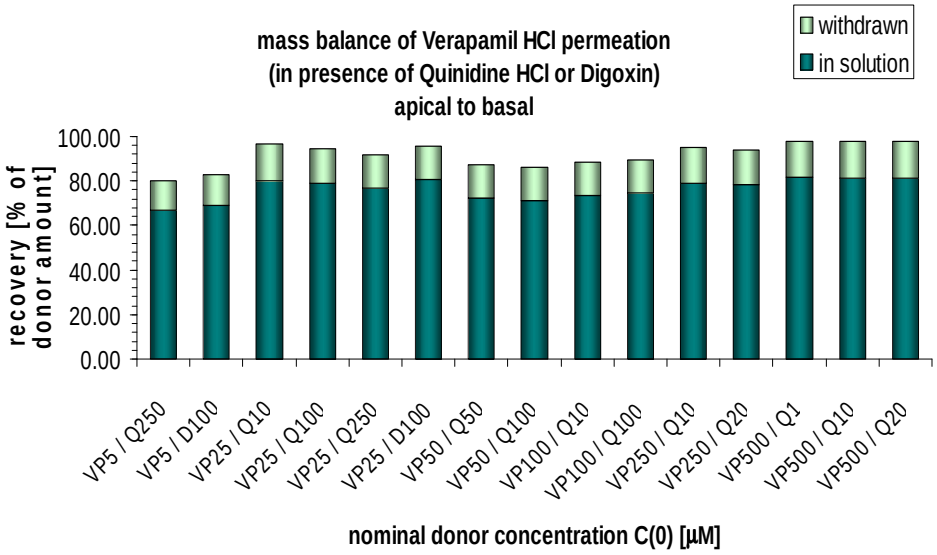

Figure 89: Mass balance of Verapamil transport apical to basal at 37°C in Caco-2 cells grown in Transwell plates (in presence of Digoxin or Quinidine). At least 3 wells were used per group. Numbers display concentrations in [µM].

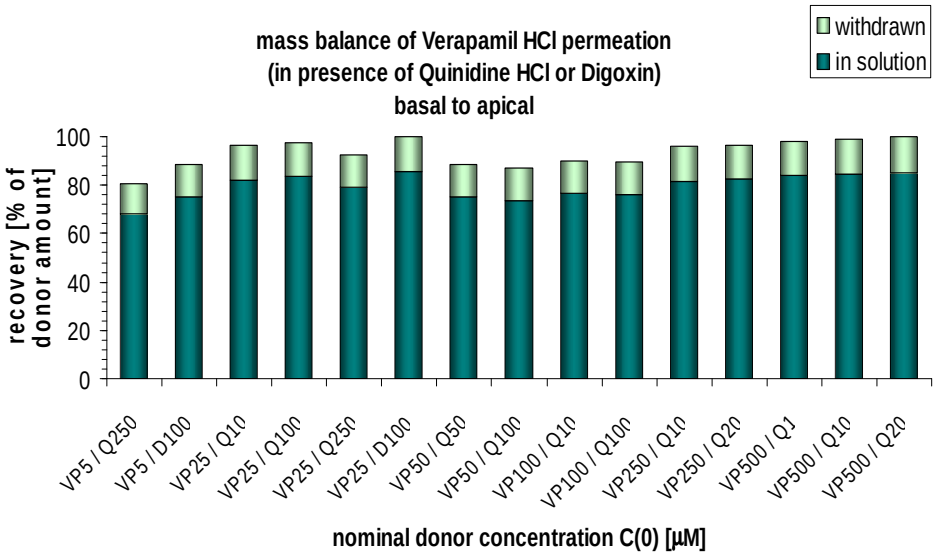

Figure 90: Mass balance of Verapamil transport basal to apical at 37°C in Caco-2 cells grown in Transwell plates (in presence of Digoxin or Quinidine). At least 3 wells were used per group. Numbers display concentrations in [µM].

8. References

Adibi, S.A. (1997). The oligopeptide transporter (Pept-1) in human intestine: biology and function. Gastroenterology. 113(1): 332 – 340.

Ambudkar, S.V., Dey, S., Hrycyna, C.A., Ramachandra, M., Pastan, I., Gottesman, M.M. (1999). Biochemical, cellular, and pharmacological aspects of the multidrug transporter. Annual review of pharmacology and toxicology. 39: 361 – 398.

Amidon, G.L., Lennernäs, H., Shah, V.P., Crison, J.R. (1995). A theoretical basis for abiopharmaceutic drug classification: the correlation of *in vitro* drug product dissolution and *in vivo* bioavailability. Pharmaceutical research. 12: 413 – 420.

Anderle, P., Niederer, E., Rubas, W., Hilgendorf, C., Spahn-Langguth, H., Wunderli-Allenspach, H., Merkle, H.P., Langguth, P. (1998). P-Glycoprotein (P-gp) mediated efflux in Caco-2 cell monolayers: the influence of culturing conditions and drug exposure on P-gp expression levels. Journal of pharmaceutical sciences. 87(6): 757 – 762.

Artursson, P. (1991 A). Cell cultures as models for drug absorption across the intestinal mucosa. Critical reviews in therapeutic drug carrier systems. 8: 305 – 350.

Artursson, P., Karlsson, J. (1991 B). Correlation between oral drug absorption in humans and apparent drug permeability coefficients in human intestinal epithelial (Caco-2) cells. Biochemical and biophysical research communications. 175(3): 880 – 885.

Artursson, P., Borchardt, R.T. (1997). Intestinal drug absorption and metabolism in cell cultures: Caco-2 and beyond. Pharmaceutical research. 14(12): 1655 – 1658.

Artursson, P., Palm, K., Luthman, K. (2001). Caco-2 monolayers in experimental and theoretical predictions of drug transport. Advanced drug delivery reviews. 46: 27 – 43.

Avdeef, A. (2001). Physicochemical profiling (solubility, permeability and charge state). Current topics in medicinal chemistry. 1: 277 – 351.

Avdeef, A. (2003). Absorption and drug development: solubility, permeability, and the charge state. John Wiley & Sons, Inc.

Bailey, C.A., Bryla, P., Malick, A.W. (1996). The use of the intestinal epithelial cell culture model, Caco-2, in pharmaceutical development. Advanced drug delivery reviews. 22(1 – 2): 85 – 103.

Balakrishnan, A., Hussainzada, N., Gonzalez, P., Bermejo, M., Swaan, P.W., Polli, J.E. (2007). Bias in estimation of transporter kinetic parameters from overexpression systems: interplay of transporter expression level and substrate affinity. Journal of pharmacology and experimental therapeutics. 320: 133-144.

Balimane, P.V., Chong, S. (2005). Cell culture-based models for intestinal permeability: a critique. Drug discovery today. 10(5): 335 – 343.

Balimane, P.V., Han J.H., Chong, S. (2006). Current industrial practices of assessing permeability and P-glycoprotein interaction. AAPS Journal. 8(1): E1-E13.

Behrens, I., Kissel, T. (2003). Do cell culture conditions influence the carrier-mediated transport of peptides in Caco-2 cell monolayers? European journal of pharmaceutical sciences. 19(5): 433 – 442.

Behrens, I., Kamm, W., Dantzig, A.H., Kissel, T. (2004). Variation of peptide transporter (PepT1 and HPT1) expression in Caco-2 cells as a function of cell origin. Journal of pharmaceutical sciences. 93(7): 1743 – 1754.

Benet, L.Z., Cummins, C.L., Wu, C.Y. (2004). Unmasking the dynamic interplay between efflux transporters and metabolic enzymes. International journal of pharmaceutics. 277: 3 – 9.

Bentz, J., Tran, T.T., Polli, J.W., Ayrton, A., Ellens, H. (2005). The steady-state Michaelis-Menten analysis of P-glycoprotein mediated transport through a confluent cell monolayer cannot predict the correct Michaelis constant Km. Pharmaceutical research. 22(10): 1667 – 77.

Bhattachar, S.N., Deschenes, L.A., Wesley, J.A. (2006). Solubility: it's not just for physical chemists. Drug discovery today. 11(21 – 22): 1012 – 1018.

Bohets, H., Annaert, P., Mannens, G., Van Beijsterveldt, L., Anciaux, K., Verboven, P., Meuldermans, W., Lavrijsen, K. (2001). Strategies for absorption screening in drug discovery and development. Current topics in medicinal chemistry. 1: 367 – 383.

Borst, P., Elferink, R.O. (2002). Mammalian ABC transporters in health and disease. Annual review of biochemistry. 71: 537 – 592.

Briske-Anderson, M.J., Finley, J.W., Newman, S.M. (1997). The influence of culture time and passage number on the morphological and physiological development of Caco-2 cells. Proceedings of the society for experimental biology and medicine. 214(3): 248 – 257.

Camenisch, G., Folkers, G. van de Waterbeemd, H. (1996). Review of theoretical passive drug absorption models: historical background, recent developments and limitations. Pharmaceutica acta Helvetiae. 71: 309 – 327.

Chan, O.H., Schmid, H.L., Kuo, B., Wright, D.S. Howson, W., Stewart, B.H. (1996). Absorption of Cam-2445, an NK1 neurokinin receptor antagonist: *In vivo*, *in situ*, and *in vitro* evaluations. Journal of pharmaceutical sciences. 85: 253 – 257.

Chan, L.M.S., Lowes, S., Hirst, B.H. (2004). The ABCs of drug transport in intestine and liver: efflux proteins limiting drug absorption and bioavailability, European journal of pharmaceutical sciences. 21: 25 – 51.

Chen, I.J., Taneja, R., Yin, D., Seo, P.R., Young, D., MacKerell, A.D. Jr, Polli, J.E. (2006). Chemical substituent effect on pyridine permeability and mechanistic insight from computational molecular descriptors. Molecular pharmaceutics. 3(6): 745 – 55.

Chen, J., Lin, H., Hu, M. (2003). Metabolism of flavonoids via enteric recycling: role of intestinal disposition. Journal of Pharmacology And Experimental Therapeutics. 304(3): 1228 – 1235

Crespi, C.L., Penman, W., Hu, M. (1996). Development of Caco-2 cells expressing high levels of cDNA-derived cytochrome P4503A4. Pharmaceutical research. 13(11): 1635 – 1641.

Cummins, C.L., Mangravite, L.M., Benet, L.Z. (2001). Characterizing the expression fo CYP3A4 and efflux transporters (P-gp, MRP1, and MRP2) in CYP3A4-transfected Caco-2 cells after induction with sodium butyrate and the phorbol ester 12-O-tetradecanoylphorbol-13-acetate. Pharmaceutical research. 18(8): 1102 – 1109.

Cussler, E.L. (1997). Diffusion. Mass transfer in fluid systems 2nd edition. Cambridge university press, Cambridge UK.

Daniel, H. (2004). Molecular and integrative physiology of intestinal peptide transport. Annual review of physiology. 66: 361 – 384.

Daugherty, A.L., Mrsny, R.J. (1999). Transcellular uptake mechanisms of the intestinal epithelial barrier Part one. Pharmaceutical science and technology today. 2(4): 144 – 151.

Delaney, J.S. (2005). Predicting aqueous solubility from structure. Drug discovery today. 10(4): 289 – 295.

Deli, M.A., Abraham, C.S., Kataoka, Y., Niwa, M. (2005). Permeability studies on *in vitro* blood-brain barrier models: physiology, pathology, and pharmacology. Cellular and molecular neurobiology. 25(1): 59 – 127.

de Waziers, I., Cugnenc, P.H., Yang, C.S., Leroux, J.P., Beaune, P.H. (1990). Cytochrome P 450 isoenzymes, epoxide hydrolase and glutathione transferases in rat

and human hepatic and extrahepatic tissues. Journal of pharmacology and experimental therapeutics. 253(1): 387 – 394.

Duvvuri, M., Feng, W., Mathis, A., Krise, J.P. (2004). A cell fractionation approach for the quantitative analysis of subcellular drug disposition. Pharmaceutical research. 21(1): 26 – 32.

Engman, H., Tannergren, C., Artursson, P., Lennernas, H. (2003). Enantioselective transport and CYP3A4-mediated metabolism of R/S-verapamil in Caco-2 cell monolayers. European journal of pharmaceutical sciences. 19(1): 57 – 65.

Eytan, G.D., Regev, R., Oren, G., Assaraf, Y.G. (1996). The role of passive transbilayer drug movement in multidrug resistance and its modulation. Journal of biological chemistry. 271: 12897 – 12902.

Eytan, G. D., Kuchel, P.W. (1999). Mechanism of action of P-glycoprotein in relation to passive membrane permeation. International review of cytology. 190: 175–250

Eytan, G. D. (2005). Mechanism of multidrug resistance in relation to passive membrane permeation. Biomedicine and pharmacotherapy. 59(3): 90 – 97.

Galijatovic, A., Otake, Y., Walle, U.K., Walle, T. (1999). Extensive metabolism of the flavonoid chrysin by human Caco-2 and Hep G2 cells. Xenobiotica 29(12): 1241 – 1256

Ghibellini, G., Leslie, E.M., Brouwer, K.L.R. (2006). Methods to evaluate biliary excretion of drugs in humans: an updated review. Molecular pharmaceutics. 3(3): 198 – 211.

Goodwin, J.T., Conradi, R.A., Ho, N.F., Burton, P.S. (2001). Physicochemical determinants of passive membrane permeability: role of solute hydrogen-bonding potential and volume. Journal of medicinal chemistry. 44(22): 3721 – 3729.

Grohganz, H., Rischer, M., Brandl, M. (2004). Adsorption of the decapeptide Cetrorelix depends both on the composition of dissolution medium and the type fo solid surface. European journal of pharmaceutical sciences. 21: 191 – 196.

Gutmann, H., Bruggisser, R., Schaffner, W., Bogman, K., Botomino, A., Drewe, J. (2002). Transport of amentoflavone across the blood-brain barrier *in vitro*. Planta Medica. 68(9):804-7.

Gutmann, H., Fricker, G., Török, M., Michael, S., Beglinger, C., Drewe, J. (1999). Evidence for different ABC-transporters in Caco-2 cells modulating drug uptake, Pharmaceutical research. 16: 402 – 407.

Hidalgo, I.J., Raub, T.J., Borchardt, R.T. (1989). Characterization of human colon carcinoma cell line (Caco-2) as a model system for intestinal epithelial permeability, Gastroenterology 96: 736–749.

Hidalgo, I.J., Li, J. (1996). Carrier-mediated transport and efflux mechanisms in Caco-2 cells. Advanced drug delivery reviews. 22: 53 – 66.

Hidalgo, I.J. (2001). Assessing the absorption of new pharmaceuticals. Current topics in medicinal chemistry. 1: 385 – 401.

Hilgendorf, C., Spahn-Langguth, H., Rhedin, M., Regardh, C.G., Lowenadler, B., Langguth, P. (2005). Selective downregulation of the MDR1 gene product in Caco-2 cells by stable transfection to prove its relevance in secretory drug transport. Molecular pharmaceutics. 2(1): 64 – 73.

Ho, N. F. H. Raub, T. J., Burton, P. S., Barsuhn, C. L., Adson, A., Audus, K. L., Borchardt, R. T. (2000). Quantitative approaches to delineate passive transport mechanisms in cell culture monolayers. In: Transport processes in pharmaceutical systems. G. L. Amidon and P. I. Lee, editiors. Marcel Dekker Ltd, New York. 219 – 316.

Hochman, J.H., Chiba, M., Nishime, J., Yamazaki, M., Lin, J.H. (2000). Influence of P-glycoprotein on the transport and metabolism of indinavir in Caco-2 cells expressing cytochrome P-450 3A4. Journal of pharmacology and experimental therapeutics. 292: 310 – 318.

Hosoya K.I., Kim K.J., Lee V.H. (1996). Age-dependent expression of P-glycoprotein gp 170 in Caco-2 cell monolayers. Pharmaceutical research. 13(6): 885-890.

Hu, M., Chen, J., Lin, H. (2003). Metabolism of flavonoids via enteric recycling: mechanistic studies of disposition of apigenin in the Caco-2 cell culture model. Journal of Pharmacology And Experimental Therapeutics. 307(1): 314 – 321.

Hunter, J., Hirst, B.H. (1997). Intestinal secretion of drugs. The role of P-glycoprotein and related drug efflux systems in limiting oral drug absorption, Advanced drug delivery reviews. 25: 129 – 157.

Ingels, F.M., Augustijns, P.F. (2003). Biological, pharmaceutical, and analytical considerations with respect to the transport media used in the absorption screening system, Caco-2. Journal of pharmaceutical sciences. 92(8): 1545 – 1558.

Jia, X., Chen, J., Lin, H., Hu, M. (2004). Disposition of flavonoids via enteric recycling: enzyme-transporter coupling affects metabolism of biochanin A and formononetin and

excretion of their phase II conjugates. Journal of Pharmacology And Experimental Therapeutics. 310(3): 1103 – 1113.

Juliano, R.L., Ling, V. (1976). A surface glycoprotein modulating drug permeability in Chinese hamster ovary cell mutants. Biochimica et biophysica acta. 455: 152 – 162.

Kansy, M., Senner, F., Gubernator, K. (1998). Physicochemical high throughput screening: parallel artificial membrane permeation assay in the description of passive absorption processes. Journal of medicinal chemistry. 41(7): 1007 – 1010.

Kapitza, S. B., Michel, B. R., van Hoogevest, P., Leigh, M. L. S, Imanidis, G. (2006). Absorption of poorly water soluble drugs subject to apical efflux using phospholipids as solubilizers in the Caco-2 cell model. European journal of pharmaceutics and biopharmaceutics. 66(1): 146 – 158.

Karlsson, J., Ungell, A.-L., Gråsjö, J., Artursson, P. (1999). Paracellular drug transport across intestinal epithelia: influence of charge and induced water flux, European journal of pharmaceutical sciences. 9: 47 – 56.

Karlsson, M., Påhlsson, C., Fowler, C.J. (2004). Reversible, temperature-dependent, and AM404-inhibitable adsorption of anandamide to cell culture wells as a confounding factor in release experiments. 22: 181 – 189.

Kasim, N.A., Whitehouse, M., Ramachandran, C., Bermejo, M., Lennernas, H., Hussain, A.S., Junginger, H.E., Stavchansky, S.A., Midha, K.K., Shah, V.P., Amidon, G.L. (2004). Molecular properties of WHO essential drugs and provisional biopharmaceutical classification. Molecular pharmaceutics. 1(1): 85 – 96.

Kennedy, T. (1997). Managing the drug discovery/development interface. Drug discovery today. 2: 436 – 444.

Keogh, J.P., Kunta, J.R. (2006). Development, validation and utility of an *in vitro* technique for assessment of potential clinical drug-drug interactions involving P-glycoprotein. European journal of pharmaceutical sciences. 27(5): 543 – 54.

Kolars, J.C., Lown, K.S., Schmiedlin-Ren, P., Ghosh, M., Fang, C., Wrighton, S.A., Merion, R.M., Watkins, P.B. (1994). CYP3A gene expression in human gut epithelium. Pharmacogenetics. 4(5): 247 – 259.

Konig, J., Nies, A.T., Cui, Y., Leier, I., Keppler, D. (1999). Conjugate export pumps of the multidrug resistance protein (MRP) family: localization, substrate specificity and MRP2-mediated drug resistance. Biochimica et biophysica acta. 141: 377 – 394.

Korjamo, T., Monkkonen, J., Uusitalo, J., Turpeinen, M., Pelkonen, O., Honkakoski, P. (2006). Metabolic and efflux properties of Caco-2 cells stably transfected with nuclear receptors. Pharmaceutical research. 23(9): 1991 – 2001.

Krishna, G., Chen, K.-J., Lin, C.-C., Nomeir, A.A. (2001). Permeability of lipophilic compounds in drug discovery using in-vitro human absorption model, Caco-2. International journal of pharmaceutics. 222: 77 – 89.

LeCluyse, E.L., Sutton, S.C. (1997). *In vitro* models for selection of development candidates. Permeability studies to define mechanism of absorption enhancement. Advanced drug delivery reviews. 23: 163 – 183.

Lee, V.H. (2000). Membrane transporters. European journal of pharmaceutical sciences. Supplement 2: S41 – 50.

Lee, Y.-J., Chung, S.-K., Shim, C.-K. (2001). The prevention of cyclosporin A adsorption to Transwell surfaces by human plasma. International journal of pharmaceutics. 224: 201 – 204.

Lenne-Gouverneur, A.-F., Lobstein, A., Haan-Archipoff, G., Duportaill, G., Anton, R., Kuhry, J.-G. (1999). Interactions of the monomeric and dimeric flavones apigenin and amentoflavone with the plasma membrane of L929 cells; a fluorescence study. Molecular membrane biology. 16: 157 – 165.

Lennernäs, H., Abrahamsson, B. (2005) The use of biopharmaceutic classification of drugs in drug discovery and development: current status and future extension. Journal of pharmacy and pharmacology. 57: 273 – 285.

Li, N.; DeMarco, V. G.; West, C.M.; Neu, J. (2003). Glutamine supports recovery from loss of transepithelial resistance and increase of permeability induced by media change in Caco-2 cells. Journal of nutritional biochemistry 14 (2003): 401 – 408

Lipinski, C.A., Lombardo, F., Dominy, B.W. and Feeney, P.J. (1997). Experimental and computational approaches to estimate solubility and permeability in drug discovery and development settings. Advanced drug delivery reviews. 23: 3 – 25.

Litman, T., Druley, T.E., Stein, W.D., Bates, S.E. (2001). From MDR to MXR: new understanding of multidrug resistance systems, their properties and clinical significance. Cellular and molecular life sciences. 58(7): 931 – 959.

Litman, T., Skovsgaard, T., Stein, W.D. (2003). Pumping of drugs by P-glycoprotein: a two-step process? Journal of pharmacology and experimental therapeutics. 307(3): 846 – 853.

Liu, Y., Hu, M. (2002). Absorption and metabolism of flavonoids in the Caco-2 cell culture model and a perused rat intestinal model. Drug Metabolism and Disposition 30(4): 370 – 377

Loo, T.W., Clarke, D.M. (2005). Recent progress in understanding the mechanism of P-glycoprotein-mediated drug efflux. Journal of membrane biology. 206: 173–185.

Ma, T. Y.; Nguyen, D.; Bui, V.; Nguyen, H.; Hoa, N. (1999). Ethanol modulation of intestinal epithelial tight junction barrier; Am. J. Physiol. 276 (Gastro-intest. Liver Physiol. 39): G965 – G974

Maeda, T., Takahashi, K., Ohtsu, N., Oguma, T., Ohnishi, T., Atsumi, R., Tamai, I. (2007). Identification of influx transporter for the quinolone antibacterial agent levofloxacin. Molecular pharmaceutics. 4(1): 85 – 94.

Makhey, V.D., Guo, A., Norris, D.A., Hu, P., Yan, J. and Sinko, P.J. (1998). Characterization of the regional intestinal kinetics of drug efflux in rat and human intestine and in Caco-2 cells. Pharmaceutical research. 15(8): 1160–1167.

Martin, A. (1993). Physical pharmacy. Physical chemical principles in the pharmaceutical sciences. 4th edition. Lea & Febiger, Philadelphia.

McKinnon, R.A., Burgess, W.M., Hall, P.M., Roberts-Thomson, S.J., Gonzalez, F.J., McManus, M.E. (1995). Characterisation of CYP3A gene subfamily expression in human gastrointestinal tissues. Gut. 36(2): 259 – 267.

Meier, M., Blatter, X.L., Seelig, A., Seelig, J. (2006). Interaction of verapamil with lipid membranes and P-glycoprotein: connecting thermodynamics and membrane structure with functional activity. Biophysical journal. 91(8): 2943 – 2955.

Meunier, V., Bourrie, M., Berger, Y., Fabre, G. (1995). The human intestinal epithelial cell line Caco-2; pharmacological and pharmacokinetic applications. Cell biology and toxicology. 11(3-4): 187-94.

Morishita, M., Peppas, N. A. (2006). Is the oral route possible for peptide and protein drug delivery? Drug Discovery Today. 11(19-20): 905 – 910.

Mosmann T. (1983). Rapid colorimetric assay for cellular growth and survival: Application to proliferation and cytotoxicity assays. J Immunol Methods 65: 55 – 63.

Nellans, H.N. (1991). Paracellular intestinal transport: modulation of absorption. Advanced drug delivery reviews. 7: 339 – 364.

Neuhoff, S., Ungell, A.L., Zamora, I., Artursson, P. (2003). pH-dependent bidirectional transport of weakly basic drugs across Caco-2 monolayers: implications for drug-drug interactions. Pharmaceutical research. 20(8): 1141 – 1148.

Neuhoff, S., Artursson, P., Zamora, I., Ungell, A.L. (2006). Impact of extracellular protein binding on passive and active drug transport across Caco-2 cells. Pharmaceutical research. 23(2): 350 – 359.

O'Leary, K.A., Day, A.J., Needs, P.W., Mellon, F.A., O'Brien, N.M., Williamson, G. (2003). Metabolism of quercetin-7- and quercetin-3-glucuronides by an *in vitro* hepatic model: the role of human beta-glucuronidase, sulfotransferase, catechol-O-methyltransferase and multi-resistant protein 2 (MRP2) in flavonoid metabolism. Biochemical pharmacology. 65(3): 479 – 91.

Pageot, L.P., Perreault, N., Basora, N., Francoeur, C., Magny, P., Beaulieu, J.F. (2000). Human cell models to study small intestinal functions: recapitulation of the crypt-villus axis. Microscopy research and technique. 49(4): 394 – 406.

Palmgrén, J.J., Mönkkönen, J., Korjamo, T., Hassinen, A., Auriola, S. (2006). Drug adsorption to plastic containers and retention of drugs in cultured cells under *in vitro* conditions. European journal of pharmaceutics and biopharmaceutics. 64: 369 – 378.

Pappenheimer, J.R.; Reiss, K.Z. (1987). Contribution of solvent drag through intercellular junctions to absorption of nutrients by the small intestine of the rat. Journal of membrane biology. 100: 123 – 136.

Pauli-Magnus, C., von Richter, O., Burk, O., Ziegler, A., Mettang, T., Eichelbaum, M., Fromm, M.F. (2000). Characterization of the major metabolites of verapamil as substrates and inhibitors of P-glycoprotein. Journal of pharmacology and experimental therapeutics. 293(2): 376 – 382.

Polli, J.W., Wring, S.A., Humphreys, J.E., Huang, L., Morgan, J.B., Webster, L.O., Serabjit-Singh CS. (2001). Rational use of *in vitro* P-glycoprotein assays in drug discovery. Journal of pharmacology and experimental therapeutics. 299(2): 620 – 628.

Rautio, J., Humphreys, J.E., Webster, L.O., Balakrishnan, A., Keogh, J.P., Kunta, J.R., Serabjit-Singh, C.J., Polli, J.W. (2006). *In vitro* P-glycoprotein inhibition assays for assessment of clinical drug interaction potential of new drug candidates: a recommendation for probe substrates. Drug metabolism and disposition. 34(5): 786 – 92.

Rodriguez-Ibáñez, M., Sánchez-Castaño, G., Montalar-Montero, M., Garrigues, T.M., Bermejo, M., Merino, V. (2006). Mathematical modelling of in situ and *in vitro* efflux of ciprofloxacin and grepafloxacin. International journal of pharmaceutics. 307(1): 33 – 41.

Rowland, M., Tozer, T.N. (1995). Clinical pharmacokinetics: Concepts and applications. Lippincott Williams & Wilkins.

Sai, Y., Tsuji, A. (2004). Transporter-mediated drug delivery: recent progress and experimental approaches. Drug discovery today. 9(16): 712 – 720.

Salama, N.N., Eddington, N.D., Fasano, A. (2006). Tight junction modulation and its relationship to drug delivery. Advanced drug delivery reviews. 58(1): 15 – 28.

Schinkel, A.H., Jonker, J.W. (2003). Mammalian drug efflux transporters of the ATP binding cassette (ABC) family: an overview. Advanced drug delivery reviews. 55(1): 3 – 29.

Schlatter, P., Gutmann, H., Drewe, J. (2006). Primary porcine proximal tubular cells as a model for transepithelial drug transport in human kidney. European journal of pharmaceutical sciences. 28(1-2): 141 – 54.

Schmiedlin-Ren, P., Thummel, K.E:, Fisher, J.M., Paine, M.F., Lown, K.S., Watkins, P.B. (1997). Expression of enzymatically active CYP3A4 by Caco-2 cells grown on extracellular matrix-coated permeable supports in the presence of 1alpha,25-dihydroxyvitamin D3. Molecular pharmacology. 51: 741 – 754.

Seydel, J.K. (2002). Function, composition, and organization of membranes. In: Drug-membrane interactions: analysis, drug distribution, modeling. Edited by Seydel, J.K:, Wiese, M. Wiley-VCH Verlag GmbH & Co. KGaA.

Shaw, A.S. (2006). Lipid rafts: now you see them, now you don't. Nature immunology. 7(11):1139 – 1142.

Shimada, T., Yamazaki, H., Mimura, M., Inui, Y., Guengerich FP. (1994). Interindividual variations in human liver cytochrome P-450 enzymes involved in the oxidation of drugs, carcinogens and toxic chemicals: studies with liver microsomes of 30 Japanese and 30 Caucasians. Journal of pharmacology and experimental therapeutics. 270(1): 414 – 423.

Shin, K., Fogg, V.C., Margolis, B. (2006). Tight junctions and cell polarity. Annual review of cell and developmental biology. 22: 207 – 235.

Shirasaka, Y., Kawasaki, M., Sakane, T., Omatsu, H., Moriya, Y., Nakamura, T., Sakaeda, T., Okumura, K., Langguth, P., Yamashita, S. (2006). Induction of human P-glycoprotein in Caco-2 cells: development of a highly sensitive assay system for P-glycoprotein-mediated drug transport. Drug metabolism and pharmacokinetics. 21(5): 414 – 423.

Simons, K., Ikonen, E. (1997). Functional rafts in cell membranes. Nature. 387(6633): 569 – 572.

Singer, S.J., Nicolson, G.L. (1972). The fluid mosaic model of the structure of cell membranes. Science. 175:720 – 731.

Smith, D.A., van de Waterbeemd, H., Walker, D.K. (2001). Chapter 3: Absorption. In: Pharmacokinetics and metabolism in drug design. Edited by D. A. Smith, H. van de Waterbeemd, D. K. Walker, R. Mannhold, H. Kubinyi, H.Timmerman. Wiley-VCH Verlag GmbH.

Stenberg, P., Norinder, U., Luthman, K., Artursson, P. (2001). Experimental and computational screening models for the prediction of intestinal drug absorption. Journal of medicinal chemistry. 44(12): 1927 – 1937.

Suzuki, H., Sugiyama, Y. (2002). Single nucleotide polymorphisms in multidrug resistance associated protein 2 (MRP2/ABCC2): its impact on drug disposition. Advanced drug delivery reviews. 54(10): 1311 – 1331.

Tada H, Shiho O, Kuroshima K, Koyama M, Tsukamoto K. (1986). An improved colorimetric assay for interleukin 2. J Immunol Methods 93:157-165.

Takagi, T., Ramachandran, C., Bermejo, M., Yamashita, S., Yu, L.X., Amidon, G.L. (2006). A provisional biopharmaceutical classification of the top 200 oral drug products in the United States, Great Britain, Spain, and Japan. Molecular pharmaceutics. 3(6): 631 – 643.

Tavelin, S., Milovic, V., Ocklind, G., Olsson, S., Artursson, P. (1999). A conditionally immortalized epithelial cell line for studies of intestinal drug transport. Journal of pharmacology and experimental therapeutics. 290(3): 1212 – 1221.

Tran, T.T., Mittal, A., Gales, T., Maleeff, B., Aldinger, T., Polli, J.W., Ayrton, A., Ellens, H., and Bentz, J. (2004). Exact kinetic analysis of passive transport across a polarized confluent MDCK cell monolayer modelled as a single barrier. Journal of pharmaceutical sciences. 93: No. 8: 2108 – 2123.

Tran, T.T., Mittal, A., Aldinger, T., Polli, J.W., Ayrton, A., Ellens, H., Bentz, J. (2005). The elementary mass action rate constants of P-gp transport for a confluent monolayer of MDCKII-hMDR1 cells. Biophysical journal. 88: 715 – 738.

Troutman, M.D., and Thakker, D.R. (2003 A). Efflux ratio connot assess P-glycoprotein-mediated attenuation of absorptive trasnsport: asymmetric effect of P-glycoprotein on

absorptive and secretory transport across Caco-2 cell monolayers. Pharmaceutical research. 20(8): 1200 – 1209.

Troutman, M.D., and Thakker, D.R. (2003 B). Novel experimental parameters to quantify the modulation of absorptive and secretory transport of compounds by P-glycoprotein in cell culture models of intestinal epithelium. Pharmaceutical research. 20(8): 1210 – 1224.

Tsuji ,A., Tamai, I. (1996). Carrier-mediated intestinal transport of drugs. Pharmaceutical research. 13(7): 963 – 977.

Usansky, H.H., Sinko, P.J. (2005). Estimating human drug oral absorption kinetics from Caco-2 permeability using an absorption-disposition model: model development and evaluation and derivation of analytical solutions for k_a and F_a. Journal of pharmacology and experimental therapeutics. 314(1): 391 –399.

Vaidyanathan, J.B., Walle, T. (2001). Transport and metabolism of the tea flavonoid (-)-epicatechin by the human intestinal cell line Caco-2. Pharmaceutical research. 18: 1420 – 1425.

van Meer, G., Simons, K.(1988). Lipid polarity and sorting in epithelial cells. Journal of cellular biochemistry. 36(1): 51 – 58.

Varma, M.V., Panchagnula, R. (2005). Prediction of *in vivo* intestinal absorption enhancement on P-glycoprotein inhibition, from rat in situ permeability. Journal of pharmaceutical sciences. 94(8): 1694 – 1704.

Vellonen, K.-S., Honkakoski, P., Urtti, A. (2004). Substrates and inhibitors of efflux proteins interfere with the MTT assay in cells and may lead to underestimation of drug toxicity. European journal of pharmaceutical sciences. 23: 181 – 188.

Venkatesh, S., Lipper, R.A. (2000). Role of the development scientist in compound lead selection and optimization. Journal of pharmaceutical sciences. 89:145 – 154.

Yahya, A.M., McElnay, J.C., D'Arcy, P.F. (1988). Drug sorption to glass and plastics. Drug metabolism and drug interactions. 6(1): 1 – 45.

Yee, S. (1997). *In vitro* permeability across Caco-2 cells (colonic) can predict *in vivo* (small intestinal) absorption in man–fact or myth. Pharmaceutical research. 14: 763-766.

Youdim K.A., Avdeef A, Abbott N.J. (2003). *In vitro* trans-monolayer permeability calculations: often forgotten assumptions. Drug Discovery Today 8(21): 997 – 1003.1

Yu, H., Cook, T.J., Sinko, P.J. (1997). Evidence for diminished functional expression of intestinal transporters in Caco-2 cell monolayers at high passages. Pharmaceutical research. 14(6): 757 – 762.

Zhang, X., Shedden, K., Rosania, G.R. (2006). A cell-based molecular transport simulator for pharmacokinetic prediction and cheminformatic exploration. Molecular pharmaceutics. 3(6): 704 -716.

Resume

David Blaser
Pharmacist

Personal Details

Name:	David Blaser
Date and place of birth:	27 December 1975
Nationality:	Swiss

PhD Study

March 2003 – May 2007	PhD study at Institute of Pharmaceutical Technology (University of Basel) under the supervision of Prof. Dr. Georgios Imanidis. Lectureship in practical courses of liquid and sterile dosageforms and semi-solid dosage forms

Supervision of the following diploma theses

May 2006 – September 2006	„Bestimmung der Wirkstoffabsorption in Caco-2-Zellkulturen bei passivem und carrier-vermitteltem Transport“ (Urs Duthaler).
February 2005 – July 2005	„Quantifizierung von Absorption, Metabolismus und apikalem Efflux in Caco-2 Zellen bei Wirkstoffgemischen“ (Chantal Krömler).

Presentations

25 – 27 October 2006	6th biennial GPEN conference, GPEN 2006, at the University of Kansas (Lawrence, Kansas) Podium presentation
1 – 3 July 2004	Midnight sun symposium on Drug Transport and Drug Delivery, at the University of Tromsø, Norway Poster presentation

Education

October 1997 – November 2002	Pharmacy studies at University of Basel, Basel, Switzerland Master in Pharmaceutical Sciences and federal diploma as pharmacist Final result state examination: 5.38 (maximum 6.00)

	Final result practical diploma thesis: 6
September 2000	3rd state examination ("Assistentenprüfung für Apotheker")
August 1999	2nd state examination ("Pharmazeutische Grundfächerprüfung")
September 1998	1st state examination („Naturwissenschaftliche Prüfung für Apotheker")
1996 and 1997	Obligatory and additional military services Function: platoon leader. Rank: lieutenant
August 1992 – December 1995	High school diploma ("Matura") at Gymnasium Liestal (specialisation in economics "Typus E"). Final result: 5.1

Work Experience

August 1999 – August 2000	Practical year at Adler Apotheke H.J. + U. Studer, Liestal, Switzerland
May 2000 – July 2000	Practical training as part of the practical year at Spitalapotheke Kantonsspital Bruderholz, Bruderholz, Switzerland

Additional Skills

Trainings	
March 2007	Quality and GMP. Continuing education course of the Pharmacenter Basel-Zürich, Switzerland
February 2007	Robust dosage form design: Innovative and effective tools for a science based road map in pharmaceutical R&D. Technology Training Center (TTC) Binzen, Germany
September / October 2004	Strategies and trends in pharmaceutical development and production. Continuing education course of the Pharmacenter Basel-Zürich, Switzerland
November 2003	Method Development for GC und HPLC, Agilent Technologies (Schweiz) AG, Basel
Languages	German (native speaker) English (fluent) French (basic to good command)
PC Literacy	Proficient user
Applications	Good command of Microsoft Office applications

As a student and PhD student I have attended lectures and courses given by

Thomas A. Kaden, Helmut Sigel, Andreas Zuberbühler, Urs Sequin, Peter Strazewski, Peter C. Hauser, Peter C. Oelhafen, Udo M. Spornitz, Lukas Landmann, Daniel Haag-Wackernagel, Hansjakob Müller, Heinz Durrer, Annetrudi Kress, Jean-Pierre Barras, Alfred Fahr, Ruth U. Leu Marseiler, Peter Erb, Christoph Moroni, Alfons Hädener, Willi Hunziker, Niggi Iberg, Michael Kessler, Roland Wormser, Rudolf Bruppacher, Kurt Hersberger, Hermann Bartels, Peter Huber, German A. Marbet, Andre Scholer, Jürgen Drewe, Stefan Krähenbühl, Raymond Schlienger, Chritoph R. Meier, Stefan Mühlebach, Christian Surber, Beat Ernst, Gert Folkers, Angelo Vedani, Willi Schaffner, Beat Meier, Karin Berger-Büter, Anna Seelig, Joachim Seelig, Heiko Heerklotz, Hans Leuenberger, Georgios Imanidis, Danielle Giron, Theodor W. Güntert